1-1-1968

Folded sandwich plate structures.

Paul P. Fazio
University of Windsor

FOLDED SANDWICH PLATE STRUCTURES

A THESIS
Submitted to the Faculty of Graduate Studies Through the
Department of Civil Engineering in Partial Fulfillment
of the Requirements for the Degree of
Philosophy Doctorate of Applied Science
at the University of Windsor

by

PAUL P. FAZIO
M.A.Sc., University of Windsor

Windsor, Ontario, Canada
May, 1968

NEX 6449

APPROVED BY:

A. B. Smith

W McVinnie

G. Abdel-Sayed

J. B. Kennedy

213297

ABSTRACT

In this study sandwich panels and folded sandwich plate structures have been investigated both analytically and experimentally. The results of flatwise and edgewise compression tests, carried out on samples of this material, have been presented in Chapter I. The shear, bending and torsional stiffness constants have been determined for sandwich panels used to build two folded plate models. Shear stiffness constants, determined by several experimental methods, vary according to the test method used. The experimental and theoretical values of the bending stiffness constants differ by only 3.6%. Torsion rigidities have been determined in Chapter III from eight square sandwich panels. Experimental deflections and stress distributions of two folded sandwich models have been presented in Chapters IV and V. One of these models (9.5 feet long) was uniformly loaded along the ridges. The other (19 feet long) was loaded laterally with air pressure. The theoretical deflections and stresses, obtained from the computer program and the theory developed for these structures in Chapter VI, compare favourably with the experimental results. The conclusions of the study and the potentials of sandwich construction in the prefabrication industry have been discussed in Chapter VIII. It is hoped that this study will promote the understanding of sandwich construction and its use in the building industry.

ACKNOWLEDGMENTS

The author owes many thanks to Dr. J. B. Kennedy (Professor and Head of the Civil Engineering Department at the University of Windsor) for his suggestions, guidance and encouragement in the completion of this work, and to the Aluminum Company of Canada (ALCAN) for sponsoring and financing this project.

The author is further indebted to:

The University of Windsor for the use of the Structural Laboratory and its competent Technicians for a period of over three years;

The Computer Center at Sir George Williams University;

His wife, Lucy, for her patience during the laborious months dedicated to the completion of this project.

TABLE OF CONTENTS

LIST OF TABLES

LIST OF ILLUSTRATIONS

NOMENCLATURE

A	=	area of cross section.
A	=	displacement transformation matrix.
A^t	=	force transformation matrix.
B	=	width of the sandwich panel.
c	=	thickness of core.
D	=	member displacement matrix in the relative coordinate system.
$\overline{D}$	=	member displacement matrix in the fixed coordinate system.
D_{qx}, D_{qy}	=	shear stiffness constants in the x- and y-directions, respectively.
D_x, D_y	=	flexural rigidities in the x- and y-directions, respectively.
D_{xy}	=	torsion rigidity constant.
$\overline{D}_z$, Δ_z	=	horizontal displacements in the fixed coordinate system.
$\overline{D}_y$, Δ_y	=	vertical displacements in the fixed coordinate system.
$\overline{D}_x$, Δ_x	=	longitudinal displacements in the fixed coordinate system.
$\overline{D}_\theta$, Δ_θ	=	ridge rotations, about the axis along the ridge, in the fixed coordinate system.
D_x, μ	=	longitudinal displacements along the plate edge.
D_y, v	=	displacements in the plane of the panel and normal to the edge.
D_z, w	=	edge displacements normal to the plane of the plate.
D_θ, θ	=	rotations at the plate edge and about the axis along the edge.

E = elastic modulus of the facings.

E_{cx}, E_{cy} = elastic moduli of the core in the x- and y-directions, respectively.

F = member force matrix in the relative coordinate system.

$\bar{F}$ = member force matrix in the fixed coordinate system.

$\bar{F}_x$, R_x = horizontal forces per unit length in the fixed coordinate system.

$\bar{F}_y$, R_y = vertical forces per unit length in the fixed coordinate system.

$\bar{F}_z$, R_z = horizontal forces per unit length in the fixed coordinate system.

$\bar{F}_\theta$, R_θ = ridge moments per unit length in the fixed coordinate system and acting about the axis along the ridge.

F_y, P = plate edge forces per unit length in the plane of the plate and normal to the edge.

F_z, Q = plate edge forces per unit length normal to the plane of the plate.

F_θ, M = plate edge moments per unit length acting about the axis along the edge.

G_{cx}, G_{cy} = shear moduli of the core material in the x- and y-directions, respectively.

G_{xyf} = modulus of elasticity in shear of the facing material.

H = horizontal component of the width of the folded plate panels.

h = thickness of a sandwich element measured from the middle planes of the facings.

I = moment of inertia of a cross section.

I_p = moment of inertia of the cross section of the sandwich panel calculated about the neutral axis normal to the facings.

K = structure stiffness matrix.

k = element stiffness matrix.

k_p = plate stiffness matrix.

k_s = slab stiffness matrix.

$\bar{k}$ = element stiffness matrix in the fixed coordinate system.

L = span length of a sandwich beam.

M_f = moment in the facings.

M_x, M_y = moments along the span of sandwich beams cut in the x- and y-directions, respectively, of the parent panel.

M_{xy} = twisting moment in the zx- and zy-planes.

m, n = side dimensions of sandwich panels subjected to torsion.

n = harmonic number.

P = concentrated load in a beam.

P = plate edge force in the plane of the sandwich panel and normal to the edge.

Q = static moment of a cross section.

Q_x, Q_y = shear forces acting in cross sections parallel to yz- and xz-plane, respectively.

r = relative displacement of the facings of a sandwich panel.

s = overall thickness of sandwich panels.

T, F_x = shear force per unit length acting along the plate edge.

t = thickness of the facings.

u = displacement at a plate edge in the direction of T.

V = vertical component of the width of the folded plate panels.

v = displacement at a plate edge in the direction of P.

V = transverse shearing force.

w = displacement at a plate edge in the direction of Q.

w_b, w_s = deflections due to bending and shear effects, respectively.

γ_x, γ_y = shear angles associated with Q_x and Q_y, respectively.

δ = deflection.

ε_x, ε_y, ε_z = strains in the x-, y- and z-directions, respectively.

λ = angles which the folded plate panels make with the horizontal.

μ = Poisson's ratio.

ρ_x, ρ_y = radii of curvature of the neutral plane of a plate in the x- and y-directions, respectively.

σ_x, σ_y, σ_z = stresses in the x-, y- and z-directions, respectively.

τ = shear stresses.

CHAPTER I

INTRODUCTION

Sandwich Construction

Sandwich constructions comprise thin strong facings bonded to each side of a thick lightweight core. By themselves, the components have little load-carrying-capacity; once bonded together, however, they produce stiff, lightweight structural members.

A sandwich member is comparable to an I-beam. The object is to place a high density, high strength material as far from the neutral axis as possible in order to get a high section modulus. Like the web of the I-beam, the core of the sandwich resists the shear loads and supports the flanges allowing them to act as a unit. The core, unlike the web, maintains a continuous support for the facings, allowing them to develop yield strength without crimping or buckling. Both the facings of the

sandwich and the flanges of the I-beam are responsible for carrying the beam bending or tensile and compressive loads.

For sandwich constructions to be effective, the adhesive which bonds the facings to the core must be capable of transmitting shear loads between the two components so these may act as a unit. The problem of bond failure is most critical for sandwiches with honeycomb cores; the structure of this core limits the contact area between facings and core to five per cent of the area of the facing.

Advantages

The most important advantage of sandwich construction is its high strength-to-weight and stiffness-to-weight ratios. For an equivalent rigidity factor an aluminum-faced honeycomb sandwich beam weighs only one-fifth that of birch or plywood, one tenth that of solid aluminum, and one-sixteenth that of solid steel.

When used in the building industry and if compared to the common methods of construction, sandwich

members lower both the framework weights and the foundation requirements. Sandwich panels are very easy to erect and provide a permanent exterior and interior finish. Because of their thinness, these panels occupy little volume, thus providing more working space in the building.

Sandwich construction has good insulating properties; it lends itself to easy removal for replacement of electrical and ducting systems; it requires less construction time on the job site; it has a long life with low maintenance; it absorbs vibrations; it makes use of materials most economically; and it offers the architect complete design freedom. Figure 1 shows a four-storey building whose enclosing walls consist of non-load-bearing sandwich panels. The building weighs only 40 lbs. per sq. ft. instead of the 120 lbs. per sq. ft. of a conventional steel-and-masonry construction system. Because of the consequent reduction in steel, concrete, and construction time, the cost of the building was only $ 15 per sq. ft. (1966). The standard panels

measured 5' x 14' and could easily be carried by one man (Fig. 1). The four walls they produced have a deadload of only 11½ tons - compared with 612 tons had the walls been of conventional brick-and-plaster.[1]

Applications

The new concept of sandwich construction was introduced in the aircraft industry during the second world war when extensive use was made of birch facing material laminated to balsa wood cores in the Havilland "Mosquito" bomber.

At present sandwich construction is used in the airborne unit of almost every aircraft and missile. Only limited application, however, has been made of this type of construction in commercial enterprises. Some of these applications are: building wall panels, flooring for house trailers, small boat hulls, shipboard doors and bulkheads, table tops, furniture, truck trailer panels and

---

[1] Figure 1 and its related information was taken from House and Home, Vol. 23, No. 10, October, 1966, p. 114. Published by McGraw Hill Inc.

doors, stressed skin buildings, etc.

Forbenfabriken Bayer A.G. of Loverkursen, Germany, is developing (1967) a self supporting automobile unit made from chemistry based materials. The sandwich construction consists of a glassfiber-reinforced plastic facing filled with polyurethane foam - a combination of extremely low weight. The car has performed satisfactorily on the test tracks.[2]

In this study sandwich panels were used as structural components in roof folded plate structures.

Flatwise Compression

In this project flatwise compression tests were carried out on 3" x 3" sandwich samples in an Instron testing machine (Figs. 2 & 3). The samples were cut from the two types of sandwich panels which were later used to build folded plate roof models. One type had one-inch-thick honeycomb paper core, the other one-inch-thick styrolite (bead formed polystyrene). The honeycomb

---

[2] Engineering Digest, Vol. 28, No. 12, December, 1967.

was Union Bag 80 (18) ½ grade - 80 lb. base, 18% resin, ½" cell size.

The specimens with the honeycomb core (Fig. 2) showed an average flatwise yield strength of 144 psi and an average value for the modulus of elasticity of 9307 psi; the styrolite samples (Fig. 3) showed the average values of 12 psi and 134 psi for the strength and modulus respectively (Table 1).

From these tests it can be seen that styrolite would make a poor core for roof structures since it would not withstand the weight of working men.

Edgewise Compression

When sandwich members are loaded as a column, the facings alone resist the axial forces while the core stabilizes the thin facings to prevent buckling. The extent to which the axial stresses in the facings are developed, before buckling occurs, depends on how well the facings are stabilized not only by the core but also by the bond between the core and the facings.

Edgewise compression tests were carried out on

TABLE 1

YIELD STRENGTHS AND MODULI OF ELASTICITY
FROM FLATWISE COMPRESSION
TESTS

Honeycomb Specimens			Styrolite Specimens		
No. of Specimens	Yield Strength in psi	Modulus of Elasticity in psi	No. of Specimens	Yield Strength in psi	Modulus of Elasticity in psi
1	120.9	7897.5	1	12.9	115.9
2	138.3	9590.0	2	12.0	154.0
3	136.0	10575.5	3	11.8	131.5
4	141.0	9165.7			
Average	134	9307	Average	12	134

several samples of both honeycomb and styrolite sandwich construction. The modes of failure of the honeycomb sandwich samples are shown in Figures 4 to 8. For almost every column, the facings buckled before developing the yield stress because the bond between the core and the facings failed. Figure 4 shows the honeycomb samples tested, their dimensions, and ultimate loads. The graphs in Figures 6, 7 and 8 show the stresses developed at failure. The accompanying drawings show the type of failure of the specimen corresponding to each curve. The load was cycled on specimen number 2 (Fig. 6).

The behaviour of the styrolite compression samples is shown in Figure 9, 10 and 11. There was no definite failure point since the facings began to buckle as soon as the load was applied. In this case, the styrolite core is not sufficiently stiff to significantly stabilize the facings. The labels in Figure 9, 10 and 11 give the dimensions of the particular sample and the load existing on the column at the time the picture was taken.

Shear, Bending and Twisting Stiffness Constants

The shear and bending stiffnesses of sandwich

construction are treated extensively in Chapter II; the twisting stiffness in Chapter III. Numerous tests were conducted on samples cut from both honeycomb and styrolite sandwich panels to determine the above stiffnesses. Some of these constants were later used in Chapter VI in the theoretical analysis of roof sandwich folded plate structures.

CHAPTER II

ANALYSIS OF SHEAR AND FLEXURAL STIFFNESSES

Introduction

Shear and flexural stiffnesses are two important properties which must be determined for any sandwich panel before it can be properly used as a structural element. A theoretical analysis of these stiffnesses is presented in the first part of this section. Four of the several methods available were employed to determine experimentally the stiffness constants of sandwich samples whose core was either paper honeycomb or styrolite; the experimental results are presented in the second part of this chapter. A general evaluation of the different experimental methods and theories postulated concludes this study on shear and flexural stiffnesses.

Shear Stiffness

The shear stiffness, D_{qx}, is defined as the ratio of shear (Q_x) to shear angle (γ_x) or, in equation form,

$$D_{qx} = \frac{Q_x}{\gamma_x} \quad \text{.....(1)}$$

when only Q_x is acting. Similarly,

$$D_{qy} = \frac{Q_y}{\gamma_y} \quad \text{.....(2)}$$

For the honeycomb and styrolite cores treated in this report the elastic moduli, E_{cx} and E_{cy}, may be assumed to be zero (See Fig. 36). Hence, the internal moment of a loaded sandwich beam (Fig. 12-a) will be resisted entirely by the facings as shown in Figure 12(b). The core will carry only the shear τ_{xy} which remains constant throughout any cross section perpendicular to the x-axis. Due to this shear distribution, the cross sections will slide over one another, but will remain plane producing shear strains which are constant for the total depth of the beam and equal to the shear angle γ_x or γ_y (Fig. 12-c).

The shear force Q_x at any cross section A, perpendicular to the x-axis, can be written as $A\tau_{xy} = AG_{cx}\gamma_x$ where G_{cx} is the shear modulus of the core material. Substituting these expressions into Eq. (1), the shear stiffness D_{qx} will become

$$D_{qx} = G_{cx}A \quad \text{.....(3)}$$

When the thickness of the facings is very small compared

tc the overall depth of the beam, the area of the cross section for Equation (3) is taken as hd where h is the distance between the neutral axes of the facings and d is the width of the section. For a one-inch-wide sandwich beam with a core such as paper honeycomb or styrolite, the shear stiffness is given by the following expression:

$$D_{qx} = G_{cx}h \quad \ldots\ldots\ldots\ldots(4)$$

Similarly,

$$D_{qy} = G_{cy}h \quad \ldots\ldots\ldots\ldots(5)$$

It should be noted that if the core is rigid enough to assure interaction between the facings, the cross sections of the plate generally tend to warp out of their plane condition when subjected to shear (p. 170 of reference 83). If warpage is significant, the shear strain, γ_x, in Eq. (1) is no longer constant; it becomes

$$\gamma_x = \frac{\tau_{xy}}{G_{cx}} = \frac{Q_x Q}{IdG_{cx}} \quad \ldots\ldots\ldots\ldots(6)$$

where I is the moment of inertia ($in.^4$) of the section and Q is the static moment of the area ($in.^3$) above the plane on which the shear τ_{xy} is being considered. Integration of γ_x through the core will yield the relative displacement, r, of the two facings.

$$r = \int_0^c \gamma_x dz = \frac{Q_x}{IdG_{cx}} \int_0^c Qdz \quad .....(7)$$

where c is the depth of the core. It is assumed in Eq. (7) that no shear strain occurs in the facings. The average shear angle γ_x can be taken as r/h. By substituting this angle into Equation (1) the following expression is obtained for the shear stiffness, D_{qx}, per unit width:

$$D_{qx} = \frac{IG_{cy}h}{\int_0^c Qdz} \quad .....(8)$$

Similarly,

$$D_{qy} = \frac{IG_{cy}h}{\int_0^c Qdz} \quad .....(9)$$

Flexural Stiffness

Let us consider a sandwich element cut out of a panel by two pairs of planes parallel to the xz and yz planes as shown in Figure 31. It is assumed that during bending the lateral sides of this element will remain plane and perpendicular to the neutral surface of the plate. The curvatures of this neutral surface are $1/\rho_x$ and $1/\rho_y$ in sections parallel to the xz and yz planes respectively and are considered positive if concave upward. The strains in any layer z distant from the neutral surface and within the facings can be written as

$$\varepsilon_x = \frac{z}{\rho_x} \qquad \varepsilon_y = \frac{z}{\rho_y} \quad \text{.....(10)}$$

Hook's law yields the following equations:

$$\varepsilon_x = \frac{1}{E} (\sigma_x - \mu\sigma_y) \quad \text{.....(11)}$$

$$\varepsilon_y = \frac{1}{E} (\sigma_y - \mu\sigma_x) \quad \text{.....(12)}$$

The corresponding stresses are

$$\sigma_x = \frac{Ez}{1-\mu^2} (\frac{1}{\rho_x} + \frac{1}{\rho_y}) = \frac{Ez}{1-\mu^2}(\frac{\partial^2 w}{\partial x^2} + \mu\frac{\partial^2 w}{\partial y^2}) \quad \text{.....(13)}$$

$$\sigma_y = \frac{Ez}{1-\mu^2} (\frac{1}{\rho_y} + \frac{1}{\rho_x}) = \frac{Ez}{1-\mu^2}(\frac{\partial^2 w}{\partial y^2} + \mu\frac{\partial^2 w}{\partial x^2}) \quad \text{.....(14)}$$

since the curvatures $1/\rho_x$ and $1/\rho_y$ are approximately equal to $\frac{\partial^2 w}{\partial x^2}$ and $\frac{\partial^2 w}{\partial y^2}$, respectively, where w is the displacement of the neutral plane in the z-direction. The normal stresses are distributed on the cross sections of the facings only and can be reduced to couples equal and opposite to the external moments. Hence, we can write the following equations:

$$2\int_{\frac{c}{2}}^{\frac{s}{2}} \sigma_x z\ (1)\ dz = M_x \quad \text{.....(15)}$$

$$2\int_{\frac{c}{2}}^{\frac{s}{2}} \sigma_y z\ (1)\ dz = M_y \quad \text{.....(16)}$$

where s is the overall thickness of the sandwich panel.

Substituting Eqs. (13) and (14) into (15) and (16) respectively, we obtain the two expressions:

$$M_x = D\left(\frac{\partial^2 w}{\partial x^2} + \mu \frac{\partial^2 w}{\partial y^2}\right) \quad \ldots\ldots\ldots\ldots\ldots\ldots\ldots \quad (17)$$

$$M_y = D\left(\frac{\partial^2 w}{\partial y^2} + \mu \frac{\partial^2 w}{\partial x^2}\right) \quad \ldots\ldots\ldots\ldots\ldots\ldots\ldots \quad (18)$$

where

$$D = \frac{2E}{1-\mu^2} \int_{\frac{c}{2}}^{\frac{s}{2}} z^2 dz$$

Hence, $$D = \frac{E(s^3 - c^3)}{12\ (1-\mu^2)} \quad \ldots\ldots\ldots\ldots\ldots\ldots\ldots \quad (19)$$

Equation (19) yields the theoretical value for the flexural stiffness of a sandwich panel. If the facings are made of homogeneous material and the core does not contribute to the flexural rigidity then D has the same value for both x and y-directions. If not, the different flexural stiffnesses (denoted by D_x and D_y) can be derived from Eqs. (11) and (12) by substituting the proper values of the elastic properties of the material.

Single Block Shear Test

The frame assembly shown in Figures 13 and 14 was used to test sandwich specimens under shear. Forces P were applied at the end fittings of the frame

by an Instron machine whose cross-head speed had been preset at .05 inches per minute. A typical load-displacement curve plotted by the loading machine is shown in Figure 15.

Eleven samples (2" x 12") were tested: three had been cut from honeycomb sandwich panels in the transversal direction, four from honeycomb panels in the longitudinal direction, and four had been cut from styrolite sandwich panels. The facings of the samples were glued to the face plates of the testing assembly with resin adhesives. The alignment of the test apparatus was such that the plane in which the load acted (Fig. 13-a) passed through the corners of the specimen, thus minimizing moments in the core.

Since the relative displacement of the facings, r, and the shear angle, γ, in the core (Fig. 13-b) are relatively small, they can be related in the following way.

$$\gamma = \frac{r}{c} \simeq \frac{r}{h} \quad \text{.....(20)}$$

where c is the thickness of the core. The shear stress, τ, can be calculated by dividing the load, p, applied to the specimen, by the area, A, of one facing and then multiplying it by cos θ, where the angle θ is shown in

Figure 13(a). Substituting for δ and γ into Eqs. (4) or (5) the shear stiffness becomes

$$D_q = \frac{\tau}{\gamma} h = \left(\frac{P}{r}\right) \frac{h^2}{A} \cos \theta \quad \ldots\ldots\ldots (21)$$

Equation (21) will yield the value for D_{qx} or D_{qy} depending on the direction in the panel along which the particular specimen has been cut. It can be seen from Figure 13(a) that the angle θ increases as the length of the specimen decreases. For a twelve-inch specimen, if the correcting factor cos θ in Eq. (21) were neglected, the change in the results would be less than .4%.

The results of the Single Block Shear Tests are given in Table II. As an example, let us consider specimen number 5 whose load-displacement curve appears in Figure 15. Substituting in Eq. (21), D_{qx} can be calculated as follows:

$$D_{qx} = \left(\frac{550}{.018}\right) \frac{(1.025)^2}{23.872} \frac{11.936}{(11.936^2 + 1.025^2)^{1/2}}$$

$$D_{qx} = 1326 \text{ lb.}$$

It may be noted that the term P/r in Equation (21) is the slope of the curve in figure 15, h = 1.025", A = 23.872 in^2.

TABLE II

RESULTS OF SINGLE BLOCK SHEAR STIFFNESS TESTS

NO.	TYPE OF CORE	SHEAR STIFFNESS D_q in lb.	SHEAR STRESS AT FAILURE IN PSI	DIRECTION** OF SAMPLE
1	Honeycomb	1035	35.6	y
2	Honeycomb	970	29.3	x
3	Honeycomb	964	31.1	x
4*	Honeycomb	1526	45.6	y
5	Honeycomb	1326	31.1	x
6*	Honeycomb	1260	52.6	Y
7	Honeycomb	890	26.9	y
8	Styrolite	184	13.7	-
9	Styrolite	184	13.3	-
10	Styrolite	160	13.0	-
11	Styrolite	172	12.1	-
Av.	Honeycomb	D_{qx} = 1087	30.5	x
Av.	Honeycomb	D_{qy} = 1178	40.2	y
Av.	Styrolite	D_q = 175	13.0	-

* Failure occurred in the core. The other honeycomb sandwich specimens delaminated as shown in Figure 14.

** For the orientation of the honeycomb core see Figure 36.

and the length of the specimen is 11.936". Since specimen number 5 was cut along the longitudinal axis (x axis) of a honeycomb sandwich panel, the resulting shear stiffness is denoted by D_{qx}. The stiffnesses in the x and y directions are expected to differ because of the nature of the honeycomb cells (Fig. 36). The average values for D_{qx} and D_{qy} in Table II, however, show a difference of 10% which may be considered negligible when the wide scatter of the value of individual stiffnesses is considered. The styrolite core was assumed to have the same shear stiffness along any direction in its own plane.

The ultimate shear stresses of the cores are also given in Table II. In the case of honeycomb sandwich samples, failures usually occurred in the bond between the core and the facings. For the two cases in which failure occurred in the core the ultimate shear was much higher (See Table II).

The Three-Point Loading Shear Stiffness Test

The deflection, w, at midspan of a simply supported sandwich beam with a concentrated load, P, at the center (Fig. 16-a) is the sum of the deflection due to bending and the deflection due to shear. In equation form we have:

$$\delta = \frac{PL^3}{48D} + \frac{PL}{4D_q} \quad \text{.....(22)}$$

where D is the bending stiffness and D_q is the shear stiffness of the beam. The value for D can be calculated from Eq. (19) and the deflection, δ, can be measured experimentally. Substituting into Eq. (22) a value for D_q can then be obtained.

Seven beams were each tested three times according to the Three-Point Loading Stiffness Test. Three of these beams had honeycomb core (x-direction), four had styrolite core. Figures (16(a) and 16(b) show the set up of the test and the dimensions of specimen number 5 of Table III. These dimensions remained constant for all the samples. For the Styrolite sandwich beams four dial indicators were used (Fig. 17) to measure the compression of the core as well as the deflection of the beam. For the honeycomb sandwich samples only one dial indicator at midspan was used. The load P was plotted versus the deflection δ for each beam. Figure 16(c) shows such a graph for beam number 5. The reciprocal of the slope of this graph is $\delta/P = .0149$. To correct for the compression of the core, one half of the sum of the displacements, read from dial indicators located on top of the supports, was subtracted from the averaged deflection of the two dial

TABLE III

SHEAR STIFFNESSES D_q (THREE-POINT-LOADING TEST)

Beam No.	1	2	3	4	5	6	7
Core	H.C.*	H.C.	H.C.	S*	S	S	S
D_q in lb per 1" width	2290	2600	2509	242	233	235	210
Average D_q per 1" width	Honeycomb 2466			Styrolite 230			

* H.C. stands for honeycomb
S stands for styrolite

TABLE IV

SHEAR STIFFNESS D_q (FOUR-POINT-LOADING TEST)

Beam No.	Core	Size	Shear Stiffness D_q in lb/Unit Width	Average
1	Honeycomb	2" x 22"	4135	
2	Honeycomb	2" x 22"	4064	4100
3	Honeycomb	6" x 60"	2584	
4	Honeycomb	6" x 60"	2232	
5	Honeycomb	6" x 60"	2368	
6	Honeycomb	6" x 60"	2152	2334
7	Styrolite	6" x 60"	84	
8	Styrolite	6" x 60"	92	
9	Styrolite	6" x 60"	109	
10	Styrolite	6" x 60"	92	94

indicators at midspan.

Numerical values from Figure 16 can now be substituted into Eq. (22) to find the shear stiffness D_q for beam number 5 of table III.

$$.0149 = \frac{58^3}{48\ (906{,}500)} + \frac{58}{4D_q}$$

from which D_q = 1400 lb. for the six-inch wide beam. The bending stiffness D, for a six-inch wide beam, was calculated from Eq. (19).

$$D = \frac{10.25 \times 10^6\ (1.050^3 - 1.000^3)\ 6}{12\ (1 - .33^2)} = 906{,}500\ \text{lb-in}^2$$

Table III gives the shear stiffnesses per unit width for the seven beams tested.

The Four-Point Loading Shear Stiffness Test

The deflection, δ, at midspan of a simply supported sandwich beam, loaded at quarter points by concentrated loads P/2 as shown in Figure 18(a), is given by the following equation:

$$\delta = \frac{11PL^3}{768D} + \frac{PL}{8D_q} \qquad \text{.....(23)}$$

where the first and second term yield the bending deflection and the shear deflection respectively. The bending

stiffness D has already been discussed in the previous article and it was found to have a value of 906,500/6 lb-in^2 per unit inch of width.

Ten samples were each tested three times according to this method. The description and dimensions are given along with the shear stiffness values in Table IV.

The experimental set-up is shown in Figure 19. The load was applied by an Instron machine whose cross head was preset at a constant speed (0.02 inches per minute for the 60" beam).

Load-deflection curves such as the one shown in Figure 18 were plotted for each beam. The reciprocal of the slope and the dimensions shown in Figure 18 are substituted in Eq. (23) to find the shear stiffness constant for beam number 8 of Table IV.

$$.0161 = \frac{11 \times 58^3}{768 \times 906{,}500} = \frac{58}{8D_q}$$

from which $D_q = 553$ lb for a six-inch wide beam.

It is worth noting that in calculating D_q for beam number 3 of Table IV, Eq. (12) becomes, after numerical values have been substituted,

$$.03528 - .03083 = \frac{7.25}{D_q}$$

The difference of the two relatively equal numbers on the left-hand side of the equation may give rise to large inaccuracies.

The Five-Point Loading Shear Stiffness Test

A sandwich beam loaded by the five-point method is shown in Figure 20. The beam rests on two supports, each a distance a from the middle of the beam. Two equal down-loads (W) are applied at the ends, each a distance b beyond the points of support. A load 2P acts at midspan (Figs. 21 & 22).

The two sets of loads (2W and 2P) will produce opposite bending deflections at the middle of the beam (Fig. 21). A ratio of the loads can be selected so that these bending deflections cancel each other. Then the net shear deflection at midspan can be measured experimentally.

Letting M = Wb and taking downward deflections and "hogging" moments as positive, the central deflection can be written as

$$\delta = \frac{Pa^3}{3D} - \frac{Ma^2}{2D} + \frac{Pa}{D_q} \quad \text{.....(24)}$$

The first two terms of the above equation represent the bending deflections; the third term represents the deflection due to shear.

When

$$\frac{Pa}{M} = \frac{3}{2} \quad \ldots\ldots\ldots\ldots\ldots\ldots\ldots\ldots (25)$$

the first two terms of Eq. (24) cancel out leaving the following relationship:

$$\frac{\delta}{a} = \frac{P}{D_q} \quad \ldots\ldots\ldots\ldots\ldots\ldots\ldots\ldots (26)$$

If central deflections are measured for applied loads which fulfil condition (25) and δ/a is plotted against P (Figs. 22 & 23), a straight line with slope equal to $1/D_q$ will result.

Instead of maintaining a constant ratio between P and M (See Equation 25), a more practical method would be to measure δ for a large number of values of P and M varied independently and then plot δ/M against Pa/M. A straight line should result having the ordinates $3/2D_q$ at Pa/M = 3/2 and $a^2/2D$ at Pa/M = 0 (Figs. 24 & 25). When P = O, Eq. (24) yields

$$D = - \frac{M}{\delta} \frac{a^2}{2} \quad \ldots\ldots\ldots\ldots\ldots\ldots\ldots\ldots (27)$$

In a third procedure, several suitable combinations of a, b and W are selected. For each combination, load (2P) is varied and the central deflections recorded.

Load-deflection curves are then plotted as shown in Figure 26. An additional line satisfying Eq. (25) is drawn and the value of its slope, P/δ, is substituted in Eq. (26) to evaluate the shear stiffness D_q. The load-deflection curves for M_1, M_2, ... M_n intersect the line $P = 0$ at $-\delta_1$, $-\delta_2$, ... $-\delta_n$ respectively. Any quotient $\frac{M_n}{\delta_n}$ can be substituted in Eq. (27) to evaluate the bending stiffness, D.

Both the second and third procedures yield experimental values for both the shear and bending stiffnesses; the first procedure yields the experimental value for the shear stiffness only.

Seven beams (three with paper honeycomb and four with styrolite core) were tested according to both procedure I (Figs. 22 & 23) and procedure II (Figs. 24 & 25). Figure 22 shows the physical dimensions of beam number 2 (Table V); these dimensions remain constant for all seven samples. The stiffness constants are calculated directly on the graphs in Figures 22 to 25, and then tabulated in Table V. The average shear stiffnesses for the honeycomb and the styrolite sandwich samples are 2952 and 264 lb. per unit width respectively; the average bending stiffnesses are 152,622 and 157,139 lb-in^2 per unit width respectively. According to Eq. (19) the bending stiffness is 151,667 psi for both types of specimens; the difference between experimental and theoretical values is .6% and 3.6%

TABLE V

SHEAR AND BENDING STIFFNESSES BY THE FIVE-POINT-LOADING TEST

Beam No	Core	Test No.	D_q in lb per unit Width		D in lb-in^2 per unit width
			Pr. I (Fig 22)	Pr. II (Fig 13)	
1	Honeycomb	1	2670		
		2	2490		
		3	2730		
		4		2820	151,667
2	Honeycomb	1	3205		
		2	3200		
		3	3360		
		4		2780	154,600
3	Honeycomb	1	3590		
		2	2780		
		3	2700		
		4		3090	151,600
4	Styrolite	1	264		
		2	269		
		3	289		
		4		287	157,667
5	Styrolite	1	273		
		2	289		
		3	237		
		4		265	167,750
6	Styrolite	1	254		
		2	244		
		3	262		
		4		244	-
7	Styrolite	1	259		
		2	260		
		3	271		
		4		260	146,000
Av.	Honeycomb		D_q = 2952		D = 152,622
Av.	Styrolite		D_q = 264		D = 157,139

for honeycomb and styrolite samples respectively.

Discussion

Single Block Shear Test:- The specimens for the Single Block Shear Test are rather expensive to manufacture since they must be glued to the face plates of the testing assembly (Fig. 13-a). When under load, these face plates will tend to bend as shown in Figure 13(c). Such bending, although small for weak cores, tends to overestimate the shear displacement, thus reducing the value of the shear stiffness of the core. For stiffer cores, such as aluminum honeycomb, the discrepancy due to the bending of faces was found to be surprisingly large (about 15%) (48).[3]

The shear distribution in the core is not uniformly distributed, but it follows a curve similar to that shown in Figure 27(b). This distribution is given by the Volkersen analysis of lap joints (87). Since the two cores analyzed in this report were very flexible and the face plates of the testing apparatus were ½ in. thick aluminum, the Volkersen correction may be considered negligible.

The transverse component of the load (P.sin θ)

---

3 Underlined numbers in brackets indicate references at the end of the Thesis.

also contributes to the deformation which is totally ascribed to shear. The results of this test (Table II) were low and widely scattered.

The Double-Block Shear Test:- The principle and problems of this test are similar to those of the Single-Block Shear Test; Figure 27(a) shows the test set-up. The shear distribution according to Volkersen analysis is shown in Figure 27 (b). For the paper honeycomb and styrolite cores, this distribution may be considered constant. But for cores with shear modulus G_c between 15,000 and 30,000 psi the modulus could be as much as 40% too low (42) if the proper shear distribution is not considered. Further problems arise from the instability of the test apparatus as shown in Figure 27(c). The direct transversal compression on the core may cause buckling of the cell walls. Some of the objections against the double-block shear test may be overcome by using bridge pieces (Fig. 27-d) to stabilize the test frame, or by using the double double-block set-up (Fig. 27-e). These modifications, however, would make the test more complicated and more expensive.

The two block shear tests described above are much more complicated that they appear to be at first. The corrections which must be made involve theories not commonly known.

The Three-Point Loading Shear Stiffness Test:-

The experimental results of Table III show consistency. The average values of shear stiffness are 2466 and 230 lb for the honeycomb and styrolite sandwiches respectively. These stiffnesses are considerably larger than their corresponding values obtained from the single-block shear test (Table II), but lower than the values given by the five-point loading test (Table V).

The engineer's formula (Eq. 22) was used to find D_q for the three-point loading test. This equation, as it stands, is not completely accurate. Because of the bending stiffness of the faces and the compressibility of the core, the loads which are applied to the faces of the sandwich element are not transmitted as shear stresses on the immediate cross sections of the core. Figure 28 represents a more realistic distribution of shear stresses. It is worth noting that the modified shear stress tends to reduce the shear strain while the compressibility of the core tends to increase it.

Equation (22) can be improved by adding a correction factor γ to the left hand side (42). If the overhangs of the beam beyond the supports are larger than the thickness of the beam, the correction factor is constant for different spans. The correction factory, γ, can be determined by measuring the deflection, δ, for different

spans of the beam and substituting back into Eq. (22).

The effect of core compressibility and shear distribution can also be overcome by using a theory of bending based on the principle of virtual displacements (36) and the total strain energy stored in the beam during deformation.

The Four-Point Loading Shear Test:- The experimental shear stiffness values obtained from the four-point loading shear test are shown in Table IV; this method yields very low shear stiffness values for the styrolite sandwich beams (94 lb). The 60-inch honeycomb beams show the same stiffness (about 2400 lb) as when tested by the three-point loading test. The shorter honeycomb beams (22") show a much larger stiffness (4100 lb).

A modified shear distribution could be drawn for this method as it was done in Figure 28 for the three-point-loading test. This modified shear distribution indicates that a shorter beam would tend to give higher values for D_q.

Generally this test is not very suitable for the determination of the shear stiffness of the core since only pure bending occurs between the central loads; shear and bending deflections occur at the end quarter spans. The method can be used, however, in conjunction with the three-point loading test to determine the bending stiffness

as well as the shear stiffness from the two Eqs. (22) and (23).

Three honeycomb sandwich beams were analysed by this procedure; the resulting average bending stiffness was found to be 140,200 lb-in.^{2} per unit width (7% lower than the theoretical value).

The Five-Point Loading Shear Stiffness Test:- The experimental results given by the five-point loading test (see Table V) are relatively consistent. The experimental bending stiffnesses for honeycomb and styrolite beams differ only by .6% and 3.6% respectively from the theoretical values. Three procedures may be used within this method to determine the shear and bending stiffnesses (see Figs. 22, 24 and 26). The second and third procedures (Figs. 24 & 26) yield both the shear as well as the bending stiffnesses; the first method (Fig. 22) yields the shear stiffness only.

The beam in the five-point loading method rotates through a much smaller angle in the region of the supports than it would in either the three or four-point loading methods. Smaller errors arising from the simple roller support can, therefore, be expected in this method. The secondary moments in the facings (Fig. 29) exist in all sandwich beams subjected to bending tests; these moments tend to reduce shear deformations.

The five-point loading beam test yields both shear and bending stiffnesses, produces consistent results, and is relatively economic when compared to other methods.

Theoretical Methods:- Analytical solutions are also available to determine the shear modulus of cores. Penzien and Didriksson (64) have examined the problem of theoretically predicting the effective shear modulus of honeycomb core materials by examining the behaviour of a single honeycomb cell under shear forces. The effects resulting from boundary conditions which prevent warpage of the cells have also been considered in the analysis. They conclude that the warpage constraints have little effect on the shear stiffness except when the ratio of core cell length to its lateral dimension becomes relatively small.

Kelsey, Gellatly and Clark (42) have developed expressions for upper and lower limits to the shear stiffness constant of honeycomb sandwich cores by applying the Unit Displacement and Unit Load methods.

Hoffman (37) has made a study on the Poisson's ratio for honeycomb cores. If the hexagonal cells are close to being equiangular (Fig. 30-a), Poisson's ratio is close to one. The ratio, however, will vary substantially with cell shape.

The above theories assume that the geometry of the cell is completely defined as in Figure 30(a). This

condition, however, does not always exist in practice. Figure 30(b) shows the configuration of a typical sample of honeycomb core made of Kraft paper ribbons. It is doubtful that the behaviour of such core could be predicted by the above theories.

Conclusion

The shear stiffness constant can be determined by several different methods. Consistent results are usually obtained when identical specimens are tested under the same set of conditions. When the dimensions of specimens and the testing conditions or methods are changed, however, the resulting stiffnesses usually vary widely. It is wise to study the behaviour of sandwich specimens under each test method before the results can be effectively used.

The shear stiffness constants recommended for the honeycomb and styrolite cores studied in this report are 3000 and 260 lb per unit width as given by the five-point loading beam test (Table V). This method showed most consistency and subjected the specimens to bending moments at the supports. This is the type of condition to which the panels in the folded plate models (studied in later chapters) will be subjected.

The theoretical value for the bending stiffness constant (151,667 psi) can be used. The experimental results given by the five-point loading test are within 3.6%.

Manufacturers must carefully consider the shear properties of their core materials. Sufficient graphs based upon different test methods should be provided to the design engineer to promote the use of sandwich construction. The shear modulus should be selected from the graph obtained from the test method which most closely approaches the loading conditions of the structure being designed.

CHAPTER III

TORSION RIGIDITY OF SANDWICH PANELS

Introduction

When a twisting moment M_{xy} is applied to the cross sectional faces of a rectangular sandwich panel, as shown in Fig. 31, the panel will undergo a twist $\frac{\partial^2 w}{\partial x \partial y}$. This twist varies directly as the moment applied and inversely as the torsion rigidity, D_{xy}, of the panel.

$$\frac{M_{xy}}{D_{xy}} = \frac{\partial^2 w}{\partial x \partial y} \quad \text{.....(28)}$$

In this chapter an expression is derived for the torsion rigidity constant, D_{xy}, for sandwich panels with cores such as paper honeycomb or styrolite. The theoretical value of D_{xy} is compared with results obtained from experiments carried out on eight sandwich panels.

Theoretical Study

The dotted element of the panel shown in Fig. 31 is reproduced and analysed in Figures 32, 33 & 34. The element will shift relative to the coordinate system x, y and z as shown in Figure 32 and it will distort as shown

in Figure 33. From Figure 32 it can be seen that the displacement of any point on line af in the x-direction is

$$u = -z \frac{\partial w}{\partial x} \quad \text{.....(29)}$$

where $\frac{\partial w}{\partial x}$ is the rotation of the element in the xz-plane. Similarly, if the rotation of the element face adef in the yz-plane were shown, it could be seen that the displacement of any point on line af in the y-direction is

$$v = -z \frac{\partial w}{\partial y} \quad \text{.....(30)}$$

where $\frac{\partial w}{\partial y}$ is the rotation of the element in the yz-plane.

From Figure 33 the relative displacements of points b and d at the top facing, due to the distortion of the element, are $\frac{\partial v}{\partial x} dx$ and $\frac{\partial u}{\partial y} dy$ respectively. The total displacements of these two points due to both the rotation and distortion of the element are (Fig. 34)

$$v + \frac{\partial v}{\partial x} dx \quad \text{.....(31)}$$

$$u + \frac{\partial u}{\partial x} dy \quad \text{.....(32)}$$

The shear strain of any membrane parallel to the xy-plane is

$$\gamma_{xy} = \frac{\partial v}{\partial x} + \frac{\partial u}{\partial y} \quad \text{.....(33)}$$

From Eqs. (29) and (30)

$$\frac{\partial u}{\partial y} = -z \frac{\partial^2 w}{\partial x \partial y} \text{ and } \frac{\partial v}{\partial x} = -z \frac{\partial^2 w}{\partial x \partial y} \quad \text{.....(34)}$$

Hence,

$$\tau_{xy} = -2G_{xy} z \frac{\partial^2 w}{\partial x \partial y} \quad \text{.....(35)}$$

The twisting moment M_{xy} can be expressed in terms of the shear stress τ_{xy}. It must be realized, however, that the only stresses which can be developed in an element of paper honeycomb core are σ_z, τ_{yz}, τ_{zy}, τ_{xz} and τ_{zx} (Fig. 35). The stresses σ_x, σ_y, τ_{xy}, τ_{yx} are essentially equal to zero since the only factor contributing to their corresponding stiffnesses E_x, E_y and G_{xy} is the bending rigidity of the paper ribbons making up the cells of the honeycomb core (Fig. 36). Therefore, the shear moment M_{xy} develops shear stresses τ_{xy} only in the facings of the sandwich element. The following equation can then be written:

$$M_{xy} = (2t) \left(\frac{h}{2}\right) \tau_{xy} \quad \text{.....(36)}$$

Substituting Eq. (35) into Eq. (36) and $-\frac{h}{2}$ for z

$$M_{xy} = (G_{xyf} h^2 t) \frac{\partial^2 w}{\partial w \partial y} \quad \text{.....(37)}$$

where G_{xyf} is the modulus of elasticity in shear of the facing material, h is the thickness of the panel measured from center to center of the facings and t is the thickness of the facings. By comparing Eq. (37) to Eq. (28) the following expression can be written for the torsion rigidity constant, D_{xy}.

$$D_{xy} = h^2 t \, G_{xyf} \quad \text{.....(38)}$$

The above formula is applicable to all sandwich panels with cores of negligible shear rigidity G_{xy}. It is important to note that this shear rigidity should not be confused with the other shear rigidities G_{xz} and G_{yz}.

It has already been shown in Fig. 32 how line af, originally perpendicular to the xy-plane, rotates through an angle of $\frac{\partial w}{\partial x}$ in xz-plane and an angle of $\frac{\partial w}{\partial y}$ in the yz-plane. The angle of twist of this line is $\frac{\partial^2 w}{\partial x \partial y}$. If x and y are the ordinates of line af in the xy-plane then its vertical displacement is

$$w = xy \frac{\partial^2 w}{\partial x \partial y} \quad \text{.....(39)}$$

The loading system acting on the rectangular panel shown in Figure 37 is statically equivalent to a twisting moment M_{xy} equal to P/2 distributed around the

edges of the panel. If distortions due to shear are not permitted to occur by properly reinforcing the edges of the panel, then rectangular cross-sections of the panel before loading will remain rectangular after loading (Fig. 37). By using Eq. (39) the deflection at the free end of the panel in Figure 37 is

$$\delta = mn \frac{\partial^2 w}{\partial x \partial y} \quad \text{.....(40)}$$

where m and n are the dimensions of the panel being tested (Fig. 37). From Eqs. (28) and (40) and noting that $M_{xy} = P/2$ the following equation can be derived

$$D_{xy} = \tfrac{1}{2} mn \left(\frac{P}{\delta}\right) \quad \text{.....(41)}$$

Eq. (41) can be used to find experimental values for the torsion constant, D_{xy}, for panels tested as shown in Figure 37.

Experimental Study

Eight square sandwich panels (24" x 24") were tested in torsion. Four of the panels had paper honeycomb cores and four styrolite cores. The physical properties of these two core materials have been discussed in Chapter I. The edges of the panels were reinforced with either plaster of Paris mixed with cement or with resin to avoid distortions due to shear stresses. The experimental set-ups can be best understood by studying Figures 38 to 42 inclusive.

The panels with honeycomb core were loaded at the free corner by the cross-head of an Instron machine (Figs. 38 & 39) whose downward movement had been preset at .05 inches per minute. At the diagonally opposite corner a downward reaction P , equal to the applied load, was developed by the swivel disc of a clamp (Figs. 40 & 41). The ball-bearing disc behaved like a pin support. Rollers provided the other two diagonally opposite corners with upward reactions each equal to P. The rollers were set on a beam which sat on the load cell of the Instron. The test machine plotted a curve of the load 2P registered by the load cell vs. the corresponding downward displacement δ of the cross-head at the free corner of the plate.

Figures 40 and 41 show the experimental set-up used to twist the panels with styrolite core. In this case the load was applied by suspending weights at the free corner of the panel. A clamp held down the diagonally opposite corner while rollers supported the remaining two corners. The data was recorded manually.

The experimental set-ups (Figs. 38 to 42) show the presence of strain gauges measuring strains at the middle of the panel and dial indicators measuring deflections in one quadrant of the panel. To calculate the experimental torsion rigidity, D_{xy}, however, the deflection at the free corner only is required. Hence, the additional

measurements are neither presented nor discussed in this report.

The experimental values for D_{xy} for the eight panels tested are given in Table VI. Load-deflection curves such as those shown in Figure 43 were drawn for each panel. The slope of these curves is P/δ. From Eq. (41), from the slope of curve A of Figure 43 and from the dimensions given in Figure 42, one can calculate the torsion rigidity for panel number 3 of Table VI. Hence,

$$D_{xy} = \tfrac{1}{2} \times 23.29 \times 23.29 \times \frac{87}{1} = 23{,}867 \text{ lb-in.}$$

According to Eq. (38), the theoretical value of D_{xy} is

$$D_{xy} = (1.025)^2 \ (.025) \ (4 \times 10^6) = 105{,}063 \text{ lb-in.}$$

Since the terms h, t, and G_{xyf} in Eq. (38) are the same for all panels tested, the theoretical torsion rigidity is 105,000 lb-in. for all cases.

Discussion of Results and Conclusions

The experimental values of D_{xy} are from 1/6 to 1/4 of the theoretical value. The larger values in Table VI were obtained from panels with better edge reinforcement. The value P/δ used in Eq. (38) was obtained from curves such as those shown in Figure 43. Curve A belongs to a panel

TABLE VI

EXPERIMENTAL TORSIONAL RIGIDITIES, D_{xy}

Sample Number	Type of Core	Experimental Torsion Rigidity, D_{xy} in lb.-in.	
		Values as Calculated	Values Rounded off to Closest 1000
1	Honeycomb	28,707	29,000
2	Honeycomb	21,697	22,000
3	Honeycomb	23,867	24,000
4	Honeycomb	26,308	26,000
5	Styrolite	18,443	18,000
6	Styrolite	34,716	35,000
7	Styrolite	29,834	30,000
8	Styrolite	15,731	16,000

with honeycomb core. The value P/δ is calculated directly from the straight portion of the graph. For the panels with styrolite core the load-deflection curves were similar to curve B (Fig. 43), but the value P/δ was taken as the slope of the tangent at the origin. This explains why some of the torsion rigidities of panels with styrolite core are larger than those of panels with honeycomb core. The former rigidities, however, decrease with increase in load; they are not constant as the rigidities given by honeycomb sandwich panels.

Figures 39 and 41 show the behaviour of panels under excessive torsion load. The failure does not occur in the facings, as one would expect, but in the reinforcement around the edges. In cases of pure torsion, rectangular cross-sections before loading should remain rectangular after loading. This condition is obviously violated in the samples tested (Figs. 39 & 41). The failures were caused by shear in the core around the edges. It can, therefore, be seen how important it is to have very rigid stiffness around the edges of the panel to carry the vertical shear forces caused by the loads applied at the corners.

It is not sufficient to reinforce these edges with plaster of Paris or resins; rigid stiffening devices should be employed. Whatever reinforcement is provided at the

edges, it should not be continuous around the corners, as this condition would contribute to the torsion rigidity of the sandwich panels.

The following additional points should be noted:

1) The compressibility of the core under load would contribute to deflections, thus lowering the torsion rigidity.
2) The effects due to shear would be less significant if larger panels were used in the tests.
3) The experimental set-up shown in Figures 40 and 41 is simpler, but not as accurate as that shown in Figures 38 and 39. In the latter case the rate of displacement of the free corner of the panel can be preset and the data is automatically recorded by the Instron Testing Machine.

The experimental values of D_{xy} shown in Table VI on one end, and the theoretical D_{xy} on the other, supply the boundaries of a region wherein lies a reliable D_{xy}; its value can be found by performing the torsion tests according to the recommendations set forth in this chapter. The scatter of the experimental results and their large differences from the theoretical value should enable the reader to appreciate the importance of proper reinforcement around the edges of the panels.

CHAPTER IV

EXPERIMENTAL STUDY
OF A 9.5-FOOT FOLDED SANDWICH PLATE MODEL

Introduction

Many studies have been made on sandwich panels (See Literature cited). Yet, very little investigation has been carried out on the performance of an integrated structural system made up of these panels.

The folded sandwich plate model shown in Figure 44 was built and tested to study the feasibility of introducing this type of light structure into the building industry. The component sandwich panels have honeycomb core and aluminum facings (Fig. 22-b). Flatwise and edgewise compression properties of these panels have been analysed in Chapter I, the shear and bending properties in Chapter II, and the torsion properties in Chapter III.

In this chapter the assembling and testing of the 9.5-foot folded plate model is treated. Two methods of loading are discussed. The location and results of the dial indicators and the strain gauges are presented. The experimental deflections and stresses, obtained from several tests, are plotted and discussed. A detailed

account of the failure process of the model, as its ultimate load of about 178 pounds per square foot was approached, is included at the end of this chapter.

Assembling the 9.5-Foot Folded Plate Model

The model (Fig. 44) was assembled by joining sandwich panels (after due preparation) along their longitudinal sides, with specially fabricated aluminum channels.

Before the panels were connected to one another, their longitudinal edges were bevelled at thirty degrees and reinforced with a plastic auto body filler (Fig. 45). The reinforcement was introduced to avoid any possible local crushing along the edges during the assembling operation. Holes (.070" in diameter) were drilled in the webs of the connecting channels (Fig. 46) at a distance of seven inches from center to center. (Cables of the loading trees were later suspended through these holes as shown in Figures 50 and 53).

After the holes in the web were completed, the next step was to temporarily insert the panel edges into their corresponding connecting channels and drill holes for one-quarter-inch bolts through the channel flanges and the panel between them (Fig. 47). The midspan section was then determined and the channels were removed. Strain gauge locations were selected on the top surface of the

panels; the corresponding points on the bottom surface were found by using the graduated fork shown in Figure 48. The strain gauges were next installed, complete with leads and protective coating, on the separate panels.

The components were now ready to be assembled into the folded plate structure. The two supporting end diaphragms were cut out of one-inch-thick plywood and set on heavy beams (Fig. 49). The diaphragms were placed at the proper span distance of 9'-5" from center to center. The sandwich panels were then placed on the supports and connected along their longitudinal edges, with the type of joint shown in Figure 50. The channel flanges were secured to the facings of the panels with bolts and a 3M-resin cement. The cement provided a good uniform bond between the flanges and the facings, thus avoiding stress concentrations in the regions around the bolts. The bolts, on the other hand, tightened the flanges onto the facings allowing the cement to set and develop a good bond. In case the cement should fail under load the bolts would then come into play and avoid collapse of the model.

The 1/16" cables to be suspended through the holes in the webs of the channels were found to have an ultimate strength of about 470 lb. each when tested (Fig. 51). A typical assembly containing the cable was tested by suspending from it a dead load of over 300 lb. for several

days (Fig. 52); no failure occurred. Loading trees were then suspended from these cables (Fig. 53 and 57) at each of the five internal ridges. The concentrated loads placed on the platforms of the tree, would be uniformly distributed along the ridge of the model. A total load of about 5000 lbs. could be safely applied along each ridge according to the capacity of the 1/16" cables; this load was estimated to be more than sufficient to fail the model.

To record the deflections at midspan of the model a total of twenty-seven dial indicators were installed across this section as shown in Figure 54. The dial indicators were supported by magnetic bases placed on steel I-beams spanning across midspan as shown in Figures 56, 57 and 58. The beams were supported by A-frames which were fixed to the floor.

The locations, on the model, of the rosette strain gauges, which had been installed on the separate panels, are shown in Figure 55. The thirty rosettes at midspan would permit a study of the critical longitudinal stresses, while the ten at the section, one foot from the face of the support, would show the critical shear stresses in the model. The wire leads, from the strain gauges, were soldered to five-channel adaptors and connected to an

automatic ditital strain recorder. The model was now ready to be tested.

Loading the 9.5 - Foot Model

The initial load consisted of standard 50-lb. weights placed on the platforms of the loading trees. Fig. 56 shows a test where all five interior ridges were loaded, while Figure 57 shows a test where only ridges 3 and 5 (Fig. 44) were subjected to load.

After several tests with the available 100 pieces of 50-lb. weights, it was realized that failure of the model was far from imminent; rather, two to three hundred additional 50-lb. weights would have been required to fail the model. Such a large amount of dead weight would not only make loading and unloading too laborious, but could produce safety hazards in the event of the failure of the model and tipping of the loaded platforms. It was, therefore, decided to switch to an hydraulic system of loading (Fig. 58).

The cross bars and the platforms of the loading trees (Fig. 53) were reinforced. The two platforms of each loading tree were then bridged with wide flange beams. Hydraulic rams were placed at midspan of these beams and jacked against a portal frame anchored to the floor. The

rams were connected to an oil pressure line from an hydraulic testing machine (Fig. 61). The oil pressure in the rams was thus controlled and indicated on the dial of the machine.

Support Conditions of the 9.5-Foot Model

The ends of the model were uniformly supported (Fig. 59) for one set of tests and point supported at the five internal ridges (Fig. 60 and 61) for a second set of tests. The uniform support was acquired by lifting the model, spreading an auto body filler on the supports and lowering the model again. The body filler molded around the edges and hardened, thus providing a continuous support. Point supports, simulating columns, were supplied by lifting the model and introducing blocks of hard wood under the five internal ridges of the model.

Presentation and Discussion of Experimental Deflections

The experimental midspan deflections of ten different tests is presented and discussed in this section.

In Figure 62 the immediate deflections, caused by a load of 5000 lbs. (standard weights) uniformly distributed along the five internal ridges (Fig. 56), are compared to the long term deflections caused by the same load

acting on the structure over a period of 166 hours. The creep which occurred over this span of time was less than five percent of the immediate deflection; its major part occurred during the first 24 hours after loading. The creep recovered within a few days after unloading. The ends of the model were continuously supported.

In a different test (Fig. 63) hydraulic rams were used to load the model with 11,300 lbs. (about 110 lbs. per sq. ft.) uniformly distributed along the five internal ridges (Fig. 58). The maximum vertical deflection of 0.198 inches occurred at the middle ridge, the least (.147") at the exterior ridges. It is worth noting here that .198" is much smaller than L/360 or .3138, which is often regarded as the maximum allowable deflection. The experimental stresses in the model for this test are shown in Figures 76 and 77. They will be discussed in the next section of this chapter.

Figure 64 shows the deflections caused by 4,800 lbs. of dead weights uniformly distributed along ridges 2, 4 and 6 (Fig. 44). The ends of the model are continuously supported. This test simulates the loading conditions of snow accumulated in roof valleys, which could be of a considerable size in a prototype structure and would thus collect large amounts of snow. The maximum deflection, in

this test, occurs at the outside ridges; the minimum at the middle ridge.

In the following test ridges 3 and 5 (Fig. 44) were each uniformly loaded with 24,000 lbs. of dead weights (Fig. 57). The ends of the model were uniformly supported. The deflections are presented in Figure 65. In this test we can see the behaviour of the model when used as a floor-bearing structure supporting the floor loads at the two upper interior ridges only. The maximum vertical deflection (.104") occurs at the middle ridge, the minimum (.038") at the exterior ridges.

Figure 66 shows the deflections due to a uniformly distributed load of 3980 lbs., applied at ridge 5 (Fig. 44) with an hydraulic ram. The same load was then applied at ridge 3 and the resulting deflections were plotted in Figure 67. The ends of the model were continuously supported. Since ridges 3 and 5 are symmetrical about the center of the section, the deflections of the two tests at symmetrically opposite ridges should be the same. This equality (neglecting small percentage differences) can be seen in Figures 66 and 67. The model was subjected to a considerable amount of twist in these two tests; the deflections varied from a maximum of about .120" at the loaded ridge to about 0" at the farthest

exterior ridge.

The model was subjected to an even greater twist in the next two tests where ridges 2 and 6 were loaded independently with a uniform load of 2550 lbs. (hydraulic ram). The ends of the model were again uniformly supported. The vertical deflection varied from a maximum of about .210" at one exterior ridge to about 0" at the other. (See Figs. 68 and 69). The equality of the deflection values (neglecting small percentage differences) can again be seen at symmetrically opposite ridges.

From Figures 70 and 71 we can compare the deflections of two different tests which have similar load but different support conditions. In the test of Figure 70 the ends of the model are uniformly supported and the middle ridge is subjected to a uniform load of 3710 lbs. applied with an hydraulic ram (Fig. 72). In the test of Figure 71 the ends are point supported at the five interior ridges and the middle ridge subjected to a smaller uniform load of 3160 lbs. The deflections of the latter test were almost double the deflections of the former. Hence, it can be seen that when point supports are used, the load-carrying capacity of the model is reduced by almost 50%. The point supports tend to introduce stress concentrations and local delaminations at the ends of the model.

It should be noted that the distortion of the

panels of the folded plate model shown in the deflection drawings are greatly exaggerated because the scale used for the deflections was much greater than the scale used for the model section.

The experimental deflections in Figures 63 to 69, inclusive, have been compared with their corresponding theoretical deflections in Figures 129 to 135, inclusive, in Chapter VII.

Presentation and Discussion of Experimental Stresses

Forty rosettes were applied on the model as shown in Figure 55. A computer program was written to resolve the strains recorded by these gauges into stresses at various directions. Figure 73 shows:

(1) The three strains (underlined) of a rosette in microinches per inch;

(2) The principal stresses of +190 psi and +3223 psi acting along principal planes which make angles of 43.69° and 133.69°, respectively, with the axis of the horizontal element of the gauge;

(3) The maximum shear stresses of 1516 psi acting along planes oriented at 45° from the principal planes;

(4) The stresses (+1707 psi) normal to the maximum shear stresses;

(5) The normal stresses +1637 psi and +1776 psi in the x and y-direction, respectively, and the associated shear stresses 1514 psi;

(6) The normal stresses +3221 psi and +192 psi in the x' and y'-direction, respectively, and the associated shear stresses 69 psi.

A study is now made of the experimental stresses in the model caused by a load of 11,300 lbs. uniformly distributed along the five interior ridges (See Figs. 58 and 63).

Longitudinal stresses obtained from gauges installed on the top facing at the midspan section of the model were plotted in Figure 74. Each plate is analysed separately. The vertical dotted lines and the underlined numbers indicate the location of the gauges and the magnitude of the stresses. A curve is then drawn and extrapolated to obtain graphically the stresses at the extreme fibers of the plates, which coincide with the ridges (denoted by circled numbers) of the folded plate model. The distribution of longitudinal stresses across the plates is essentially linear in every case, but the location of the neutral axis varies from plate to plate. The above procedure was repeated for the gauges installed on the

bottom facing at the midspan section of the model. The results are plotted in Figure 75.

At each ridge the stresses of the adjacent facings were averaged and plotted in Figure 76. The solid line indicates the stress distribution in the top facing of the model; the dotted line represents the stress distribution in the bottom facing. Negative numbers denote compressive stresses in psi. It is worth noting that the maximum compressive stresses occur in the top facings at the upper ridges, while the maximum tensile stresses are found in the bottom facings at the lower ridges. The neutral axis moves upward as we move from middle to external panels.

The experimental stresses in Figure 76 have been compared with their corresponding theoretical stresses in Figure 136 in Chapter VII.

The state of stress at five points in the top and bottom facings, at a cross-section one foot away from the face of the support, is shown in Figure 77. The five points have been analysed by five rosette strain gauges located on the top facing and five additional rosettes installed on the bottom facing directly below the top gauges as shown in Figures 77(a) and 55(c). The strains were converted to principal stresses according to the procedure shown in Figure 73. The results from the top gauges

are drawn in Figure 77(b), those from the bottom gauges in Figure 77(c). The direction of the principal stresses varies from 2^{o} to 9^{o} from top to bottom facing. In general, however, the direction of the different types of stresses remains the same. Maximum transversal shears lie on planes oriented from 2 to 15 degrees from the transversal planes of the plates. Strain gauge 2 (S.G. 2) and strain gauge 3 (S.G. 3) show compressive principal stresses in the top facing and tensile principal stresses in bottom facing. This state of stress is caused by the support reactions acting normal to the plane of the panel. The transversal shear stresses at midspan varied from 0 to 60 psi which can be considered negligible as predicted by the ordinary beam theory.

Failure of the 9.5-Foot Model

The sequence of failures for the 9.5-Foot folded plate model is shown by the circled numbers in Figure 78. All failures occurred at the ends of the model and consisted mainly of delaminations between the facings and the core. Failures 1 and 2 (Fig. 78) occurred near the point supports as a uniform load of 2680 lbs. was being applied along ridge 2; they were caused by the high concentration of shear stresses at these points. The extent and location of these two failures are shown in Figure 79. Failure 1,

which was essentially identical to failure 2, is further illustrated in Figure 80. To prevent propagation of these delaminations in subsequent tests, holes were drilled and bolts were used to tighten the facings against the core.

Ridge 6 (Fig. 44) was selected to be loaded next. To avoid early delaminations, regions near the point supports were reinforced with bolts. This reinforcement proved to be ineffective, however, since failure 3 (Fig. 78) occurred at a uniform load of 2110 lbs., about 25% lower than the load which caused failures 1 and 2. Rather, the vibrations of the drill must have weakened the bond around the reinforced area, thus causing delaminations prematurely. Failure 3 is of the same general nature as failures 1 and 2 shown in Figures 79 and 80.

In the subsequent test, all five internal ridges were uniformly loaded with hydraulic rams (Fig. 61); the model remained point supported. At a total load of 5660 lbs. the aluminum facings, which had delaminated in the first three failures, had opened up considerably, while regions near the other point supports also began to delaminate. The model was unloaded and the point supports were removed, since these would have caused complete failure of the structure at relatively low loads.

The five interior ridges were reloaded. At a total load of about 13,000 lbs., failure 4 occurred as

plate 3 began to buckle at the east end (Fig. 81). This section had been clamped with bolts before any tests were carried out because of delaminations which had occurred while the model was being assembled. The buckling seemed to be initiated by a protrusion in the support, barely perceptible in Figure 81. At the same load of about 13,000 lbs., failure 5 (Fig. 78) occured at the west end of plate 4 as it began to buckle. The nature of failure 5 was essentially the same as that of failure 4.

As the load was slowly increased failures 4 and 5 distorted further. Figure 82 shows the increase bending of failure 5 at the west end of plate 4 as the total load was increased from 13,000 lbs. to 14,700 lbs. At this latter load (14,700 lbs.) plate 5 began to buckle at the east end (Failure 6). At 16,000 lbs. both plates 5 and 6 delaminated and continued to buckle at the east end of ridge 5 as shown in Figure 83. The label in this figure should read east end rather than west end; the signs were mixed up in the confusion arising from the quickly developing distortions of the model. These photos were taken while the loading was being applied and failures were occurring.

Failure 7 (Fig. 78) occurred at a load of 17,200 lbs. as plate 6 failed in shear at the west end. This failure was characterized by a loud bang and simultaneous

upward bulging of the top facing along an inclined line. Similar failures occurred at the west ends of plate 5 at a load of 17,600 lbs. and of plates 3 and 4 at a load of 17,750 lbs. The end view of the above failures can be seen in Figure 84 (note wrong sign). At the ultimate load of 17,750 lbs. (178 lbs. per sq. ft.), the model kept on deforming without further load increase. In this final stage the connecting channel of ridge 5 opened up and cracked at the underside; and a transversal ripple formed at midspan of plate 6 (Fig. 84).

It should be noted that the shear failures were precipitated by the delamination of the load between core and facings. These failures occurred in a direction perpendicular to the principal compressive stresses which are given in Figure 77.

Further Observations on the Failed Model

After total collapse, the strain gauge wires were cut off; the delaminations were marked and dimensioned on the top and bottom facings; the model was taken down from the supports and placed upright on its end for photographs (Figs. 85 and 86). The model possessed a considerable amount of rigidity even after having been taken down.

To study the contribution of the connecting channels to the strength of the model, 12-inch samples were cut out at midspan of each ridge (Fig. 87) and tested in compression as shown in Figure 88. Universal joints were placed at both ends of the compressive samples to simulate pin connections. Buckling of the flanges occurred at loads ranging around 10,000 lbs.

CHAPTER V

EXPERIMENTAL STUDY OF A 19-FOOT FOLDED SANDWICH PLATE MODEL

Introduction

The 19-foot model shown in Figure 89 was built and tested to obtain additional experimental data to compare with the theoretical results in Chapter VII. This structure was similar, in many ways, to the first model (Fig. 44) studied in Chapter IV: the geometry of the section, the connection channels, the thickness of the panels, and the material of the facings were substantially the same.

The 9.5-foot model differed from the 19-foot model in the span and in core material; the core for the former consisted of Kraft honeycomb paper, for the latter it consisted of styrolite. Since the first model had failed in shear at the ends, it was estimated that, by doubling the span from 9.5 feet to 19 feet for the second model, a bending failure at midspan would be assured.

This chapter presents and discusses the assembling and testing of the 19-foot model, the air pressure loading system, the experimental deflections and stresses of several tests, the failure process of the model as the ultimate load of 75.4 lbs. per sq. ft. is approached, and

the exposure to outside weather of the model after its failure.

Assembling the 19-Foot Model and the Pressure Box

The assembling procedure of the 19-foot model varied only slightly from that of the 9.5-foot model. The edges of the panel were not bevelled. The resin cement was applied directly on the painted surface of the facings; paint had been removed along the longitudinal edges of the panels for the first model. Because of the compressibility of the core, the ends of the panels resting on the supports were reinforced with channels made out of the same aluminum sheets as the facings.

The forty rosette strain gauges were installed at midspan and at one foot away from the face of the support as specified in Figures 55(b) and (c). The wires of the gauges on the top facings were taped against the surface to avoid stress concentrations in the pressure bag; the connecting channels were also taped (Fig. 91).

The end supports consisted of two-by-fours glued and bolted against one-inch thick plywood panels bolted to the heavy beams. These wood panels extended high enough above the model to form the two shorter sides of the pressure box. The other two sides of the box were added by securing two-by-tens to the columns of the test

frame as shown in Figure 90. The longitudinal edges of the model were free and independent of the sides of the box with a clearance of about one inch.

Two sheets of plastic (each six mills thick) were loosely laid over the model and taped around the rim of the box to form the bottom of the pressure bag (Fig. 91). Special attention was paid to the four corners of the box and to regions around columns to avoid possible air leaks. Crevices and gaps between the edges of the model and the sides of the box had been sealed with rubber sheets glued to the vertical sides of the wood frame and flapping over the model (Fig. 91). The rubber seals, along the longitudinal sides of the model, did not interfere with the free movement of the two exterior ridges of the structure; yet, they provided a smooth continuous surface for the plastic bottom of the bag to press against.

A large sheet of rubber (20' long, 12' wide, 1/16" thick) was prepared on the floor (Fig. 90), complete with five valves and reinforcing boards glued along the two longitudinal edges. The rubber sheet was then hoisted on to the top of the model and its edges were sealed around the rim of the box with glue and nails. The five valves, placed at the middle and four corners of the rubber sheet, were connected to a multi-tube manometer by means of plastic conduits. These valves made it possible

to check and measure the air pressure at different points in the pressure box.

To measure the deflections of the model, twenty-seven dial indicators were set on its bottom surface (Figs. 92 and 93) at the same relative locations as shown in Figure 54. The dials were supported by magnetic bases set on a steel portal frame anchored to the floor. The strain gauges were connected to the automatic data acquisition system. The set-up was now ready for preliminary tests.

Air was pumped into the pressure bag to test it for leaks. The top layer of rubber soon bulged into the shape shown in Figure 94. It was estimated that the rubber would have failed due to tensile membrane stresses at a very low pressure of .095 lbs. per sq. in. or 13.7 lbs. per sq. ft. After no significant leaks were detected in the bag, a sturdy wood platform was built to support the top membrane as shown in Figure 95. Regular tests followed.

Presentation and Discussion of Experimental Deflections

The experimental deflections at midspan of the 19-foot model are presented and discussed below for ten different tests.

Figure 96 shows the deflections in inches at midspan when the model was subjected to a pressure of .1625 psi (23.4 lbs. per sq. ft.). This pressure is equivalent to about 4,900 lbs. of vertical load uniformly distributed over the total horizontal area of the model. The maximum vertical deflection of about one inch occurred at the two outside ridges, the minimum of .317" occurred at the middle ridge. The deflections in this test were essentially equal at symmetrically opposite ridges (Fig. 96). These deflections will be compared with the theoretical ones in Chapter VII.

The air pressure in the above test was then increased to .2708 psi (40 lbs. per sq. ft.) acting perpendicularly to the surface of the panels. This pressure constituted a total vertical uniform load of 8145 lbs. The deflections increased proportionally with the load as shown in Figure 97. The symmetry of these deflections was upset a little at this point of loading since ridge 1 (Fig. 89) began to touch the side of the pressure box at the frame column (Fig. 95). The maximum deflection occurred at ridge 7, the minimum at the middle ridge.

In a subsequent test, the air pressure was increased to .3430 psi (49.4 lbs. per sq. ft. or 10,317 lbs. of vertical uniform load on the model). The deflections

at midspan can be seen in Figure 98. The symmetry of the readings was upset again by the interference of the column at ridge 1. Ridge 7 underwent a displacement of over three inches measured perpendicular to the plane of panel 6, while the middle ridge deflected only .823". It can be seen from these results (Fig. 98) that this pressure loading tends to bend the model about the middle ridge.

An intermediate support was introduced for the next seven tests. The point support consisted of a one-inch pipe sitting on a load cell and supporting a different ridge for each test (Fig. 106). In every test, the support was placed two feet west (Fig. 89) of midspan, and the structure was loaded with a uniform pressure of 26 lbs. per sq. ft.

The reaction given by the load cell and the relative displacement of the ridge at the intermediate support are shown for each test in Figures 99 to 105, inclusive. The force reaction at the point support changes from one test to another, even though this reaction would be expected to remain the same at symmetrically opposite ridges. As an example, let us look at Figures 102 and 103. The reaction of the load cell is 1250 lbs. when the support is under ridge 2 (Fig. 102), but 3275 lbs. (Fig. 103) when the support is under ridge 6 (symmetrically

opposite to ridge 2). The deflections at symmetrically opposite ridges also differ. The reaction change was undoubtedly due to the following facts:

(1) The degree of the initial tightness of the support against the ridges may have varied from test to test;

(2) A different load cell was used for each ridge and each cell may have undergone different strains under load;

(3) The bearing area of the model above the support may have reacted differently from ridge to ridge.

It should be noted from the results shown in Figures 99 to 103, inclusive, that the supported ridges are subjected to additional transversal moments due to the support. A significant twist occurs in the structure when ridges 2 (Fig. 102) and 3 (Fig. 103) are supported independently. The deflections vary from less than .1" at the supported ridge to over one inch at the farthest exterior ridge.

Fig. 106 shows a typical point support with a ball bearing between the pipe and ridge 5. The deflections, which resulted from this test, have been plotted in Fig. 101. The photo in Figure 106 was taken looking towards the east end of the model. The cross sections

in Figures 96 to 105, inclusive, were drawn as seen when looking towards the west end of the model. The support was set at two feet west of midspan where a series of strain gauges and dial indicators were located.

The experimental deflections in Figures 96, 97, and 98 have been compared with their corresponding theoretical deflections in Figures 138, 139 and 140 in Chapter VII.

Presentation and Discussion of Stress Results

The strains obtained from the forty rosette strain gauges (See Fig. 55) were resolved into stresses according to a procedure outlined in Figure 73. Figures 107, 108, 109 and 110 show the longitudinal stresses in psi in the top and bottom facings at the midspan section when the 19-foot model was subjected to pressures of 13, 23.4, 26 and 39 psf. respectively. The maximum tensile and compressive stresses at the ridges of the model were determined by extrapolation as it was done for the 9.5-foot model in Figures 73 and 74.

It can be seen in Figures 107 to 110, inclusive, that the maximum compressive longitudinal stresses occur in the top facings at the top ridges (except for ridge 7 in Figs. 107 and 108). One would expect the

maximum tensile longitudinal stresses to occur in the bottom facings at the bottom ridges as they did for the 9.5-foot model (Fig. 76). At ridges 2 and 5 in Figures 107 and 108 and at ridge 6 in Figures 109 and 110, however, the maximum tensile stress occurred in the top facing. This state of stress was due to high transversal stresses resulting from the moments at these ridges. The moments were caused by the air pressure acting on the cantilevered exterior panels. This state of stress is not shown at ridge 2 in Figures 109 and 110, since the free end of panel 1 was partially supported by the side of the pressure box when the model was subjected to the loads indicated in these two figures (Figs. 109 and 110).

The minimum longitudinal tensile stresses occur at the middle ridge; the maximum longitudinal compressive stresses are found at the two top interior ridges (ridges 3 and 5). In general, the stresses in the 19-foot model tend to be a little irregular when compared with the stresses in the 9.5-foot model (Fig. 76). It should be remembered that the styrolite core was very compressible (See Chapter I), thus providing little support to stabilize the facings. When the facings tended to buckle locally, the stresses were perturbed.

The experimental stresses in Figures 107, 108

and 109 have been compared with their corresponding theoretical stresses in Figures 141, 142, and 143 in Chapter VII.

Failure of the 19-Foot Model

After the series of tests with intermediate supports was completed, load was applied to the model with intent to fail it.

No intermediate supports were used at first. At a pressure of 44.2 lbs. per sq. ft., the connecting channel of ridge 6, near the east end of the model, delaminated from the facings of the panels (Fig. 111); the resin glue had failed. The bolts, however, kept the connection tight and prevented any further development of the failure. As the pressure was increased to 46.8 lbs. per sq. ft., the connecting channel of ridge 5 at the east end also delaminated. The west end showed no such failure.

Under this load (46.8 lbs. per sq. ft.), the two exterior panels (No. 1 and 6) had deflected so much that ridges 1 and 2 became exposed at the bottom rim of the pressure box (a deflection of over three inches). Ridge 1 is shown in Figure 112 in this deflected position. Had the pressure been increased, the rubber seal would have slid off the top of the model and the plastic sheets would have been exposed to rupture. The model was

unloaded and intermediate point supports were introduced at midspan of the two exterior ridges (Fig. 113). Pressure was applied once more.

Local buckling began to occur in the bearing surface above the point supports, at ridge 7 when the load was 39.0 lbs. per sq. ft., at ridge 1 when the load was 44.2 lbs. per sq. ft. It should be noted here that ridge 1 was also partially supported at the frame column (Fig. 95). As the pressure was increased to 49.4 lbs. per sq. ft., the deformation above the point support at ridge 7 extended towards ridge 6 (Fig. 114); plate 6 was now excessively deformed. At 52.0 lbs. per sq. ft. random noises were heard from the model. At 54.6 lbs. per sq. ft. the distortions of the two exterior panels indicated that:

(1) Local ultimate failure in the exterior ridges,

(2) Cantilever failure of the exterior panels at quarter spans, and

(3) Consequent failure of the pressure bag,

were imminent. The model was unloaded.

To get complete failure across the midspan section of the model, an additional test was carried out in which the exterior ridges were supported at approximately every thirty inches by clamps fastened to the sides of the pressure box. These sides had been reinforced and further supported at the middle (Figs. 115 and 116).

The pressure was applied and, as it was increased to 57.2 lbs. per sq. ft., ripples began to form in the facings along the top ridges propagating from midspan to quarter points. Deflections readings were taken at loads of 62.4 and 67.6 lbs. per sq. ft. All the dial indicators at midspan were removed, except for one at the middle ridge. The pressure was slowly increased. At 75.4 lbs. per sq. ft. the top ridges (3 and 5) buckled in compression at midspan. The pressure dropped to 54.6 lbs. per sq. ft. and remained constant. The nature of the failure at the bottom of the model can be seen from Figure 116, from the top in Figure 117. The black strips along the sides of the box are the rubber seals.

Figure 118 shows the deflections in inches at midspan when the model was subjected to a load of 67.6 lbs. per sq. ft. and after ridges 3 and 5 had buckled at a load of 75.4 lbs. per sq. ft. The vertical deflection at midspan of the middle ridge had increased from 1.6" (67.6 psf) to 2.3" after buckling (75.4 psf).

Model Exposed to Outside Weather

After failure, the model was taken out of the structural frame; it had a saddle shape, but remained stiff (Figure 119). The 19-foot model was placed upright

on ridge 7 and rolled along the floor out through the doors of the lab. It was loaded on a transport truck and delivered to a private home, where it was installed as the roof of a patio (Fig. 120).

The model was turned with its bottom up to shed water and to avoid giving the impression of failing above people's heads. Liquid asphalt was brushed over the connecting channels to plug holes which had developed during failure. The model has already withstood the loads of snow and wind for one winter; it remains stiff and waterproof.

CHAPTER VI

FOLDED SANDWICH PLATE STRUCTURES
THEORETICAL ANALYSIS AND COMPUTER PROGRAM

Introduction

A folded sandwich plate structure is made up of a series of adjoining sandwich panels mutually supporting each other and rigidly connected along their common edges (Figs. 44 & 89). It is usually closed off at its ends by diaphragms which act as end supports. Numerous contributions have been made to the theoretical and experimental studies of folded plates made out of plywood, metal, or concrete. A review of some of these methods can be found in an earlier work by P. P. Fazio (23). An extensive bibliography is given in reference 65. Very little has been done, however, to analyze folded sandwich plate structures.

In this chapter a direct stiffness method of analysis, presented by DeFries-Skene and Scordelis (18) for ordinary folded plate structures, has been employed to develop a theory which effectively predicts the behaviour of folded sandwich plates when subjected to a variety of loads. In this theory, the basic individual panel can be analyzed by various methods. The resulting

boundary functions, relating the forces to the corresponding displacements, are arranged into matrix form. By performing a set of operations on these element matrices, one can derive a general stiffness matrix relating all the external forces to their corresponding displacements and vice versa. The general stiffness matrix is a band matrix (its non-zero terms are grouped along the main diagonal) and thus well conditioned for inversion. This analytical approach is direct and straightforward; it lends itself to simple computer analysis.

A general computer program has been written for folded sandwich plate structures. The only input requirements are: the geometrical data of the cross section, the properties of the materials used, and the loading conditions of the structure. The computer prints out, in tabular form and under proper headings, the joint displacements, the internal forces and internal stresses. A sequence of intermediate matrices and results will also be printed out if a number larger than zero is punched on a special data card.

In the following chapter, theoretical deflections and stresses obtained from the computer program are compared to their corresponding experimental values given in Chapters IV and V.

Method of Analysis - The General Stiffness Method

Applicability:- The general stiffness method may be used to study a structure under the following conditions:

(1) The structure is made up of a finite number of structural components connected at a finite number of joints.

(2) Each joint having m degrees of freedom will suffer m different displacements and be subjected to m different forces; if a displacement is known its corresponding force is unknown, and vice versa.

Once all the joint forces and displacements have been determined, the internal forces and stresses of the structural elements can be found. In case of folded sandwich plates the elements are the sandwich panels and the joints or nodal points lie in the connecting channels. The two exterior channels are also considered in this category.

Basic Assumptions:- The following assumptions are made:

(1) The relation between forces and displacements is linear. Hence, the principal of superposition can be utilized.

(2) The panels are rigidly connected along the ridges.

(3) Each panel is rectangular with top and bottom facings of equal thickness and of the same material.

(4) The end diaphragms are infinitely stiff parallel to their own plane, but perfectly flexible normal to their own plane.

Degrees of Freedom:- Each ridge or joint can undergo four different displacements. It can move vertically and horizontally in a plane parallel to the end diaphragms; it can displace longitudinally parallel to the joint; and it can rotate about the longitudinal axis of the ridge.

Since each plate has two edges, it will have eight degrees of freedom. There will be eight element forces and eight element displacements.

Coordinate Systems:- Two coordinate systems are used to facilitate the analysis of a structure: the fixed system and the relative system.

The displacements and forces acting at a joint are expressed in the fixed coordinate system as shown in Figure 121. This system is fixed with respect to the structure; the sign convention is as follows:

(1) Horizontal forces, $\bar{F}_z$, R_z, and displacements, $\bar{D}_z$, and Δ_z, are positive from left to right.

(2) Vertical forces, $\bar{F}_y$, R_y, and displacements, $\bar{D}_y$, Δ_y, are positive downward.

(3) Horizontal forces, $\bar{F}_x$, R_x, and displacements, $\bar{D}_x$, Δ_x, are positive away from midspan.

(4) Ridge moments, $\bar{F}_\theta$, R_θ, and rotations $\bar{D}_\theta$, Δ_θ, are positive counterclockwise.

Figure 122 shows the forces, $\bar{F}$ (force per unit length), and the displacements, $\bar{D}$, at the edges of the plates. The symbols R and Δ represent force per unit length and displacement, respectively, acting at the joint in the fixed coordinate system.

The relative coordinate system is oriented along the direction of the panel. The forces and displacements studied in this system are shown in Figure 123. The symbols and their sign convention are explained below:

(1) The symbol T or F_x is shear force per unit length acting along the plate edge; u or D_x represent the displacement along the plate edge. Both force and displacement are positive away from midspan.

(2) Force, P or F_y, per unit length along the plate edge and displacement, v or D_y, along

the plate edge, are in the plane of the plate and normal to the edge. These are positive if they produce tension in the cross section of the plate.

(3) Force, Q or F_z, per unit length and displacement, w or D_z, are both normal to the plane of the plate. They are positive if they tend to rotate the plate cross section clockwise.

(4) Moment, M or F_θ, per unit length and displacement, θ or D_θ, are found around the axis along the edge; they are both positive if acting counterclockwise.

Transformation of Coordinate Systems:- Figure 124 shows the relationship between displacements in the relative and fixed coordinate systems, whereas Figure 125 presents the relationship between forces in the relative and fixed coordinate systems. From Figure 124 the following relationships can be derived:

$$\theta_1 = D_{\theta 1} = \bar{D}_{\theta 1} \quad \text{.....(42-a)}$$

$$\theta_2 = D_{\theta 2} = \bar{D}_{\theta 2} \quad \text{.....(42-b)}$$

$$u_1 = D_{x1} = \bar{D}_{x1} \quad \text{.....(42-c)}$$

$$u_2 = D_{x2} = \bar{D}_{x2} \quad \text{.....(42-d)}$$

Furthermore,

$$v_1 = D_{y1} = \bar{D}_{y1}\left(\frac{V}{B}\right) - \bar{D}_{z1}\left(\frac{H}{B}\right) \quad \text{.....(43-a)}$$

$$v_2 = D_{y2} = -\bar{D}_{y2}\left(\frac{V}{B}\right) + \bar{D}_{z2}\left(\frac{H}{B}\right) \quad \text{.....(43-b)}$$

$$w_1 = D_{z1} = -\bar{D}_{y1}\left(\frac{H}{B}\right) - \bar{D}_{z1}\left(\frac{V}{B}\right) \quad \text{.....(43-c)}$$

$$w_2 = D_{z2} = \bar{D}_{y2}\left(\frac{H}{B}\right) + \bar{D}_{z2}\left(\frac{V}{B}\right) \quad \text{.....(43-d)}$$

Subscripts 1 and 2 refer to the edges of the plate. Equations (42) and (43) can be written in matrix form.

$$\begin{bmatrix} \theta_1 \\ \theta_2 \\ w_1 \\ w_2 \\ u_1 \\ u_2 \\ v_1 \\ v_2 \end{bmatrix} = \begin{bmatrix} D_{\theta 1} \\ D_{\theta 2} \\ D_{z1} \\ D_{z2} \\ D_{x1} \\ D_{x2} \\ D_{y1} \\ D_{y2} \end{bmatrix} = \begin{bmatrix} 0 & 0 & 0 & 1 & 0 & 0 & 0 & 0 \\ 0 & 0 & 0 & 0 & 0 & 0 & 0 & 1 \\ -\frac{V}{B} & -\frac{H}{B} & 0 & 0 & 0 & 0 & 0 & 0 \\ 0 & 0 & 0 & 0 & \frac{V}{B} & \frac{H}{B} & 0 & 0 \\ 0 & 0 & 1 & 0 & 0 & 0 & 0 & 0 \\ 0 & 0 & 0 & 0 & 0 & 0 & 1 & 0 \\ -\frac{H}{B} & \frac{V}{B} & 0 & 0 & 0 & 0 & 0 & 0 \\ 0 & 0 & 0 & 0 & \frac{H}{B} & -\frac{V}{B} & 0 & 0 \end{bmatrix} \begin{bmatrix} \bar{D}_{z1} \\ \bar{D}_{y1} \\ \bar{D}_{x1} \\ \bar{D}_{\theta 1} \\ \bar{D}_{z2} \\ \bar{D}_{y2} \\ \bar{D}_{x2} \\ \bar{D}_{\theta 2} \end{bmatrix} \quad \text{(44-a)}$$

Symbolically relation (44-a) becomes

$$\{D\} = |A| \{\bar{D}\} \quad \text{.....(44-b)}$$

The matrix $|A|$ is called the transformation matrix. The same procedure is repeated for Figure 125. Hence,

$$F_{\theta 1} = \bar{F}_{\theta 1} = M_1 \quad \text{.....(45-a)}$$

$$F_{\theta 2} = \bar{F}_{\theta 2} = M_2 \quad \text{.....(45-b)}$$

$$F_{x1} = \bar{F}_{x1} = T_1 \quad \text{.....(45-c)}$$

$$F_{x2} = \bar{F}_{x2} = T_2 \quad \text{.....(45-d)}$$

$$P_1 = -\bar{F}_{z1} \left(\frac{H}{B}\right) = \bar{F}_{y1} \left(\frac{V}{B}\right) \quad \text{.....(46-a)}$$

$$P_2 = \bar{F}_{z2} \left(\frac{H}{B}\right) - \bar{F}_{y2} \left(\frac{V}{B}\right) \quad \text{.....(46-b)}$$

$$Q_1 = -\bar{F}_{z1} \left(\frac{V}{B}\right) - \bar{F}_{y1} \left(\frac{H}{B}\right) \quad \text{.....(46-c)}$$

$$Q_2 = \bar{F}_{z2} \left(\frac{V}{B}\right) + \bar{F}_{y2} \left(\frac{H}{B}\right) \quad \text{.....(46-d)}$$

Equations (45) and (46) can be written in matrix form as follows:

$$\begin{bmatrix} M_1 \\ M_2 \\ Q_1 \\ Q_2 \\ T_1 \\ T_2 \\ P_1 \\ P_2 \end{bmatrix} = \begin{bmatrix} 0 & 0 & 0 & 1 & 0 & 0 & 0 & 0 \\ 0 & 0 & 0 & 0 & 0 & 0 & 0 & 1 \\ -\frac{V}{B} & -\frac{H}{B} & 0 & 0 & 0 & 0 & 0 & 0 \\ 0 & 0 & 0 & 0 & \frac{V}{B} & \frac{H}{B} & 0 & 0 \\ 0 & 0 & 1 & 0 & 0 & 0 & 0 & 0 \\ 0 & 0 & 0 & 0 & 0 & 0 & 1 & 0 \\ -\frac{H}{B} & \frac{V}{B} & 0 & 0 & 0 & 0 & 0 & 0 \\ 0 & 0 & 0 & 0 & \frac{H}{B} & -\frac{V}{B} & 0 & 0 \end{bmatrix} \begin{bmatrix} \bar{F}_{z1} \\ \bar{F}_{y1} \\ \bar{F}_{x1} \\ \bar{F}_{\theta 1} \\ \bar{F}_{z2} \\ \bar{F}_{y2} \\ \bar{F}_{x2} \\ \bar{F}_{\theta 2} \end{bmatrix} \qquad (47\text{-a})$$

Symbolically, relations (47-a) can be written as

$$\{F\} = |A| \{\bar{F}\} \qquad (47\text{-b})$$

where $|A|$ is the transformation matrix.

Figure 125 can be used to establish the following additional relationships:

$$\bar{F}_{z1} = -Q_1 \left(\frac{V}{B}\right) - P_1 \left(\frac{H}{B}\right) \quad \text{.....(48-a)}$$

$$\bar{F}_{z2} = Q_2 \left(\frac{V}{B}\right) + P_2 \left(\frac{H}{B}\right) \quad \text{.....(48-b)}$$

$$\bar{F}_{y1} = Q_1 \left(\frac{H}{B}\right) + P_1 \left(\frac{V}{B}\right) \quad \text{.....(48-c)}$$

$$\bar{F}_{y2} = Q_2 \left(\frac{H}{B}\right) - P_2 \left(\frac{V}{B}\right) \quad \text{.....(48-d)}$$

$$\bar{F}_{\theta 1} = M_1 \quad \text{.....(49-a)}$$

$$\bar{F}_{\theta 2} = M_2 \quad \text{.....(49-b)}$$

$$\bar{F}_{x1} = T_1 \quad \text{.....(49-c)}$$

$$\bar{F}_{x2} = T_2 \quad \text{.....(49-d)}$$

Equations (48) and (49) can be written in matrix form as follows:

$$\begin{bmatrix} \bar{F}_{z1} \\ \bar{F}_{y1} \\ \bar{F}_{x1} \\ \bar{F}_{\theta 1} \\ \bar{F}_{z2} \\ \bar{F}_{y2} \\ \bar{F}_{x2} \\ \bar{F}_{\theta 2} \end{bmatrix} = \begin{bmatrix} 0 & 0 & -\frac{V}{B} & 0 & 0 & 0 & -\frac{H}{B} & 0 \\ 0 & 0 & -\frac{H}{B} & 0 & 0 & 0 & \frac{V}{B} & 0 \\ 0 & 0 & 0 & 0 & 1 & 0 & 0 & 0 \\ 1 & 0 & 0 & 0 & 0 & 0 & 0 & 0 \\ 0 & 0 & 0 & \frac{V}{B} & 0 & 0 & 0 & \frac{H}{B} \\ 0 & 0 & 0 & \frac{H}{B} & 0 & 0 & 0 & -\frac{V}{B} \\ 0 & 0 & 0 & 0 & 0 & 1 & 0 & 0 \\ 0 & 1 & 0 & 0 & 0 & 0 & 0 & 0 \end{bmatrix} \begin{bmatrix} M_1 \\ M_2 \\ Q_1 \\ Q_2 \\ T_1 \\ T_2 \\ P_1 \\ P_2 \end{bmatrix} \quad \text{(50-a)}$$

Symbolically, relations (50-a) can be written as

$$\{\bar{F}\} = |A^t| \{F\} \quad \text{.....(50-b)}$$

where $|A^t|$ is the transpose of A. The similarity between Equations (50-b) and (47-b) should be noted.

Element Stiffness Matrix:- The element stiffness matrix relates the element forces F in the relative system to the corresponding displacements D. The size of this matrix is (8 by 8) and is formed by grouping together the slab stiffness (4 by 4) and the plate stiffness (4 by 4) matrices. The following two assumptions are involved in the construction of the element stiffness matrix:

(1) The slab stiffness matrix is determined by the performance of one-way sandwich beams spanning between longitudinal ridges.

(2) Membrane stresses produced in the facings of each panel by longitudinal plate action may be calculated by elementary beam theory.

The equations of this section will confirm that the slab stiffness and plate stiffness of the individual elements are independent of each other.

Slab Stiffness:- The slab stiffness matrix must

take into account the shear stiffness of the sandwich strip being considered. The bending and shear displacements in a sandwich beam, due to a set of general forces, are shown in Figure 126. The total rotation, θ_1, due both to bending and shear effects can be written as follows:

$$\theta_1 = \frac{B}{6D}(2M_1 - M_2) - \frac{w_{b1}}{B} - \frac{w_{b2}}{B} - \frac{w_{s1}}{B} - \frac{w_{s2}}{B} \quad \text{.....(51)}$$

where w_b and w_s are the deflections due to bending and shear effects, respectively; D is the bending stiffness. It should be noted that if the last two terms on the right-hand side are dropped, Equation (51) becomes a standard slope deflection equation.

From Figure 126(b) and from the theory of Chapter II the following relation can be written:

$$w_{s1} + w_{s2} = \frac{Q_1 B}{D_q} = \frac{Q_2 B}{D_q} \quad \text{.....(52)}$$

Where D_q is the shear stiffness of the sandwich beam. Also,

$$Q_1 B = Q_2 B = M_1 + M_2 \quad \text{.....(53)}$$

Equations (52) and (53) are substituted into Equation (51); after simplification, the following relation can be written:

$$\theta_1 = M_1 \left(\frac{B}{3D} - \frac{1}{BD_q}\right) + M_2 \left(-\frac{B}{6D} - \frac{1}{BD_q}\right) - \frac{w_{b1}}{B} - \frac{w_{b2}}{B} \quad \ldots.(54)$$

The procedure can be repeated to write a similar equation for θ_2. Hence,

$$\theta_2 = M_1 \left(-\frac{B}{6D} - \frac{1}{BD_q}\right) + M_2 \left(\frac{B}{3D} - \frac{1}{BD_q}\right) - \frac{w_{b1}}{B} - \frac{w_{b2}}{B} \quad \ldots..(55)$$

From Equations (54) and (55) one may solve for M_1 and M_2. After due simplification the following two equations result:

$$M_1 = \frac{4D(B^2D_q-3D)}{B(B^2D_q-12D)}(\theta_1) + \frac{2D(B^2D_q+6D)}{B(B^2D_q-12D)}(\theta_2)$$

$$+ \frac{6D_qD}{B^2D_q-12D}(w_{b1}) + \frac{6D_qD}{B^2D_q-12D}(w_{b2}) \quad \ldots....(56)$$

$$M_2 = \frac{2D(B^2D_q+6D)}{B(B^2D_q-12D)}(\theta_1) + \frac{4D(B^2D_q-3D)}{B(B^2D_q-12D)}(\theta_2)$$

$$+ \frac{6D_qD}{B^2D_q-12D}(w_{b1}) + \frac{6D_qD}{B^2D_q-12D}(w_{b2}) \quad \ldots....(57)$$

$$\begin{bmatrix} M_1 \\ M_2 \\ Q_1 \\ Q_2 \end{bmatrix} = \begin{bmatrix} \frac{4D(B^2D_q-3D)}{B(B^2D_q-12D)} & \frac{2D(B^2D_q+6D)}{B(B^2D_q-12D)} & \frac{6D_qD}{B^2D_q-12D} & \frac{6D_qD}{B^2D_q-12D} \\ \frac{2D(B^2D_q+6D)}{B(B^2D_q-12D)} & \frac{4D(B^2D_q-3D)}{B(B^2D_q-12D)} & \frac{6D_qD}{B^2D_q-12D} & \frac{6D_qD}{B^2D_q-12D} \\ \frac{6D_qD}{B^2D_q-12D} & \frac{6D_qD}{B^2D_q-12D} & \frac{12D_qD}{B(B^2D_q-12D)} & \frac{12D_qD}{B(B^2D_q-12D)} \\ \frac{6D_qD}{B^2D_q-12D} & \frac{6D_qD}{B^2D_q-12D} & \frac{12D_qD}{B(B^2D_q-12D)} & \frac{12D_qD}{B(B^2D_q-12D)} \end{bmatrix} \begin{bmatrix} \theta_1 \\ \theta_2 \\ w_{b1} \\ w_{b2} \end{bmatrix} \quad \ldots\ldots(58)$$

By substituting Equations (56) and (57) into Equation (53), general expressions for Q_1 and Q_2 can be written. The four equations for M_1, M_2, Q_1 and Q_2 have been written in matrix form as Equation (58). They can also be written symbolically as

$$\{F_s\} = |k_s| \{D_s\} \quad \ldots\ldots\ldots\ldots (59)$$

Where $\{F_s\}$ denotes the slab forces, $\{D_s\}$ the slab displacements, and $|k_s|$ the slab stiffness matrix.

It is worth noting in Equations (58) that the angles, θ, are the total rotations due to both bending and shear effects. Whereas, the deflections w_b are those caused by bending only. It is necessary to use Equation (52) in conjunction with Equations (58) to solve for the total deflection, w.

Plate Stiffness:- Figure 127 shows the displacement and force patterns produced in each panel by longitudinal plate action. The plate stiffness matrix can be determined from these patterns. In Figure 127(a) the displacements along the longitudinal edges and in the plane of the panel are assumed to have a sine distribution. Hence,

$$v' = 1 \sin \frac{n\pi x}{L} \quad \text{for } n = 1, 2, 3 \ldots\text{etc.} \quad (60)$$

The forces corresponding to this displacement will also have a sine distribution, namely

$$p' = \frac{2Et}{B} \sin \frac{n\pi x}{L} \quad \ldots\ldots\ldots\ldots\ldots\ldots \quad (61)$$

The longitudinal displacements are shown in Figure 127(b). These are assumed to be zero at midspan and maximum at the ends of the panel, and have the following distribution:

$$u' = 1 \cos \frac{n\pi x}{L} \quad \ldots\ldots\ldots\ldots\ldots\ldots \quad (62)$$

The corresponding forces T' (Fig. 127-b) are determined as follows:

$$\frac{d(-u')}{dx} = 2 \int_{\frac{L}{2}}^{\frac{L}{2}+x} \frac{2T'dx}{2tBE} = 2 \int_{\frac{L}{2}}^{\frac{L}{2}+x} \frac{2T'dx}{AE}$$

$$\frac{d^2(-u')}{dx^2} = \frac{4T'}{AE} \quad \ldots\ldots\ldots\ldots \quad (63)$$

where $A = 2tB$.

Differentiating Equation (62) and substituting in Equation (63), the following expression for T' is obtained:

$$T' = \frac{AE}{4} \frac{n^2\pi^2}{L^2} \cos \frac{n\pi x}{L} \quad \ldots\ldots\ldots\ldots\ldots\ldots (64)$$

Where A is the area of the cross section of the facings and E their modulus of elasticity.

Figure 127(c) shows longitudinal bending displacements; rotation of the ends of the panel is restrained. The distribution is assumed to be

$$v'' = 1 \sin \frac{n\pi x}{L} \quad \ldots\ldots\ldots\ldots\ldots (65)$$

The corresponding forces, T" and P" (Fig. 127-c), are determined as follows:

$$T'' \, Bdx = Vdx = \left(\int_{\frac{L}{2}}^{\frac{L}{2} + x} 2P'' \, dx \right) dx \quad \ldots\ldots\ldots (66)$$

where V is the transverse shearing force. Also

$$\frac{V}{GA} = - \frac{dv''}{2dx} \quad \ldots\ldots\ldots\ldots\ldots\ldots (67)$$

From the above two Equations and replacing G by $\frac{E}{2(1+\mu)}$, the following expression can be written:

$$T'' = -\frac{EAn\pi}{4(1+\mu)BL} \cos \frac{n\pi x}{L} \quad \ldots\ldots\ldots\ldots\ldots \quad (68)$$

where μ is the Poisson's ratio for the facings. From Equation (66)

$$T''B = \int_{\frac{L}{2}}^{\frac{L}{2}+x} 2P''dx \quad \ldots\ldots\ldots\ldots\ldots\ldots \quad (69)$$

Differentiating once with respect to x we obtain

$$B \frac{dT''}{dx} = 2P'' \quad \ldots\ldots\ldots\ldots\ldots\ldots\ldots \quad (70)$$

Equation (68) is differentiated with respect to x and substituted in Equation (70). Hence,

$$P'' = \frac{EAn^2\pi^2}{8(1+\mu)L^2} \sin \frac{n\pi x}{L} \quad \ldots\ldots\ldots\ldots\ldots \quad (71)$$

The end restraints in Figure 127(c), once released, give rise to the displacements shown in Figure 127(d). The distribution of these displacements along the panel can be assumed to be

$$u'' = 1 \cos \frac{n\pi x}{L} \quad \text{.....(72)}$$

The corresponding forces, T" and P" (Fig. 127-d), can be determined as follows:

$$\frac{M\ (\frac{B}{2})}{EI_p} = \frac{1}{2}\frac{du''}{dx} = -\frac{1}{2}\frac{n\pi}{L} \sin \frac{n\pi x}{L} \quad \text{.....(73)}$$

where M is the bending moment. Because deflection v" = 0,

$$\frac{d^2v''}{dx^2} = \frac{M}{EI_p} - \frac{1}{GA}\frac{dV}{dx} = 0 \quad \text{.....(74)}$$

Hence,

$$\frac{1}{GA}\ \frac{dV}{dx} = \frac{1}{GA}\ (2P'') = \frac{M}{EI_p} = -\frac{1}{B}\frac{n\pi}{L} \sin \frac{n\pi x}{L} \quad \text{.....(75)}$$

From which

$$P'' = -\frac{EAn\pi}{4(1+\mu)BL} \sin \frac{n\pi x}{L} \quad \text{.....(76)}$$

From Figure 127(d) the following can be written:

$$T''\ dxB = Vdx - dM = \left(\int \frac{dV}{dx}\ dx\right)\ dx - \left(\frac{dM}{dx}\right)\ dx \quad \text{.....(77)}$$

Since $\frac{dV}{dx} = GA\ \frac{M}{EI_p}$, (See Equations 74 and 75),

Equation (77) can be written as

$$T''B = GA \int \frac{M}{EI_p} dx - \frac{dM}{dx} \quad \text{.....(78)}$$

Integrating Equation (73) the following is obtained:

$$\int \frac{M}{EI_p} dx = \frac{1}{B} \cos \frac{n\pi x}{L} + C \quad \text{.....(79)}$$

where the constant of integration can be shown to be equal to zero for all odd values of n. When Equation (73) is differentiated,

$$\frac{dM}{dx} = - \frac{EI_p}{B} \frac{n^2\pi^2}{L^2} \cos \frac{n\pi x}{L} \quad \text{.....(80)}$$

Substituting Equations (79) and (80) into Equation (78), the distribution for Forces T" is found to be

$$T'' = \left[\frac{EA}{2(1+\mu)B^2} + \frac{EI_p n^2\pi^2}{B^2L^2} \right] \cos \frac{n\pi x}{L} \quad \text{.....(81)}$$

Equations 60, 61, 62, 64, 65, 68, 71, 72, 76 and 81 can be written in matrix form.

See Equations (82-a)

$$\begin{bmatrix} T' \\ T'' \\ P' \\ P'' \end{bmatrix} = \begin{bmatrix} \frac{AEn^2\pi^2}{4L^2} & 0 & 0 & 0 \\ 0 & \frac{EA}{2(1+\mu)B^2} + \frac{EI_p n^2\pi^2}{B^2L^2} & 0 & -\frac{EAn\pi}{4(1+\mu)BL} \\ 0 & 0 & \frac{2Et}{B} & 0 \\ 0 & -\frac{EAn\pi}{4(1+\mu)BL} & 0 & \frac{EAn^2\pi^2}{8(1+\mu)L^2} \end{bmatrix} \begin{bmatrix} u' \\ u'' \\ v' \\ v'' \end{bmatrix} \quad ..(82\text{-a})$$

Symbolically Equations (82-a) can be written as

$$\{F'_p\} = |k'_p| \{D'_p\} \quad \text{.....(82-b)}$$

where $\{F'_p\}$ denotes forces, $\{D'_p\}$ displacements and $|k'_p|$ is the stiffness matrix.

From Figure 127, the following relations can be verified:

$$u' = u_1 + u_2 \quad \text{.....(83-a)}$$

$$u'' = u_1 - u_2 \quad \text{.....(83-b)}$$

$$v' = v_1 + v_2 \quad \text{.....(83-c)}$$

$$v'' = v_1 - v_2 \quad \text{.....(83-d)}$$

The subscripts 1 and 2 indicate the respective edges of the plate. In matrix form Equations (83) become:

$$\begin{bmatrix} u' \\ u'' \\ v' \\ v'' \end{bmatrix} = \{D'_p\} = \begin{bmatrix} 1 & 1 & 0 & 0 \\ 1 & -1 & 0 & 0 \\ 0 & 0 & 1 & 1 \\ 0 & 0 & 1 & -1 \end{bmatrix} \begin{bmatrix} u_1 \\ u_2 \\ v_1 \\ v_2 \end{bmatrix} = |C|\{D_p\} \quad \text{..(84)}$$

in which $\{D_p\}$ represents the displacements in the plate system and $|C|$ is the transformation matrix.

A set of equations similar to Equations (83) can now be written to relate the forces assumed in Figure 127 with those shown in Figure 123(a). The result can be expressed as follows:

$$\{F_p\} = |C|\{F'_p\} \quad \text{.....(85)}$$

in which $\{F_p\}$ represents the forces in the plate system.

Equations (82), (83), and (85) can be combined to yield:

$$\{F_p\} = |C||k'_p|\{D'_p\} = |C||k'_p||C|\{D_p\} = |k_p|\{D_p\} \quad \text{....(86)}$$

Hence the plate stiffness matrix can be written as

$$|k_p| = |C||k'_p||C| \quad \text{.....(87)}$$

The element stiffness matrix can now be formed for each panel by combining the slab and plate systems. Hence,

$$\begin{bmatrix} F_s \\ \\ F_p \end{bmatrix} = \begin{bmatrix} k_s & 0 \\ & \\ 0 & k_p \end{bmatrix} \times \begin{bmatrix} D_s \\ \\ D_p \end{bmatrix} \quad \text{.....(88-a)}$$

Symbolically, the above can be written as

$$\{F\} = |k|\{D\} \quad \text{.....(88-b)}$$

in which $|k|$ is the element stiffness matrix in the relative coordinate system. This stiffness can be transformed into the fixed coordinate system by combining Equations (44), (50) and (88). Hence, for plate number n,

$$\{\bar{F}\}_n = |A^t|_n\{F\}_n = |A^t|_n|k|_n\{D\}_n$$

$$= |A^t|_n|k|_n|A|_n\{\bar{D}\}_n = |\bar{k}|_n\{\bar{D}\}_n \quad \text{.....(89)}$$

From the above equation, $|\bar{k}|_n$ is the element stiffness matrix which relates the forces to the displacements in the fixed coordinate system and can be written as follows:

$$|\bar{k}|_n = |A^t|_n|k|_n|A|_n \quad \text{.....(90)}$$

Structure Stiffness Matrix:- The structure stiffness matrix, $|K|$, can be formed by properly combining the element stiffness matrices. If two consecutive plates are numbered m and n (n = m+1), edge 2 of plate m and edge 1 of plate n are common and undergo the same four displacements along

their common joint. It should be noted that these four displacements are related to their corresponding forces by both the last quadrant of the stiffness matrix for plate m and the first quadrant of the stiffness matrix for plate n. Hence, the structure stiffness matrix, $|K|$, can be formed by assembling the element stiffness matrices successively along the diagonal in such a pattern so that the elements in the last quadrant of one matrix can be added to the corresponding elements in the first quadrant of the following matrix. The size of matrix $|K|$ is $4(x+1)$ by $4(x+1)$ where x is the total number of the panels making up the structure.

The general stiffness matrix relates all the joint forces to their corresponding displacements. Once all the joint forces and displacements are known, the element forces in the relative system can be found by substituting back into the appropriate equations. For example, Equation (44) can be used to transform the displacements from the fixed to the relative coordinate system; these displacements can then be substituted into Equation (88) to find the stresses in the panels.

Fourier Components of Loadings and Displacements:- The equations in this Chapter have been devised for joint loads only. Surface loading can be reduced to joint loading, however, by applying, at the ridges, an equivalent set of fixed-end moments and shears. This set of forces is computed by

assuming each panel acting as one-way slab fixed along its longitudinal edges.

The distribution of all applied forces and displacements is taken as that given by harmonics of Fourier series. By choosing the proper series it is possible to analyse the structure under different types of loading without making any revisions in the theory presented in this chapter. Some of the Fourier series which represent the most common types of loadings are given below; it is assumed that the series end at n = 11:

1. A concentrated load δ_o at midspan is represented by:

$$R_y = \frac{2\delta_o}{\pi}\left(1 \sin \frac{\pi x}{L} - 1 \sin \frac{3\pi x}{L} + \ldots\ldots - 1 \sin \frac{11\pi x}{L}\right) \quad \ldots(91)$$

2. A uniform load with intensity δ_o at midspan is represented by:

$$R_x = \frac{4\delta_o}{\pi}\left(1 \sin \frac{\pi x}{L} + \frac{1}{3} \sin \frac{3\pi x}{L} + \ldots\ldots + \frac{1}{11} \sin \frac{11\pi x}{L}\right) \quad \ldots(92)$$

3. A prestressing force of δ_o applied at the ends of the panels (by a straight cable in a longitudinal direction, for example) is represented by:

$$R_x = \frac{4\delta_o}{L}\left(1 \cos \frac{\pi x}{L} + 1 \cos \frac{3\pi x}{L} + \ldots\ldots + 1 \cos \frac{11\pi x}{L}\right) \quad \ldots(93)$$

The structure is analysed for each of the components in brackets in the selected Fourier series. The results of each harmonic are added to yield the final stresses and deflections.

Computer Program

A program has been written in the Fortran language for the Control Data Corporation (CDC) 3300 computer. This machine has a 65k words (24 bits each) of core storage; full floating point and character hardware; seven disk drives with a total capacity of 56 million characters; five tape units; two printers, card readers, and one punch; one plotter; twelve local cathode ray display terminals; a multi-plexor connecting up to the TWX network. The computer has a cycle time of 1.25 micro seconds and runs approximately 50% faster than the IBM 1044 on compute bound jobs. The memory is roughly equivalent to 256k bytes on the IBM 360 series.

The program was used to find theoretical stresses and deflections of the two folded sandwich plate structures analysed in Chapters IV and V. Both of these structures had six panels and seven ridges. The running time for one loading condition was 1 minute, 35.301 seconds; for 21 different loading conditions, 18 minutes, 16.739 seconds.

The number of panels which can be handled by the program is restricted only by the storage capacity of the

computer; this number can be further increased by making proper use of disk storage and some minor adjustments in the program. An infinite number of structures and loading conditions can be analysed consecutively by this program.

The structures can be subjected to any type of loading which can be represented by Fourier series. With few minor revisions in the program, analysis can be made of folded sandwich plates with panels of different width and whose top and bottom facings vary in thickness.

Because of its length, the computer program will not be presented here; its general outline follows closely that given by the matrix sequence of operations set forth in the theory of the previous section. The form of input and output together with a flow chart are discussed below.

Input:- The following data is punched on the data cards in the order outlined below:

(1) If any number larger than zero is punched in the first ten spaces of this card, all the intermediate matrices calculated by the computer will be printed out along with the final results. If a blank card is used, the print-out will be exactly as shown on pages 235 to 238, inclusive;

(2) The number of structures to be analysed consecutively;

(3) The modulus of elasticity and Poisson's ratio of the facings;

(4) The thickness of the facings, the thickness of the panels, the width of the panels, the span length, and the number of panels in the structure;

(5) The cross sectional area, in square inches, of the facings and connecting channels for each plate;

(6) The moments of inertia of each panel, in $in.^4$, taken about the axis which runs through the centroid of the cross section and which is perpendicular to the plane of the panel;

(7) The angles which the plates make with the horizontal as shown in Figures 44 and 89;

(8) The shear stiffness constant of the sandwich panels taken in the transversal direction;

(9) Number of loading conditions applied to each structure;

(10) If a number larger than zero is punched in the first ten spaces of this card the loading consists of a uniform pressure applied perpendicular to the surfaces of the panels. This pressure is given in psi by card number 11. If data card No. 10 is blank, on the other hand, it indicates joint loads applied at the ridges of the structure.

Since each ridge can be subjected to four different joint loads, the number of cards required to transmit this data to the computer would be $4(n+1)/8$, where n is the number of plates in the structure and 8 is the number of forces to be punched on each card.

It should be noted that more than one card would be required in cases 4, 5 and 6 where the number of panels per structure exceeds 8.

Additional loading conditions can be analysed by adding loading data cards similar to those following card number 9; whereas, additional structures can be analysed by adding data cards similar to those following card number 2.

Output:- If the intermediate matrices are not printed out the complete output for one structure and one loading condition is given on pages 107 to 113, inclusive.

Page 107 presents the data input. Pages 108 and 109 consist of the displacements, in inches, calculated along each ridge at intervals of .1 (span length). The tenth interval occurs over the supports where the displacement is equal to zero as verified in these answers. Symmetry exists along each ridge at points equidistant from midspan. Similarly, pages 110, 111, and 112 of the output present the internal forces (lbs. per in.) and moments (lbs-in per in.) acting along the two longitudinal edges of each plate. These

forces are numbered from 1 to 8 and represent M_1, M_2, Q_1, Q_2, T_1, T_2, P_1 and P_2 respectively. Figure 123(a) shows these forces acting on a plate element.

On page 113 are found the longitudinal stresses along the edges of each plate. It is worth noting that edge 2 of plate n and edge 1 of plate n+1 are adjacent to one another, and undergo the same stresses as shown by the computer answers.

Computer Program Flow Chart:- The flow chart shown in Figure 128 lists in a chronological order the steps which are followed in solving the problem.

STRUCTURE NUMBER 1

GEOMETRICAL DATA

MODULUS OF ELASTICITY OF THE FACINGS	=	10250000.00000
POISSON S RATIO OF THE FACINGS	=	.33000
THICKNESS OF THE FACINGS IN IN.	=	.02500
THICKNESS OF THE SANDWICH PANELS	=	1.02500
WIDTHS OF THE SANDWICH PANELS IN IN.	=	23.75000
SPAN LENGTH OF THE STRUCTURE IN IN.	=	113.00000
NUMBER OF SANDWICH PANELS	=	6

CROSS SECTIONAL AREAS OF FACINGS AND CHANNELS PER PANEL IN SQ. IN.

1.40250 1.61650 1.61650 1.61650 1.61650 1.40250

MOMENTS OF INERTIA OF THE SANDWICH PANELS IN IN. TO THE FOURTH POWER

78.81140 113.46490 113.46490 113.46490 113.46490 78.81140

ANGLES IN RADIANS EACH PANEL MAKES WITH THE HORIZONTAL MEASURED COUNTERCLOCKWISE

330.35000 29.65000 330.25000 29.55000 330.45000 29.60000

STIFFNESS CONSTANTS

BENDING STIFFNESS = 152000
SHEAR STIFFNESS = 3075

LOADING CONDITION NUMBER 1

FORCES ACTING AT RIDGES

	FZ	FY	FX	FO
RIDGE 1	0	0	0	0
RIDGE 2	0	2.000000000E 01	0	0
RIDGE 3	0	2.000000000E 01	0	0
RIDGE 4	0	2.000000000E 01	0	0
RIDGE 5	0	2.000000000E 01	0	0
RIDGE 6	0	2.000000000E 01	0	0
RIDGE 7	0	0	0	0

STRUCTURE NUMBER 1. LOADING CONDITION NUMBER 1

DISPLACEMENT MATRIX DIS(28,10) FORMED BY ADDING MATRICES DIS(28,10) FOR N=1,11.

THE DISPLACEMENTS BELOW ARE GIVEN AT INTERVALS OF .1(SPAN LENGTH) ALONG EACH RIDGE.

RIDGE 1. TRANSVERSAL DISPLACEMENT, RZ, IN INCHES.

1.46163381E-03	3.31529529E-03	4.62690005E-03	5.41458708E-03	5.74448047E-03
5.41458716E-03	4.62690026E-03	3.31529552E-03	1.46163418E-03	1.46662776E-10

RIDGE 1. VERTICAL DISPLACEMENT, RY, IN INCHES.

4.06629508E-02	7.59834641E-02	1.03600983E-01	1.21114053E-01	1.27041683E-01
1.21114055E-01	1.03600987E-01	7.59834696E-02	4.06629574E-02	7.19321936E-09

RIDGE 1. LONGITUDINAL DISPLACEMENT, RX, IN INCHES.

-1.86821504E-02	-1.58757817E-02	-1.16912669E-02	-6.25365615E-03	-5.47721344E-10
-6.25365514E-03	-1.16912661E-02	-1.58757811E-02	-1.86821500E-02	-1.97487720E-02

RIDGE 1. ROTATION, RO, IN RADIANS.

-3.27628510E-04	-6.29470243E-04	-8.53680340E-04	-9.91814141E-04	-1.04115148E-03
-9.91814157E-04	-8.53680373E-04	-6.29470293E-04	-3.27628568E-04	-5.33747471E-11

RIDGE 2. TRANSVERSAL DISPLACEMENT, RZ, IN INCHES.

-1.91845453E-03	-3.68311685E-03	-4.99605943E-03	-5.80573531E-03	-6.09445412E-03
-5.80573541E-03	-4.99605962E-03	-3.68311711E-03	-1.91845687E-03	-3.13358646E-10

RIDGE 2. VERTICAL DISPLACEMENT, RY, IN INCHES.

4.76724078E-02	8.92020608E-02	1.21452872E-01	1.41831625E-01	1.48755424E-01
1.41831628E-01	1.21452876E-01	8.92020672E-02	4.76724155E-02	8.38099885E-09

RIDGE 2. LONGITUDINAL DISPLACEMENT, RX, IN INCHES.

2.07182695E-02	1.76059140E-02	1.29667692E-02	6.93688923E-03	6.07614982E-10
6.93688811E-03	1.29667683E-02	1.76059133E-02	2.07182691E-02	2.19244597E-02

RIDGE 2. ROTATION, RO, IN RADIANS.

-3.27628501E-04	-6.29470232E-04	-8.53680317E-04	-9.91814112E-04	-1.04115145E-03
-9.91814127E-04	-8.53680349E-04	-6.29470276E-04	-3.27628559E-04	-5.33747453E-11

RIDGE 3. TRANSVERSAL DISPLACEMENT, RZ, IN INCHES.

7.29081579E-04	1.38019967E-03	1.89048868E-03	2.21475254E-03	2.32583647E-03
2.21475257E-03	1.89048876E-03	1.38019977E-03	7.29081699E-04	1.26705711E-10

RIDGE 3. VERTICAL DISPLACEMENT, RY, IN INCHES.

5.23066535E-02	9.80666858E-02	1.33510664E-01	1.55875547E-01	1.63499713E-01
1.55875550E-01	1.33510669E-01	9.80666928E-02	5.23066619E-02	9.16008020E-09

RIDGE 3. LONGITUDINAL DISPLACEMENT, RX, IN INCHES.

-2.29096454E-02	-1.94680611E-02	-1.43385736E-02	-7.67099288E-03	-6.71928464E-10
-7.67099163E-03	-1.43385726E-02	-1.94680604E-02	-2.29096449E-02	-2.42436790E-02

RIDGE 3. ROTATION, RO, IN RADIANS.

-1.25299639E-04	-2.36965451E-04	-3.24745859E-04	-3.80610355E-04	-3.99713514E-04
-3.80619361E-04	-3.24745871E-04	-2.36965448E-04	-1.25299659E-04	-2.18578916E-11

RIDGE 4. TRANSVERSAL DISPLACEMENT, RZ, IN INCHES.

-1.00415077E-04	-1.89062028E-04	-2.57475754E-04	-3.00551597E-04	-3.15321837E-04
-3.00551402E-04	-2.57475764E-04	-1.89062042E-04	-1.00415094E-04	-1.74236606E-11

RIDGE 4. VERTICAL DISPLACEMENT, DY, IN INCHES.

5.37834694E-02	1.00864010E-01	1.37332736E-01	1.61349810E-01	1.68197503E-01
1.60349813E-01	1.37332741E-01	1.00864026E-01	5.37834781E-02	9.41661802E-09

RIDGE 4. LONGITUDINAL DISPLACEMENT, DX, IN INCHES.

2.33353176E-02	1.98208445E-02	1.46043580E-02	7.81270956E-03	6.84315402E-10
7.81270830E-03	1.46043570E-02	1.98208438E-02	2.33353172E-02	2.46035784E-02

RIDGE 4. ROTATION, RO, IN RADIANS.

-1.23459365E-05	-2.30391970E-05	-3.12985042E-05	-3.64991668E-05	-3.82640758E-05
-3.64991674E-05	-3.12985053E-05	-2.30391987E-05	-1.23459364E-05	-2.17495210E-12

RIDGE 5. TRANSVERSAL DISPLACEMENT, RZ, IN INCHES.

-7.50550886E-04	-1.42017484E-03	-1.94495202E-03	-2.27841008E-03	-2.39258857E-03
-2.27841012E-03	-1.94495210E-03	-1.42017497E-03	-7.50551009E-04	-1.30535140E-10

RIDGE 5. VERTICAL DISPLACEMENT, DY, IN INCHES.

5.26170344E-02	9.86444471E-02	1.34295954E-01	1.56791367E-01	1.64459716E-01
1.56791370E-01	1.34295959E-01	9.86448542E-02	5.26170434E-02	9.21496992E-09

RIDGE 5. LONGITUDINAL DISPLACEMENT, DX, IN INCHES.

-2.29378410E-02	-1.94920065E-02	-1.43563568E-02	-7.68060687E-03	-6.72776017E-10
-7.68060562E-03	-1.43563558E-02	-1.94920058E-02	-2.29378406E-02	-2.42736347E-02

RIDGE 5. ROTATION, RO, IN RADIANS.

1.19483082E-04	2.26046393E-04	3.09876402E-04	3.63257857E-04	3.81501188E-04
3.63257863E-04	3.09876414E-04	2.26046409E-04	1.19483102E-04	2.08416759E-11

RIDGE 6. TRANSVERSAL DISPLACEMENT, RZ, IN INCHES.

1.92850340E-03	3.70193008E-03	5.02117898E-03	5.83666936E-03	6.12471845E-03
5.83666945E-03	5.02117917E-03	3.70191036E-03	1.92850374E-03	3.15051990E-10

RIDGE 6. VERTICAL DISPLACEMENT, DY, IN INCHES.

4.79062028E-02	8.96399055E-02	1.22048868E-01	1.42527443E-01	1.49485216E-01
1.42527445E-01	1.22048872E-01	8.96399120E-02	4.79062105E-02	8.43103498E-09

RIDGE 6. LONGITUDINAL DISPLACEMENT, DX, IN INCHES.

2.07772039E-02	1.76559942E-02	1.30036627E-02	6.95663263E-03	6.09344690E-10
6.95663150E-03	1.30036617E-02	1.76559936E-02	2.07772035E-02	2.19868328E-02

RIDGE 6. ROTATION, RO, IN RADIANS.

3.40687228E-04	6.53710453E-04	8.86538332E-04	1.03008935E-03	1.08125485E-03
1.03008937E-03	8.86538365E-04	6.53710498E-04	3.40687288E-04	5.56922125E-11

RIDGE 7. TRANSVERSAL DISPLACEMENT, RZ, IN INCHES.

-1.59720866E-03	-3.56787221E-03	-4.97001998E-03	-5.81477645E-03	-6.16398219E-03
-5.81477654E-03	-4.97002020E-03	-3.56787246E-03	-1.59720905E-03	-1.70642512E-10

RIDGE 7. VERTICAL DISPLACEMENT, DY, IN INCHES.

4.96033142E-02	7.59138072E-02	1.03509124E-01	1.21008660E-01	1.26932010E-01
1.21008662E-01	1.03509128E-01	7.59138127E-02	4.06033207E-02	7.18573140E-09

RIDGE 7. LONGITUDINAL DISPLACEMENT, DX, IN INCHES.

-1.87460083E-02	-1.59300576E-02	-1.17311311E-02	-6.27490752E-03	-5.49578733E-10
-6.27490651E-03	-1.17311303E-02	-1.59301570E-02	-1.87460079E-02	-1.98362590E-02

RIDGE 7. ROTATION, RO, IN RADIANS.

3.40687206E-04	6.53710410E-04	8.86538272E-04	1.03008928E-03	1.08125477E-03
1.03008930E-03	8.86538306E-04	6.53710456E-04	3.40687266E-04	5.56922086E-11

STRUCTURE NUMBER 1. LOADING CONDITION NUMBER 1

FORCE MATRIX SELEAD(8,10,6) FORMED BY ADDING MATRICES SELEM(8,10,6) FOR N=1,11.

THE FORCES BELOW ARE GIVEN AT INTERVALS OF .1(SPAN LENGTH) ALONG THE EDGES OF EACH PLATE.

PLATE 1	FORCE 1				
	-4.71540523E-07	-8.94986998E-07	-1.22924619E-06	-1.44465339E-06	-1.51919085E-06
	-1.44465341E-06	-1.22924424E-06	-8.94987063E-07	-4.71540601E-07	-8.18401405E-14
PLATE 1	FORCE 2				
	-3.52793627E-07	-6.55559587E-07	-9.01197100E-07	-1.03472265E-06	-1.09840767E-06
	-1.03472266E-06	-9.01197135E-07	-6.55559631E-07	-3.52793689E-07	-5.63479037E-14
PLATE 1	FORCE 3				
	-3.56401955E-08	-6.71536354E-08	-9.22871630E-08	-1.07449952E-07	-1.13430360E-07
	-1.07449954E-07	-9.22871666E-08	-6.71536401E-08	-3.56402016E-08	-5.95424981E-15
PLATE 1	FORCE 4				
	-3.56401955E-08	-6.71536354E-08	-9.22871630E-08	-1.07449952E-07	-1.13430360E-07
	-1.07449954E-07	-9.22871666E-08	-6.71536401E-08	-3.56402016E-08	-5.95424981E-15
PLATE 1	FORCE 5				
	7.16068111E-09	5.95228074E-09	4.85321439E-09	2.77632533E-09	1.51667814E-16
	2.77632510E-09	4.85321428E-09	5.95228073E-09	7.16068097E-09	7.80710252E-09
PLATE 1	FORCE 6				
	1.24446928E 01	1.07766878E 01	8.67163714E 00	5.58352224E 00	6.15017334E-07
	5.58352158E 00	8.67163674E 00	1.07766875E 01	1.24446926E 01	1.42313719E 01
PLATE 1	FORCE 7				
	3.11772660E-08	6.13253813E-08	8.50848355E-08	1.02646140E-07	1.06578227E-07
	1.02646142E-07	8.50848389E-08	6.13253863E-08	3.11772709E-08	5.81643739E-15
PLATE 1	FORCE 8				
	2.33036665E 01	1.97310282E 01	2.02141177E 01	2.14849294E 01	1.95511078E 01
	2.14849298E 01	2.02141169E 01	1.97310293E 01	2.33036652E 01	8.29752102E-06
PLATE 2	FORCE 1				
	-3.43705221E-07	-6.67217758E-07	-9.13030682E-07	-1.09566159E-06	-1.14152454E-06
	-1.09566161E-06	-9.13030517E-07	-6.67217811E-07	-3.43705275E-07	-6.41954576E-14
PLATE 2	FORCE 2				
	2.58980910E 00	5.02406054E 00	6.77036016E 00	7.82329181E 00	8.21040440E 00
	7.82329192E 00	6.77036041E 00	5.02406088E 00	2.58980958E 00	4.03415463E-07
PLATE 2	FORCE 3				
	1.09044583E-01	2.11539370E-01	2.85067767E-01	3.29401725E-01	3.45701201E-01
	3.29401730E-01	2.85067778E-01	2.11539384E-01	1.09044603E-01	1.69859206E-08
PLATE 2	FORCE 4				
	1.09044583E-01	2.11539370E-01	2.85067767E-01	3.29401725E-01	3.45701201E-01
	3.29401730E-01	2.85067778E-01	2.11539384E-01	1.09044603E-01	1.69859206E-08
PLATE 2	FORCE 5				
	-1.24446928E 01	-1.07766878E 01	-8.67163715E 00	-5.58352224E 00	-6.15017335E-07
	-5.58352158E 00	-8.67163674E 00	-1.07766876E 01	-1.24446926E 01	-1.42313720E 01
PLATE 2	FORCE 6				
	-2.91701749E 00	-2.51261487E 00	-1.97458799E 00	-1.21547194E 00	-1.27654040E-07
	-1.21547179E 00	-1.97458788E 00	-2.51261481E 00	-2.91701745E 00	-3.24582158E 00
PLATE 2	FORCE 7				
	2.32415931E 01	1.96106115E 01	2.00518461E 01	2.12974213E 01	1.93543217E 01
	2.12974217E 01	2.00518453E 01	1.96106127E 01	2.32415918E 01	8.28785154E-06
PLATE 2	FORCE 8				
	-2.28827143E 01	-1.89628151E 01	-1.91950435E 01	-2.03143188E 01	-1.83288389E 01
	-2.03143194E 01	-1.91950427E 01	-1.89628161E 01	-2.28827129E 01	-8.22379197E-06
PLATE 3	FORCE 1				
	-2.58980942E 0	-5.02406115E 00	-6.77036100E 00	-7.82329279E 0	-8.21040544E 00
	-7.82329241E 0	-6.77036128E 00	-5.02406149E 00	-2.58980990E 0	-4.03415718E-07

PLATE 3	FORCE 2				
	-1.14400201E 00	-2.285[illegible]11E 00	-3.014234[illegible]E 00	-3.41[illegible]439E 00	-3.58385263E 00
	-3.41855444E 00	-3.[illegible]234[illegible]E 00	-2.28580525E 00	-1.144002[illegible]E 00	-1.51474093E-07
PLATE 3	FORCE 3				
	-1.57213113E-01	-3.[illegible]7783843E-01	-4.119829[illegible]E-01	-4.73340935E-01	-4.96600341E-01
	-4.73340942E-01	-4.11983000E-01	-3.[illegible]7783863E-01	-1.57213144E-01	-2.33637816E-08
PLATE 3	FORCE 4				
	-1.57213113E-01	-3.[illegible]7783843E-01	-4.11982985E-01	-4.73340935E-01	-4.96600341E-01
	-4.73340942E-01	-4.11983000E-01	-3.[illegible]7783863E-01	-1.57213144E-01	-2.33637816E-08
PLATE 3	FORCE 5				
	2.91701757E 00	2.51261494E 00	1.97458803E 00	1.21547197E 00	1.27654042E-07
	1.21547161E 00	1.97458793E 00	2.51261488E 00	2.91701753E 00	3.26582167E 00
PLATE 3	FORCE 6				
	1.25374137E-02	1.18876161E-02	1.37809399E-02	1.35991834E-02	1.99970254E-09
	1.35991824E-02	1.37809403E-02	1.18876167E-02	1.25374137E-02	2.02854009E-02
PLATE 3	FORCE 7				
	-2.29332292E 01	-1.90370811E 01	-1.92871391E 01	-2.04173968E 01	-1.84339456E 01
	-2.04173972E 01	-1.92871383E 01	-1.90370822E 01	-2.29332268E 01	-8.23665840E-06
PLATE 3	FORCE 8				
	2.34873549E 01	2.00670743E 01	2.06559744E 01	2.19891834E 01	2.00770086E 01
	2.19891838E 01	2.06559736E 01	2.00670754E 01	2.34873527E 01	8.32911166E-06
PLATE 4	FORCE 1				
	1.14400201E 00	2.285[illegible]11E 00	3.014234[illegible]E 00	3.41855437E 00	3.58385261E 00
	3.41855442E 00	3.[illegible]234[illegible]E 00	2.28580524E 00	1.14400225E 00	1.51474092E-07
PLATE 4	FORCE 2				
	2.83141344E 00	5.47410057E 00	7.38127369E 00	8.53544432E 00	8.95684803E 00
	8.53544444E 00	7.38127396E 00	5.47410104E 00	2.83141395E 00	4.46086933E-07
PLATE 4	FORCE 3				
	1.67385914E-01	3.26732876E-01	4.37705625E-01	5.03326263E-01	5.28029503E-01
	5.03326271E-01	4.37705641E-01	3.26732898E-01	1.67385946E-01	2.51604643E-08
PLATE 4	FORCE 4				
	1.67385914E-01	3.26732876E-01	4.37705625E-01	5.03326263E-01	5.28029503E-01
	5.03326271E-01	4.37705641E-01	3.26732898E-01	1.67385946E-01	2.51604643E-08
PLATE 4	FORCE 5				
	-1.25375057E-02	-1.[illegible]876[illegible]E-02	-1.37809965E-02	-1.35992129E-02	-1.99970514E-09
	-1.35992123E-02	-1.37[illegible]9965E-02	-1.18876953E-02	-1.25375057E-02	-2.02854974E-02
PLATE 4	FORCE 6				
	2.73422432E 00	2.35[illegible]41E 00	1.45006499E 00	1.13797835E 00	1.19436249E-07
	1.13797853E 00	1.35[illegible]E 00	2.35402335E 00	2.73422487E 00	3.06016988E 00
PLATE 4	FORCE 7				
	2.34360335E 01	2.[illegible]E 01	2.06014244E 01	2.19301842E 01	2.00210479E 01
	2.19301847E 01	2.[illegible]E 01	2.06017712E 01	2.34360082E 01	8.31164051E-06
PLATE 4	FORCE 8				
	-2.30956474E 01	-1.[illegible]E 01	-1.93190045E 01	-2.04466995E 01	-1.84524503E 01
	-2.04467003E 01	-1.[illegible]E 01	-1.93183265E 01	-2.30956465E 01	-8.26628952E-06
PLATE 5	FORCE 1				
	-2.83141331E 00	-5.47411[illegible]E 00	-7.38127336E 00	-8.53544394E 00	-8.95684763E 00
	-8.53544405E 00	-7.38127365E 00	-5.47410080E 00	-2.83141383E 00	-4.46086911E-07
PLATE 5	FORCE 2				
	-2.31557547E-07	-6.42393581E-07	-6.27644423E-07	-7.42979889E-07	-7.81990821E-07
	-7.42978402E-07	-6.27644423E-07	-6.42393521E-07	-2.31557585E-07	-4.04333778E-14
PLATE 5	FORCE 3				
	-1.19217412E-01	-2.30[illegible]E-01	-3.10790423E-01	-3.59387143E-01	-3.77130458E-01
	-3.59387149E-01	-3.10790494E-01	-2.30488473E-01	-1.19217434E-01	-1.87826084E-08
PLATE 5	FORCE 4				
	-1.19217412E-01	-2.30[illegible]E-01	-3.10790423E-01	-3.59387143E-01	-3.77130458E-01
	-3.59387149E-01	-3.10790494E-01	-2.30488473E-01	-1.19217434E-01	-1.87826084E-08

PLATE 5	FORCE 5				
	-2.73422487E 01	-2.33[illegible]37E 00	-1.45006496E 00	-1.13797866E 00	-1.19416247E-07
	-1.13797452E 01	-1.[illegible]496E 01	-2.35492031E 00	-2.73422482E 00	-3.06016082E 00
PLATE 5	FORCE 6				
	-1.24221754E 01	-1.07543993E 01	-8.66187230E 00	-5.58278503E 00	-6.15525549E-07
	-5.58278497E 00	-8.66187190E 00	-1.07583991E 01	-1.24221756E 01	-1.42126084E 01
PLATE 5	FORCE 7				
	-2.29817414E 01	-1.90262432E 01	-1.92475543E 01	-2.03650981E 01	-1.83669030E 01
	-2.03650983E 01	-1.92476635E 01	-1.90262443E 01	-2.29817400E 01	-8.26267426E-06
PLATE 5	FORCE 8				
	2.32957423E 01	1.96627707E 01	2.01091300E 01	2.13593172E 01	1.94137199E 01
	2.13593176E 01	2.01091292E 01	1.96627719E 01	2.32957415E 01	8.30601655E-06
PLATE 6	FORCE 1				
	8.95533474E-08	1.79861546E-07	2.76836544E-07	3.35884805E-07	3.58122634E-07
	3.35884811E-07	2.76836558E-07	1.79861563E-07	8.95534125E-08	1.52890929E-14
PLATE 6	FORCE 2				
	-1.92437393E-07	-3.59608901E-07	-4.84537485E-07	-5.41209007E-07	-5.86966053E-07
	-5.41209016E-07	-4.84538802E-07	-3.59608927E-07	-1.92437424E-07	-3.36459351E-14
PLATE 6	FORCE 3				
	-3.85660980E-10	-7.58667331E-11	1.41877643E-09	2.39938449E-09	2.78123480E-09
	2.39938459E-09	1.41877669E-09	-7.58665763E-11	-3.85660993E-10	-1.04054345E-16
PLATE 6	FORCE 4				
	-3.85660980E-10	-7.58667331E-11	1.41877643E-09	2.39938449E-09	2.78123480E-09
	2.39938459E-09	1.41877669E-09	-7.58665763E-11	-3.85660993E-10	-1.04054345E-16
PLATE 6	FORCE 5				
	1.24221757E 01	1.07543993E 01	8.66187228E 00	5.58278562E 00	6.15525548E-07
	5.58278496E 00	8.66187188E 00	1.07583990E 01	1.24221755E 01	1.42126084E 01
PLATE 6	FORCE 6				
	-7.44843321E-09	-6.21373232E-09	-4.97973461E-09	-2.81584028E-09	-2.42009595E-16
	-2.81585980E-09	-4.97973431E-09	-6.21373220E-09	-7.44843297E-09	-8.07631295E-09
PLATE 6	FORCE 7				
	2.33749020E 01	1.98032442E 01	2.02953724E 01	2.15743434E 01	1.96372463E 01
	2.15743439E 01	2.02953716E 01	1.98032454E 01	2.33749007E 01	8.32078414E-06
PLATE 6	FORCE 8				
	1.96097486E-08	3.64080349E-08	5.16548846E-08	6.02710842E-08	6.35081960E-08
	6.02710850E-08	5.16548870E-08	3.64080372E-08	1.96097522E-08	2.96694339E-15

STRUCTURE NUMBER 1. LOADING CONDITION NUMBER 1

LONGITUDINAL STRESS MATRIX EXTRAN(12,10) FORMED BY ADDING MATRICES EXTRAN(12,10) FOR I=1,11.

THE STRESSES BELOW ARE GIVEN AT INTERVALS OF .1(SPAN LENGTH) ALONG THE EDGES OF EACH PLATE.

PLATE 1	EDGE 1				
	-1.93924144E 03	-3.44086280E 03	-4.51928090E 03	-5.16753036E 03	-5.38142259E 03
	-5.16753042E 03	-4.51928104E 03	-3.44086302E 03	-1.93924217E 03	-3.54275122E-04
PLATE 1	EDGE 2				
	2.30630862E 03	3.94743140E 03	5.14513279E 03	5.87113091E 03	6.09392790E 03
	5.87113100E 03	5.14513295E 03	3.94743166E 03	2.30630893E 03	4.48152836E-04
PLATE 2	EDGE 1				
	2.30589893E 03	3.94663665E 03	5.14406180E 03	5.86989336E 03	6.09262911E 03
	5.86989345E 03	5.14406196E 03	3.94663691E 03	2.30589925E 03	4.48089018E-04
PLATE 2	EDGE 2				
	-2.53164330E 03	-4.34642616E 03	-5.66847778E 03	-6.46906732E 03	-6.71430962E 03
	-6.46906741E 03	-5.66847795E 03	-4.34642644E 03	-2.53164365E 03	-4.89389715E-04
PLATE 3	EDGE 1				
	-2.53197469E 03	-4.34691632E 03	-5.66908601E 03	-6.46974763E 03	-6.71700332E 03
	-6.46974772E 03	-5.66908619E 03	-4.34691660E 03	-2.53197704E 03	-4.89468034E-04
PLATE 3	EDGE 2				
	2.57893270E 03	4.43150392E 03	5.78114649E 03	6.59850592E 03	6.85132590E 03
	6.59850601E 03	5.78114667E 03	4.43150420E 03	2.57893305E 03	4.97920732E-04
PLATE 4	EDGE 1				
	2.57859052E 03	4.43117719E 03	5.78078910E 03	6.59811652E 03	6.85095669E 03
	6.59811662E 03	5.78078928E 03	4.43117747E 03	2.57859084E 03	4.97815422E-04
PLATE 4	EDGE 2				
	-2.53560502E 03	-4.35254084E 03	-5.67611056E 03	-6.47759119E 03	-6.72503926E 03
	-6.47759128E 03	-5.67611073E 03	-4.35254112E 03	-2.53560537E 03	-4.93257375E-04
PLATE 5	EDGE 1				
	-2.53542490E 03	-4.35218073E 03	-5.67563569E 03	-6.47705262E 03	-6.72447464E 03
	-6.47705271E 03	-5.67563586E 03	-4.35218101E 03	-2.53542515E 03	-4.93233514E-04
PLATE 5	EDGE 2				
	2.31239144E 03	3.95784805E 03	5.15869536E 03	5.88659402E 03	6.10997583E 03
	5.88659411E 03	5.15869552E 03	3.95784830E 03	2.31239215E 03	4.49331224E-04
PLATE 6	EDGE 1				
	2.31291429E 03	3.95877517E 03	5.15992456E 03	5.88800924E 03	6.11145111E 03
	5.88800932E 03	5.15992472E 03	3.95877543E 03	2.31291491E 03	4.49436691E-04
PLATE 6	EDGE 2				
	-1.94572818E 03	-3.45252278E 03	-4.53473527E 03	-5.18529904E 03	-5.39895989E 03
	-5.18529911E 03	-4.53473541E 03	-3.45252300E 03	-1.94572847E 03	-3.55468997E-04

CHAPTER VII

THEORETICAL AND EXPERIMENTAL RESULTS OF THE FOLDED SANDWICH PLATE MODELS COMPARISON AND DISCUSSION

Deflections of the 9.5-Foot Folded Sandwich Plate Model

The downward displacement of the 9.5-foot model due to the compressibility of the plywood supports and the possible deflection of the beams under the supports (Fig. 49) has been estimated at 5% of the midspan deflections by considering theoretically the elastic compressibility of the plywood supports. The experimental deflections given in Chapter IV have been revised and compared with the corresponding theoretical ones as shown in Figures 129 to 135, inclusive.

Figure 129 compares the deflections for the case where ridge 2 to 6 (Fig. 44) are uniformly loaded with 2260 lbs. (Fig. 58). The percentage difference varies from about 2% at one external ridge to about 10.5% at the middle ridge. The experimental deflections for this test have been presented in Figure 63.

The deflections, due to loading applied at the bottom ridges only, are compared in Figure 130. The percentage difference varies from 5% at one exterior ridge to 15% at the middle ridge.

When the load was applied at ridges 3 and 5 the experimental and theoretical deflections differed by 4% to 8% for the five inner ridges (Fig. 131); the difference was considerably larger at the two exterior ridges where the actual rotation of panels 1 and 6 lagged behind the amount of rotation given by the theory. This discrepancy was, undoubtedly, due to the fact that the ridges were not completely rigid. It must be noted, here, that the connecting channels consisted of two components welded together at alternate four-inch intervals (Fig. 46).

From Figure 131, it can be seen that this loading condition tends to deflect the model making it concave upward transversally.

Figure 132 compares the deflections resulting from a load of 3980 lbs., uniformly distributed along ridge 5. The percentage difference varies from 0% to 7% except for the exterior ridge (No. 7) where the theoretical deflection is .026" and the experimental one is .065". The joint at ridge 6 fails to rotate the panel upward in the test. It would seem that the angle between panels 5 and 6 increases due to the flexibility of the joint.

The above argument applies equally well to the results shown in Figure 133. Since the same load of 3980 lbs. has been applied along ridge 3, symmetrically opposite to ridge 5, the theoretical and experimental deflections of

symmetrically opposite ridges remain essentially the same as in the previous test.

Figure 134 shows the deflections due to a load of 2550 uniformly distributed along ridge 2. The percentage difference are rather small except for ridges 1 and 2, where the theoretical deflections are from 20% to 25% smaller than the experimental ones. The same load of 2550 lbs. is then applied at ridge 6, symmetrically opposite to ridge 2; the results are shown in Figure 135. The similarity of Figures 134 and 135 is seen when deflections at symmetrically opposite ridges are compared.

It should be noted that ridges 1 and 7 had no connecting channels. As a result, minor local delaminations occurred along these unprotected edges during the assembling operation and developed further as the model was loaded. Hence, the stiffness of the outside panels was lowered, thus contributing to large experimental deflections in these regions.

The first indications of failure occurred in panel 6. It is interesting to see that the experimental deflections at panel 6 in Figure 135 are larger than those of panel 1 shown in Figure 134. It had been observed during the early stages of testing that the delaminations in plate 6 were more widely developed than those in plate 1.

Longitudinal Stresses of the 9.5-Foot Folded Sandwich Plate Model

An envelope for the maximum experimental longitudinal stresses, shown in Figure 76, is shown in solid lines in Figure 136; the distribution is assumed linear across the panels. The theoretical stresses, given by the computer results on page 238 are plotted on the same diagram in broken lines. The percentage difference between the theoretical and experimental stresses varies between 10% to 27%. The larger differences are found at the exterior ridges where delaminations and local buckling have occurred and the experimental stresses could not be developed. It has already been mentioned that the exterior ridges (1 & 7) had no reinforcing channels. The stresses discussed above occurred when the structure was loaded with loads of 2260 lbs. uniformly distributed along each of the five internal ridges.

A similar comparison of stresses is made in Figure 137 for the case where a load of 1600 lbs. is uniformly distributed along each of ridges 2, 4 and 6. The percentage differences vary from 0.4% to 9.7%. The larger differences occurred at ridges 2 and 6. It is interesting to see that the differences at ridges 1 and 7 are only 0.4% and 3.5% respectively; in the previous test they were 27% and 24% respectively.

It must be noted here that the test of Figure 137

was the second test performed on the structure and the delaminations at the outside ridges had not yet developed to a significant degree. The load was applied gradually with calibrated dead weights (Fig. 57) and was limited to a total of 4,800 lbs. The experimental results shown in Figure 136, on the other hand, were caused by the fourteenth test run on the structure. Delaminations had developed and propagated along ridges 1 and 7. A total load of 11,300 lbs. was applied with hydraulic rams and it was added at a faster rate than one would normally load dead weights.

In both Figures 136 and 137, the theoretical stresses are invariably larger than their corresponding experimental values. Consequently, a slight safety factor is inherent in the theory put forth in Chapter VI.

Deflections of the 19-Foot Folded Sandwich Plate Model

In Figures 138, 139 and 140, comparison is made between experimental and theoretical deflections for the surface loadings of 23.4, 40, and 49.4 psf., respectively. The experimental deflections for these cases have been presented in Figures 96, 97 and 98, in Chapter V. The correction of 5% in the deflections was not made for the 19-foot model, since the load was applied by means of a pressure chamber built on top of the structure; the pressure loads caused no net reactions at the supports.

The theoretical and experimental deflections due to a load of 23.4 psf. (Fig. 138) compare quite closely; the difference varies from 1.3% to 15.1%. When the load was increased to 40 psf, in a subsequent test, (Fig. 139), the difference of the deflections varied from 3.9% at the middle ridge to 21.5% at exterior ridge 7. At this load, ridge 1 was partially supported by the side of the pressure box; it can be seen from Figure 139 that the deflection at ridge 1 is considerably less than the deflection at ridge 7.

The pressure was then extended to 49.4 psf. The percentage difference between experimental and theoretical deflections varied between 2.5% and 43.7% (Fig. 140). The excessive deflections occurred at ridge 7, and would indicate that the core of panel 7 was stressed beyond its elastic limit. Ridge 1 continued to be partially supported laterally.

It may be concluded here that the theory can be used to predict the deflections for this type of structure with reasonable accuracy. One must be careful, however, not to exceed the elastic shear deformation of the core. This deformation is most critical at exterior panels.

Longitudinal stresses of the 19-Foot Folded Plate Model

Comparison of theoretical and experimental longitudinal stresses is made in Figures 141, 142, 143 and 144 for loading conditions of 13, 23.4, 26, and 39 psf, respectively.

The experimental stress distributions in the top and bottom facings of the model, for these tests, have been discussed in Chapter V. In Figures 141 to 144, inclusive, the envelopes of maximum experimental stresses are represented in solid lines and the corresponding theoretical stresses in broken lines.

At a uniform load of 13 psf. (Fig. 141), the theoretical stresses are generally on the conservative side, except for those at the middle ridge, where their values are 20% lower than the experimental stresses.

Figure 142 shows the theoretical stresses at the four exterior ridges (1, 2, 6 and 7) to be on the conservative side by 1.04% to 37.7%. At the three interior ridges (3, 4 and 5) the theoretical stresses are from 5.2% to 11.3% lower than the experimental values. The load in this test was 23.4 psf.

In the following comparison (Fig. 143), the stress distribution is similar to that of Figure 142. The load in this test was 26 psf. It can be seen from these two figures (Fig. 142 and 143) that the percentage differences of the theoretical and experimental stresses differ considerably from those of the previous test. The test of Figure 143 was carried out 17 tests after the test of Figure 142; the intervening tests had had intermediate supports which may have caused residual stresses and disturbed the behaviour of the

structure.

When the model was loaded with 39 psf., ridge 1 became partially supported by the side of the pressure box. Consequently, the experimental stresses at this ridge are much smaller than those at ridge 7 (Fig. 144). These stresses are 36.6% and 12.2% smaller than their corresponding theoretical values at ridges 1 and 7, respectively. Generally, the theoretical stresses remain on the conservative side except for those at the middle ridge, which are 25% lower than the experimental stresses.

The percentage differences between the experimental and theoretical results may be explained by the following reasons:

(1) The stresses obtained from the strain gauges included local stresses which might have been caused by stress concentrations along the ridges;

(2) The compressibility of the styrolite core (See Chapter I) would permit local bending of the facings under surface load. It must be remembered that the gauges were mounted on the facings, about two inches from the longitudinal axis of the ridges;

(3) The ridges were assumed completely rigid in the theory; in practice, they were welded at alternate

intervals of about four inches;

(4) Some inaccuracies arise from the resolution of uniform surface load into joint loads;

(5) Secondary moments in the facings (See Fig. 29), arising from shear deformations, have not been considered in the theory. These moments are particularly significant in ridges 2 and 6, due to the large shear deformations in panels 1 and 6 respectively.

CHAPTER VIII

CONCLUSIONS AND RECOMMENDATIONS

Conclusions

From the foregoing study, the following conclusions may be drawn:

1. Sandwich elements can behave as excellent load-carrying components in structural folded plate systems. The 9.5-foot model carried an ultimate load of 178 psf; the 19-foot model, an ultimate load of 75.4 psf.

2. Sandwich structures are relatively light. The 9.5-foot and 19-foot models covered areas of about 100 and 200 sq. ft., respectively; yet, both could be easily lifted by a few men.

3. The distribution of longitudinal stresses at the midspan sections of the structures tested was essentially linear across every plate; the location of the neutral axis varied from panel to panel.

4. At the cross sections of the models, one foot away from the face of the support, the direction of the principal stresses in the top facing varied from 2 to 9 degrees from the direction of the principal stresses in the bottom facing. Maximum transversal shear occurred in planes oriented at 2 to 15 degrees from the transversal planes of the plates.

5. The deflections at midspan of the 9.5-foot model remained much lower than the ratio, (span length in inches)/360, up to the last loading stages preceeding failure. The deflections of the 19-foot model exceeded the ratio, (span length in inches)/180, only at the unsupported ridges and for loads above 35 psf.

6. The behaviour of these structures can be closely predicted by the theory set forth in Chapter VI. The percentage differences between experimental and theoretical results seldom exceeded 15%. See Chapter VII.

7. The computer program, outlined in Chapter VI, can analyse, consecutively, several structures with different loading conditions within minutes.

8. Roof structures made with sandwich components can stand severe weather conditions without requiring the conventional asphalt roof covering if the joints are properly sealed. Since failure, the 19-foot model has been exposed to outside weather conditions for the last winter (1967-68); it has shown no deterioration.

9. The load-carrying capacity of the 9.5-foot model could have been increased by properly reinforcing the high shear stress regions near the supports and by improving the bond between the honeycomb core and the facings of the sandwich panels.

10. The buckling of the 19-foot model would have been retarded if the core had had greater stiffness in the flatwise direction to stabilize the facings. The flatwise yield strength of the styrolite used in this model was only 12 psi. Compression failures of the core, above the supports, was prevented by reinforcing the ends of the panels with aluminum channels.

11. When sandwich structures rest on point supports, a reinforcing frame should be provided around

the bearing ends, otherwise the load-carrying capacity of these structures is greatly reduced.

12. Connecting channels greatly contribute to the strength of the structure since they are generally situated at points of extreme stresses.

13. The type of connection, shown in Figure 50, can easily be made waterproof. The connection is not completely rigid, however, since the two composing channels are welded together at alternate four-inch intervals. A continuous weld would cause the resulting connecting channel to twist about its longitudinal axis.

14. The core for the sandwich panels must be selected with care: it must have enough flatwise strength to carry the load of working men and to prevent buckling of the facings; it must develop a good bond with the facings. Styrolite has little flatwise rigidity; honeycomb makes contact over only 5% of the surface of the facings.

15. Different shear tests yield different shear stiffness for the same type of sandwich. The shear stiffness of sandwich panels should be selected from the test method which most closely

approaches the loading conditions to which the panels are subjected in their parent structure.

16. The bending stiffness of sandwich panels depends mainly on the facings, when flexible cores such as honeycomb and styrolite are used.

17. In determining torsion rigidity constants, the sandwich panels must be well reinforced around the edges to avoid shear deformations.

18. When cores such as honeycomb and styrolite are used, the torsion rigidity of the sandwich panel is a function of the shear rigidities of the facings, only.

19. High edgewise compression stresses can be developed in the facings when the core and bond effectively stabilize the facings.

Recommendations

Because of its advantages (See Page 2), sandwich construction is most ideally suited for use in factory-prefabricated structural components. Serious consideration must, therefore, be given to the development of sandwich construction, since this is an age of prefabrication in the building industry.

The 1966 report of the National Commission on Technology, Automation and Economic Progress recommended prefabrication as one of the advanced production techniques which could be used to satisfy the heavy demand of sheltered space (45); the building industry quickly responded.

Apartments based on the mobile-home technology have been built. Each apartment is made up of two factory-prefabricated boxes (12' x 30') clustered around a utility core which contains bathrooms and kitchen appliances.

The concrete industry has introduced the "Techcrete" system of precast components. The system utilizes only three structural elements: floor planks of precast, prestressed, hollow-core concrete; precast, post-tensioned concrete bearing walls; and precast, prestressed shear walls. The components are assembled and made rigid by post-tensioned vertical rods and by grout pumped into the joints. At present (1968) a 500-room hotel in San Antonio, Texas, is being assembled. The components consist of modules precast as rooms which are completely finished and furnished before being hoisted into place (30).

The steel industry has introduced the storey-high, staggered steel truss scheme. The trusses support floor systems at both the top and bottom chords and are staggered so that a truss on the fourth storey is located above the middle of the span between two third-storey trusses. As a result, the clear span between trusses is double the span of the floor planks.

A system approach has also been developed in the building industry. The system aims for long-term economy by introducing structural compatibility among components such as ceiling, lighting, heating, ventilation, air conditioning, and partition systems (45).

Canada's Department of Industry is promoting, through the BEAM program, the concept of modular co-ordination to facilitate the mass production of building components and ultimately industrialize the building process. (1966 Annual Review, Department of Industry, Ottawa, Canada).

Sandwich construction could be effectively used in most of the above examples of prefabrication, reducing framework weights and foundation requirements. The light weight of the units would reduce transportation costs; the relatively small thickness of sandwich components would provide more usable space in the building.

Ultimately, after due study, the cry for space could be answered by putting buildings on the production line. A minimum number of basic elements could be made to assemble into buildings of different types and sizes. The components could incorporate plumbing, lighting, ducts, etc. and be made of such a size so that they could be easily transported to any part of the country or of the world. Because the same type of structure (a school, for example) would be produced many times, it would be feasible to devote full attention to the comfort, efficiency and function of the building at the design stage.

Many architects argue that standardization is futile, since a building becomes obsolete before leaving the drafting board. It must be remembered, however, that the desire to control most space per dollar will never change. A good design will become obsolete only when the function of the building changes; this type of change does not occur over a short period of time. Moreover, periodic improvements can be made in the design to meet new requirements.

As more and bigger building components are prefabricated, we move closer to the complete industrialization of the building process. For this process to be most successful it must exploit the advantages of sandwich construction.

Before sandwich construction can be effectively used, however, several aspects must be reviewed:

1. Proper selection of materials and adhesives;
2. Economical and rigid connections;
3. Stress distribution along the connections;
4. Mass production at low cost;
5. Fire rating requirements.

These problems remain a challenge to the design engineer. It is up to the industry and to the Government to see that new ideas are given a fair trial. The cry for space is acute. The ultimate market is a vast one.

LITERATURE CITED

1. Anderson, Melvin S., Optimum Proportions of Truss-Core and Web-Core Sandwich Plates Loaded in Compression, NASA, TN D-98.

2. Batdorf, S. B., A Simplified Method of Elastic Stability Analysis for Thin Cylindrical Shells, NACA, TR-874, 1947.

3. Batdorf, S. B. and Libove, Charles, A General Small-Deflection Theory for Flat Sandwich Plates, NASA, TR-899.

4. Batdorf, S. B. and Schildcrout, Murray, Critical Axial-Compressive Stress of a Curved Rectangular Panel with a General Chordwise Stiffner, NASA, TN 1661, Washington, 1948.

5. Batdorf, S. B., Stein, Manuel and Schildcrout, Murray, Critical Shear Stress of Curved Rectangular Panels, NASA, TN 1348, Washington, May, 1947.

6. Beam Program, Annual Review, 1966, Department of Industry, Canada.

7. Beaufait, Fred W., Analysis of Continuous Folded Plate Surface, Journal of the Structural Division, ASCE, Vol. 91, No. ST6, December, 1965.

8. Biggs, W. D. and Riley, V.R., Bending of Sandwich Beams - The Elastic Shear Modulus of Sandwich Building Core Materials, Transactions of the Engineering Institute of Canada, Vol. 8, No. A-12, Paper No: EIC-65-BR & STR 12.

9. Billington, P. David and Robert, Mark, Small Scale Model Analysis of Thin Shells, Journal of the American Concrete Institute, June, 1965, Proc. V. 62, No. 6.

10. Boley, Bruno A., Kemprur, Joseph, and Mayers, J., A Numerical Approach to the Instability Problem of Monocoque Cylinders, NACA, TN 2354, Washington, April, 1951.

11. Boyd, G. Murray, Effective Flange Width of Stiffened Plating in Longitudinal Bending, Engineering Journal, A.M.I.N.A., December 27th, 1946.

12. Buckling of Sandwich Cylinders of Finite Length under Uniform External Lateral Pressure, Forest Products Laboratory, U.S. Department of Agriculture, No. 1844-R, May, 1955.

13. Catchpole, E. J., Bonding and Sandwich Construction, The Aeroplane, June 1, 1961.

14. Cemal, A., Buckling of Sandwich Cylinder under Uniform Axial Compressive Load, Journal of Applied Mechanics, ASCE, June, 1951.

15. Chim, James, Cylindrical Shell Analysis Simplified by Beam Method, Journal of the American Concrete Institute, May, 1959, and December, 1959, Part II.

16. Clark, B. W., and Doble, R. J., Preliminary Investigation into Honeycomb Core Properties, Aero Research Ltd., Report, September, 1955.

17. Dale, F. A., and Smith, R. C. T., Grid Sandwich Panels in Compression, Australian Council for Aeronautics, Report ACA-16, April, 1945.

18. De Fries-Skene, Arnim, and Scordelis, A. C., Direct Stiffness Solution for Folded Plates, Journal of the Structural Division, ASCE, Vol. 90, No. ST4, August, 1964, Part I.

19. Dirkes, William E., High-Strength Structural Sandwich Construction, American Society of Mechanical Engineers, Paper No. 58 - MD - 10.

20. Donnell, L. H., Stability of Thin-Walled Tubes under Torsion, California Institute of Technology, NASA, Report No. TR 479.

21. Edgewise Compressive Strength of Flat Sandwich Constructions, ASTM Standards, Vol. 16, C364-61, p. 17.

22. Fahey, D. J., Dunlap, M. E. and Seidl, R. J., Thermal Insulation of Paper Honeycomb Cores and Sound Absorption of Sandwich Panels, Forest Products Laboratory, U.S. Department of Agriculture.

23. Fazio, P., Continuous Folded Plate Structures Under Uniform Load, M.A.Sc. Thesis, Department of Civil Engineering, University of Windsor, 1964.

24. Fazio, P., and Kennedy, J. B., Experimental Study of Continuous Two-Span Folded Plate Structures, Journal of Concrete and Constructional Engineering, December, 1966, p. 431 - 438.

25. Fialkorv, M. N., F.ASCE, Folded Plate Analysis by Minimum Energy Principle, Journal of the Structural Division, ASCE, June, 1962, ST. 3.

26. Flatwise Compressive Strength of Sandwich Cores, ASTM Standards, Vol. 16, C365-57, p. 21.

27. Flexure Test of Flat Sandwich Constructions, ASTM Standards, C393-62, p. 28.

28. Fulton, Robert E., Non-Linear Equations for a Shallow Unsymmetrical Sandwich Shell of Double Curvature, Department of Civil Engineering, University of Illinois, Urbana, Illinois, August, 1961.

29. Gerard, George, Bending Tests of Thin-Walled Sandwich Cylinders, Journal of Aeronautical Sciences, September, 1953.

30. Gillette, Roy W., Precast Boxes Stacked to Build 496-Room Hotel in Nine Months for HemisFair, Civil Engineer, ASCE, March, 1968.

31. Grayley, M. E., Shear Stiffness of Sandwich Panels - A Review of Test Methods, Journal of the Royal Aeronautical Society, Vol. 70, October, 1966.

32. Halsband, G., Galvanised Steel Sheet Roofing, Acier-Stahl-Steel, Vol. 21, No. 10, October, 1956, pp. 403-5.

33. Heath, W. G., Sandwich Construction, Correlation and Extension of Existing Theory of Flat Panels Subjected to Lengthwise Compression, Aircraft Engineering, July, 1960.

34. Hildebrand, F. B., Reissner, E., and Thomas, G. B., Notes on the Foundations of the Theory of Small Displacements of Orthotropic Shells, NASA, TN 1833.

35. Hoff, N. J. and Mautner, S. E., Bending and Buckling of Sandwich Beams, Journal of the Aeronautical Sciences, December, 1948.

36. Hoff, N. J. and Mautner, S. E., The Buckling of Sandwich-Type Panels, Journal of the Aeronautical Sciences, July, 1945.

37. Hoffman, G. A., Poisson's Ratio for Honeycomb Sandwich Cores, Rand Corporation, April, 1957, p. 945.

38. Holland, H., Sandwich Panels for Wing Tips, Aero Digest, Vol. 69, No. 6, December, 1954, pp. 36, 38, 40.

39. Hopkins, H. G. and Pearson, S., The Behaviour of Flat Sandwich Panels Under Uniform Transverse Loading, Royal Aircraft Establishment, Fornborough Report No. S.M.E. 3271, March, 1944.

40. Howard, H. B., The Five-Point Loading Shear Stiffness Test, Journal of the Royal Aeronautical Society, Vol. 66, September, 1962, p. 591.

41. Humke, R. K., Selection Guide for Sandwich Panel Adhesives, Product Engineering, May 26, 1958.

42. Kelsey, S., Gellantly, R. A., and Clark, B. W., The Shear Modulus of Foil Honeycomb Cores, Aircraft Engineering Journal, October, 1958.

43. Kennedy, J. B., and Fazio, P., Analysis of Continuous Folded Plate Structures, Transactions of the Engineering Institute of Canada, Vol. 9, No. A-3, Paper No. EIC-66-BR & ST9.

44. Kennedy, W. B., and Troxell, W. W., Study of Compression Panel, Supported on Four Edges, Formed of Corrugated Sheet with Flat Skin on Both Sides, NACA, Arr. No. 5803, Washington, June, 1945.

45. Kneeland, A. Godfrey, Jr., New Technology in Low-Income Housing, Civil Engineer, American Society of Civil Engineers, January, 1968.

46. Kommers, N. J. and Norris, C. E., Effects of Shear Deformation in the Core of a Flat Rectangular Sandwich Panel, Forest Products Laboratory, U.S. Department of Agriculture, Report No. 1583-A.

47. Kroll, Wilhelmina D., Mordfin, Leonard and Garland, William A., Investigation of Sandwich Construction under Lateral and Axial Loads, NACA, TN 3090.

48. Kuenzi, E. W., Mechanical Properties of Aluminum Honeycomb Cores, Forest Products Laboratory, U.S. Department of Agriculture, Report No. 1849, September, 1955.

49. Kuenzi, Edward W., Norris, Charles B., and Jenkinson, Paul M., Buckling Coefficients for Simply Supported and Clamped Flat, Rectangular Sandwich Panels under Edgewise Compression, Forest Products Laboratory, U.S. Department of Agriculture, December, 1964.

50. Kuo Tai Yen, Salerno, and Hoff, N. J., Buckling of Rectangular Sandwich Plates Subjected to Edgewise Compression with Loaded Edges Simply Supported and Unloaded Edges Clamped, NACA, TN 2556, Washington, January, 1957.

51. Langhaar, H. and Fefferman, R., Sandwich-Type Shear Panels of Wood-Aluminum Construction, Product Engineering, December, 1945.

52. Lewis, Wayne C., Deflection and Stresses in a Uniformly Loaded, Simply Supported, Rectangular Sandwich Plate, Forest Product Laboratory, U.S. Department of Agriculture, Report No. 1847-A.

53. Libove, Charles and Hubka, Ralph E., Elastic Constants for Corrugated-Core Sandwich Plates, NACA, TN 2289, Washington, February, 1951.

54. Long, J. W.,and Cremer, G. D., Sandwich Structures, Aircraft Production, Vol. 17, No. 11, January, 1955, pp. 22-31.

55. Lowy, Mortimer J., Afias, and Jaffee, Robert I., On the Development of Low-Cost, Formable, All-Metal Sandwich Panels with Corrugated Cores, Aerospace Engineering, November, 1961.

56. March, H. W., Behaviour of a Rectangular Sandwich Panel under a Uniform Lateral Load and Compressive Edge Loads, Forest Products Laboratory, U.S. Department of Agriculture, No. 1834.

57. March, H. W. and Kuenzi, Edward, Buckling of Cylinders of Sandwich Construction in Axial Compression, Forest Products Laboratory, U.S. Department of Agriculture, Report No. 1830, Revised, December, 1957.

58. Martin, Ignacio, J.M.ASCE, and Padilla, Narciso, J.M.ASCE, Precast Folded-plate Roof for a Paint Plant, Civil Engineering, ASCE, March, 1959.

59. Mush Tari, Kh. M., On the Domain of Application of Approximate Theories of Three-Layer, Applied Mechanics Review, Vol. 18, No. 1, p. 21.

60. Nardo, S. V., An Exact Solution for the Buckling Load of Flat Sandwich Panels with Loaded Edges Clamped, Journal of the Aeronautical Sciences, September, 1953.

61. Norris, Charles B. and Boller, Kenneth H., Transfer of Longitudinal Load from One Facing of a Sandwich Panel to the Other by Means of Shear in the Core, Forest Products Laboratories, U.S. Department of Agriculture, No. 1846.

62. O'Keefe, Philip, Aluminum Honeycomb Sandwich has ... Light Weight, High Strength, Good Stability, Uniform Density, Materials and Methods, December, 1952.

63. O'Sullivan, H. P., Double Block Shear Test for Foil Honeycomb Cores, Aircraft Engineering, Vol. 33, No. 385, March, 1961, p. 64-65.

64. Penzien, Joseph and Didriksson, Theodor, Effective Shear Modulus of Honeycomb Cellular Structure, AIAA Journal, Vol. 2, No. 3, March, 1964.

65. Phase I Report on Folded Plate Construction, Report of the Task Committee on Folded Plate Construction of the Committee on Masonry and Reinforced Concrete, George F. Booss, Chmn., Journal of the Structural Division, ASCE, Vol. 89, No. ST6, Proc. Paper 3741, December, 1963, p. 365.

66. Plantema, Frederick J. Sandwich Construction, The Bending and Buckling of Sandwich Beams, Plates and Shells, John Wiley and Sons, Inc., New York . London . Sydney.

67. Powell, Graham H., Comparison of Simplified Theories for Folded Plates, Journal of the Structural Division, ASCE, Vol. 91, No. ST6, December, 1965.

68. Raville, Milton E., Deflection and Stresses in a Uniformly Loaded, Simply Supported, Rectangular Sandwich Plate, Forest Products Laboratories, U.S. Department of Agriculture, No. 1962.

69. Reissner, Eric, Small Bending and Strengthening of Sandwich-Type Shells, NASA, Report No. TR-975.

70. Sanderson, Paul A. and Fischel, J. Robert, Corrugated Panels under Combined Compressions and Shear Head, Journal of the Aeronautical Sciences, June 17, 1939.

71. Saporvity, Alan D., Transverse Shear Stiffness for the Double "V" Corrugated-Core Sandwich Panel, Aerospace Engineering, September, 1959.

72. Scordelis, A. C., Matrix Formulation of the Folded Plate Equations, Journal of the Structural Division, ASCE, Vol. 86, No. ST-10, October, 1960.

73. Seide, Paul, Compressive Buckling of Flat Rectangular Metalite Type Sandwich Plates with Simply Supported Loaded Edges and Clamped Unloaded Edges, NACA, TN 2637, Washington, February, 1952.

74. Seide, Paul and Stowell, Elbridge Z., Elastic and Plastic Buckling of Simply Supported Solid-Core Sandwich Plates in Compression, NACA, Report 967.

75. Shalashilin, V. I., On the Analysis of Shells Made Out of Corrugated Material, Applied Mechanics Review, Vol. 18, No. 3, p. 194.

76. Sharma, S. P. and Goval, B. K., The Analysis of Continuous Folded Plates, An Extension of Whitney's Method, Indian Concrete Journal, December, 1963.

77. Shear Test in Flatwise Plane of Flat Sandwich Construction or Sandwich Cores, ASTM Standards, Vol. 16, C273-61, p. 6.

78. Silliman, John C., Elastic Stability Design Charts for Duraluminum Channels in Compression, Journal of the Aeronautical Sciences, June, 24-26, 1940.

79. Simpson, A. M., ASCE, Design of Folded Plate Roofs, Journal of the Structural Division, Proceedings of the American Society of Civil Engineers, (Proc. Paper 1508).

80. Spot-Welded Corrugated Sandwich Construction for Aircraft, Machinery, Vol. 94, June 10, 1959.

81. Stein, Manuel and Mayers, J., A Small-Deflection Theory for Curved Sandwich Plates, NACA, Report 1008, 1951.

82. Tai Yen, Kuo, Gunturkun, Sadettin and Pohle, Frederick V., Deflections of a Simply Supported Rectangular Sandwich Plate Subjected to Transverse Loads, NACA, TN 2581, Washington, December, 1951.

83. Timoshenko, S. Strength of Materials, Part I - Elementary Theory and Problems. Second Ed., D. Van Nostrand Co., Inc., 1940.

84. Timoshenko, S. and Goodier, J. N. Theory of Elasticity, Second Edition, 1951, McGraw-Hill.

85. Thurston, G. A., Bending and Buckling of Clamped Sandwich Plates, Journal of the Aeronautical Sciences, June, 1957.

86. Vishwanath, Tekal, Mhatre, Ramkrishna P. and Sutharamulu, Kareti, Test of a Ferro-Cement Precast Folded Plate, Journal of the Structural Division, ASCE, Vol. 91, No. ST6, December, 1965.

87. Volkersen, O., Die Neitkraft Verteilung in Sugbeans Pruchten Nietverbindungen Mit Konstanten Querschnitten, Luftfahrtforschung, Bano 15, p. 41, 1938.

88. Wang, Chi-Teh, Principle and Application of Complementary Energy Method for Thin Homogeneous and Sandwich Plates and Shells with Finite Deflections, NACA, TN 2620, Washington, February, 1952.

89. Wang, Chi-Teh, and Rao, G. V. R., A Study of an Analogous Model Giving the Non-Linear Characteristics in the Buckling Theory of Sandwich Cylinders, Journal of the Aeronautical Sciences, February, 1952.

90. Warren, Fred, Shear-Fatigue Properties of Various Sandwich Construction, Forest Products Laboratories, U.S. Department of Agriculture, No. 1837, July, 1952.

91. Wempner, G. A., Theory of Moderate Large Deflections of Thin Sandwich Shells, Transactions of the ASME, Paper No. 64-NA/APM-6.

92. Winter, George and Pei, Minglung, Hipped Plate Construction, Journal of the American Concrete Institute, Vol. 18, No. 5, January, 1947.

93. Witt, R. K., Hoppman, N. H. and Buxbaum, R. S., Determination of Elastic Constants of Orthotropic Materials with Special Reference to Laminates, ASTM Bulletin, TP 117-TP2001, December, 1953, p. 53-57.

94. Why Honeycomb in the First Place, American Machinist, Special Report No. 441, March 25, 1957.

95. Yitzhaki, David and Reiss, Max, Analysis of Folded Plates, Journal of the Structural Division, ASCE, ST-5, October, 1962.

APPENDIX
FIGURES

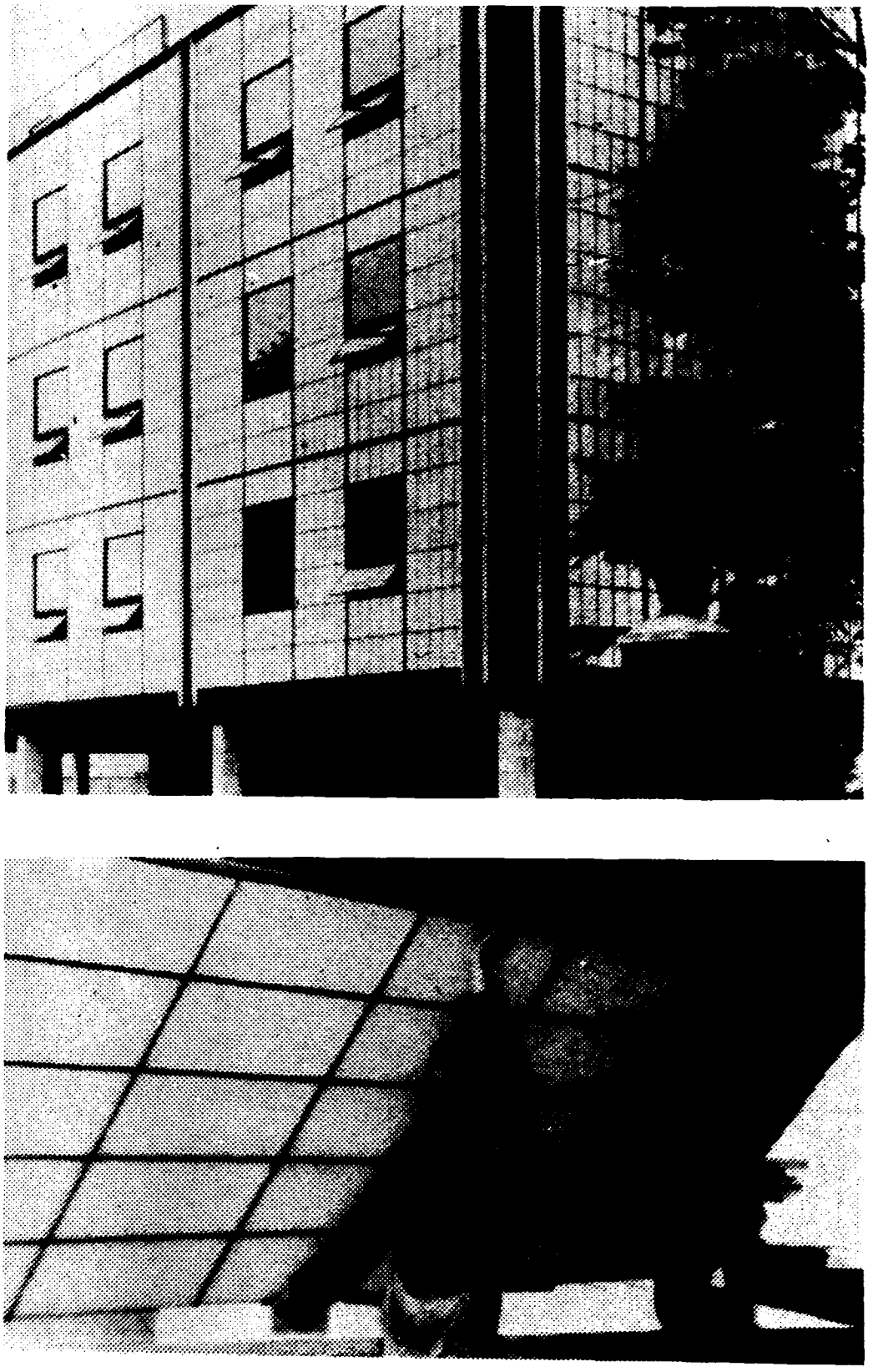

FIG. 1. FOUR STOREY BUILDING WITH SANDWICH CURTAIN WALLS

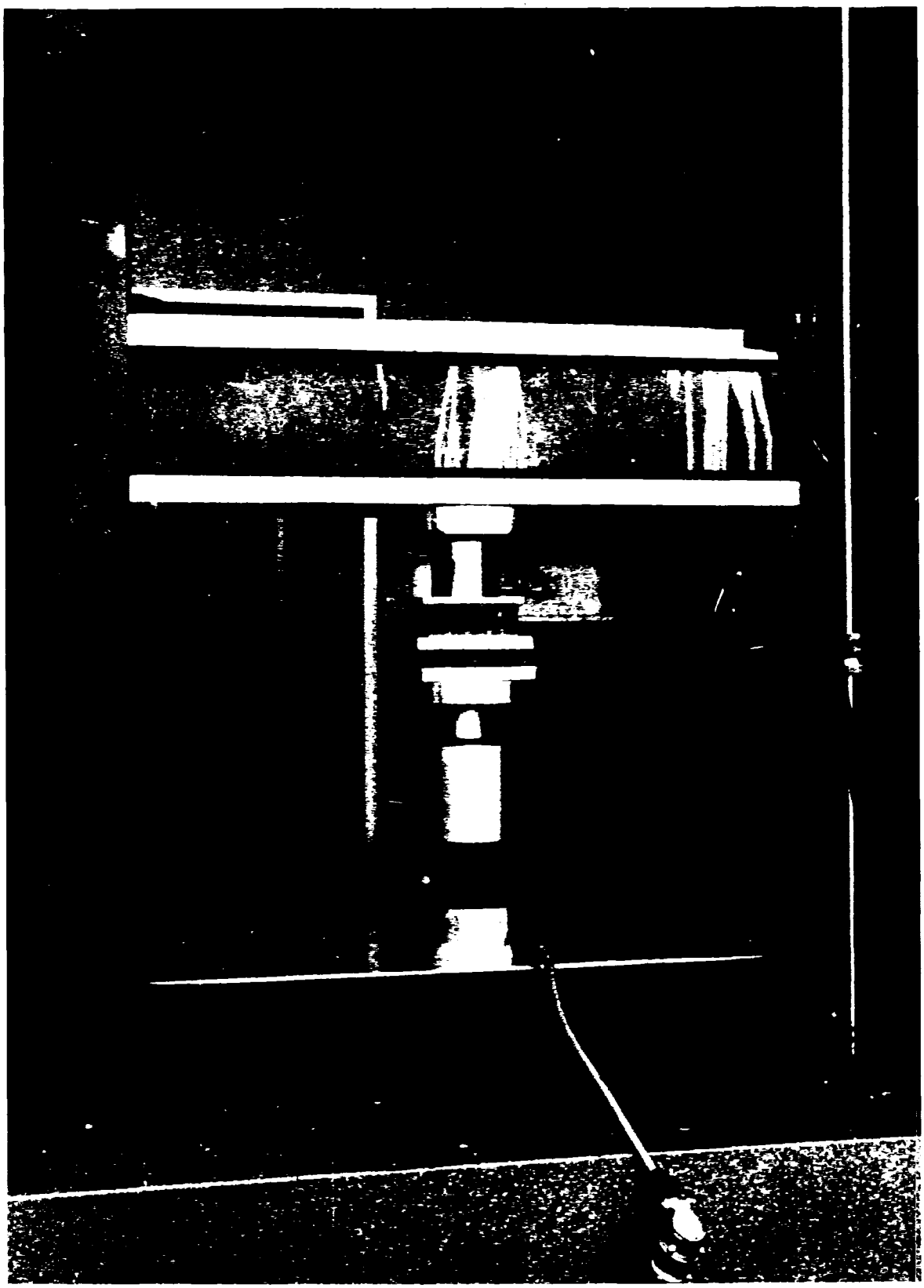

FIG. 2. FLATWISE COMPRESSION TEST ON A
3" x 3" x 1"
HONEYCOMB CORE SAMPLE

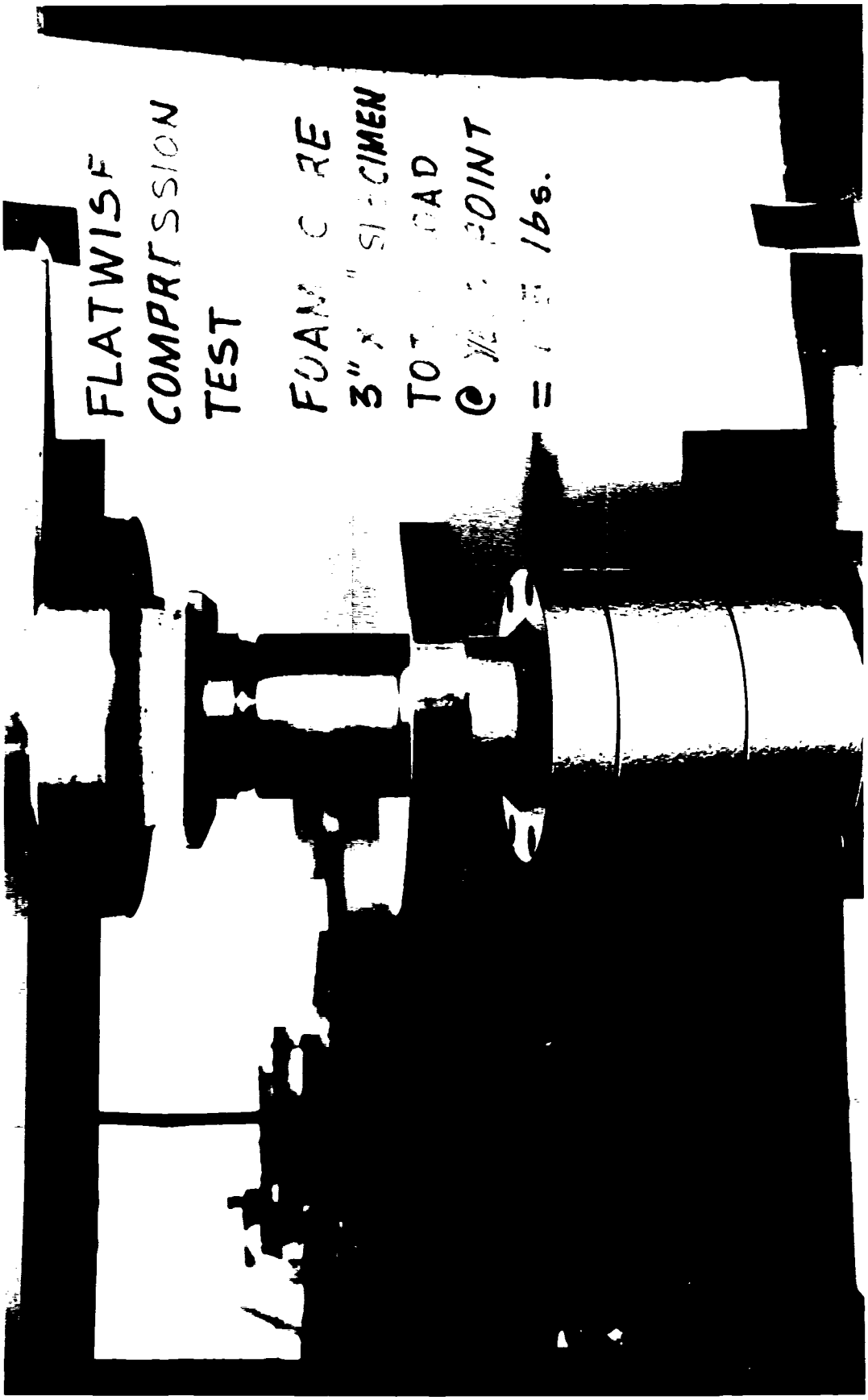

FIG. 3. FLATWISE COMPRESSION TEST ON A 3" x 3" x 1" STYROLITE CORE SAMPLE

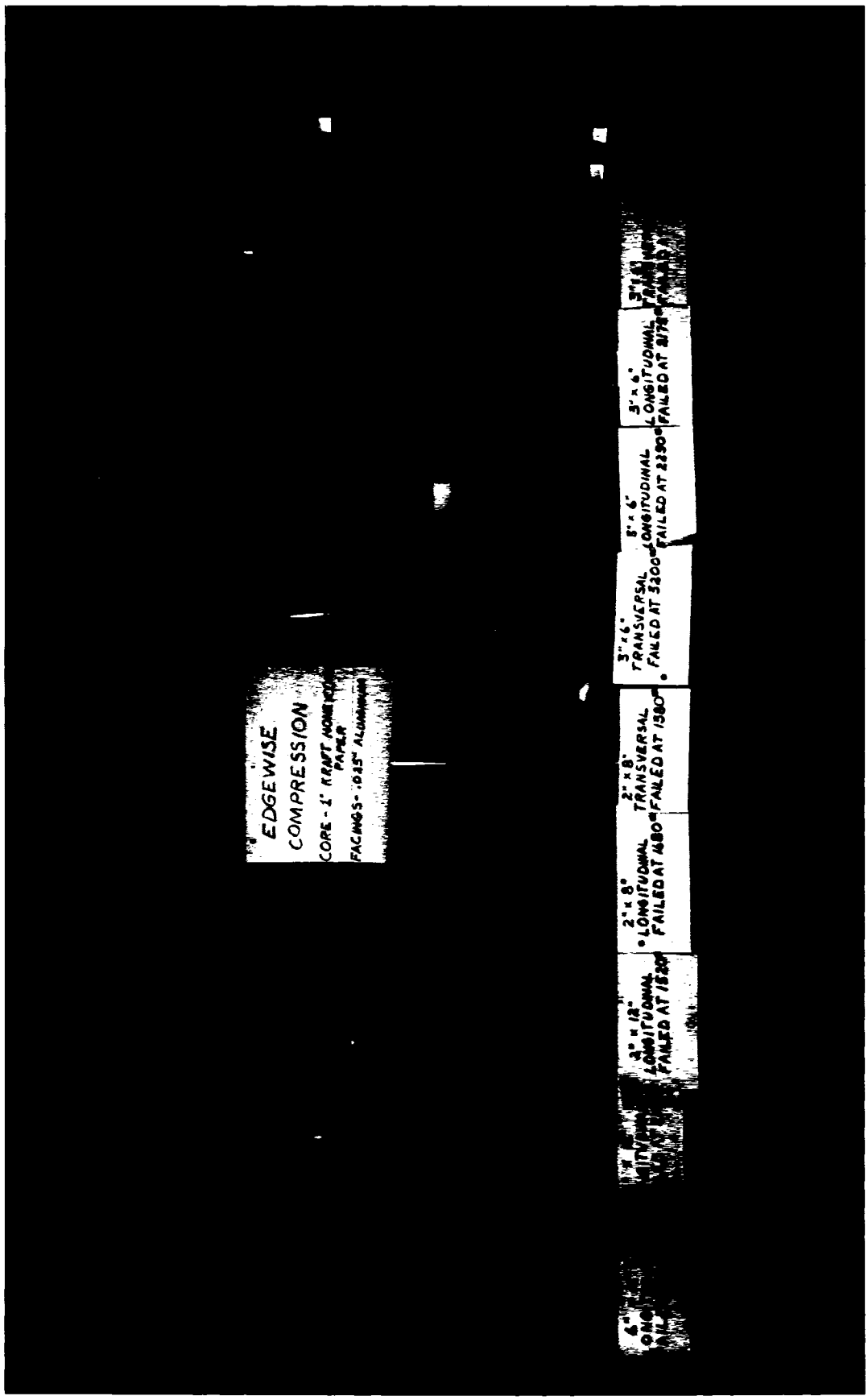

FIG. 4. HONEYCOMB SANDWICH COLUMNS AFTER FAILURE

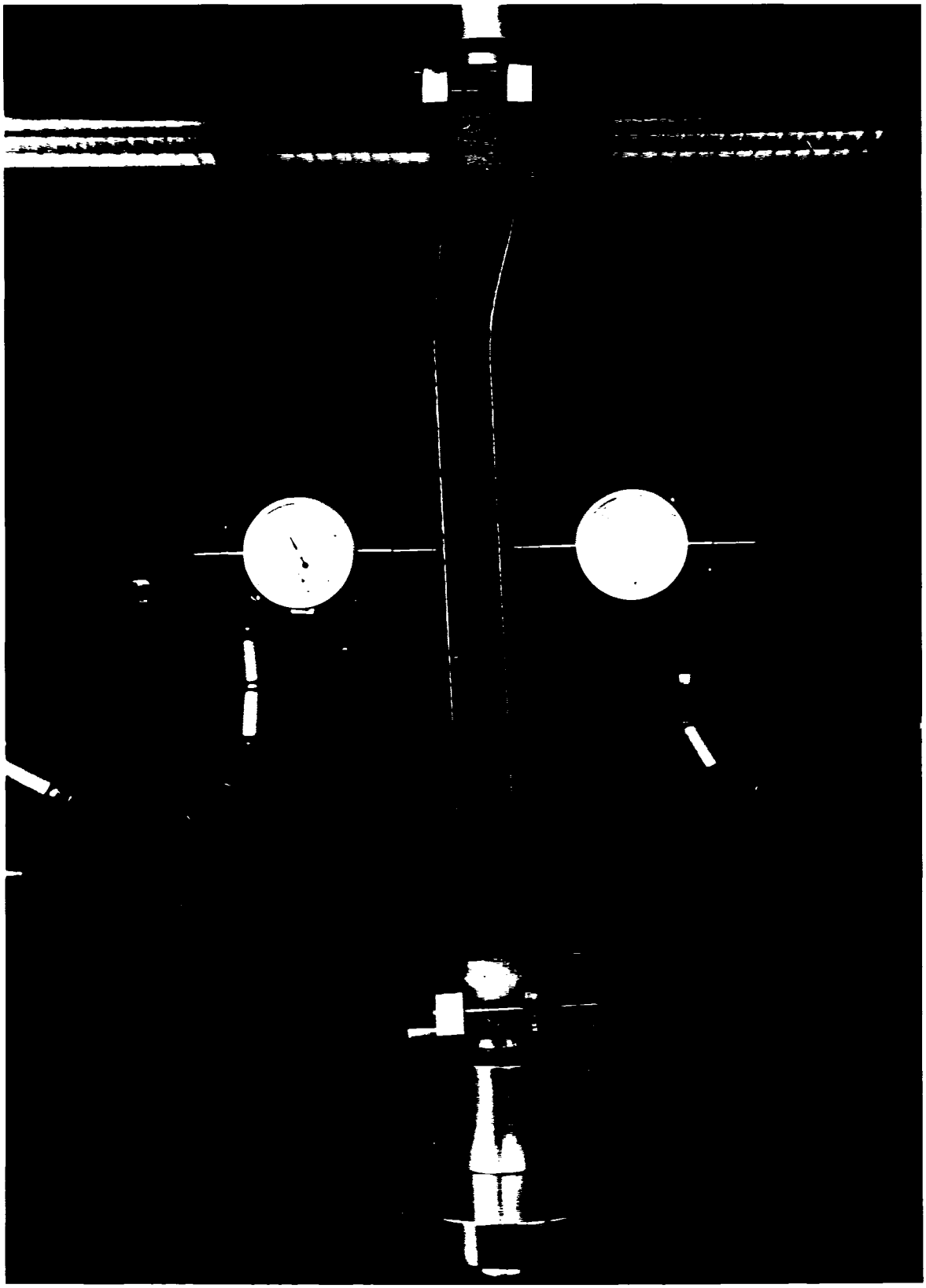

FIG. 5. HONEYCOMB SANDWICH COLUMN
(18" x 3" x 1")
TESTED IN EDGEWISE COMPRESSION

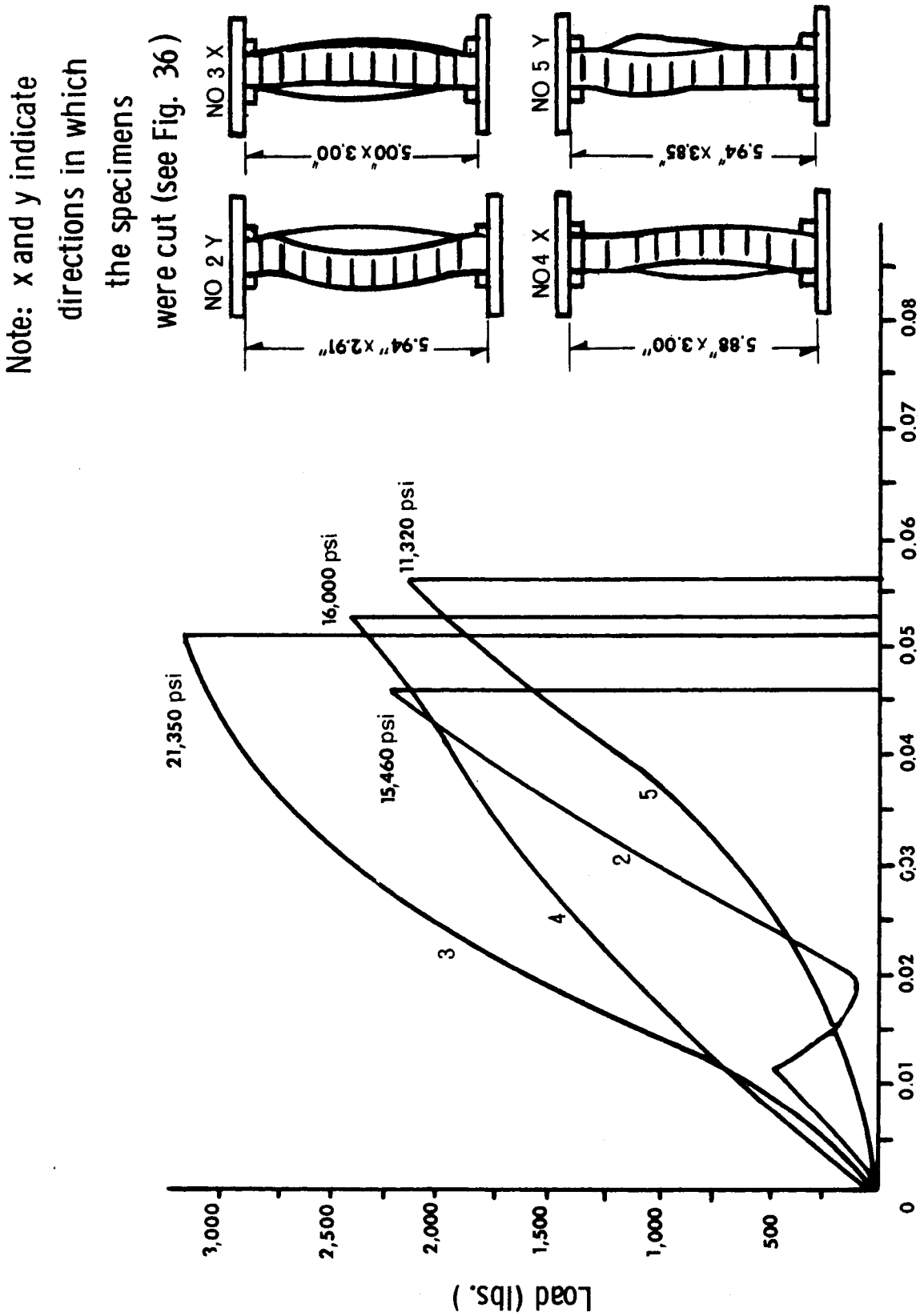

FIG. 6. LOAD-DISPLACEMENT CURVES FOR SANDWICH COLUMNS (1 TO 4)

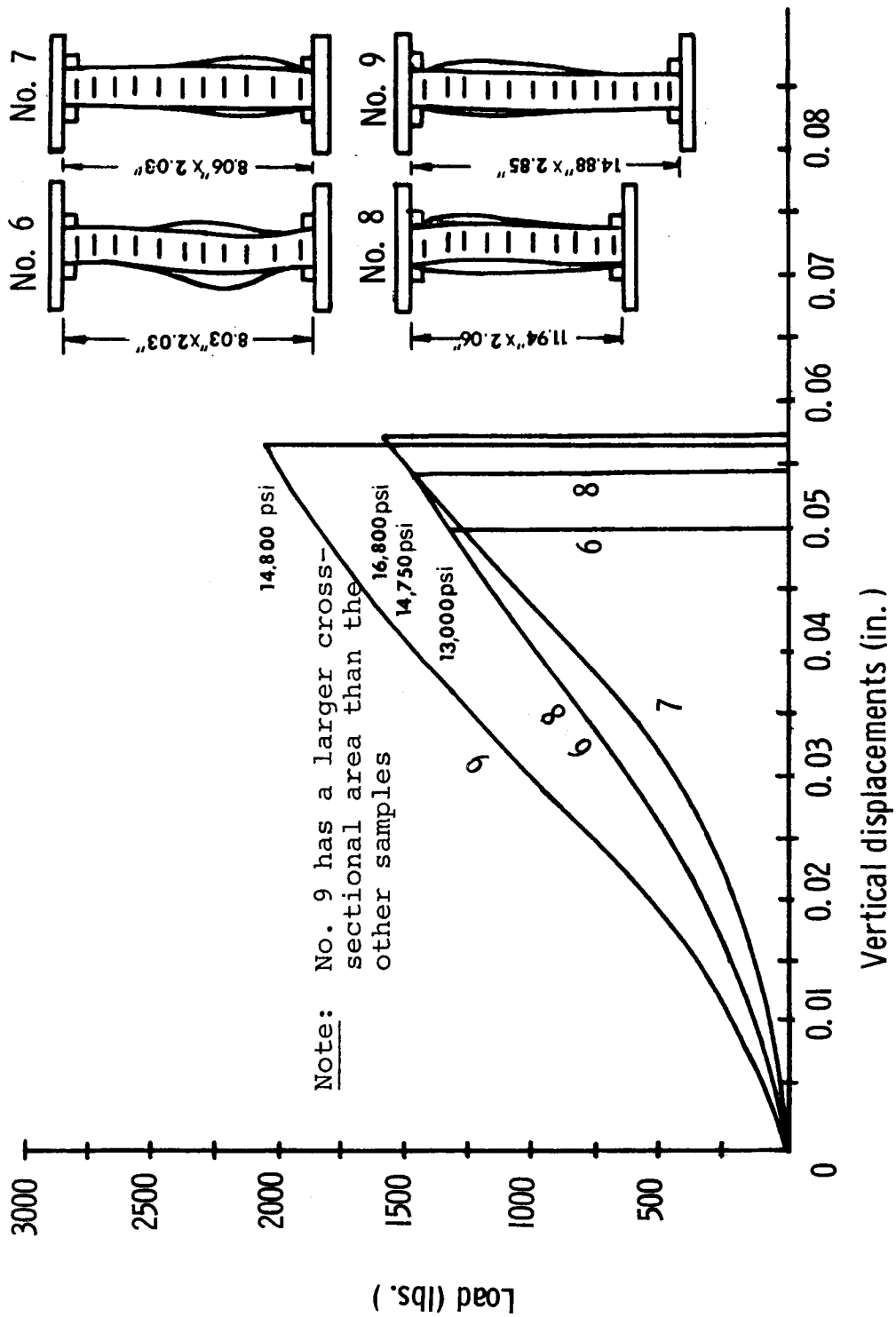

FIG. 7. LOAD-DISPLACEMENT CURVES FOR SANDWICH COLUMNS (5 TO 8)

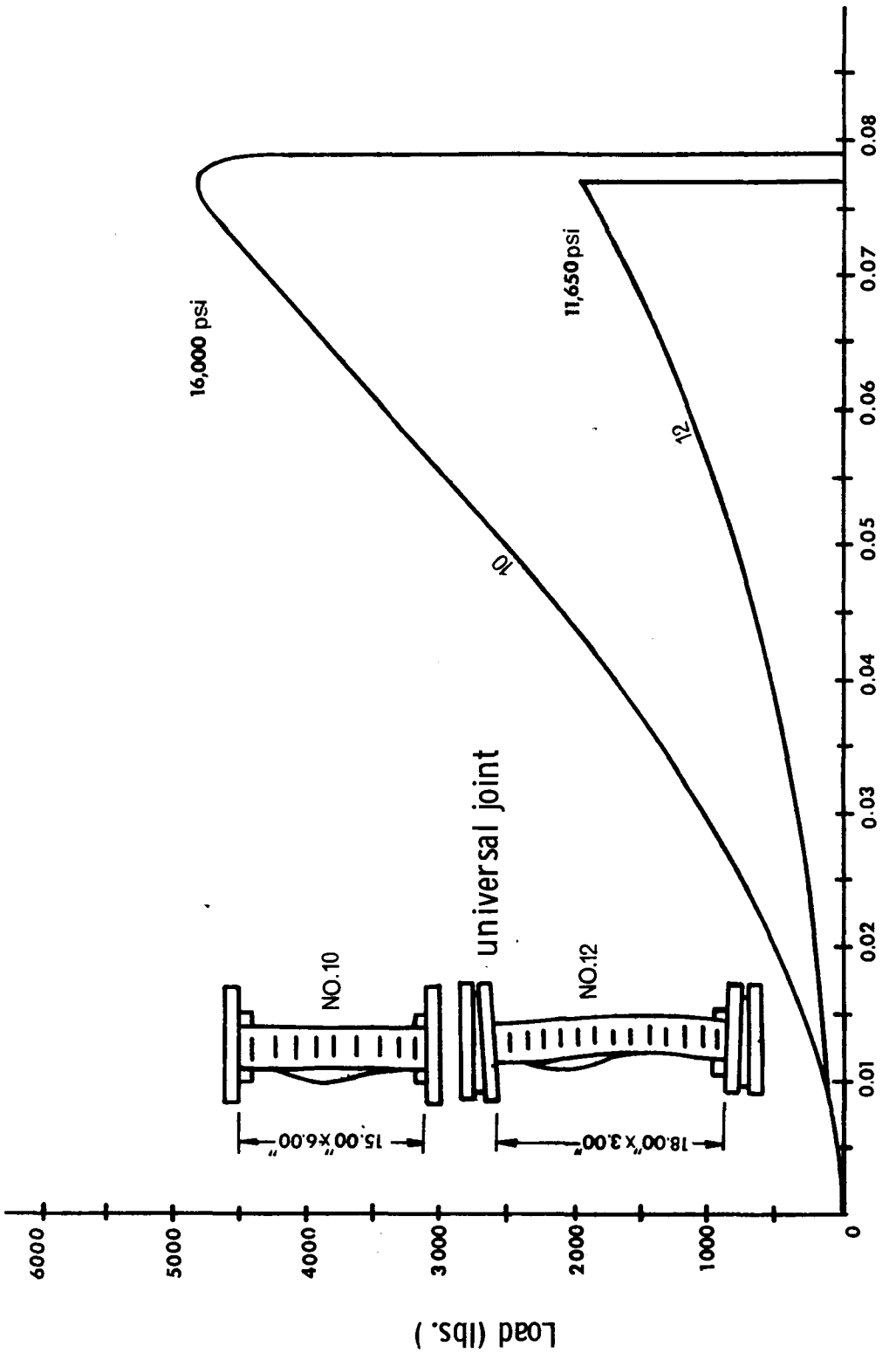

FIG. 8. LOAD-DISPLACEMENT CURVES FOR SANDWICH COLUMNS (9 AND 10)

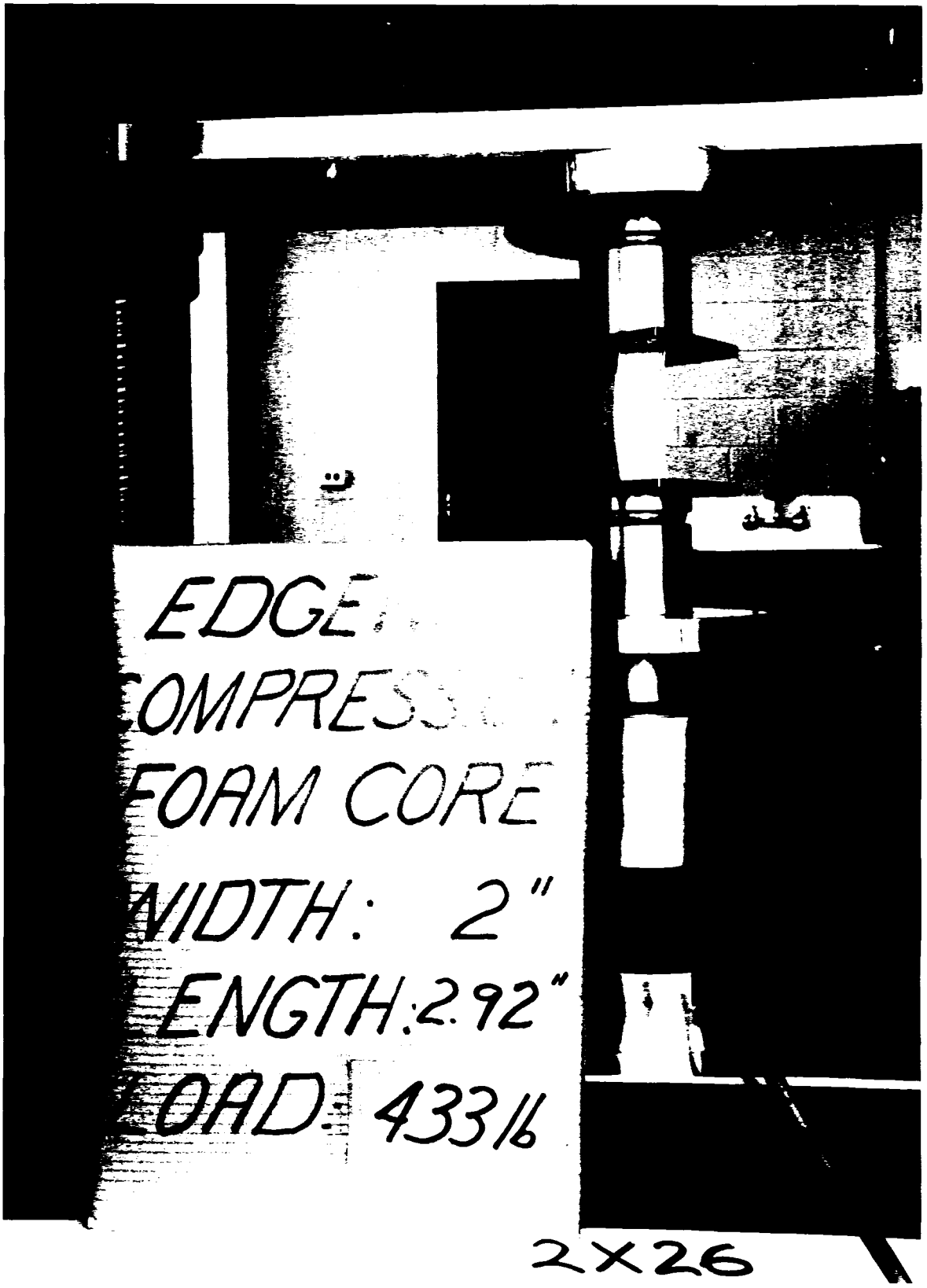

FIG. 9. EDGEWISE COMPRESSION TEST ON A
2.92" x 2" x 1"
STYROLITE SANDWICH COLUMN

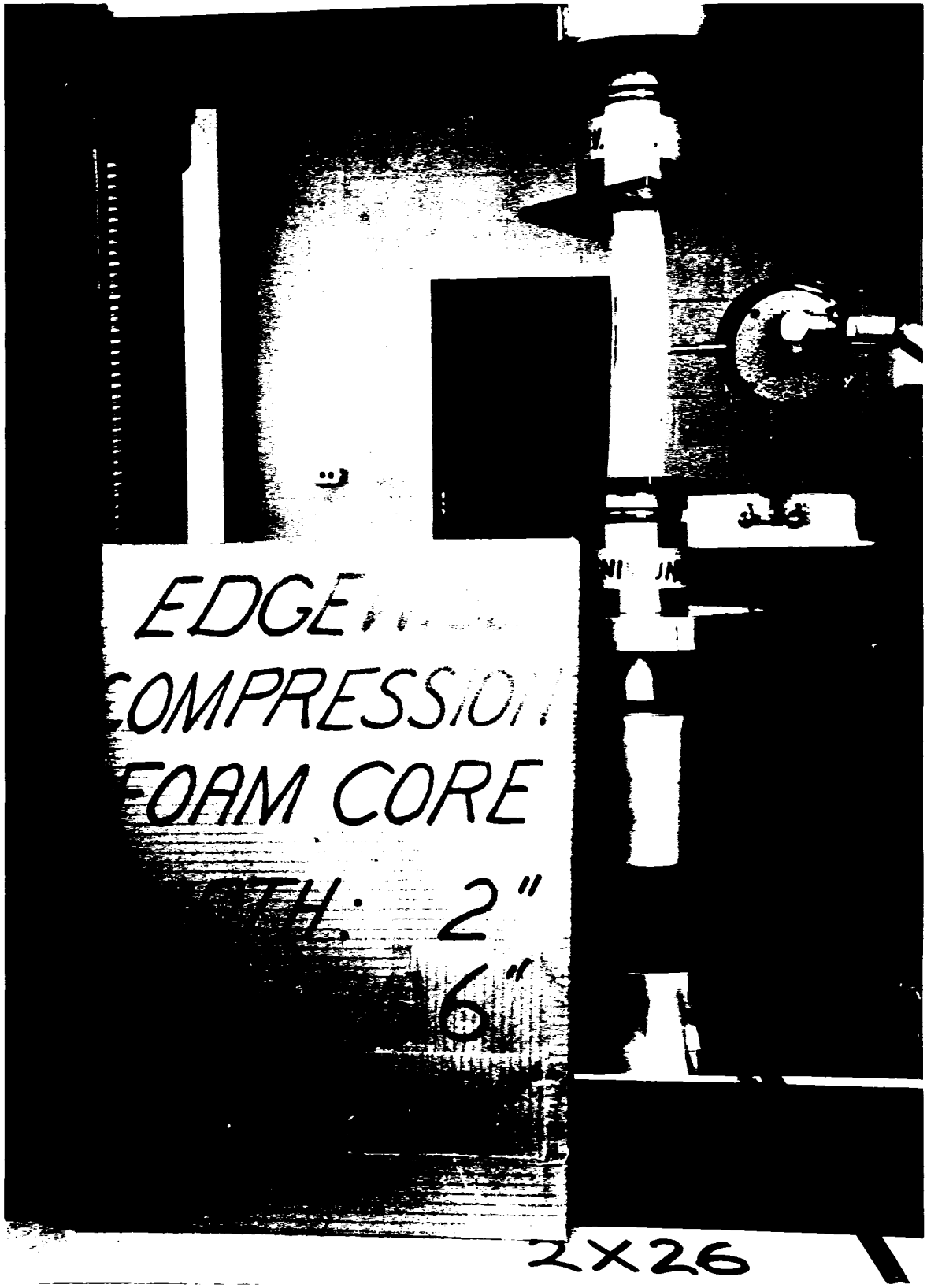

FIG. 10. EDGEWISE COMPRESSION TEST ON A
6" x 2" x 1"
STYROLITE SANDWICH COLUMN

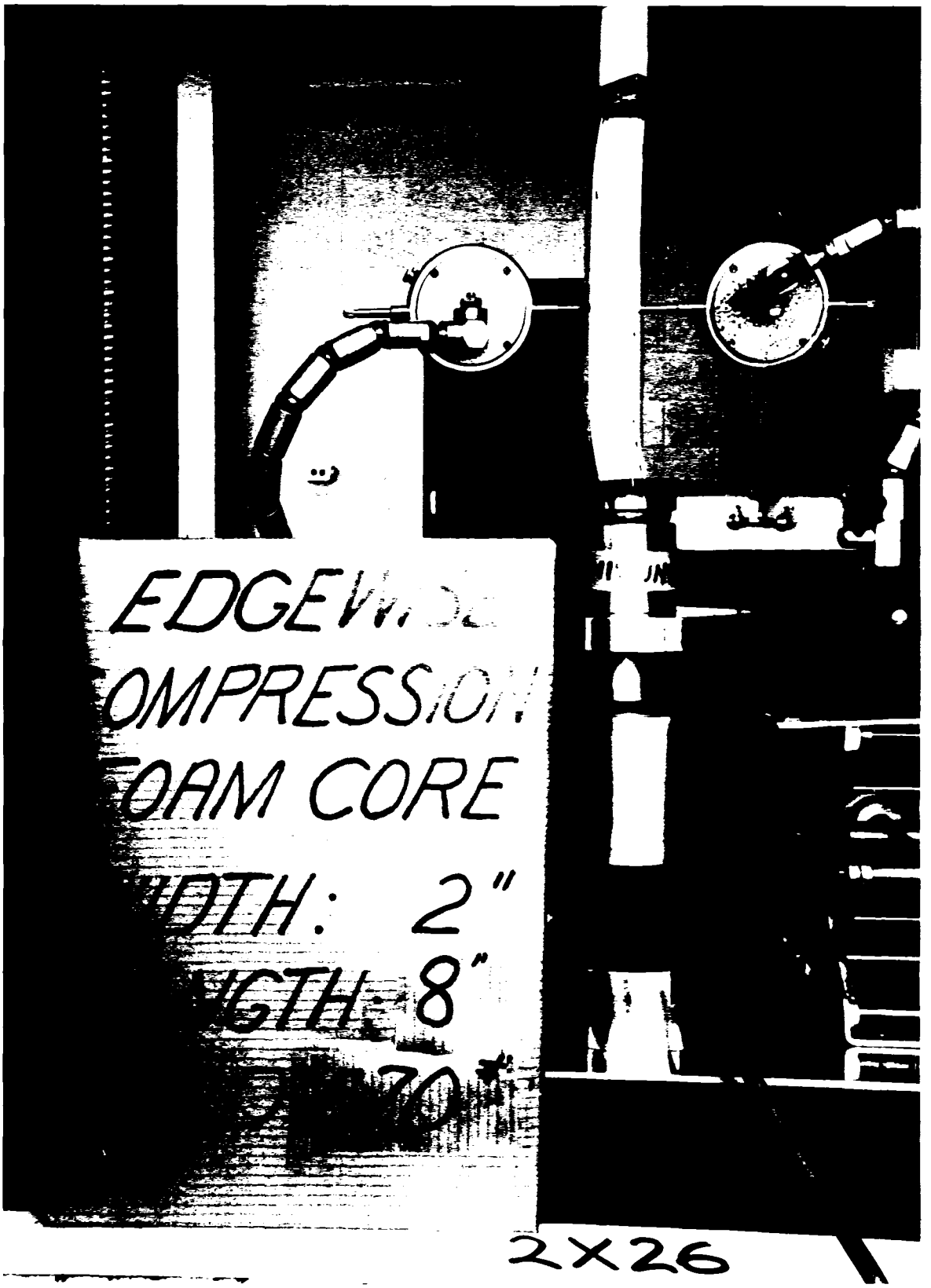

FIG. 11. EDGEWISE COMPRESSION TEST OF A
8" x 2" x 1"
STYROLITE SANDWICH COLUMN

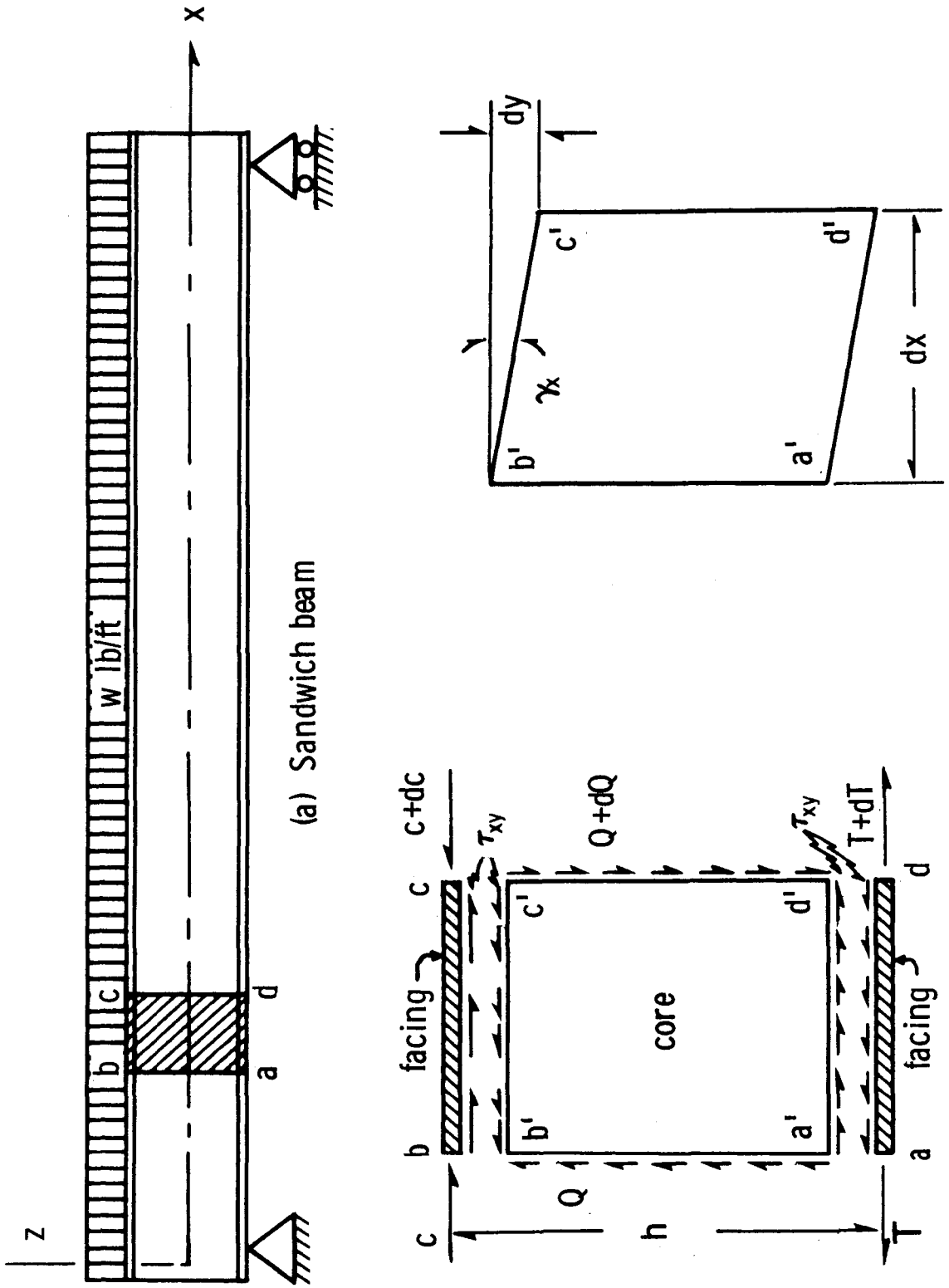

FIG. 12. SHEAR DEFORMATIONS IN A SANDWICH BEAM ELEMENT

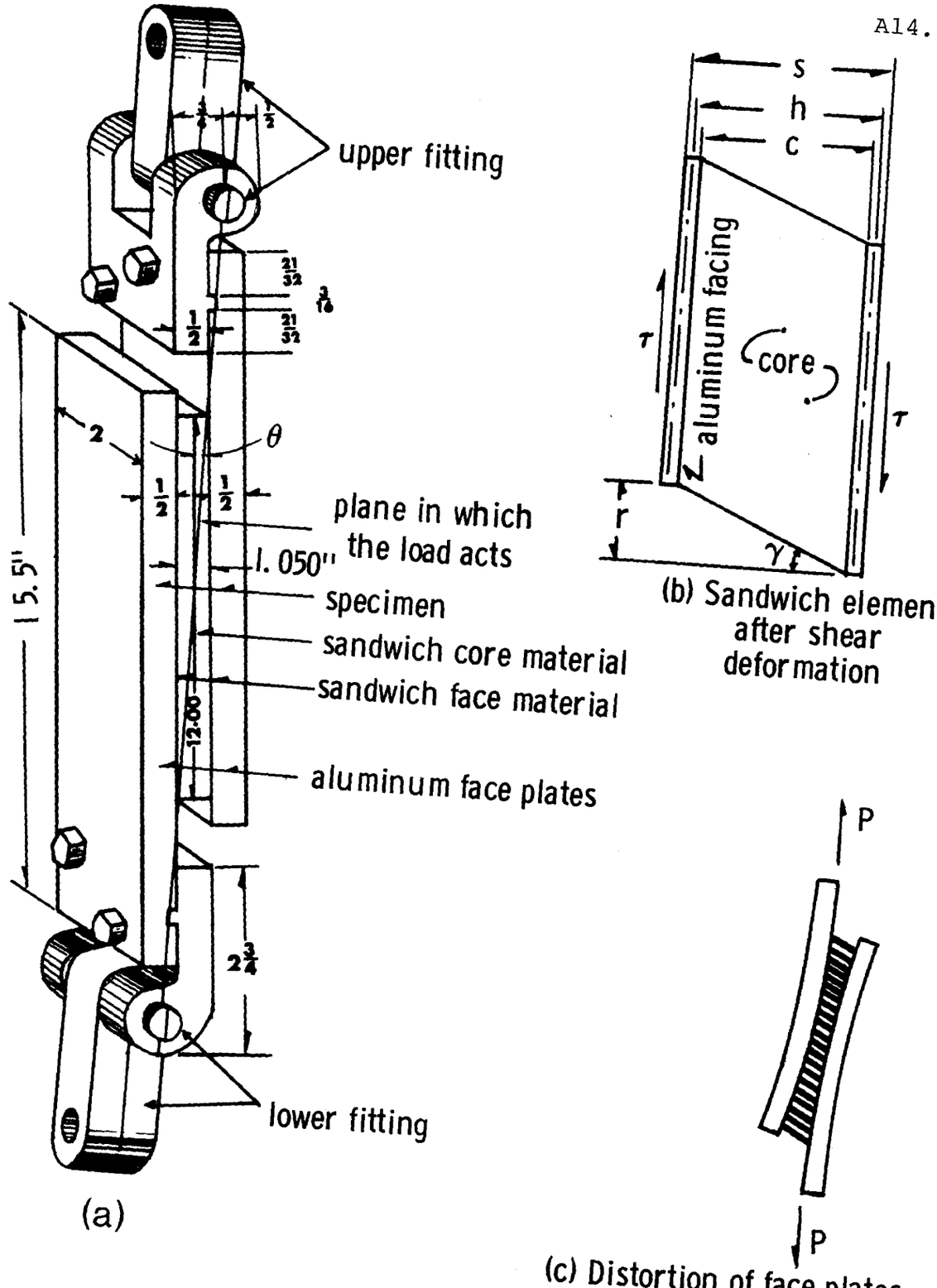

FIG. 13. DETAILS OF FRAME ASSEMBLY USED TO TEST SANDWICH MATERIALS IN SHEAR

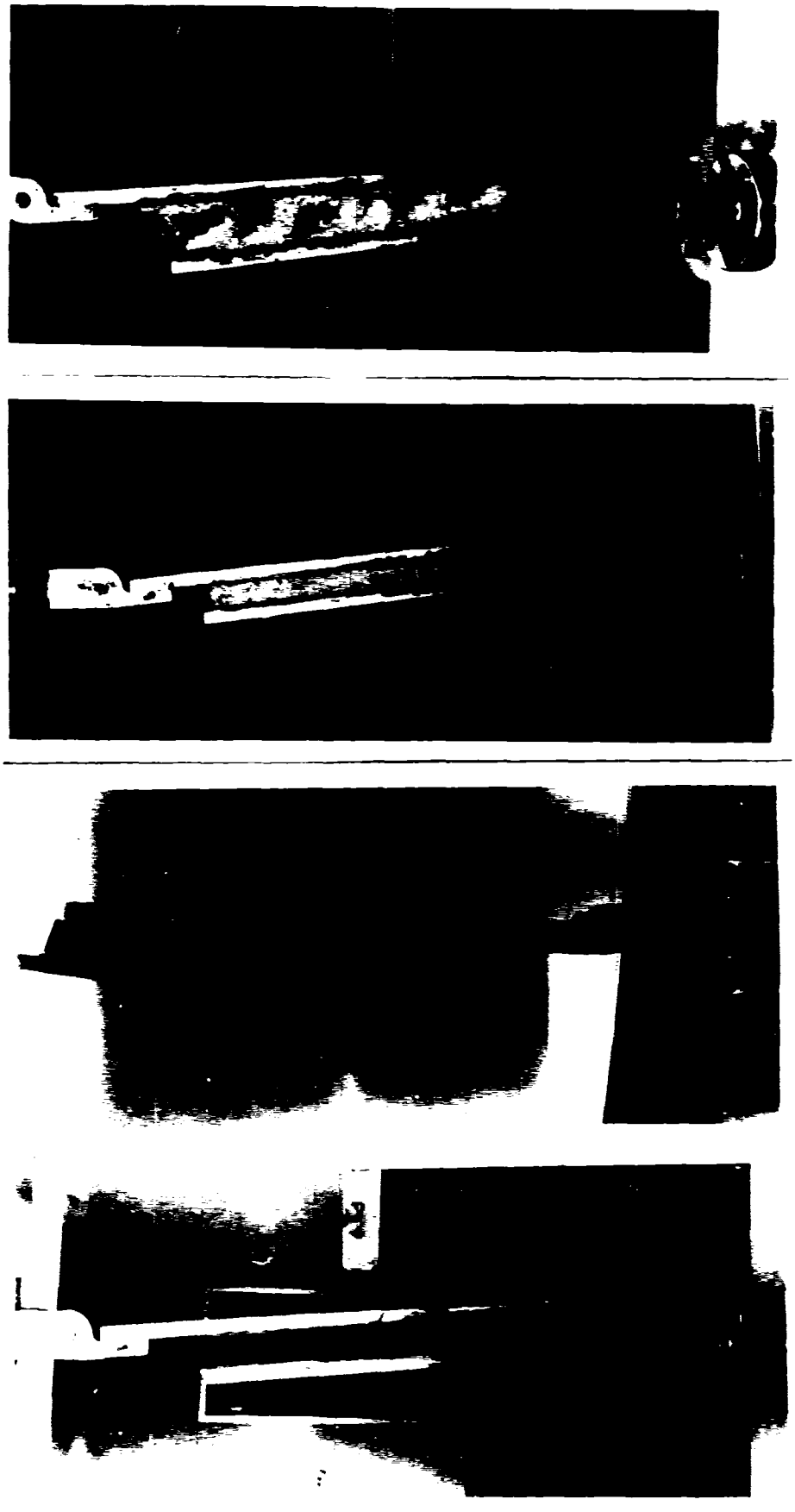

(a) Honeycomb before Failure.
(b) Honeycomb after Failure.
(c) Styrolite before Failure.
(d) Styrolite after Failure.

FIG. 14. SINGLE-BLOCK SHEAR TESTS OF HONEYCOMB AND STYROLITE CORES.

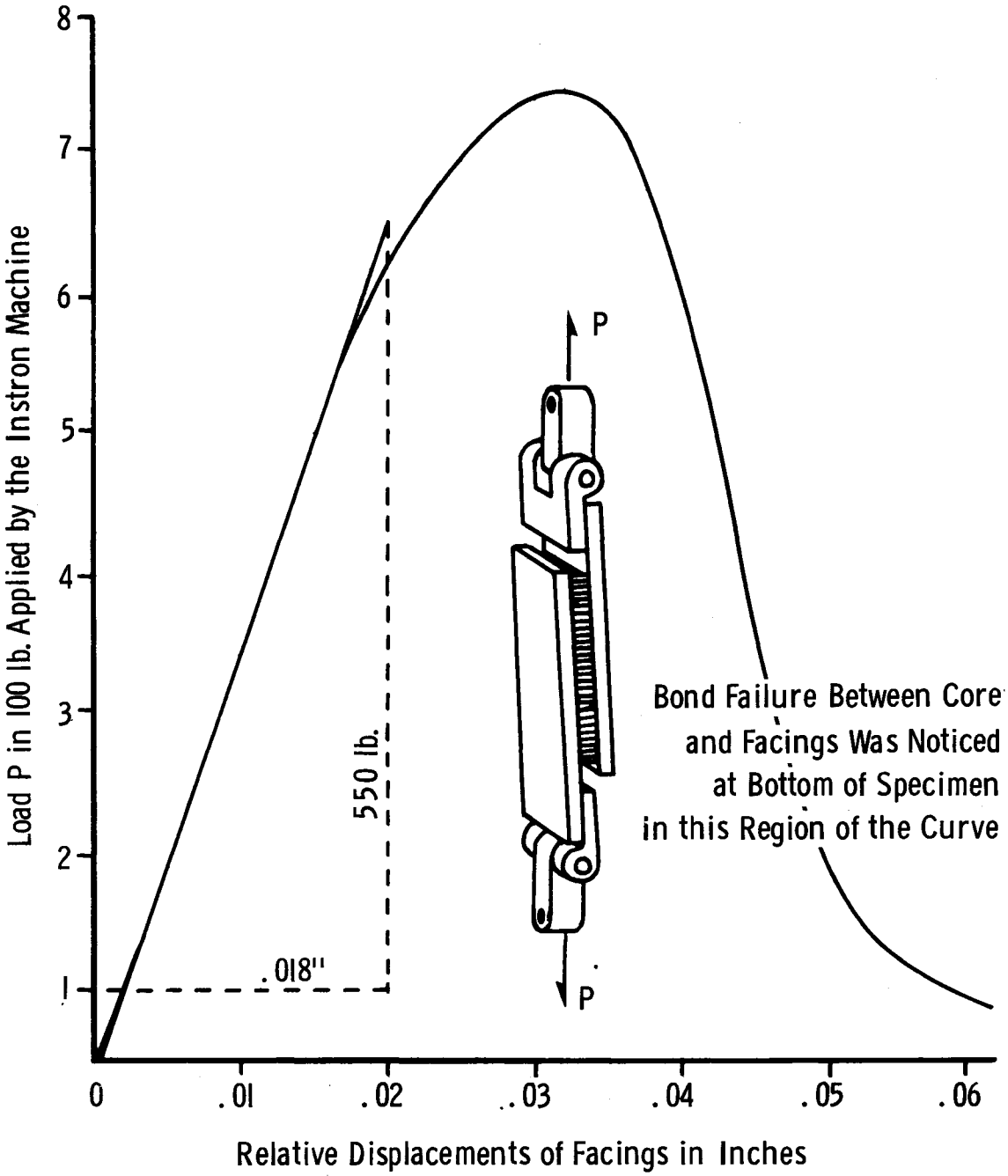

FIG. 15. LOAD DISPLACEMENT CURVE DRAWN BY THE INSTRON MACHINE FOR A HONEYCOMB SANDWICH SPECIMEN (2" x 12") TESTED ACCORDING TO THE SINGLE-BLOCK SHEAR TEST

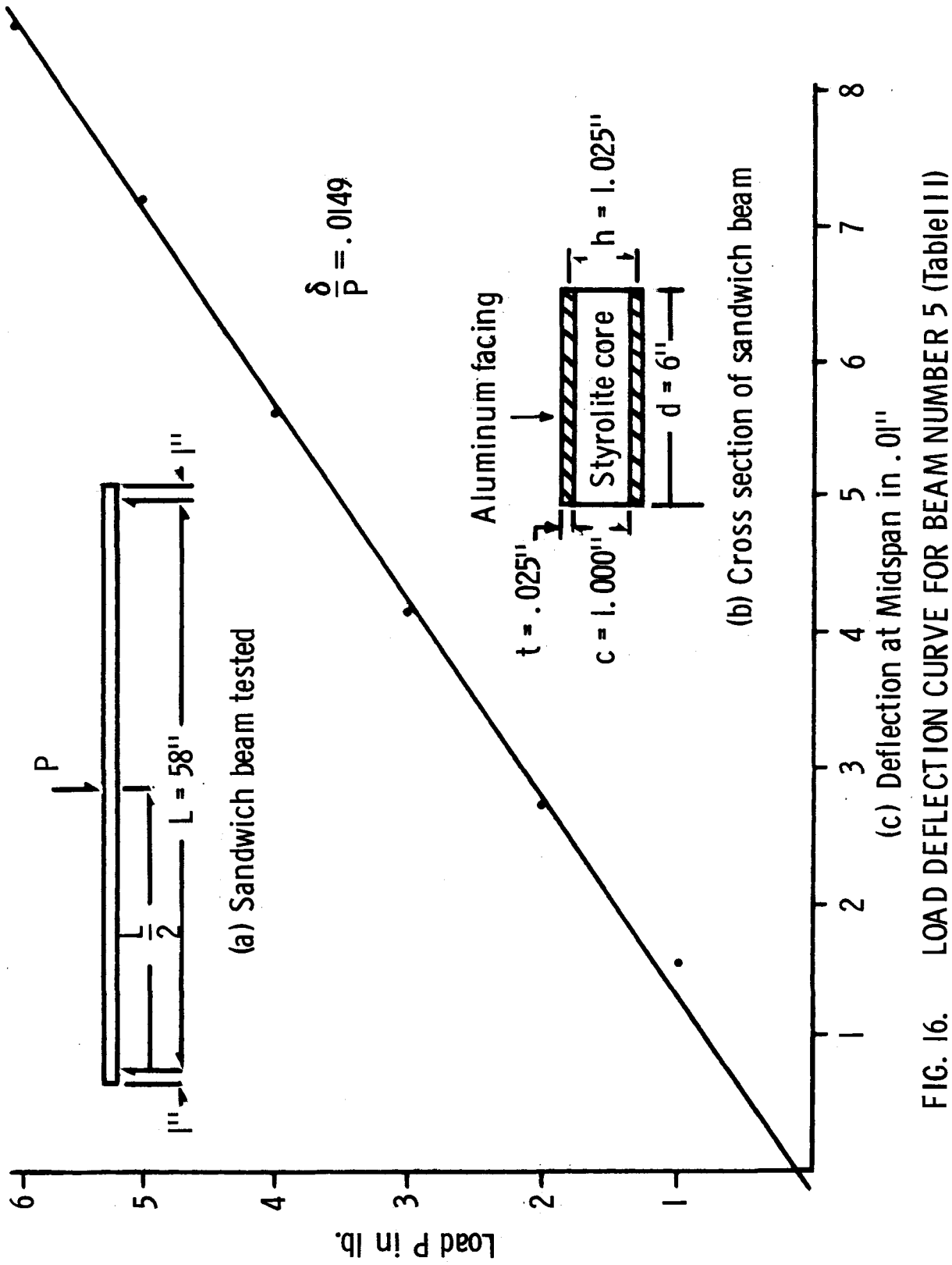

FIG. 16. LOAD DEFLECTION CURVE FOR BEAM NUMBER 5 (Table III)

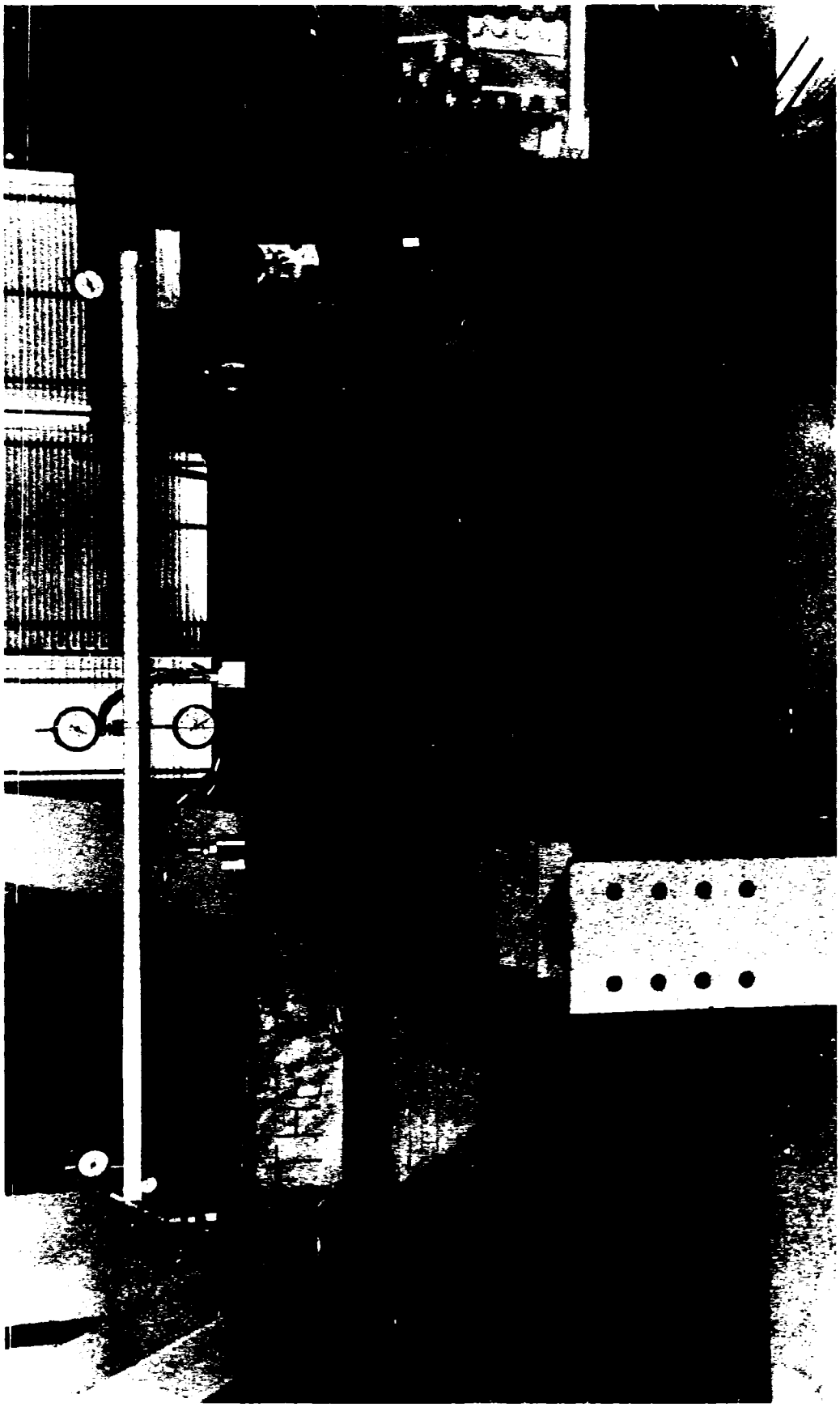

FIG. 17. STYROLITE SANDWICH BEAM TESTED BY THE THREE-POINT SHEAR STIFFNESS TEST.

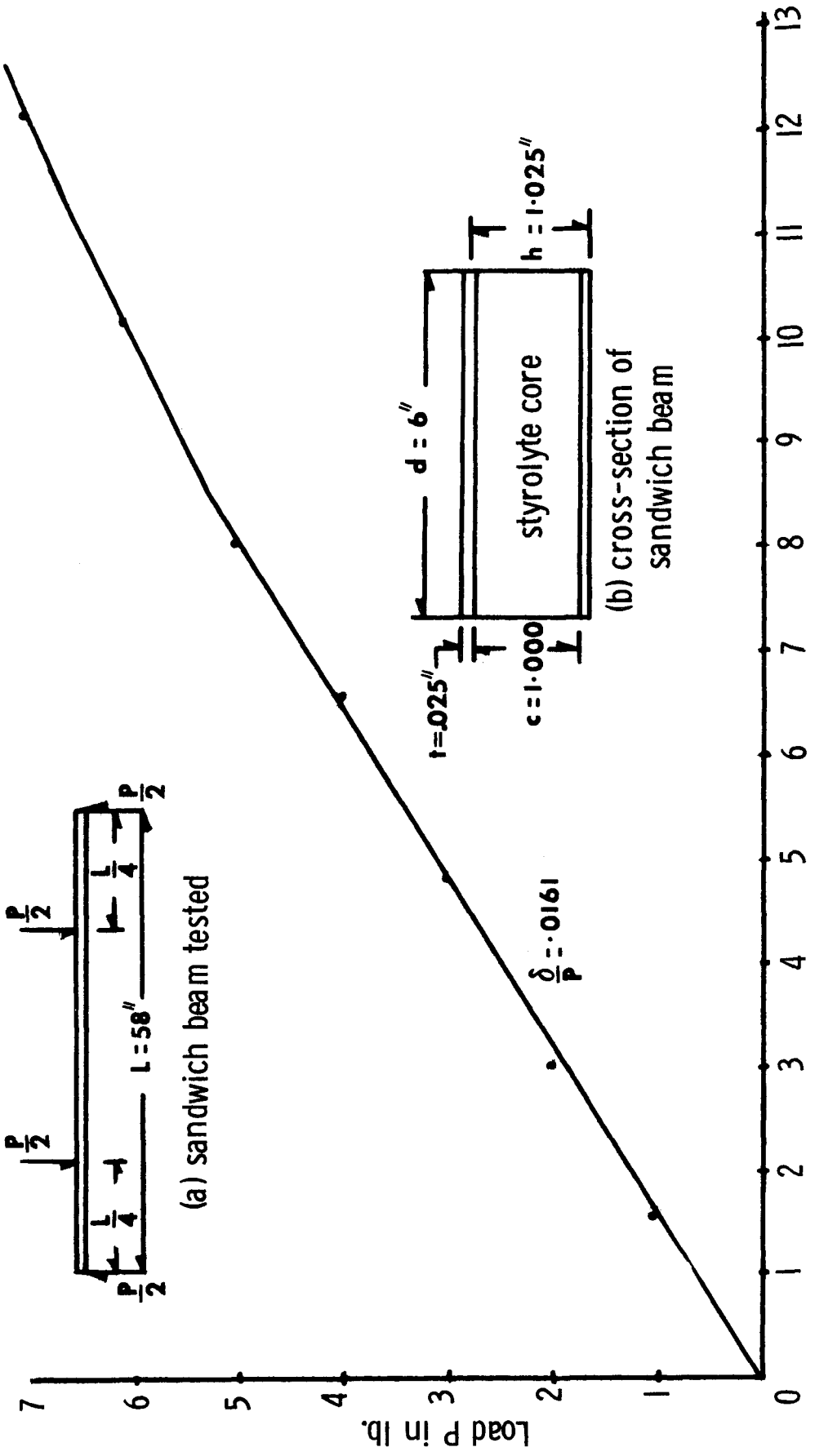

FIG. 18. LOAD DEFLECTION CURVE FOR BEAM NUMBER 8 (TABLE IV)

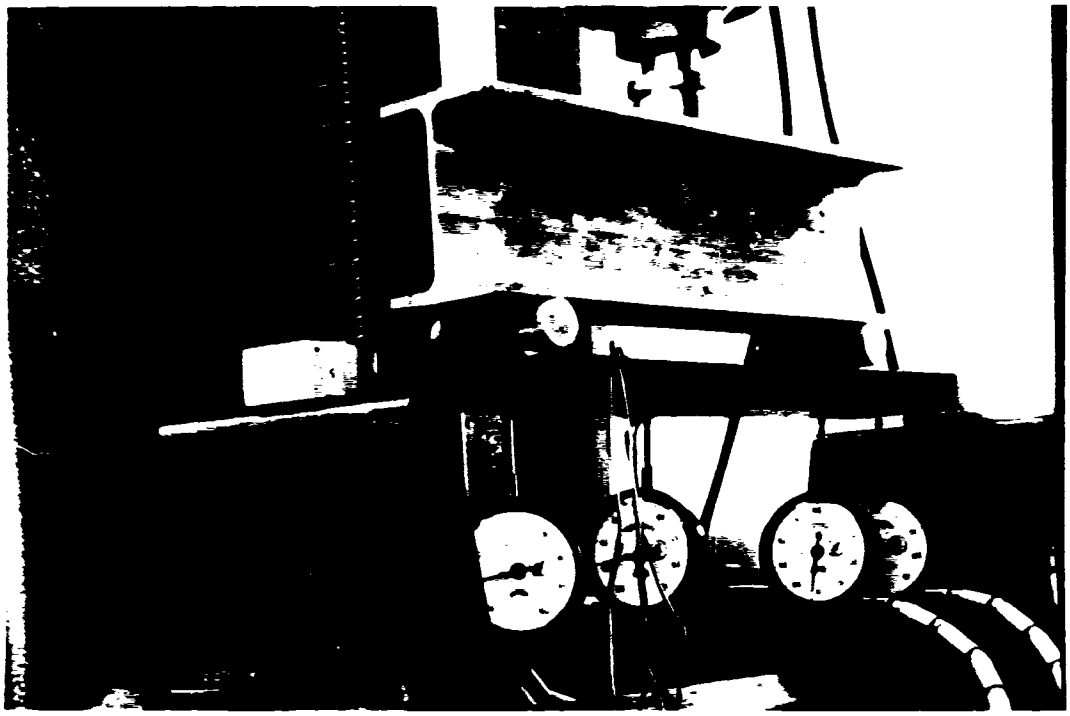

(a) Honeycomb Sandwich Beam (2" x 22")

(b) Honeycomb Sandwich Beam (6" x 60")

FIG. 19. THE FOUR-POINT SHEAR STIFFNESS TEST

FIG. 20. A STYROLITE SANDWICH BEAM TESTED BY THE FIVE-POINT SHEAR STIFFNESS METHOD.

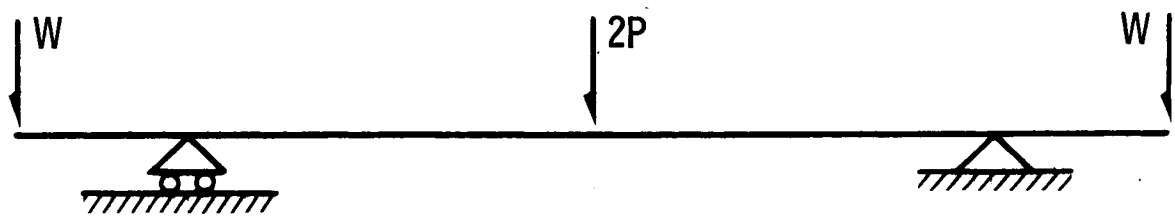

(a) Neutral plane of sandwich beam

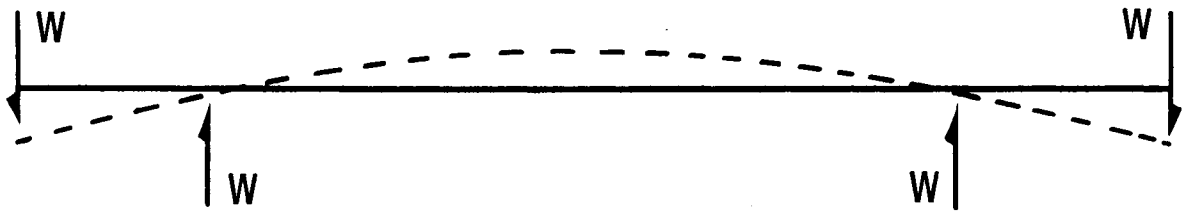

(b) Upward central deflection due to loads W

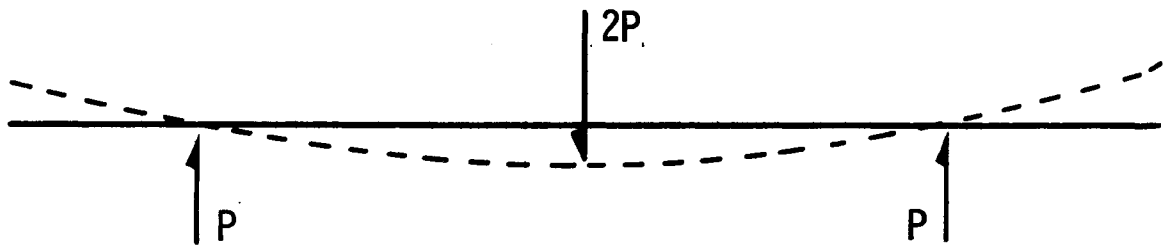

(c) Downward central deflection due to load 2P

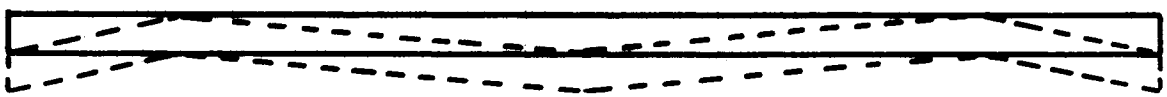

(d) Shear deflections

FIG. 21. DEFLECTIONS IN THE FIVE-POINT LOADING TEST

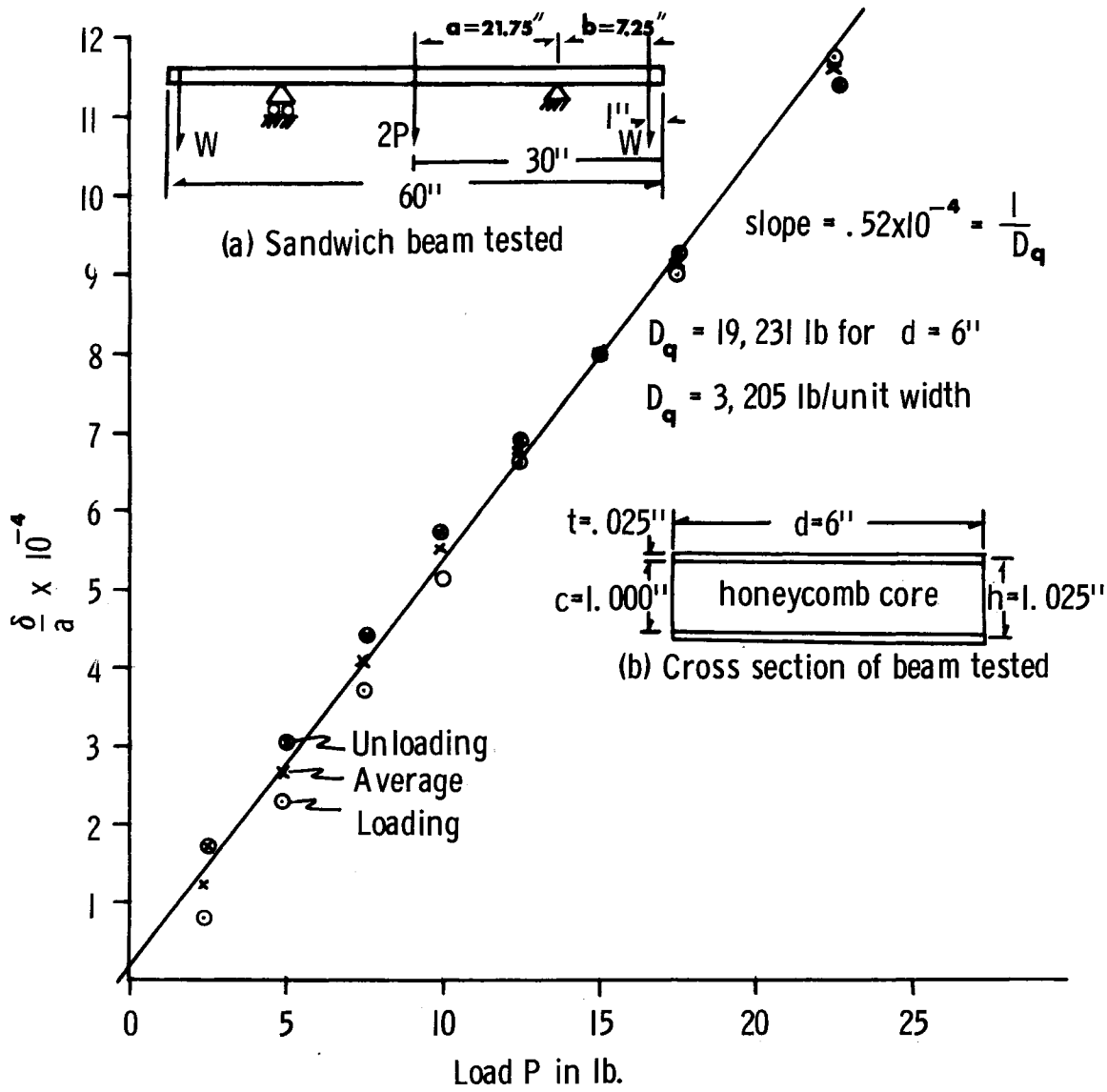

FIG. 22. THE FIVE-POINT LOADING SHEAR STIFFNESS TEST (Procedure I)
Beam No. 2 (Table V) - Test No. I - Honeycomb Core

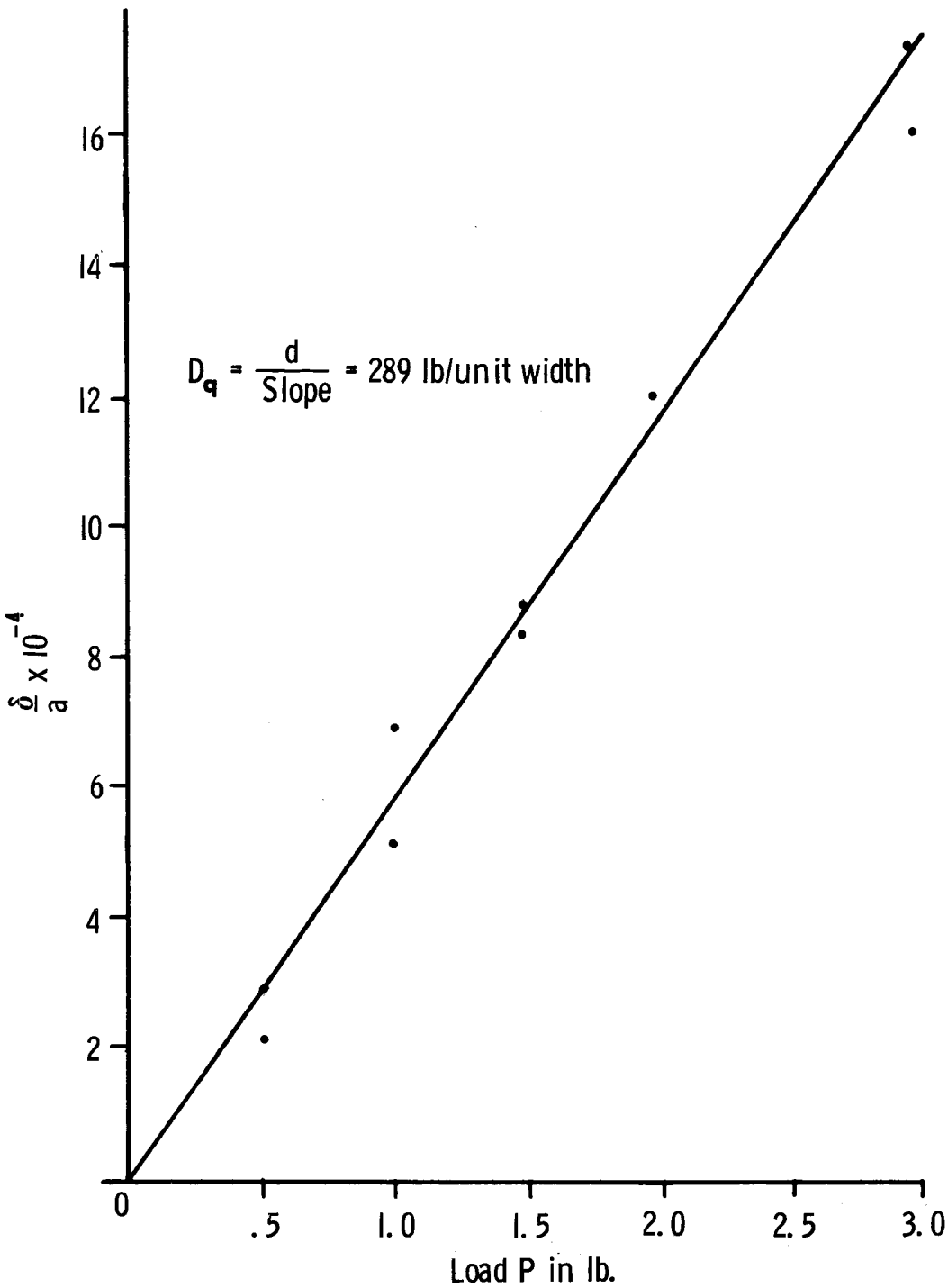

FIG. 23. THE FIVE-POINT LOADING SHEAR STIFFNESS TEST (Procedure I)
Beam No. 5 (Table V) - Test No. 2 - Styrolite Core

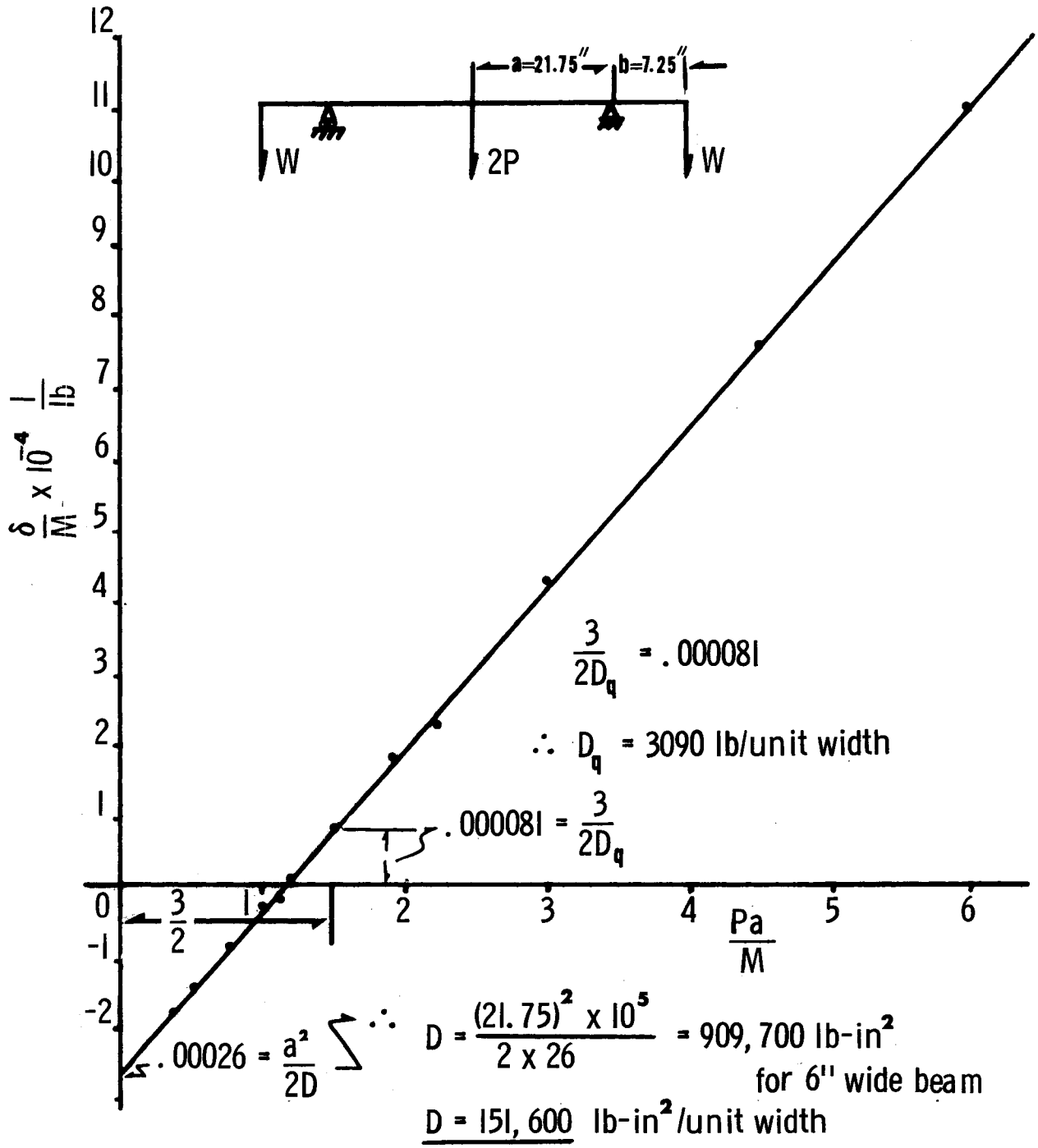

FIG. 24. THE FIVE-POINT LOADING SHEAR STIFFNESS TEST
(Procedure II)
Beam No. 3 (Table V) - Test No. 4 - Honeycomb Core

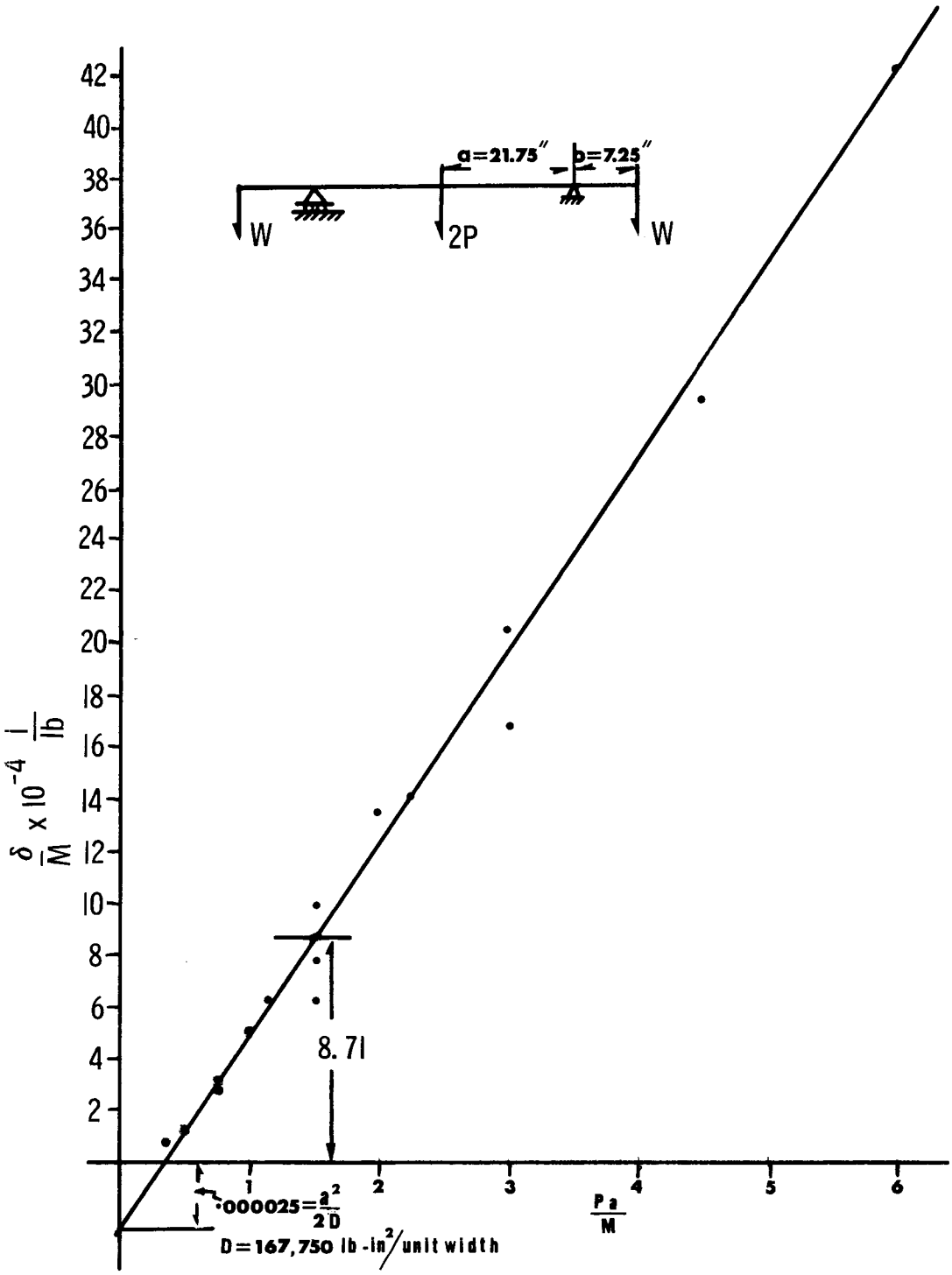

FIG. 25. THE FIVE-POINT LOADING SHEAR STIFFNESS TEST (Procedure II)
Beam No. 5 (Table V) - Test No. 4 - Styrolite Core

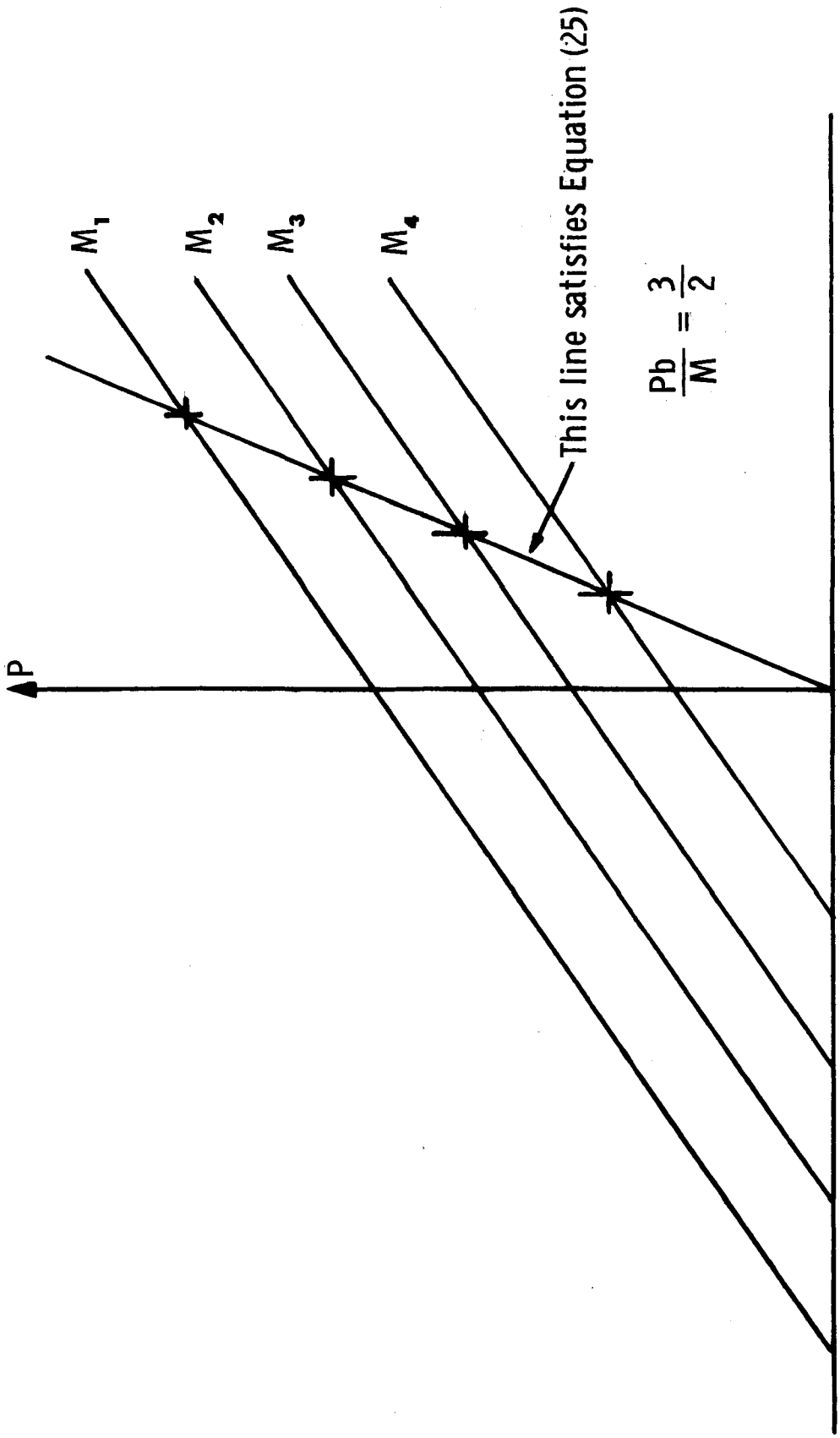

FIG. 26. THE FIVE-POINT LOADING SHEAR STIFFNESS TEST (Procedure III)

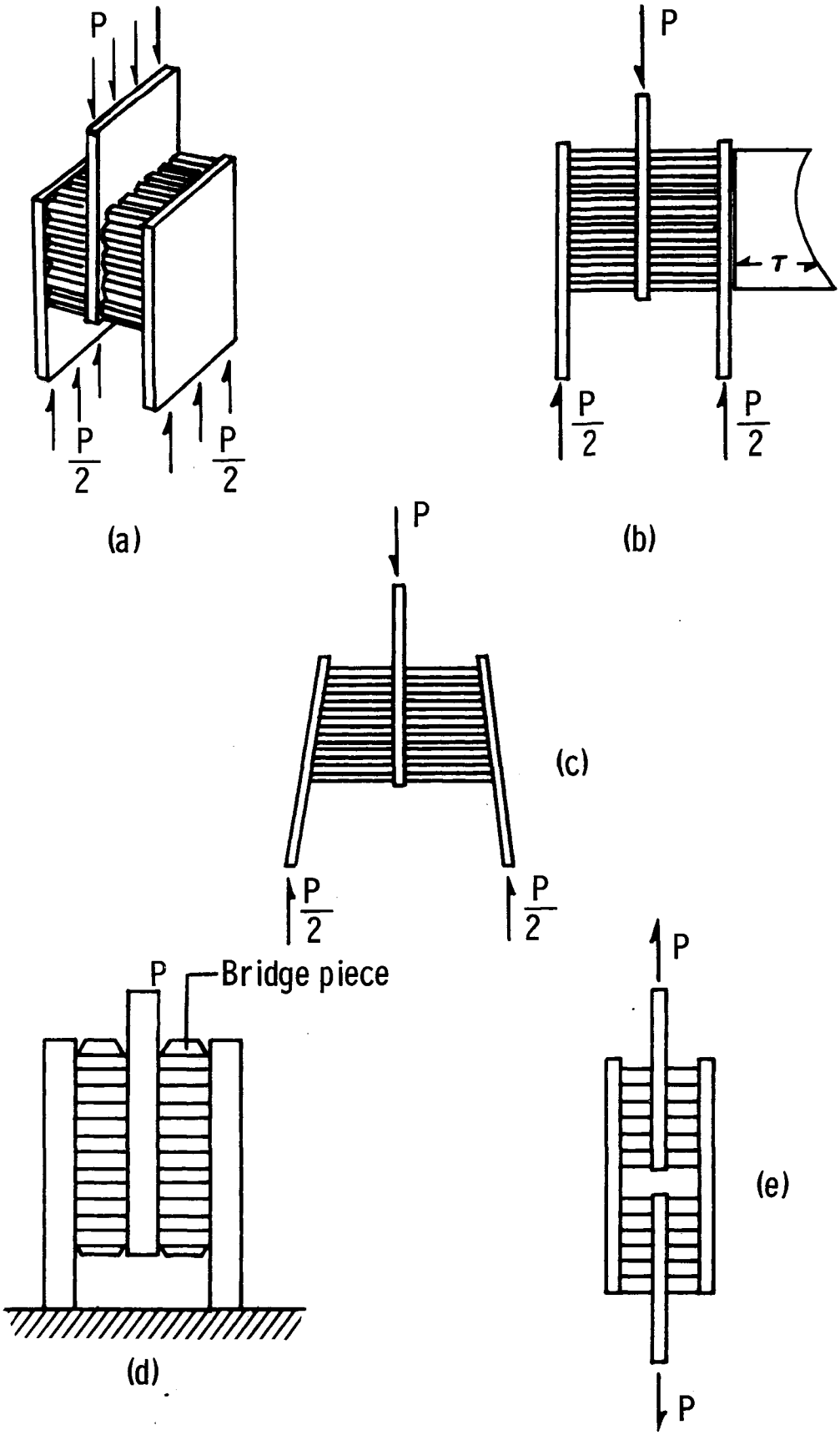

FIG. 27. BLOCK SHEAR TESTS

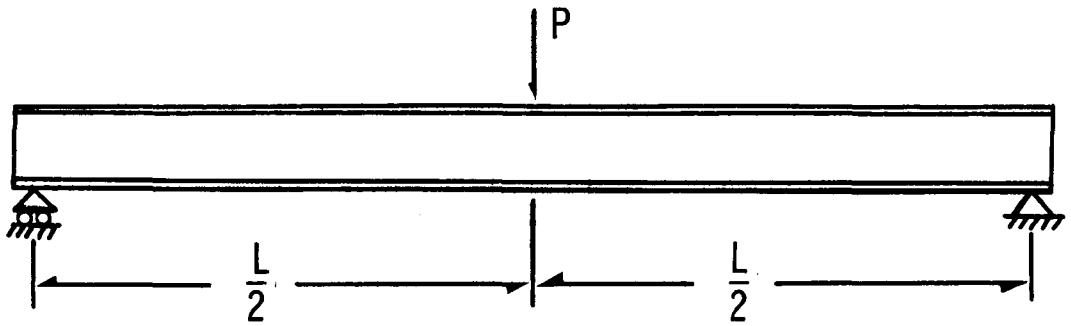

(a) Sandwich beam under the three point loading test

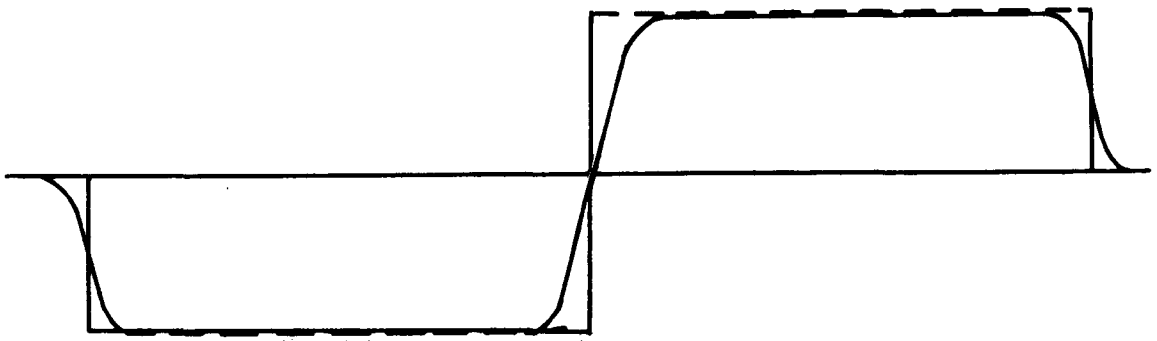

(b) Modified shear stress distribution in the core

FIG. 28. SHEAR STRESS DISTRIBUTION IN SANDWICH BEAMS SUBJECTED TO THE THREE-POINT LOADING TEST

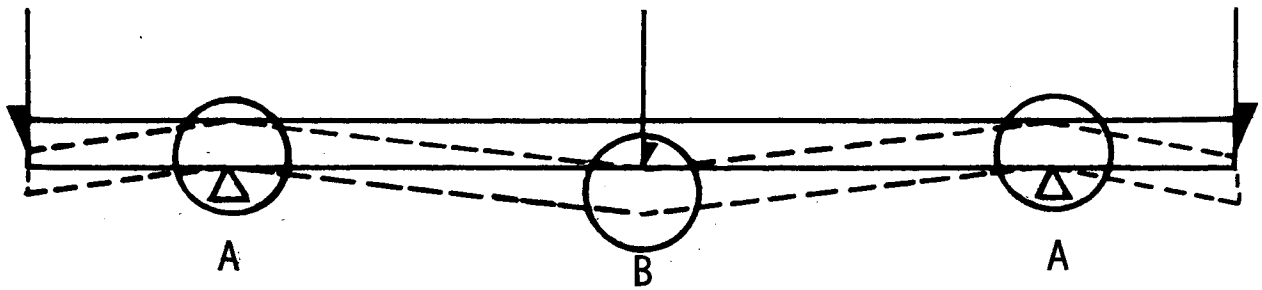

(a) Sandwich beam subjected to the five-point loading test

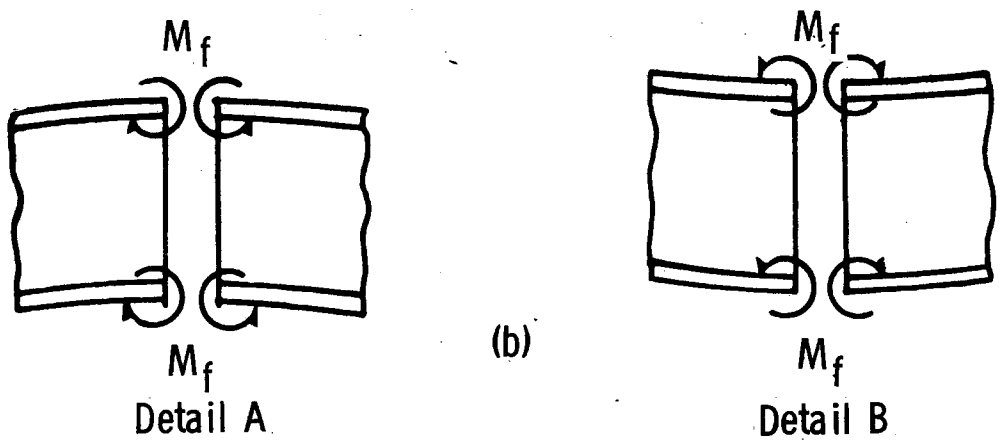

FIG. 29. SECONDARY MOMENTS IN THE FACINGS OF BEAMS SUBJECTED TO BENDING TESTS

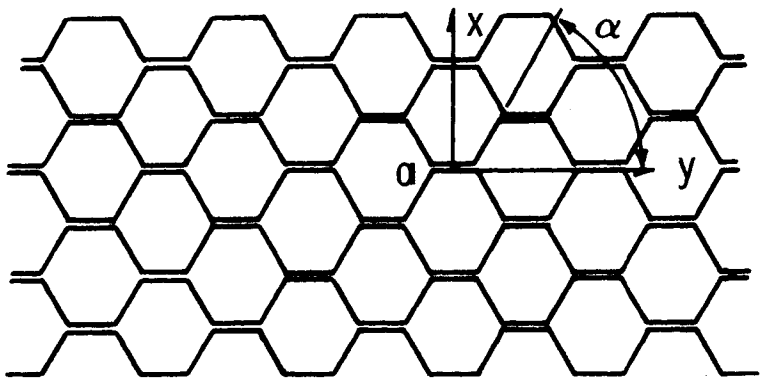

(a) Assumed configuration of equiangular hexagonal cells ($\alpha = 60^0$)

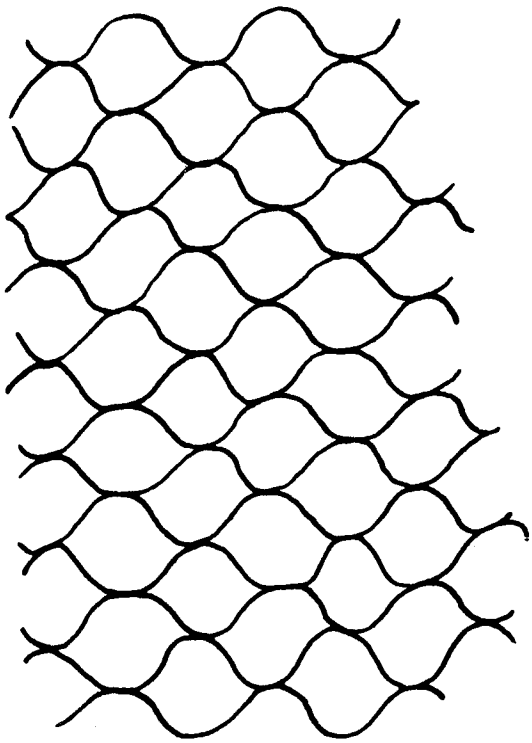

(b) Actual configuration of a typical sample of kraft paper honeycomb core

FIG. 30. DIFFERENCE BETWEEN THE ACTUAL AND ASSUMED CONFIGURATION OF PAPER HONEYCOMB CORE

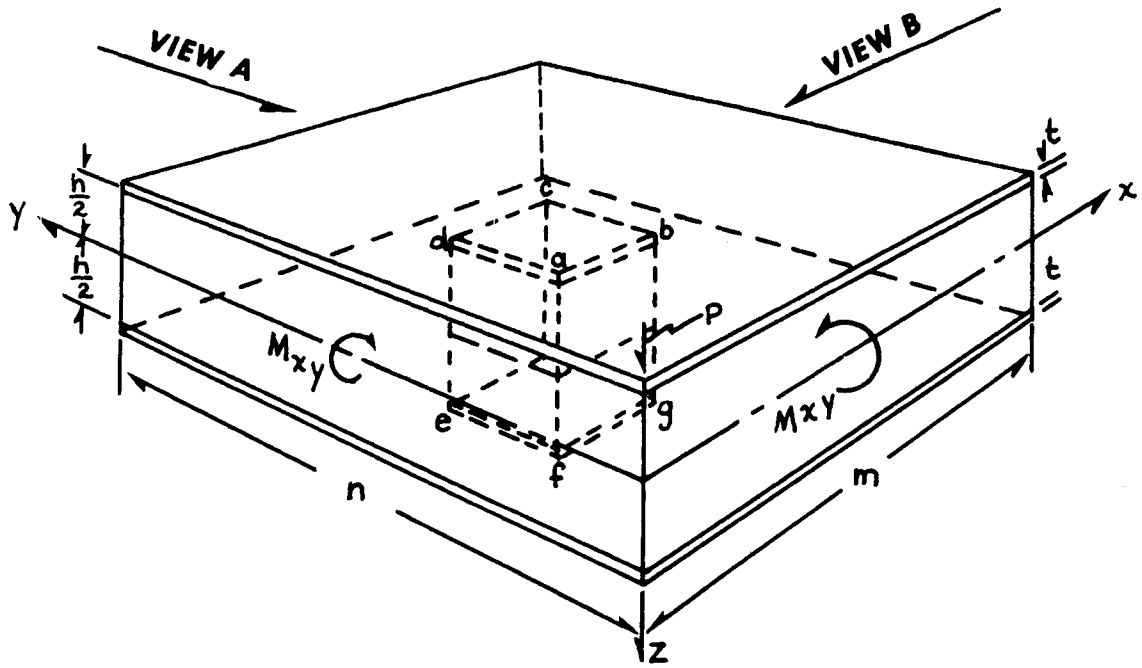

FIG. 31. RECTANGULAR SANDWICH PANEL

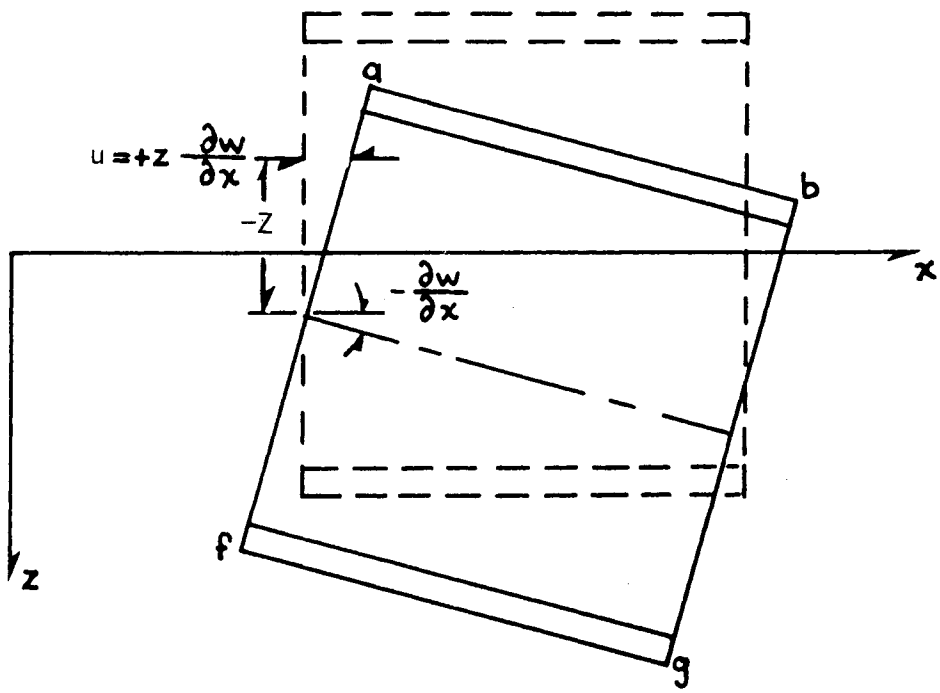

FIG. 32. FACE abfg OF DOTTED ELEMENT IN FIGURE 31 AFTER TWIST

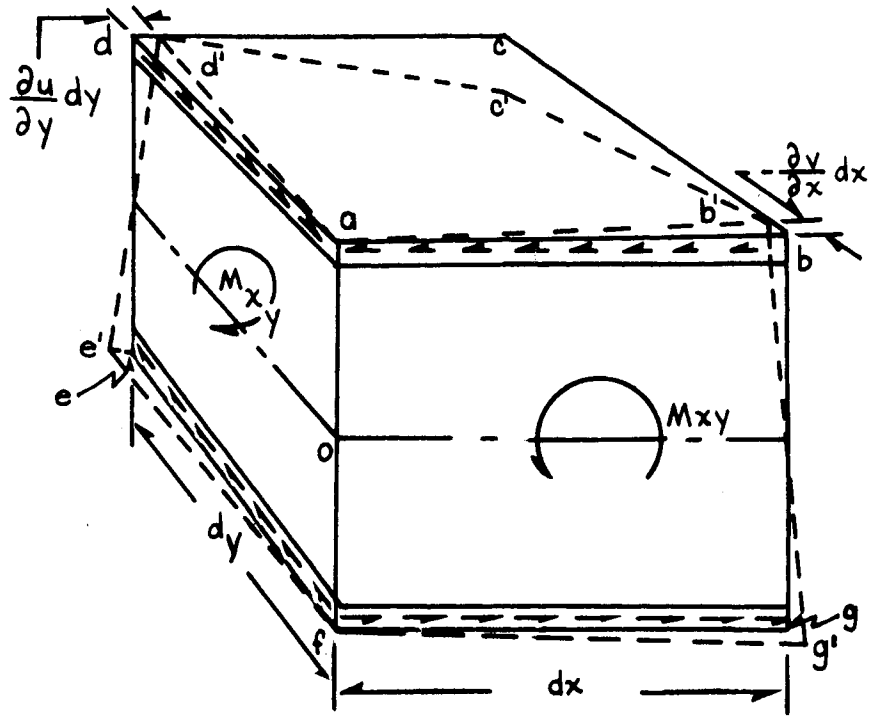

FIG. 33. DISTORTION PATTERN OF A SANDWICH ELEMENT SUBJECTED TO TWIST

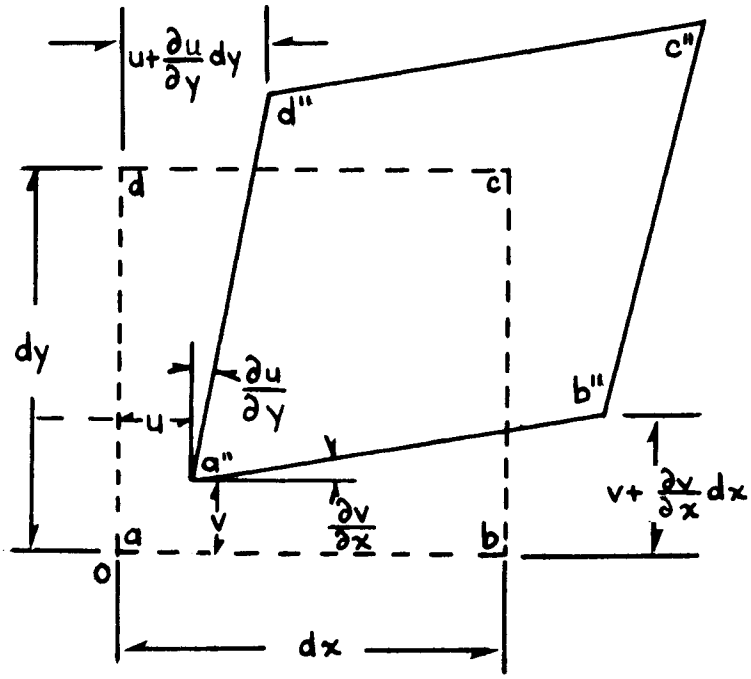

FIG. 34. DISTORTION IN THE XY-PLANE OF THE ELEMENT IN FIGURE 33

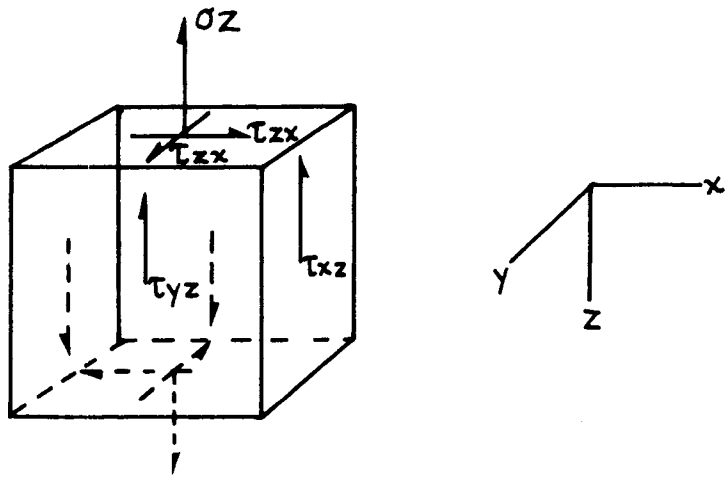

FIG. 35. STRESSES ACTING ON AN ELEMENT OF HONEYCOMB CORE

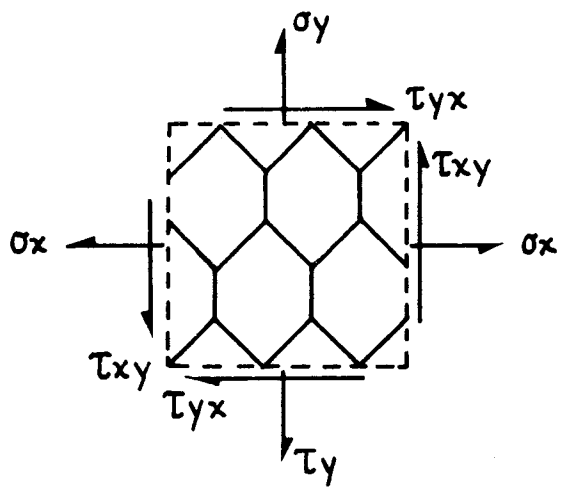

FIG. 36. PLAN VIEW OF AN ELEMENT OF HONEYCOMB CORE

$(\sigma_x = \sigma_y = \tau_{xy} = \tau_{xy} = 0)$

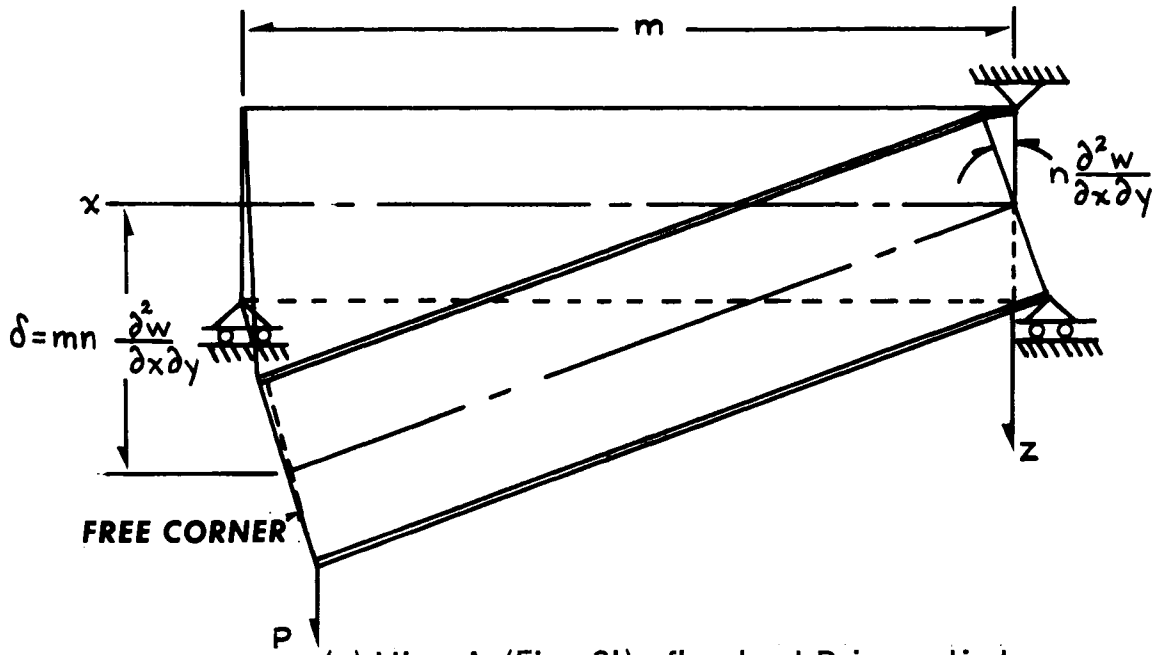

(a) View A (Fig. 31) after load P is applied

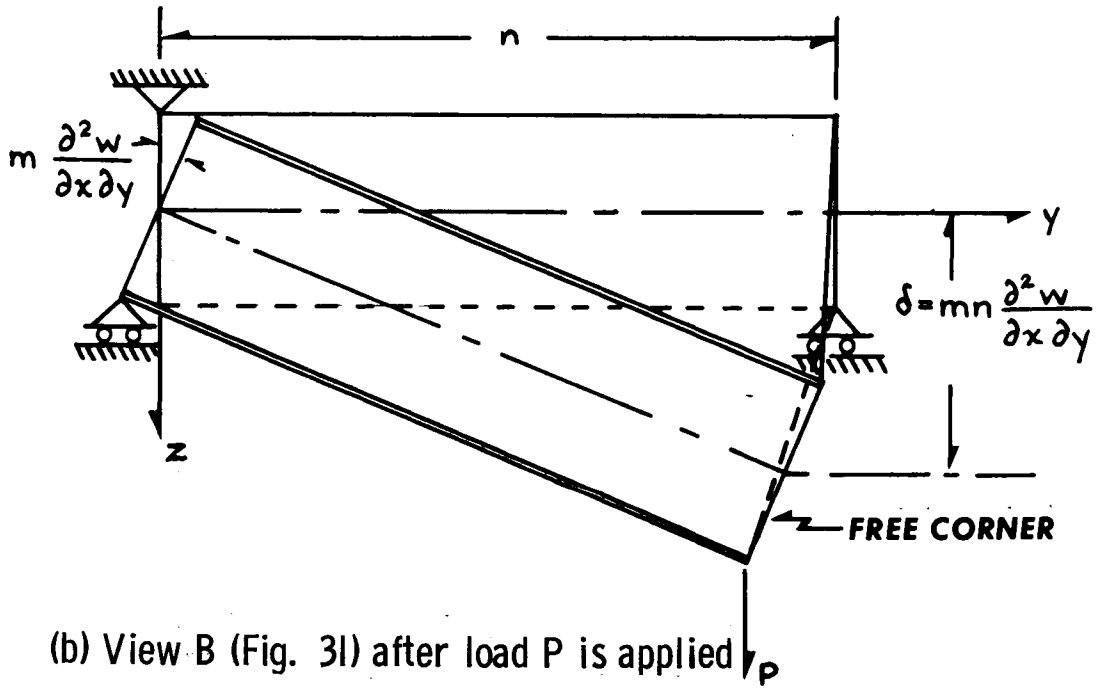

(b) View B (Fig. 31) after load P is applied

FIG. 37. SANDWICH PANEL UNDER TORSION

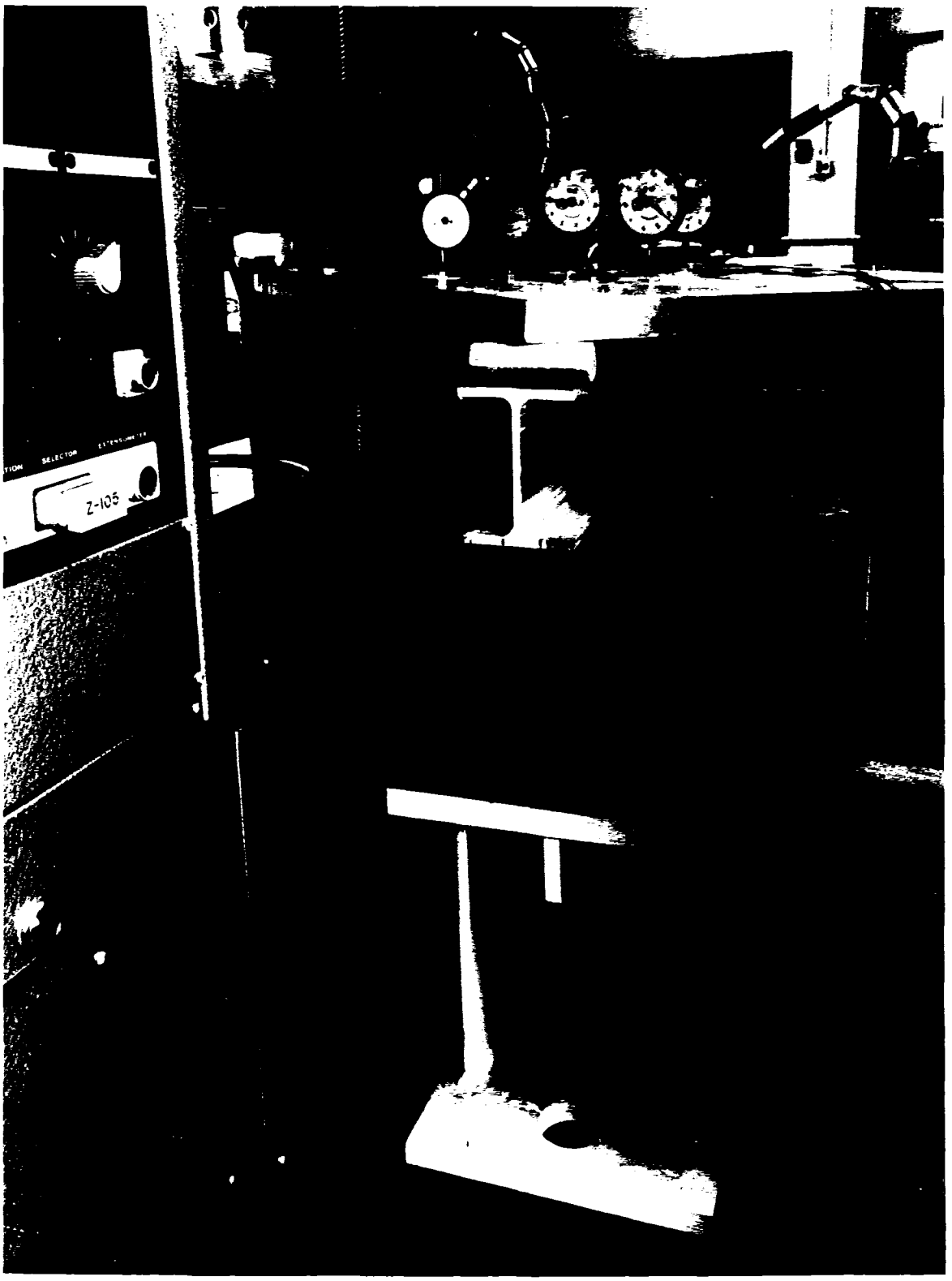

FIG. 38. EXPERIMENTAL SET-UP TO APPLY TORSION TO A SQUARE (24" x 24") SANDWICH PANEL WITH HONEYCOMB CORE.

FIG. 39. FAILURE OF A HONEYCOMB SANDWICH PANEL (24" x 24") UNDER TORSION.

FIG. 40. EXPERIMENTAL SET-UP TO APPLY TORSION TO A SQUARE (24" x 24") SANDWICH PANEL WITH STYROLITE CORE.

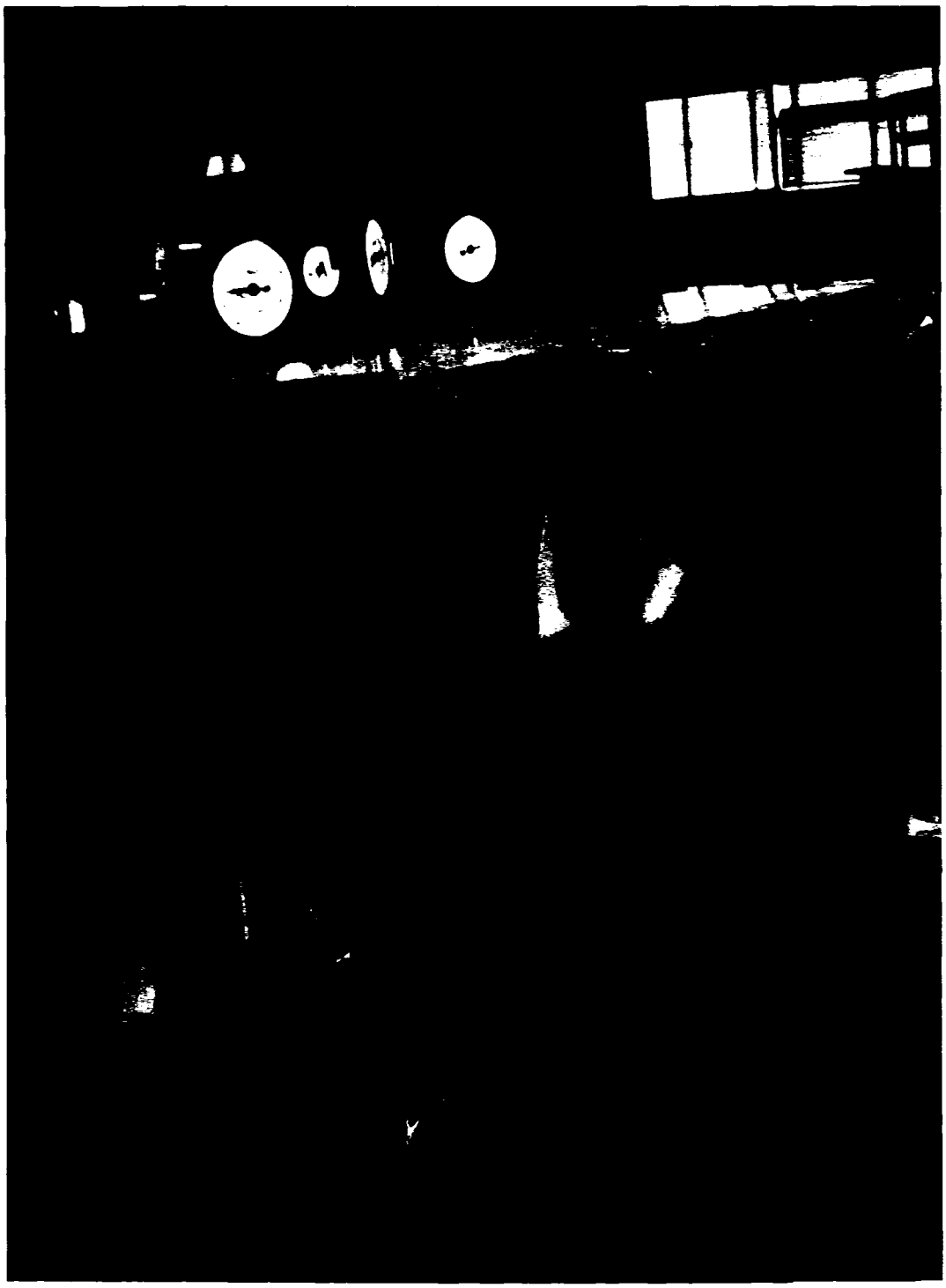

FIG. 41. LARGE DISTORTION OF A STYROLITE SANDWICH PANEL (24" x 24") UNDER TORSION.

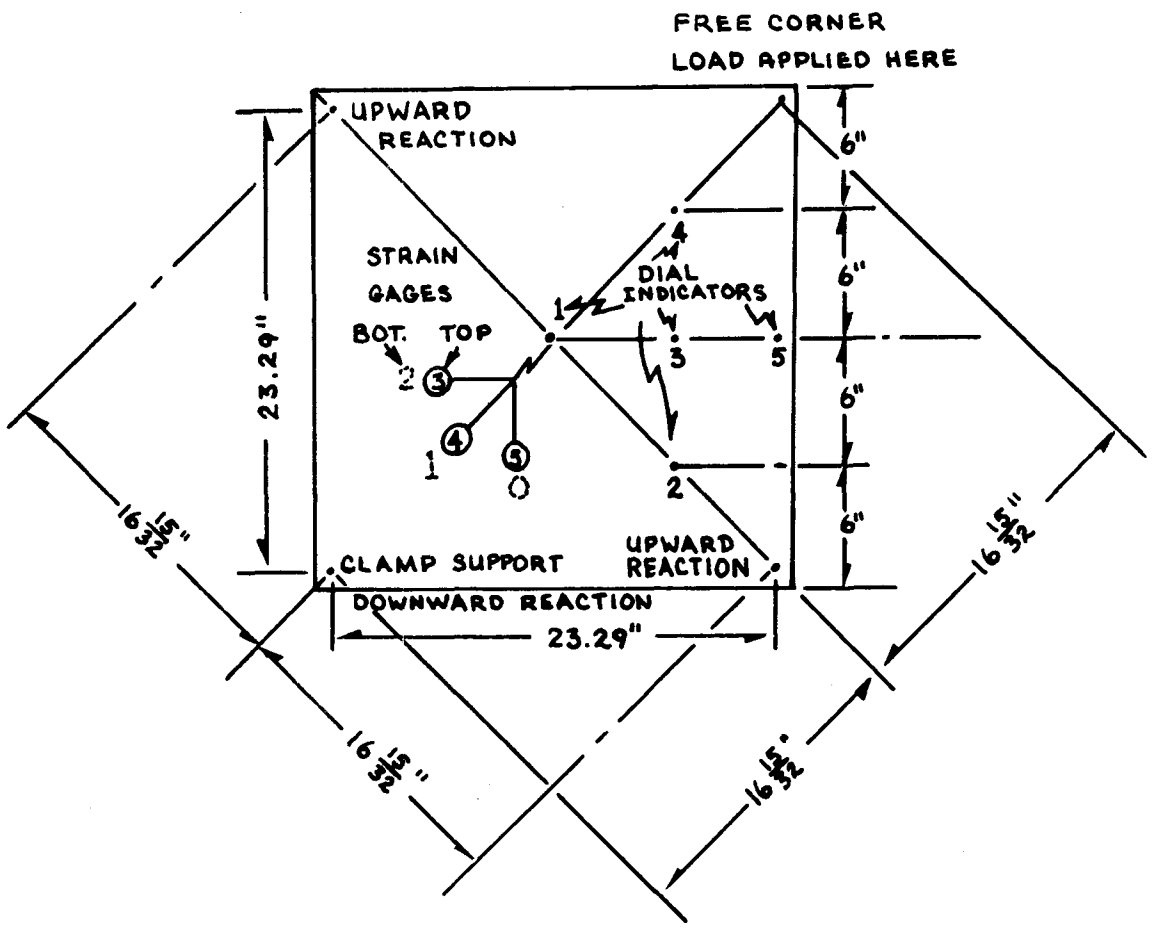

FIG. 42. PLAN VIEW OF TYPICAL TORSION SAMPLE

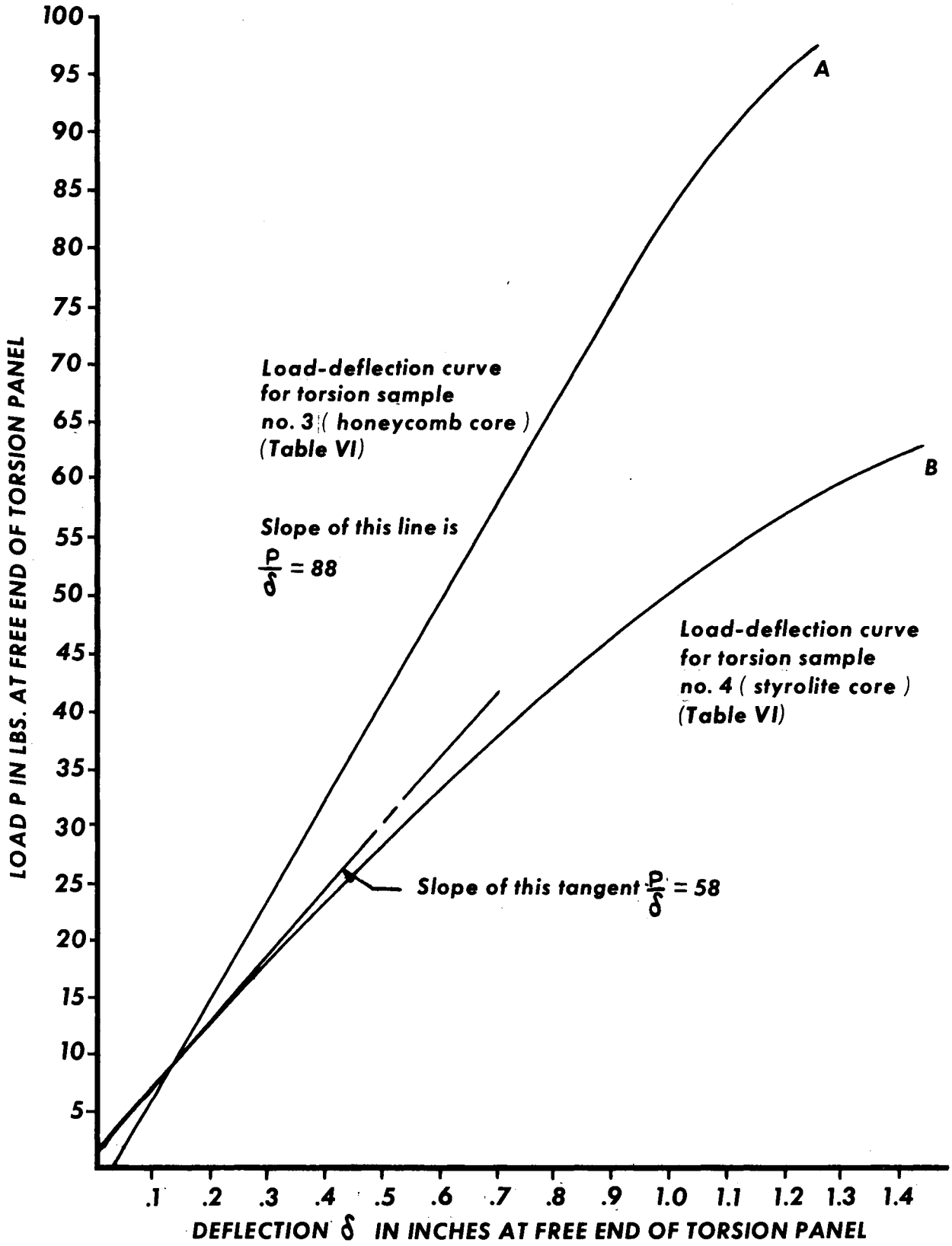

FIG. 43. LOAD-DEFLECTION CURVES FOR PANELS UNDER PURE TORSION

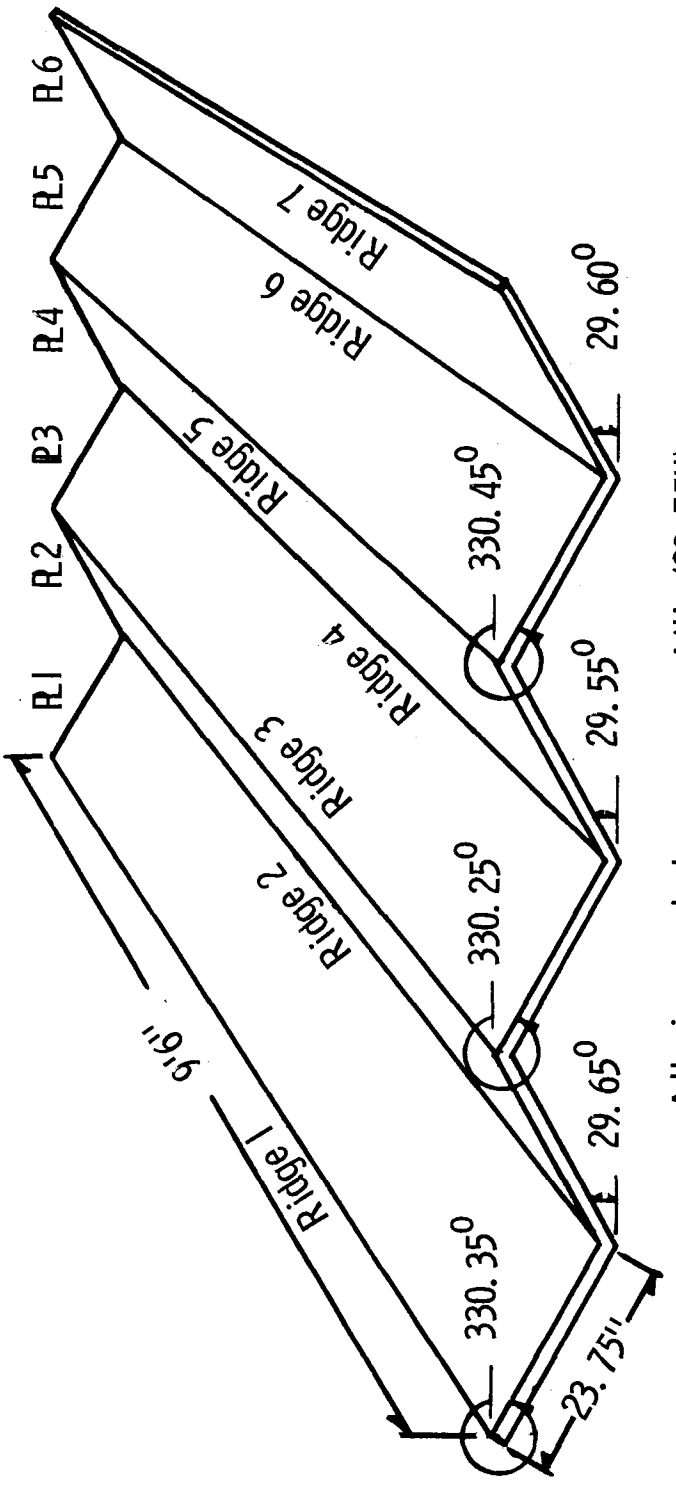

FIG. 44. FOLDED PLATE MODEL MADE UP OF SANDWICH PANELS HAVING ALUMINUM FACINGS (.025" THICK) AND HONEYCOMB CORE (1" THICK)

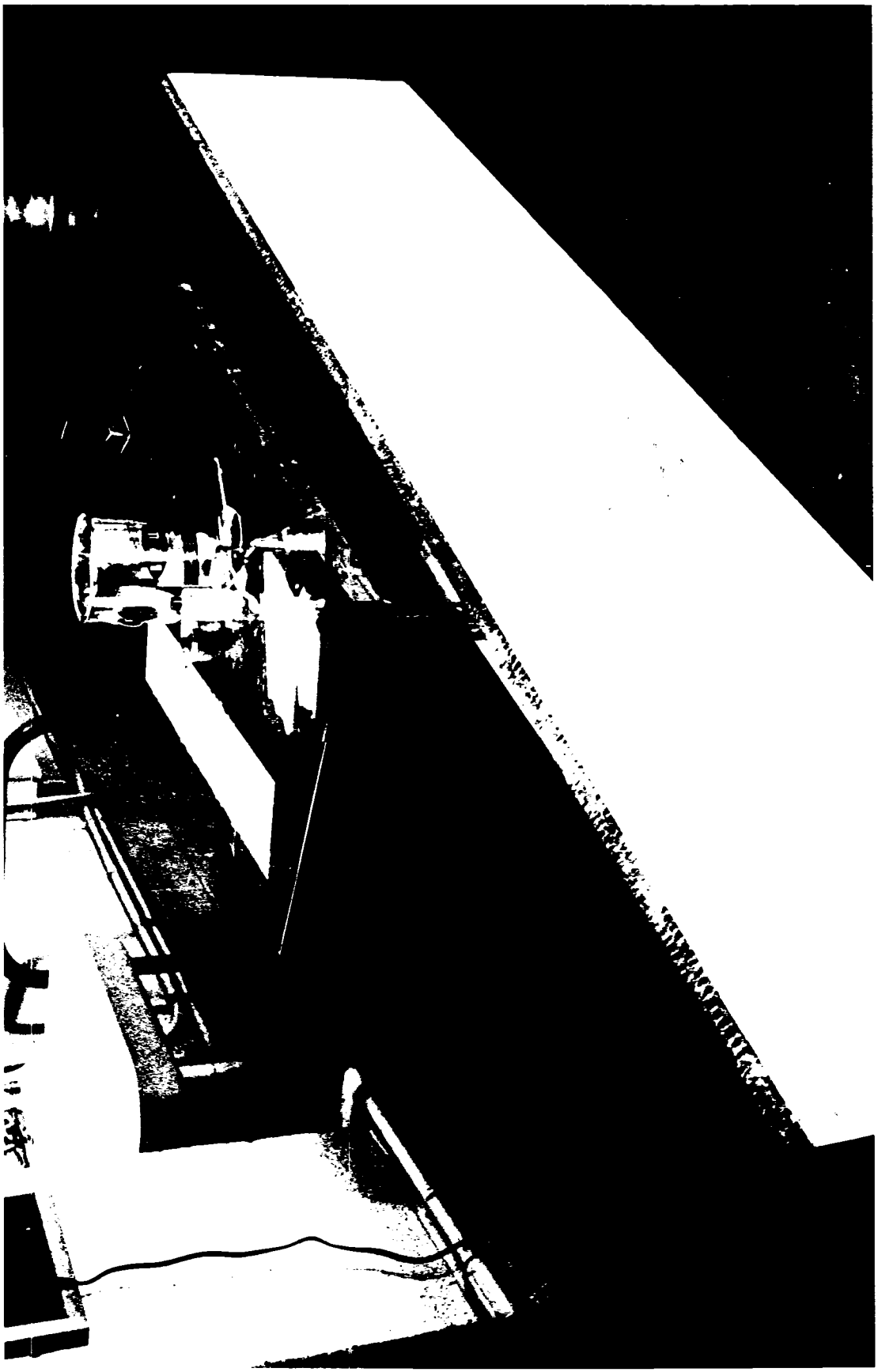

FIG. 45. HONEYCOMB SANDWICH PANEL BEVELLED AND REINFORCED AT THE EDGES

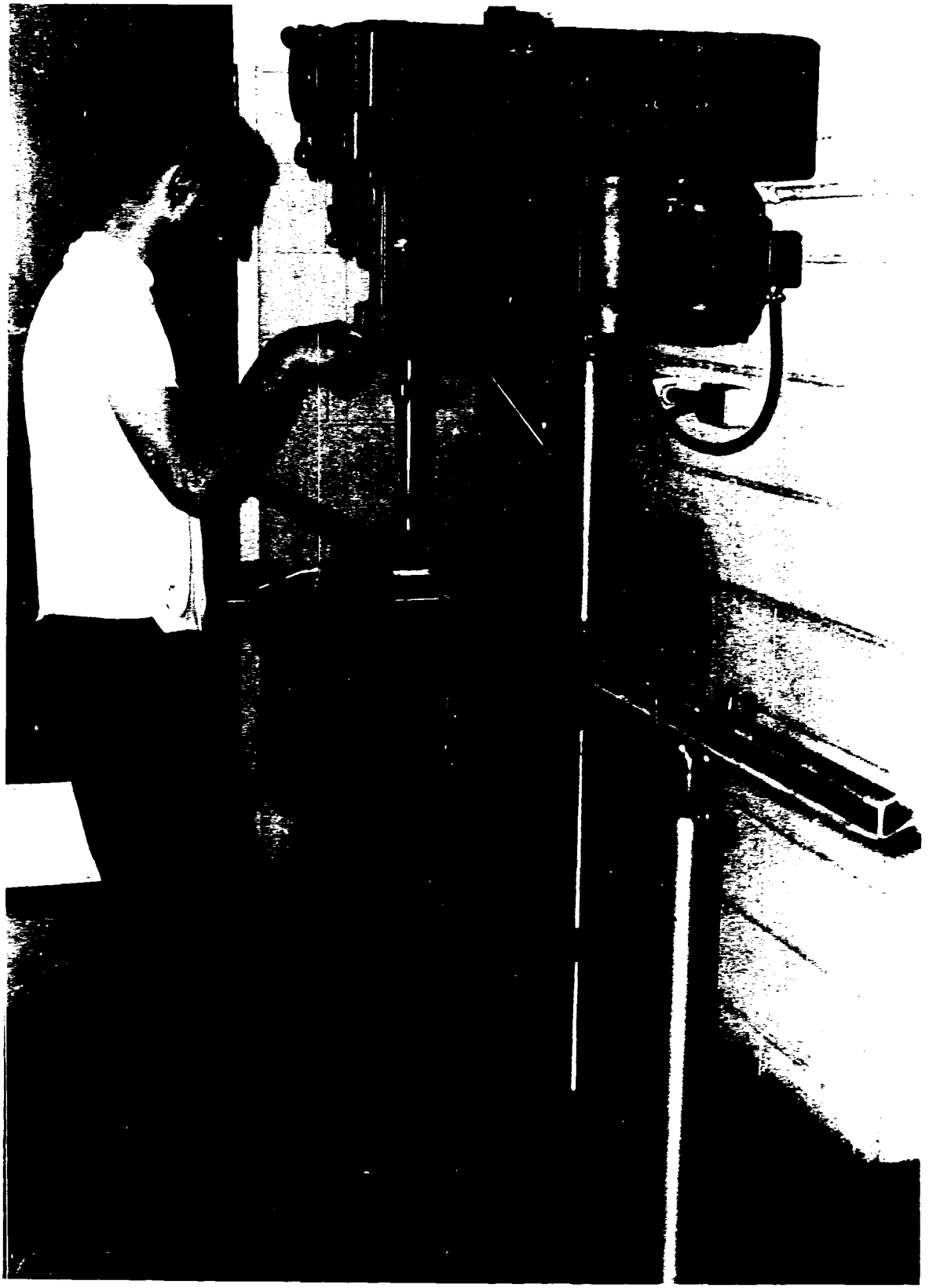

FIG. 46. HOLES ARE BEING DRILLED IN THE WEB OF THE CONNECTING CHANNELS TO SUSPEND THE CABLES OF THE LOADING TREE.

FIG. 47. HOLES FOR CONNECTING BOLTS ARE BEING DRILLED THROUGH THE FLANGES OF THE CONNECTING CHANNEL AND THE EDGE OF THE SANDWICH PANEL.

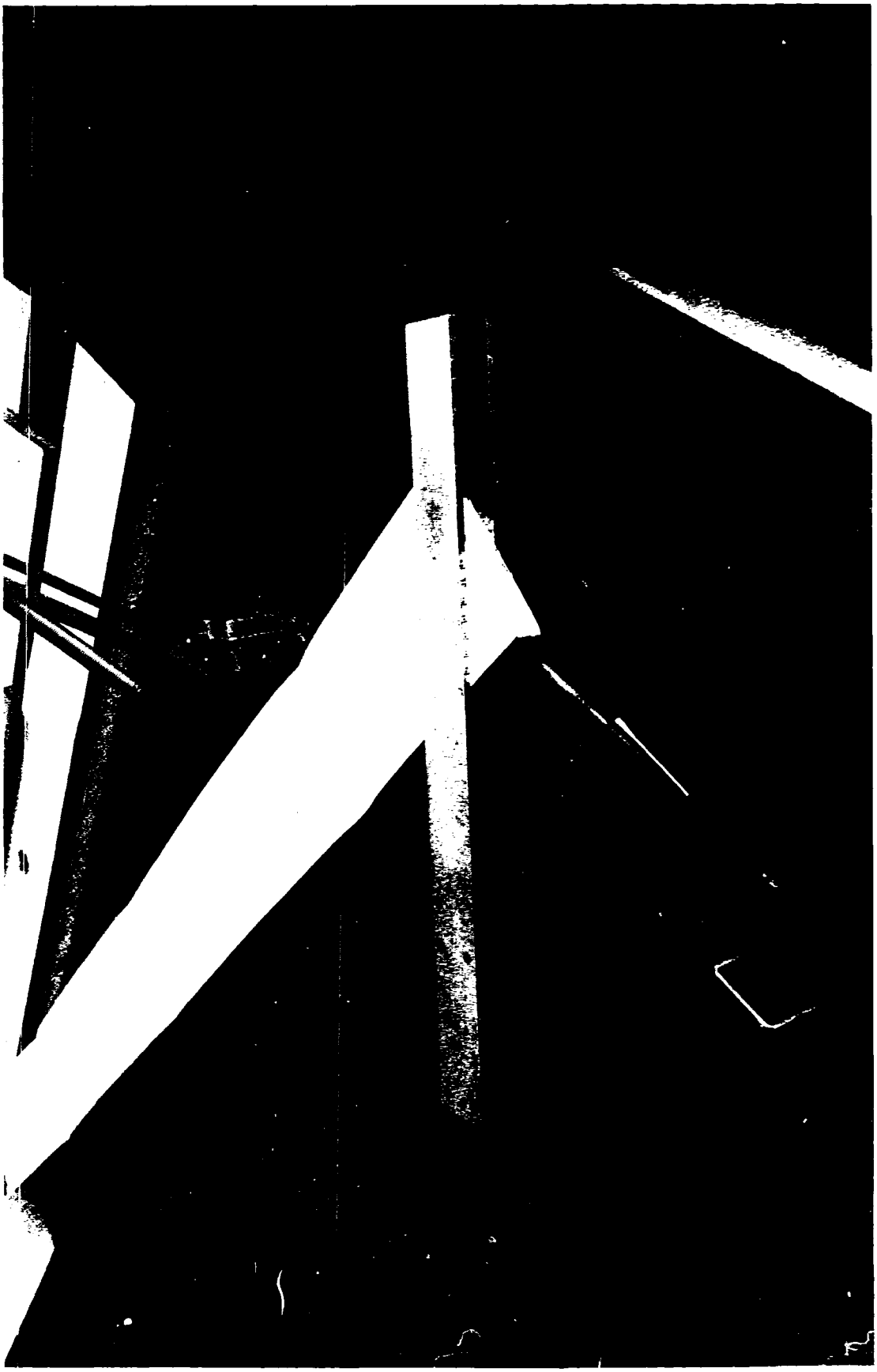

FIG. 48. GRADUATED FORK TO SELECT CORRESPONDING POINTS ON THE TOP AND BOTTOM FACINGS FOR STRAIN GAUGE LOCATIONS.

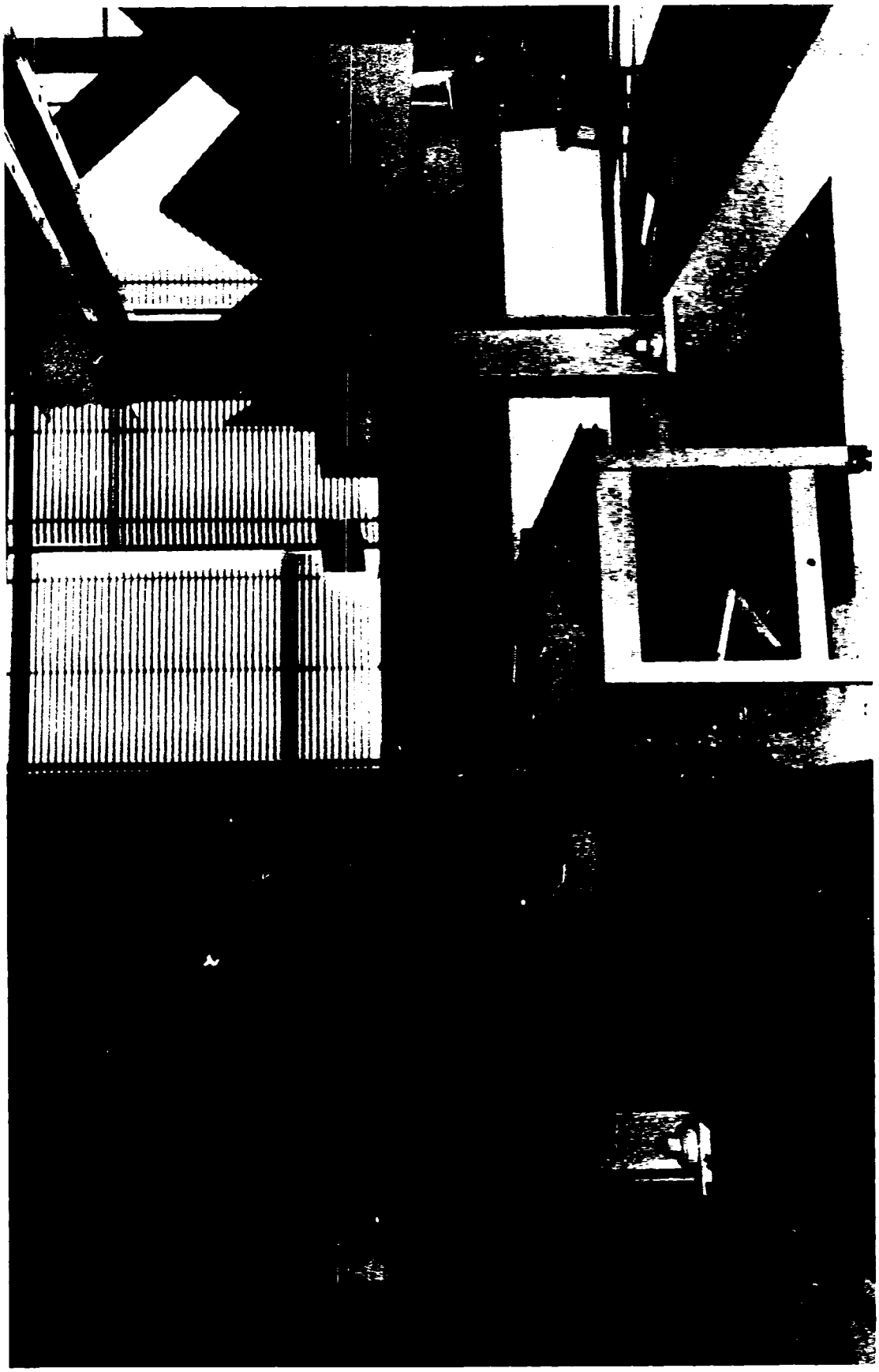

FIG. 49. SUPPORTING END-DIAPHRAGMS (ONE-INCH THICK PLYWOOD) BOLTED ON HEAVY BEAMS.

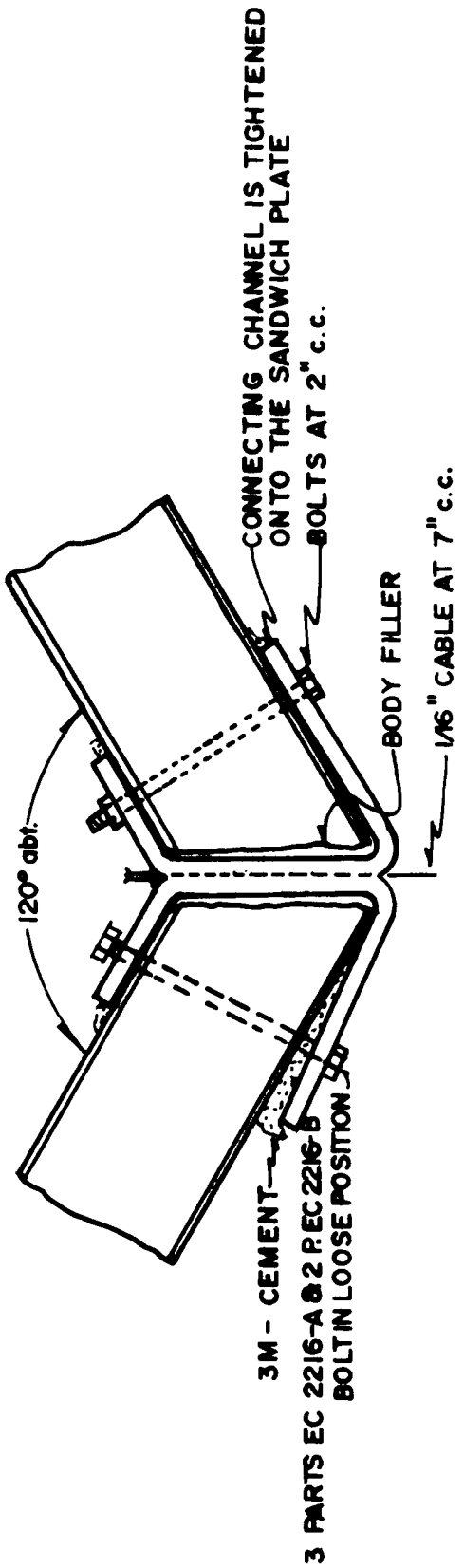

FIG. 50. TYPICAL CONNECTION USED TO JOIN SANDWICH PANELS AT THE RIDGES OF THE FOLDED PLATE MODELS

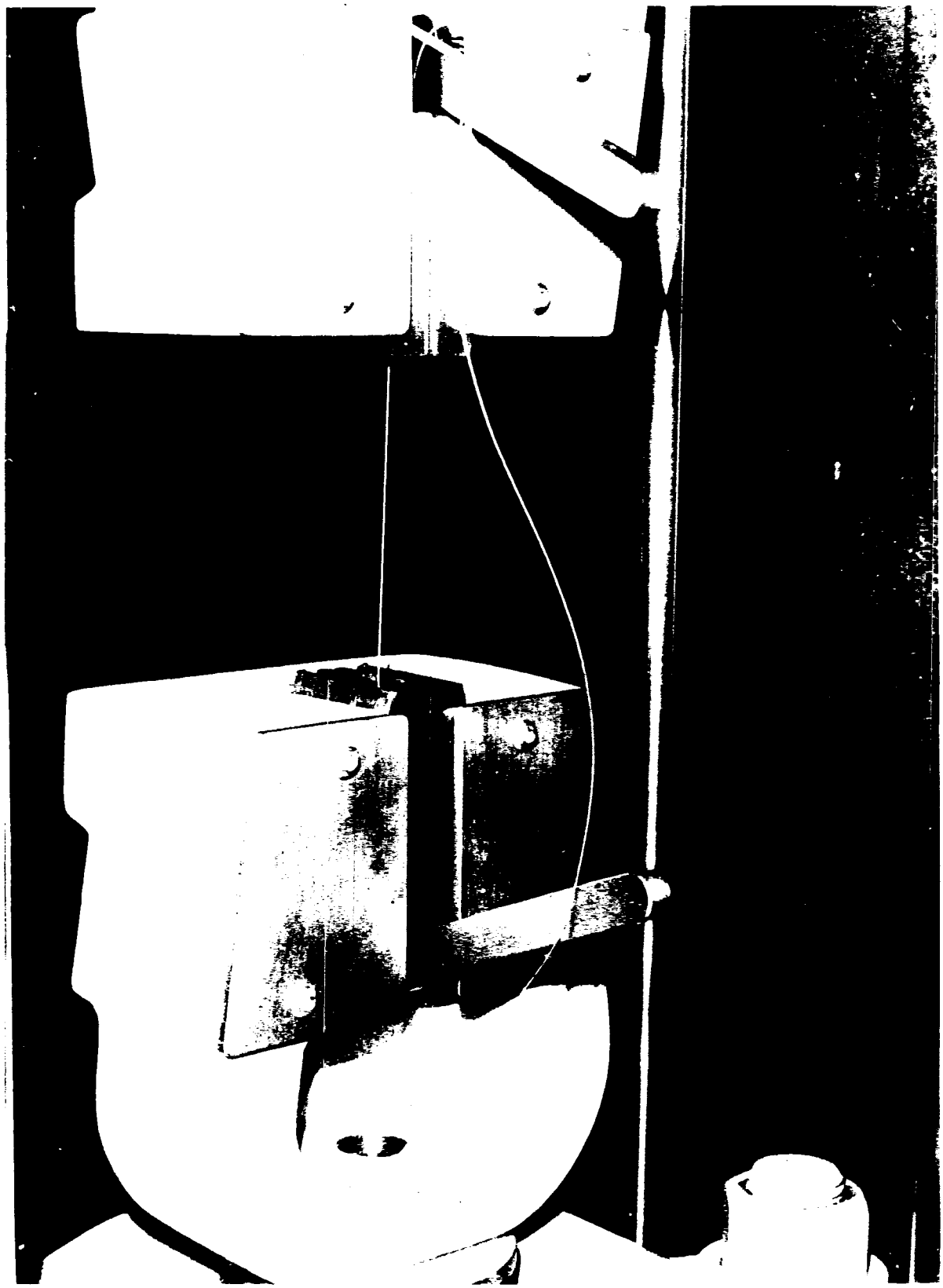

FIG. 51. ULTIMATE STRENGTH TEST OF THE CABLE (1/16" IN DIAMETER) SUSPENDED THROUGH THE HOLES IN THE WEB OF THE CONNECTING CHANNELS TO SUPPORT THE LOADING TREES.

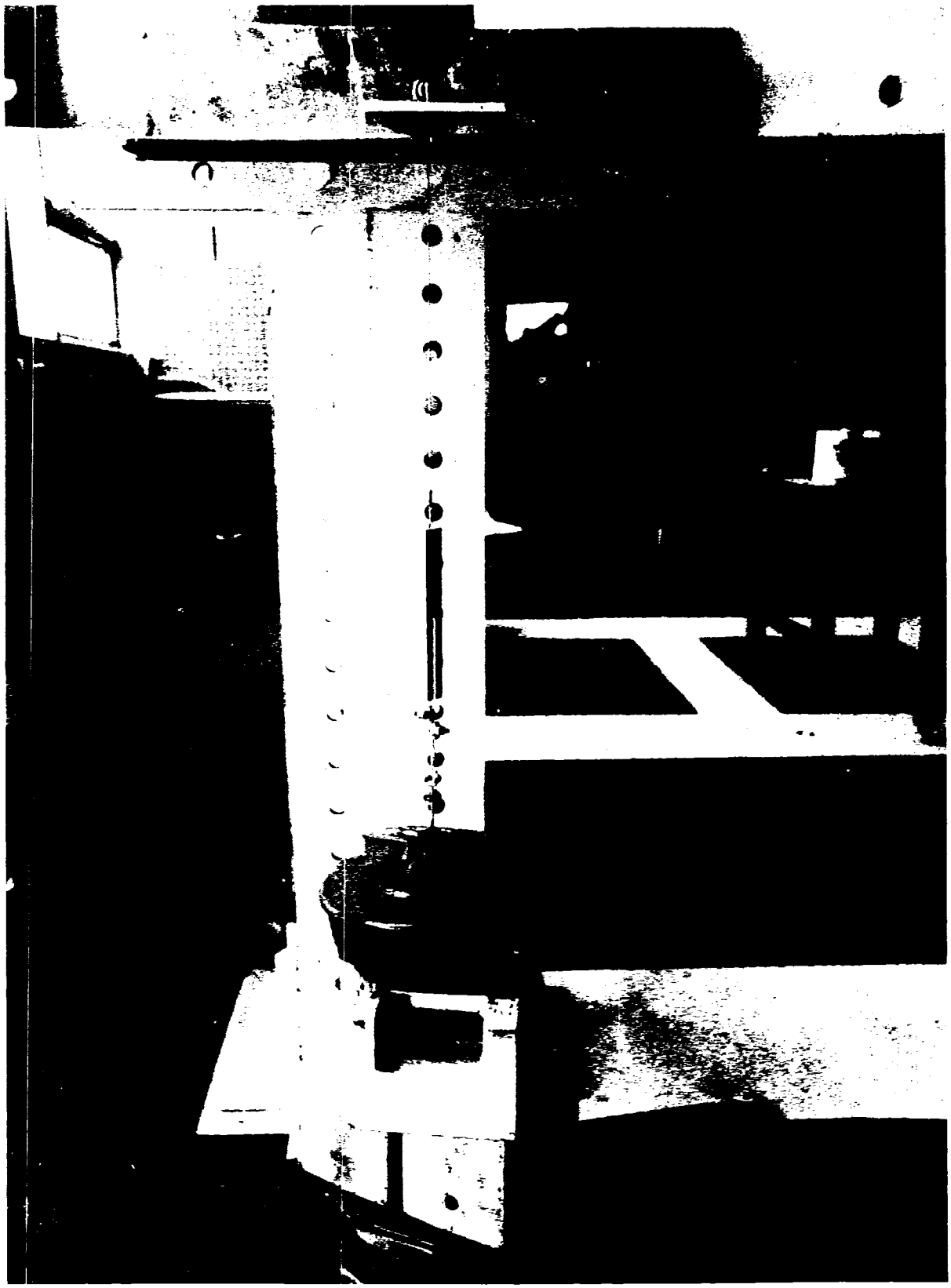

FIG. 52. CABLE ASSEMBLY USED TO SUSPEND THE LOADING TREES IS TESTED FOR STRENGTH.

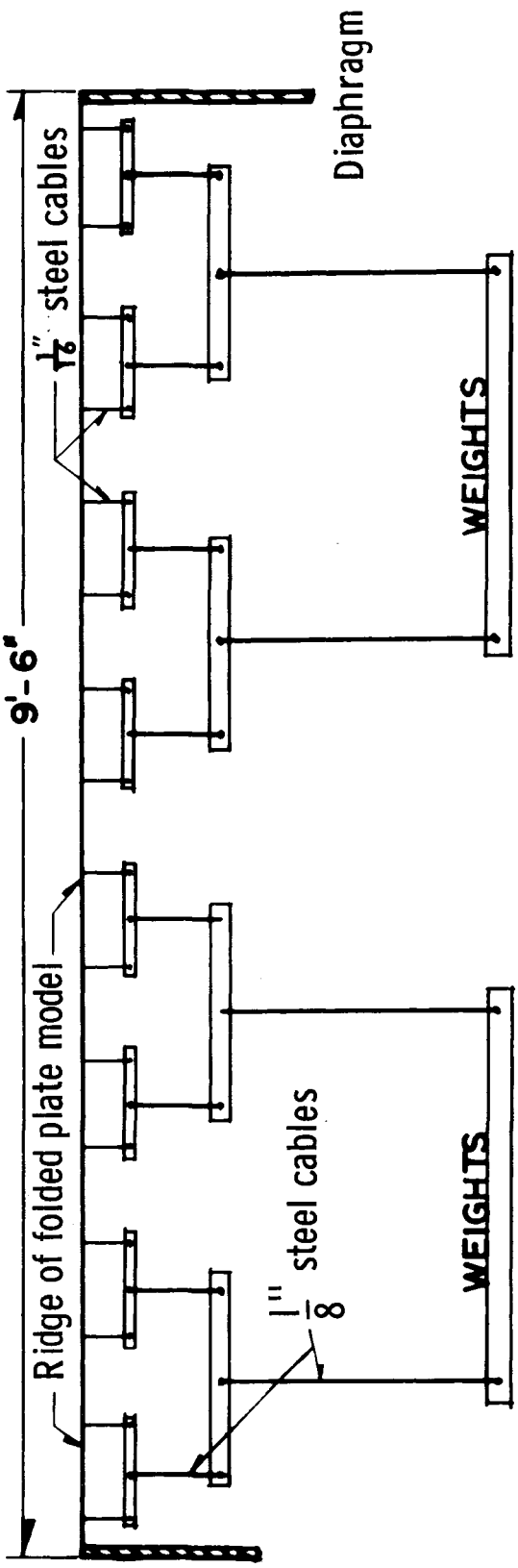

FIG. 53. TYPICAL LOADING TREE SUSPENDED AT THE INTERIOR FIVE RIDGES OF THE FOLDED PLATE MODEL

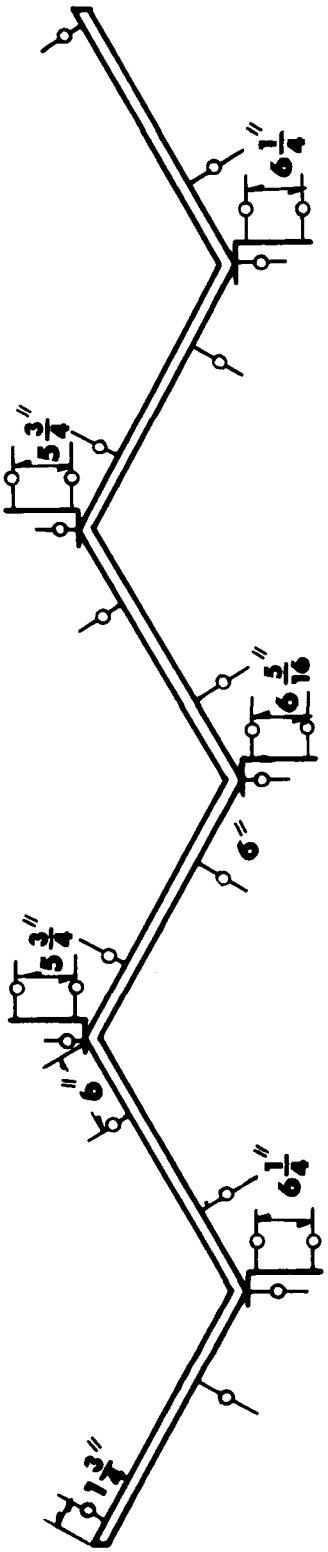

FIG. 54. SET-UP OF DIAL INDICATORS LOCATED AT MIDSPAN TO MEASURE THE DEFLECTION OF THE FOLDED PLATE MODEL

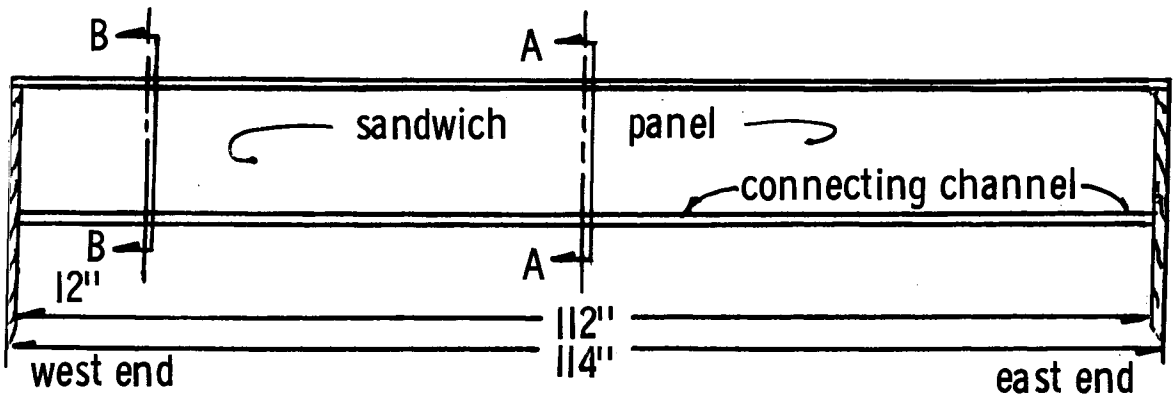

(a) Side view of folded plate model

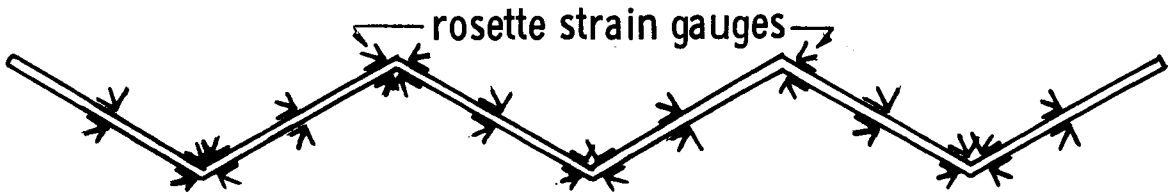

(b) Section A-A (30 rosettes = 90 channels)

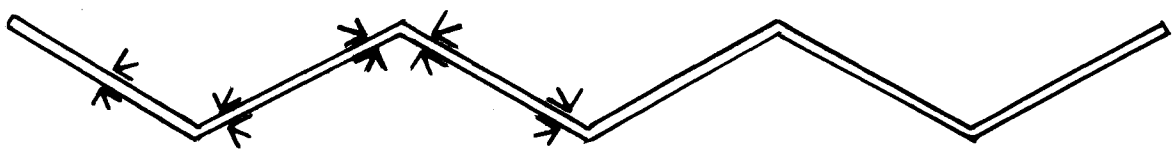

(c) Section B-B (10 rosettes = 30 channels)

FIG. 55. LOCATION OF STRAIN GAUGES INSTALLED AT MIDSPAN AND AT ONE FOOT FROM THE FACE OF THE WEST-END SUPPORT

FIG. 56. UNIFORM LOAD IS APPLIED AT THE FIVE INTERIOR RIDGES WITH STANDARD 50-LB. WEIGHTS.

FIG. 57. A UNIFORM LOAD OF 2400 LBS IS APPLIED AT EACH OF RIDGES 3 AND 5 WITH STANDARD 50-LB WEIGHTS.

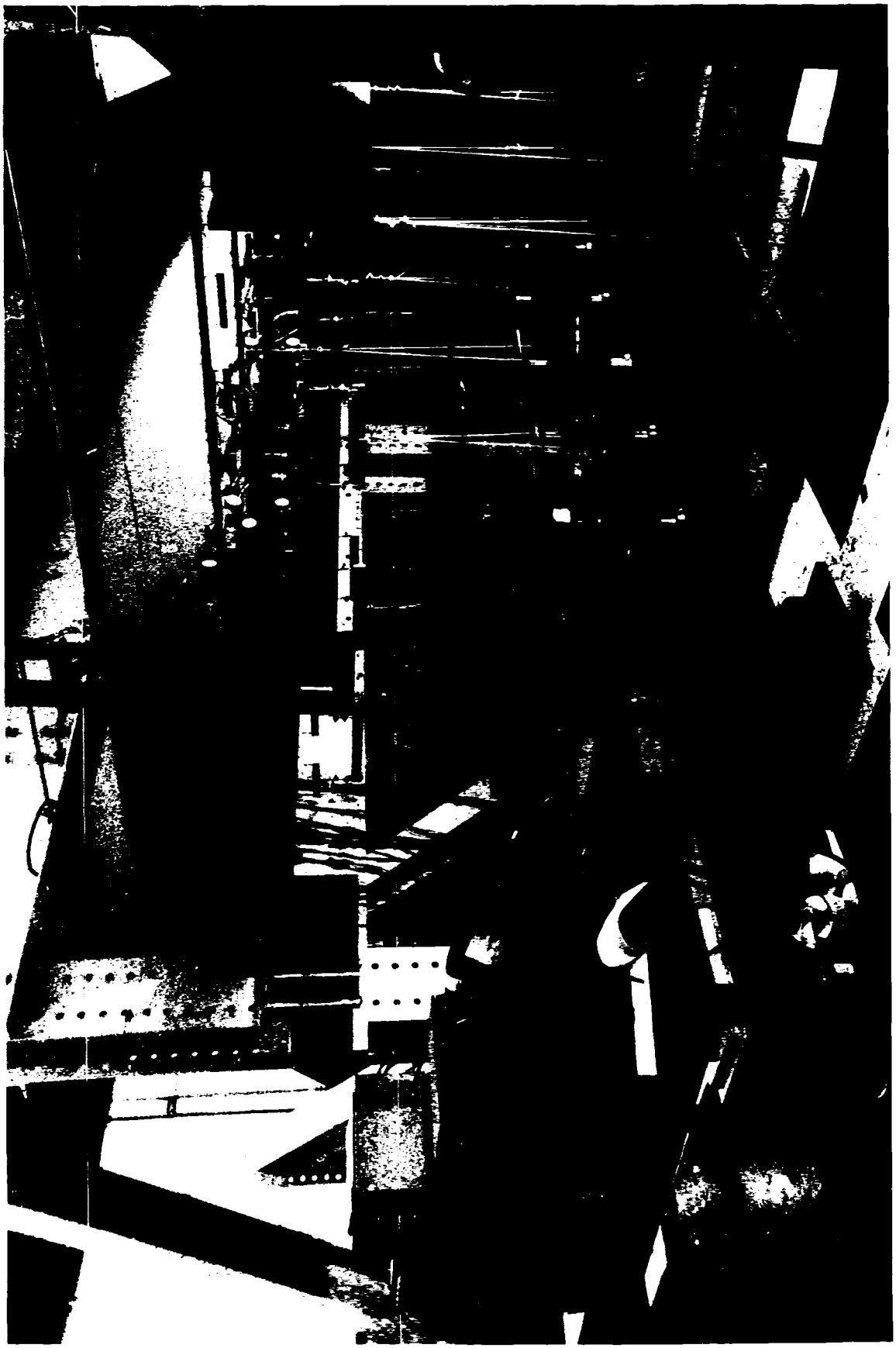

FIG. 58. UNIFORM LOAD IS APPLIED AT THE FIVE INTERNAL RIDGES WITH HYDRAULIC RAMS.

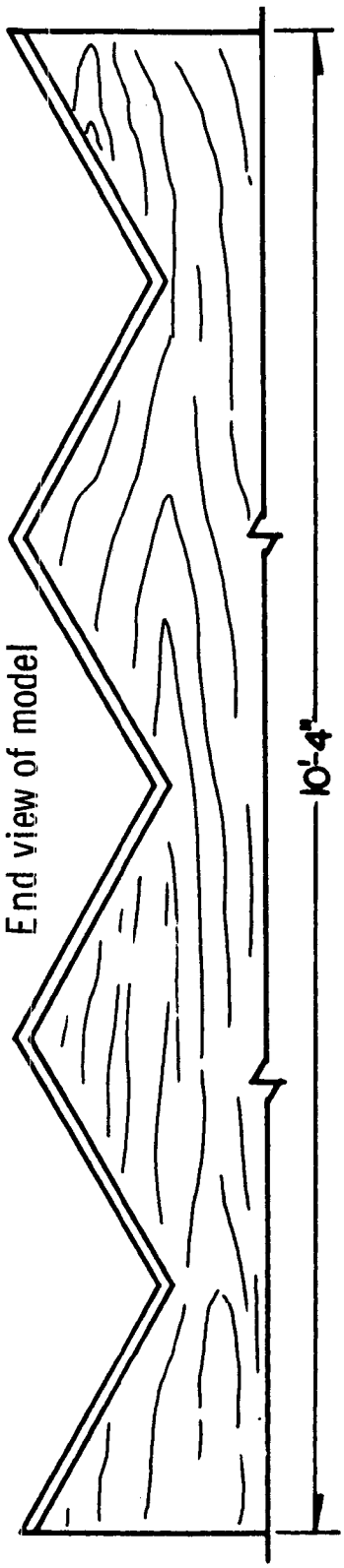

FIG. 59. ENDS OF MODEL ARE UNIFORMLY SUPPORTED

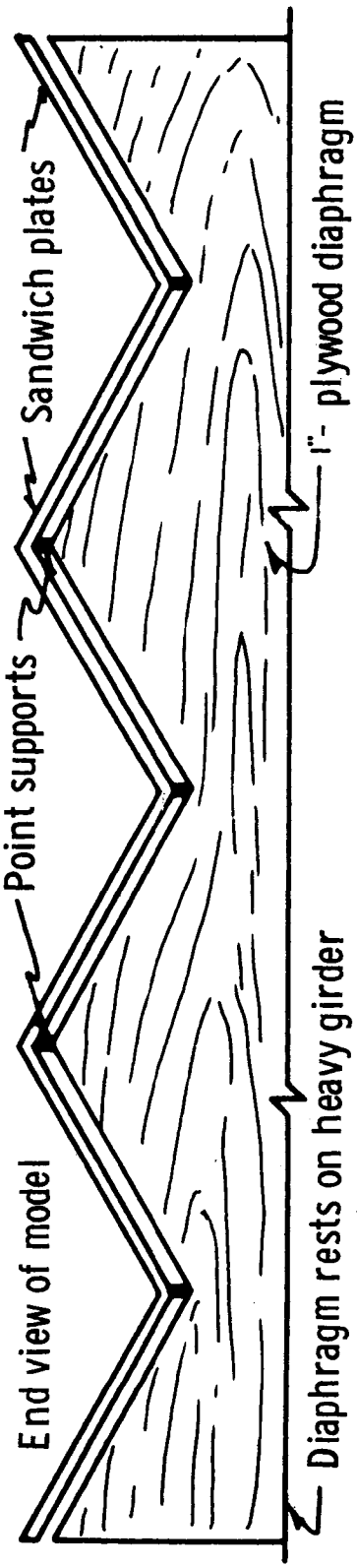

FIG. 60. ENDS OF MODEL ARE POINT SUPPORTED AT THE FIVE INTERIOR RIDGES

FIG. 61. END VIEW OF POINT SUPPORTS BETWEEN THE END DIAPHRAGMS AND THE FIVE INTERNAL RIDGES OF THE MODEL.

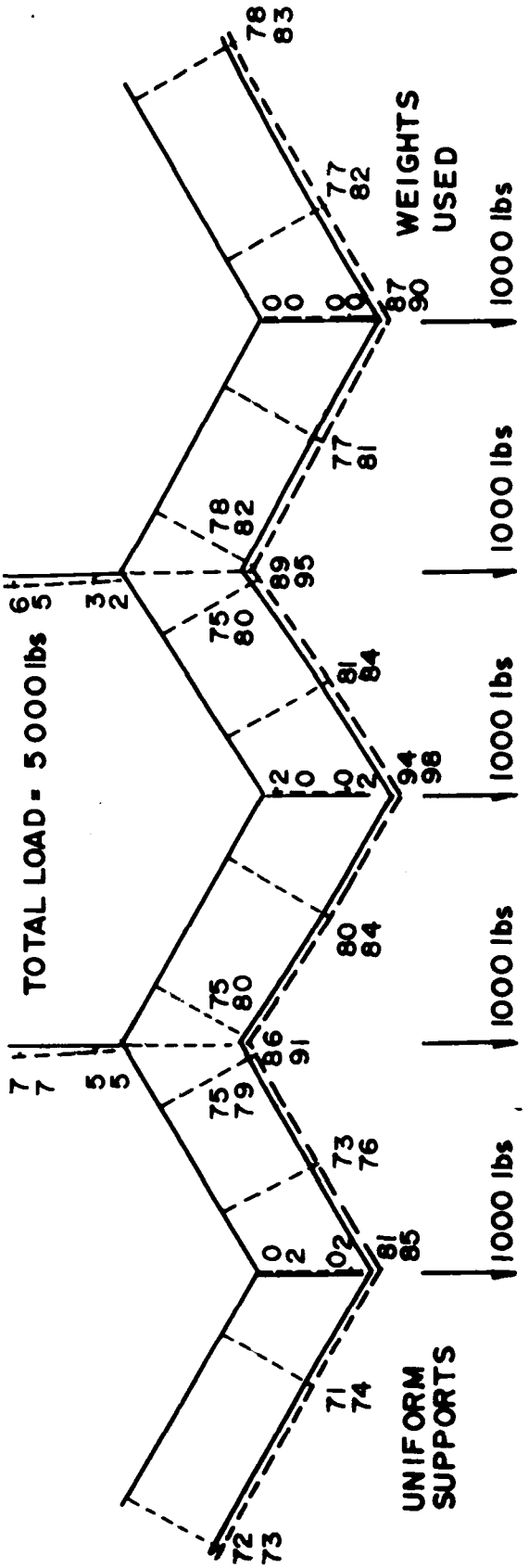

FIG. 62. STUDY OF CREEP AFTER 166 HOURS - EXPERIMENTAL DEFLECTIONS IN .001" AT MIDSPAN OF THE 9.5-FOOT FOLDED PLATE MODEL - FIVE RIDGES UNIFORMLY LOADED WITH 5000 POUNDS

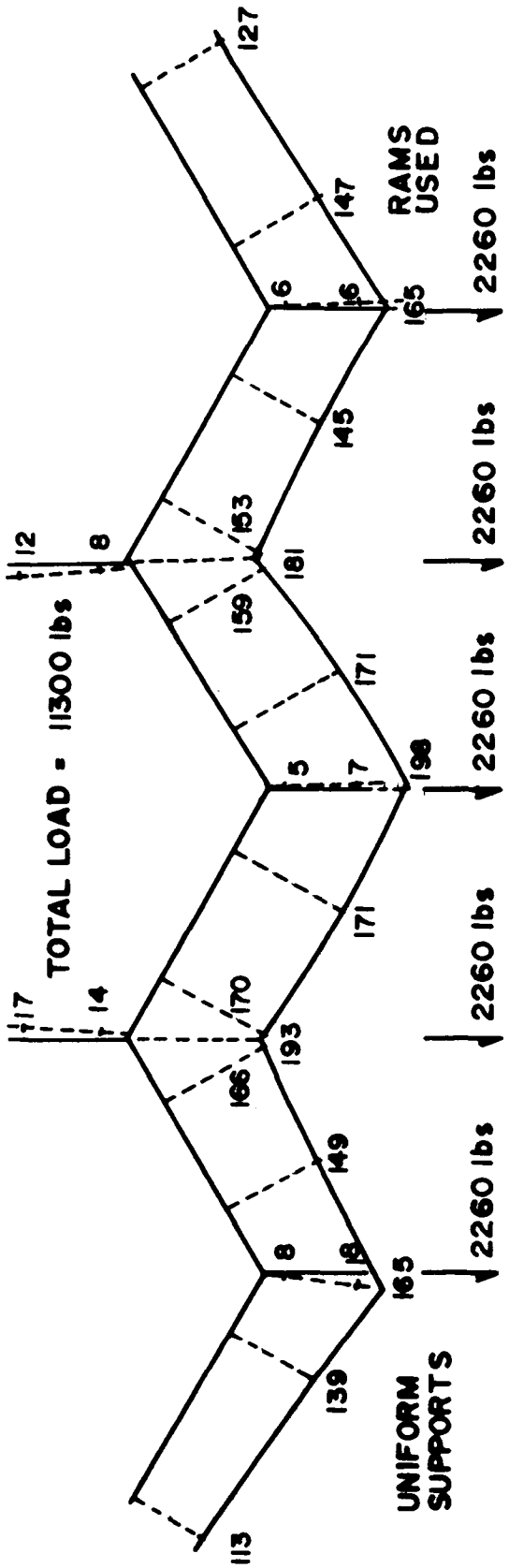

FIG. 63. EXPERIMENTAL DEFLECTIONS IN .001" AT MIDSPAN OF THE 9.5-FOOT FOLDED PLATE MODEL - FIVE RIDGES UNIFORMLY LOADED WITH 11,300 POUNDS

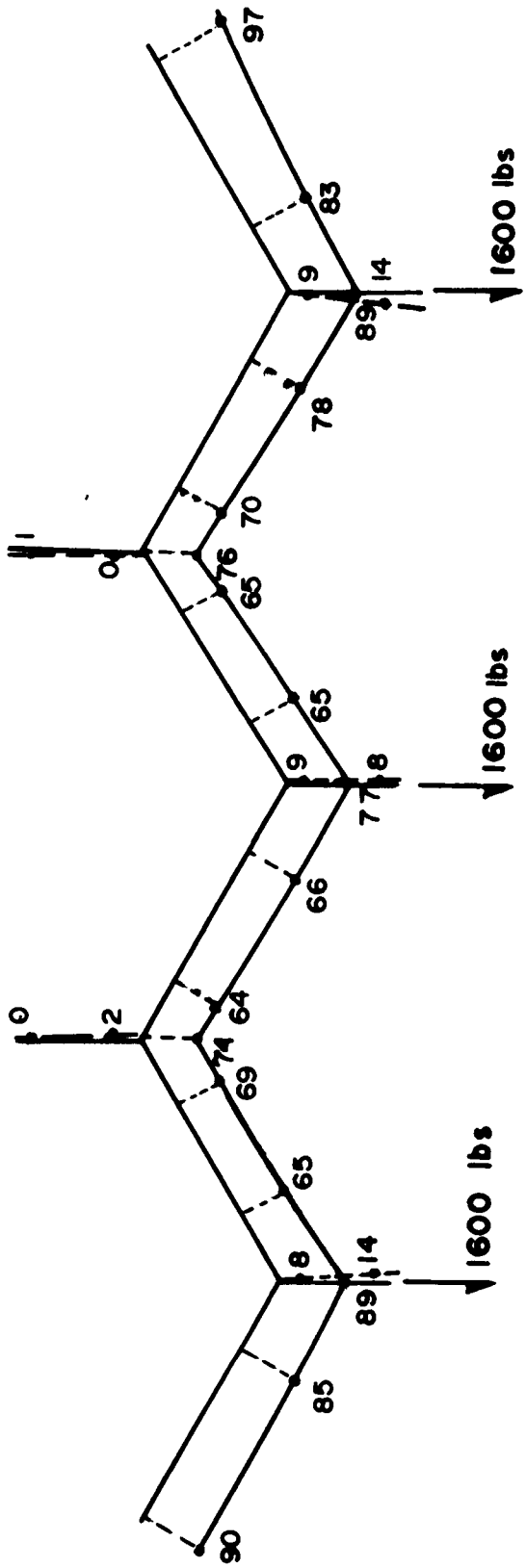

FIG. 64. EXPERIMENTAL DEFLECTIONS IN .001" AT MIDSPAN OF THE 9.5-FOOT FOLDED PLATE MODEL - RIDGES 2, 4 AND 6 EACH UNIFORMLY LOADED WITH 1600 POUNDS

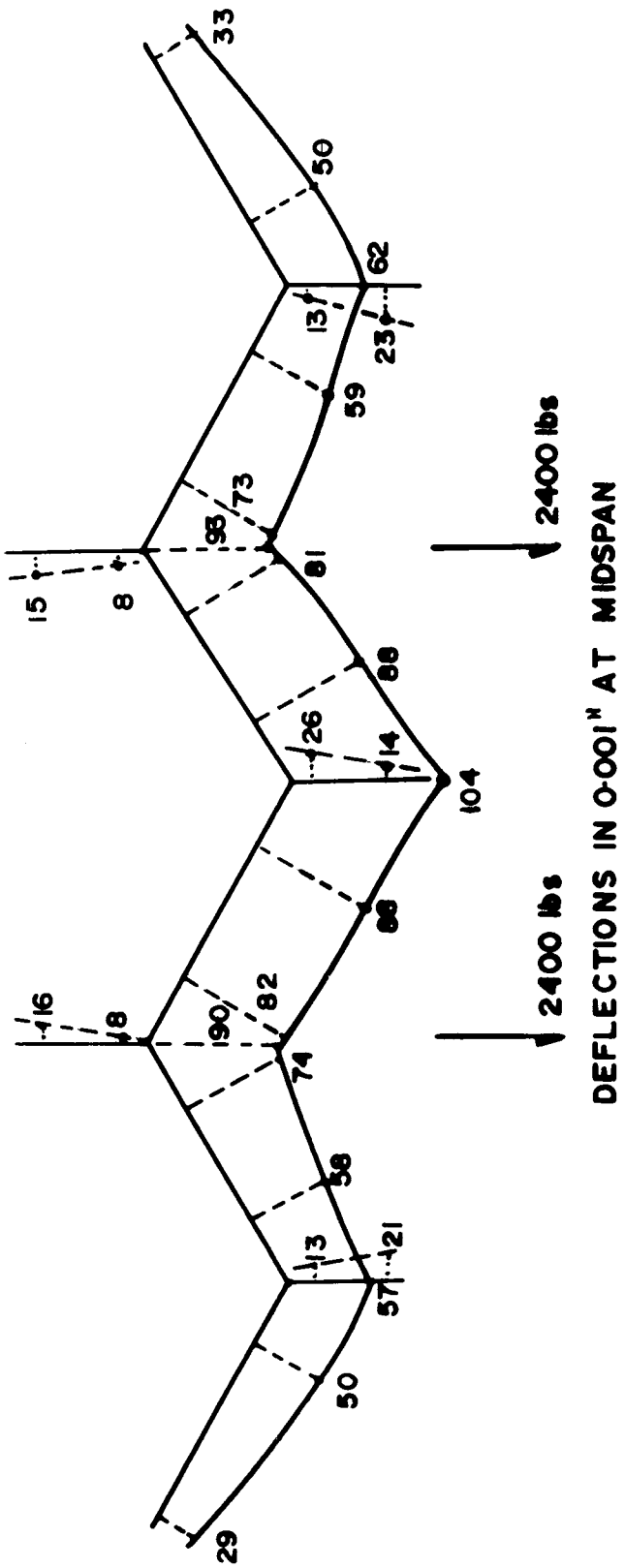

FIG. 65. EXPERIMENTAL DEFLECTIONS IN .001" AT MIDSPAN OF THE 9.5-FOOT FOLDED PLATE MODEL - RIDGES 3 AND 5 EACH UNIFORMLY LOADED WITH 2400 POUNDS

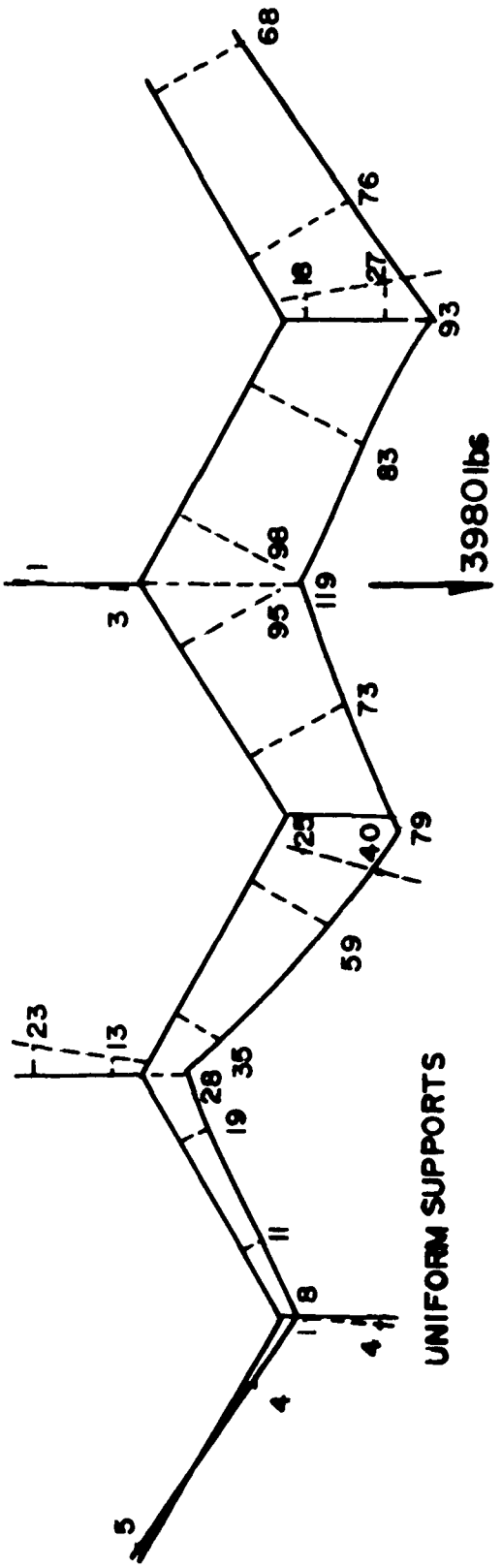

FIG. 66. EXPERIMENTAL DEFLECTIONS IN .001" AT MIDSPAN OF THE 9.5-FOOT FOLDED PLATE MODEL - RIDGE 5 UNIFORMLY LOADED WITH 3980 POUNDS

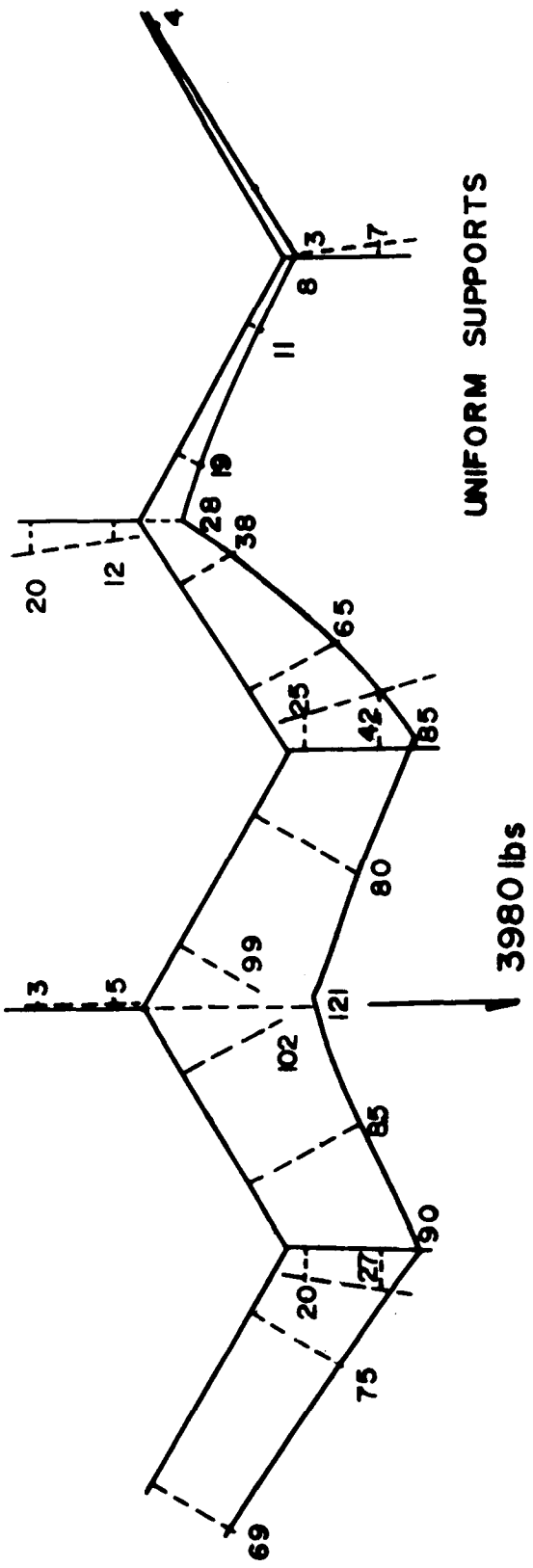

FIG. 67. EXPERIMENTAL DEFLECTIONS IN .001" AT MIDSPAN OF THE 9.5-FOOT FOLDED PLATE MODEL - RIDGE 3 UNIFORMLY SUPPORTED WITH 3980 POUNDS

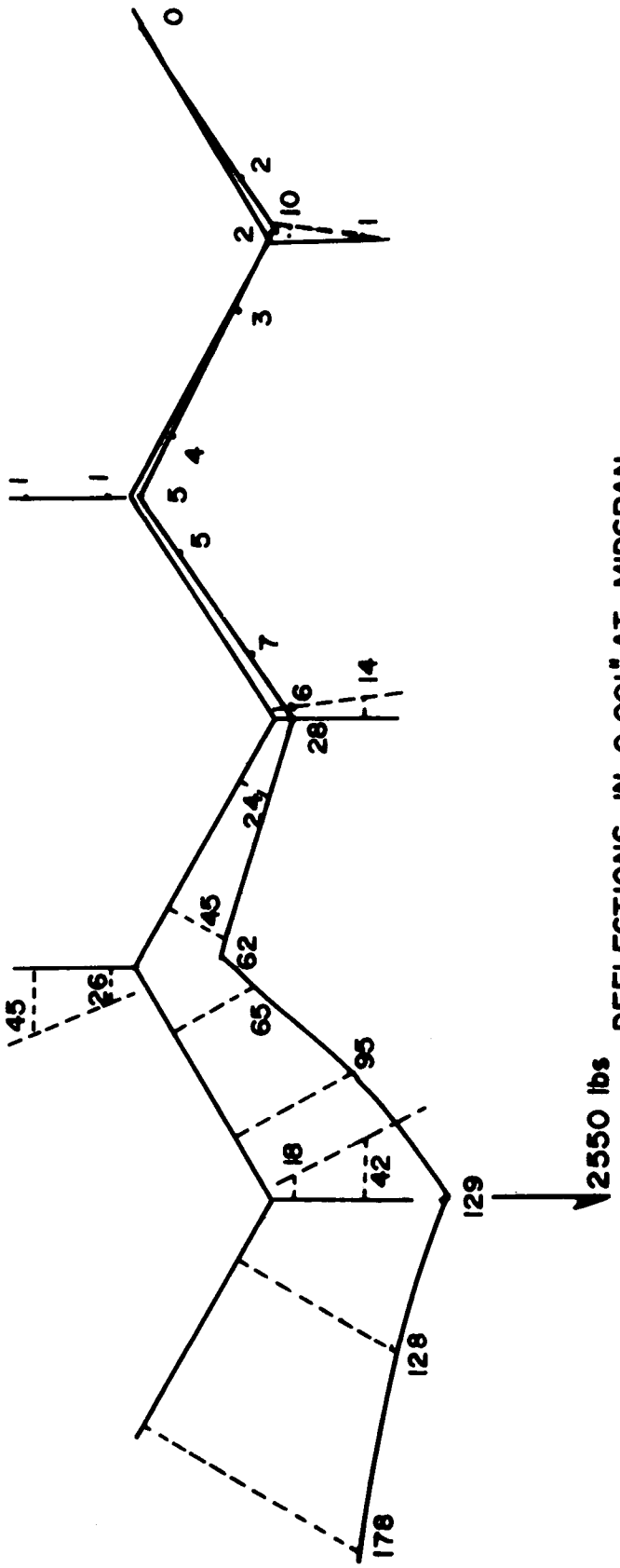

FIG. 68. EXPERIMENTAL DEFLECTIONS IN .001" AT MIDSPAN OF THE 9.5-FOOT FOLDED PLATE MODEL - RIDGE 2 UNIFORMLY LOADED WITH 2550 POUNDS

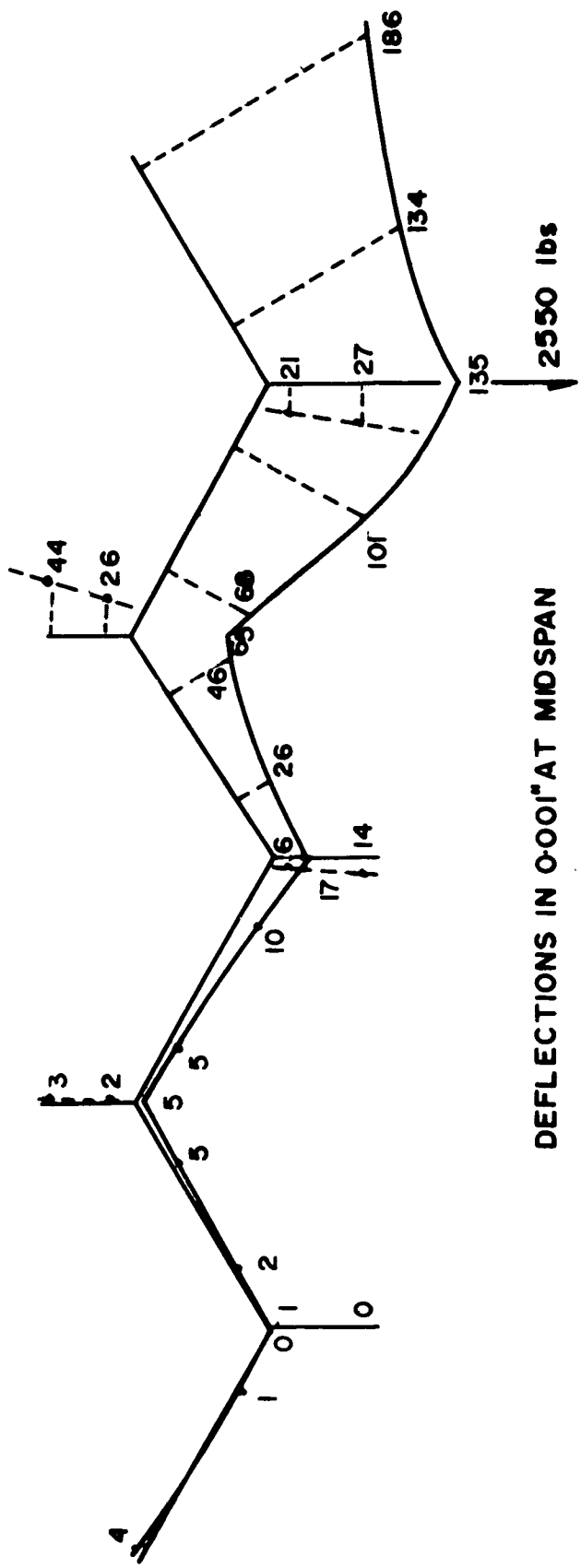

FIG. 69. EXPERIMENTAL DEFLECTIONS IN .001" AT MIDSPAN OF THE 9.5-FOOT FOLDED PLATE MODEL - RIDGE 6 UNIFORMLY LOADED WITH 2550 POUNDS

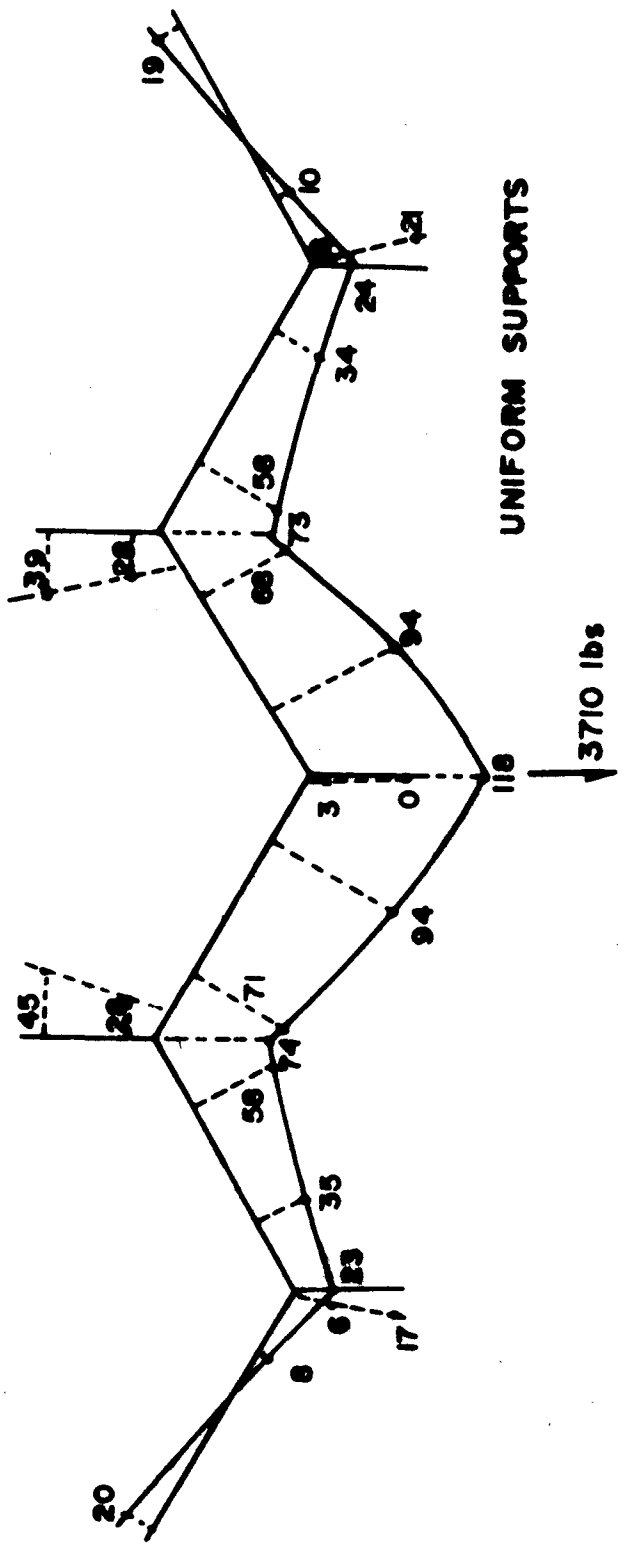

FIG. 70. EXPERIMENTAL DEFLECTIONS IN .001" AT MIDSPAN OF THE 9.5-FOOT FOLDED PLATE MODEL - RIDGE 4 UNIFORMLY LOADED WITH 3710 POUNDS

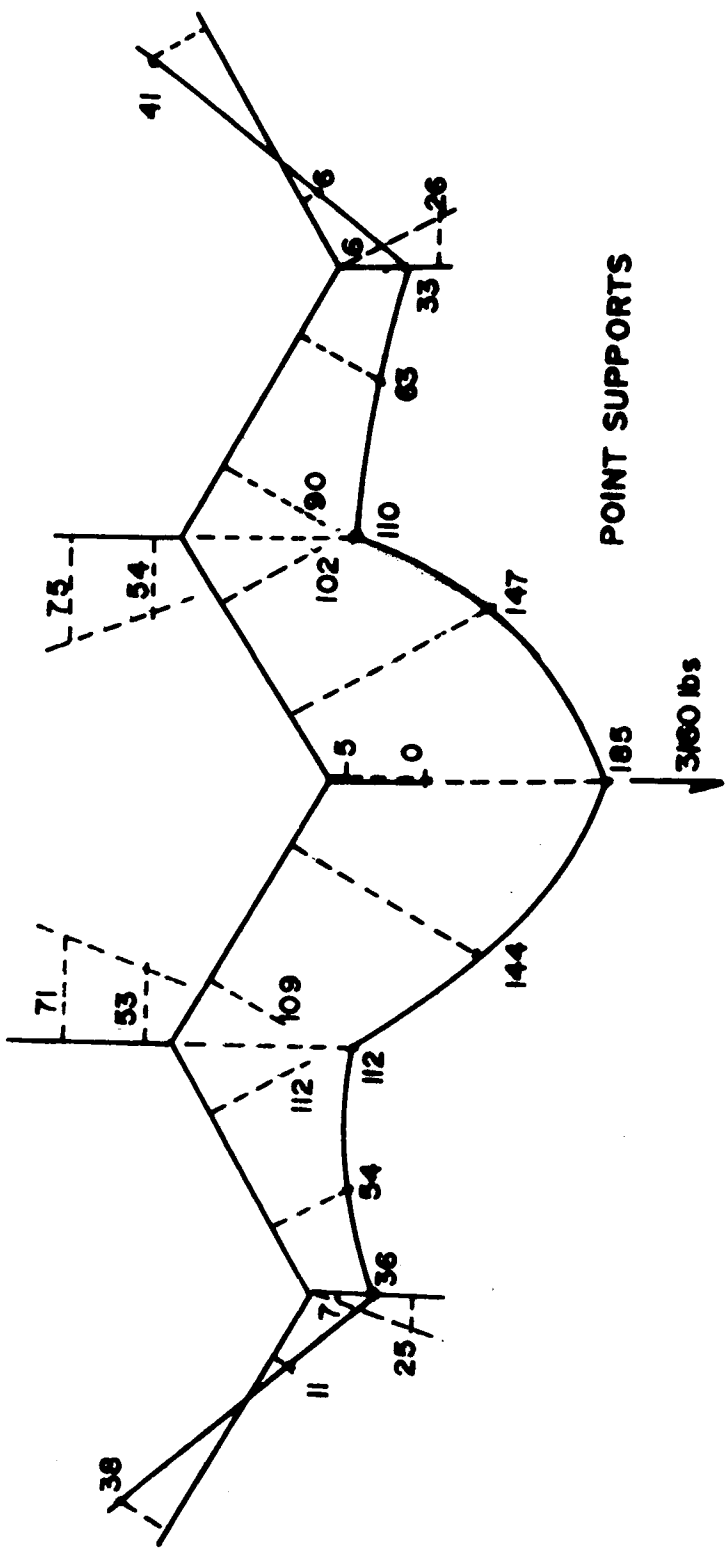

FIG. 71. EXPERIMENTAL DEFLECTIONS IN .001" AT MIDSPAN OF THE 9.5-FOOT MODEL - RIDGE 4 UNIFORMLY LOADED WITH 3160 POUNDS - POINT SUPPORTS

FIG. 72. THE 9.5-FOLDED PLATE MODEL LOADED AT RIDGE 4, WITH A HYDRAULIC RAM.

Note: All underlined numbers represent strains in μ in/in. The negative sign indicates compression, the positive sign tension. All other numbers are stresses in PSI.

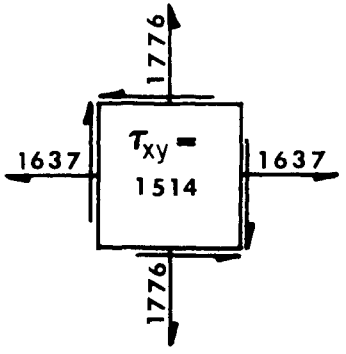

(a) Stresses at point O of figure (b)

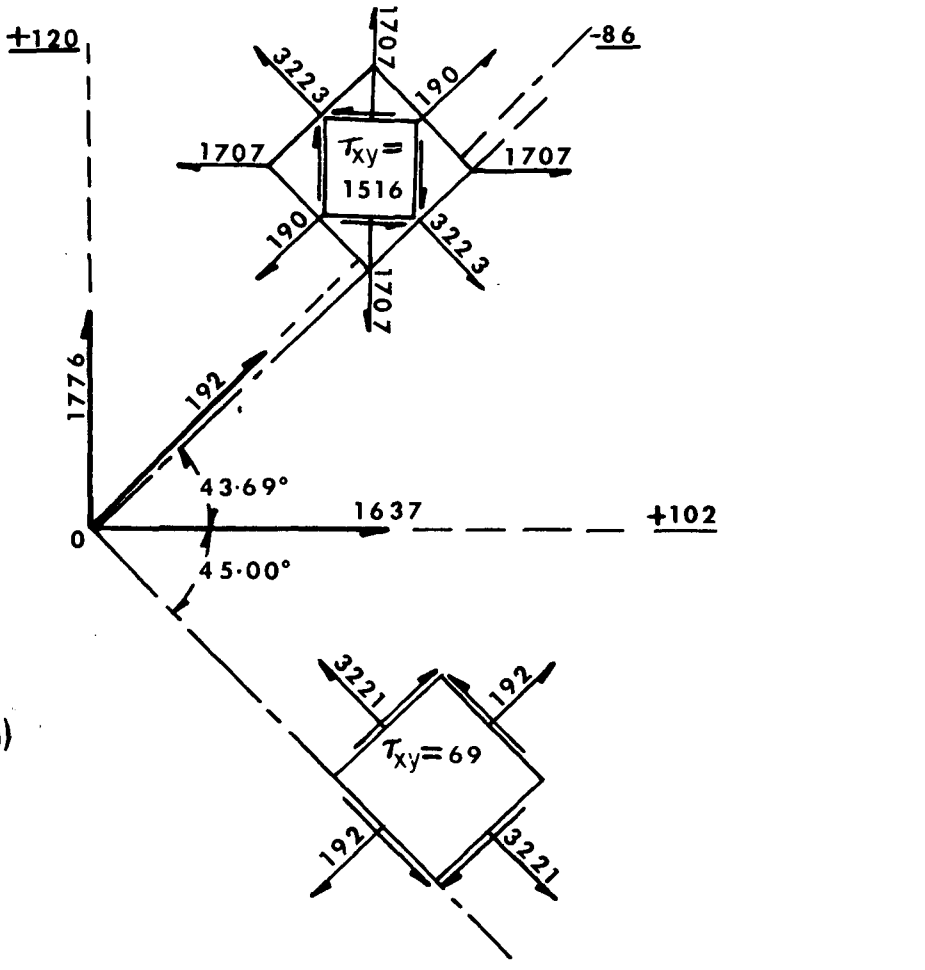

(b) Stresses and strains in various directions

FIG. 73. RESOLUTION OF STRAINS OBTAINED FROM A ROSETTE STRAIN GAUGE INTO STRESSES IN VARIOUS DIRECTIONS

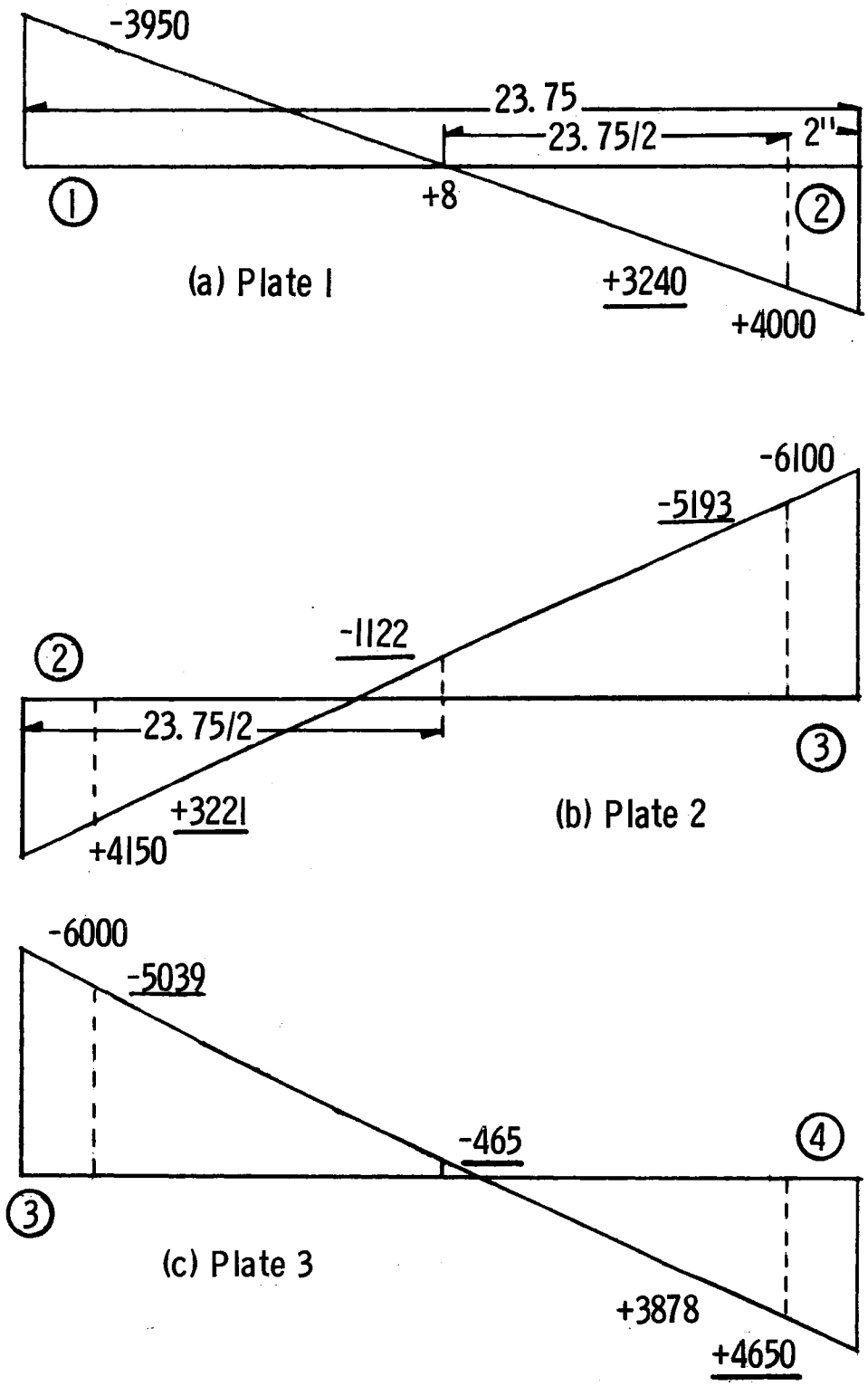

FIG. 74. EXPERIMENTAL LONGITUDINAL STRESSES IN PSI IN THE TOP FACING AT THE MIDSPAN SECTION OF THE 9.5-FOOT FOLDED PLATE MODEL WHEN LOADED AS SHOWN IN FIG. 63
(Underlined stresses are obtained from strain gauges)

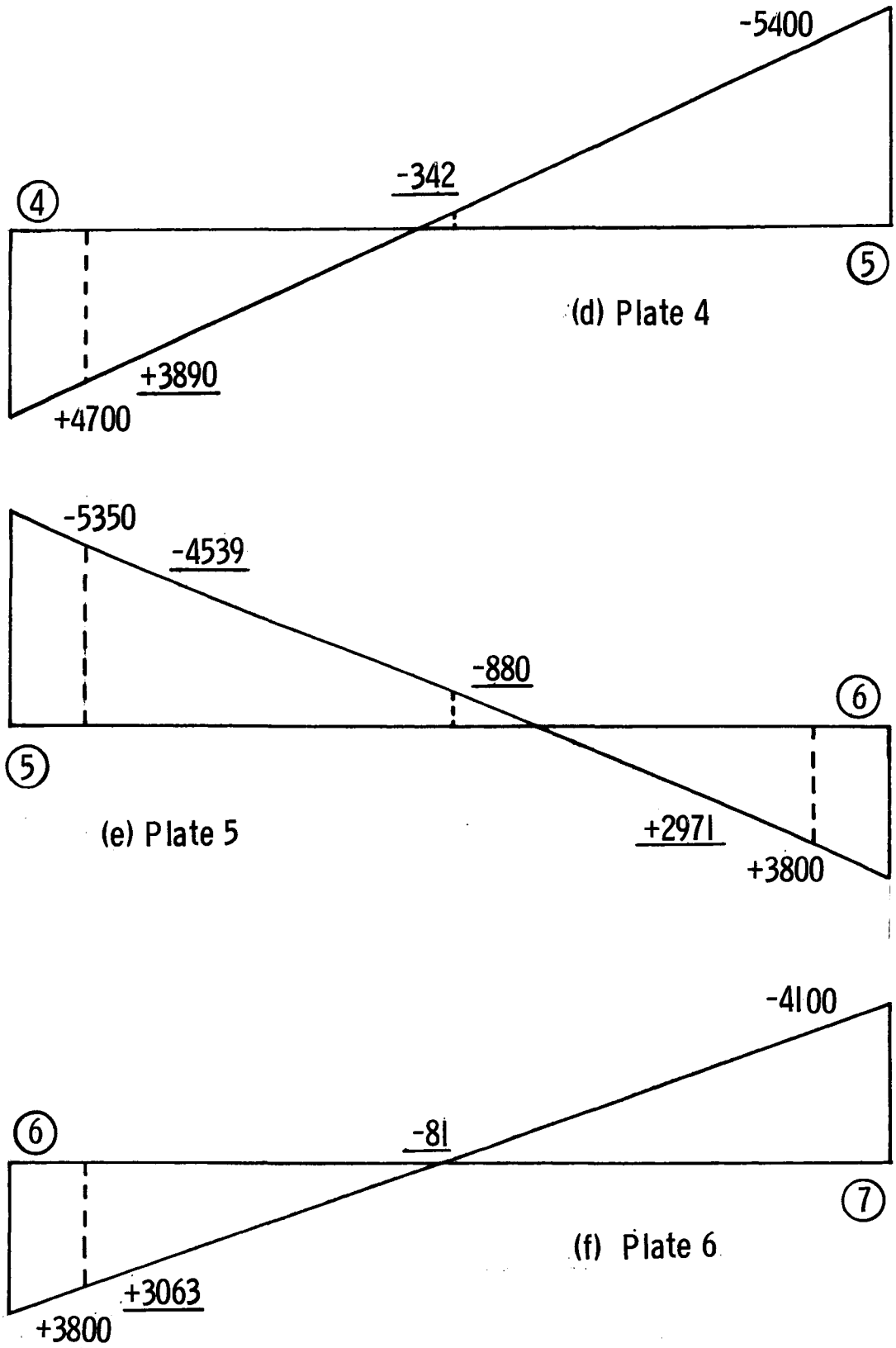

FIG. 74 (continued)

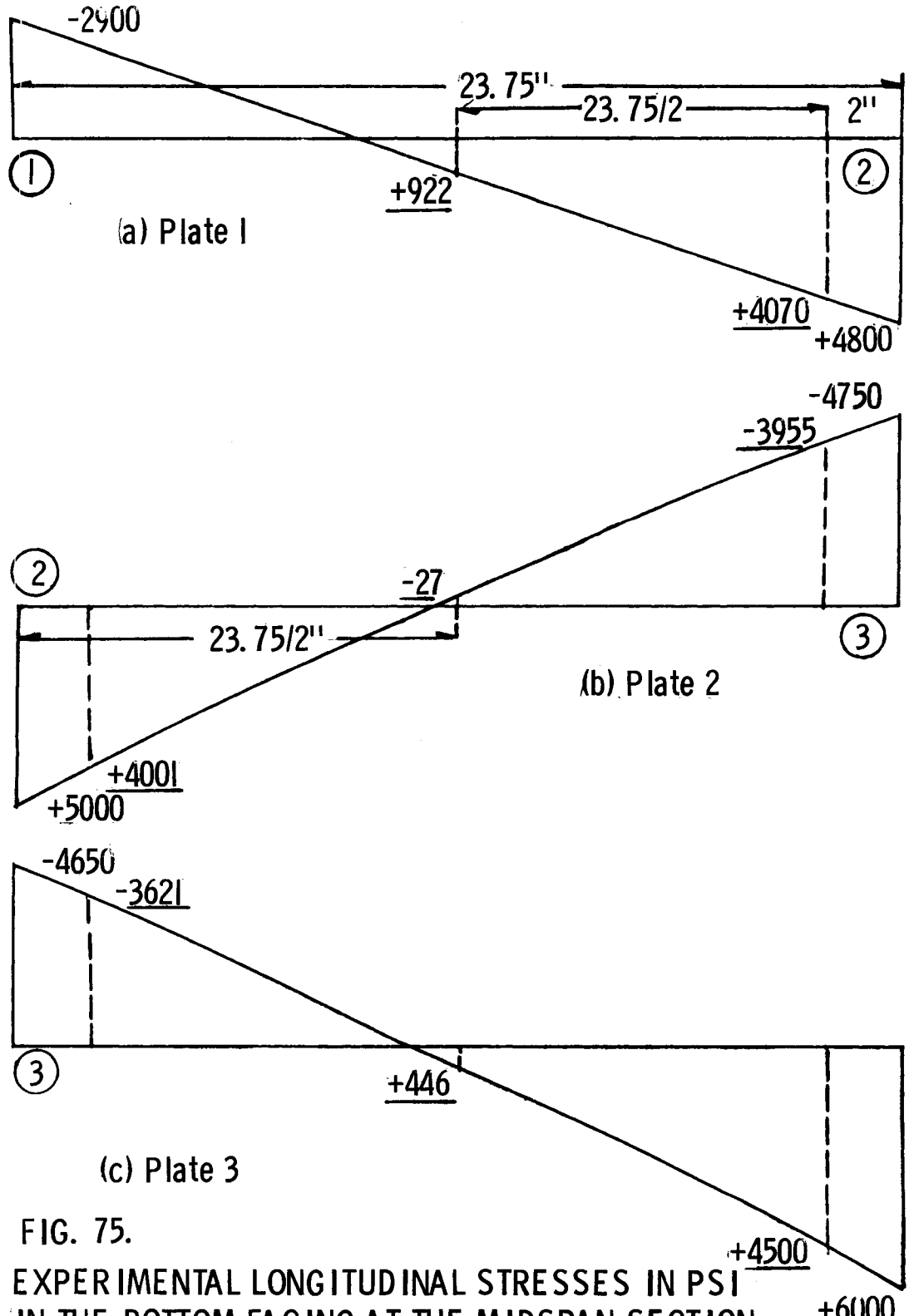

FIG. 75.

EXPERIMENTAL LONGITUDINAL STRESSES IN PSI IN THE BOTTOM FACING AT THE MIDSPAN SECTION OF THE 9.5-FOOT FOLDED PLATE MODEL WHEN LOADED AS SHOWN IN FIG. 63
(Underlined stresses are obtained from strain gauges)

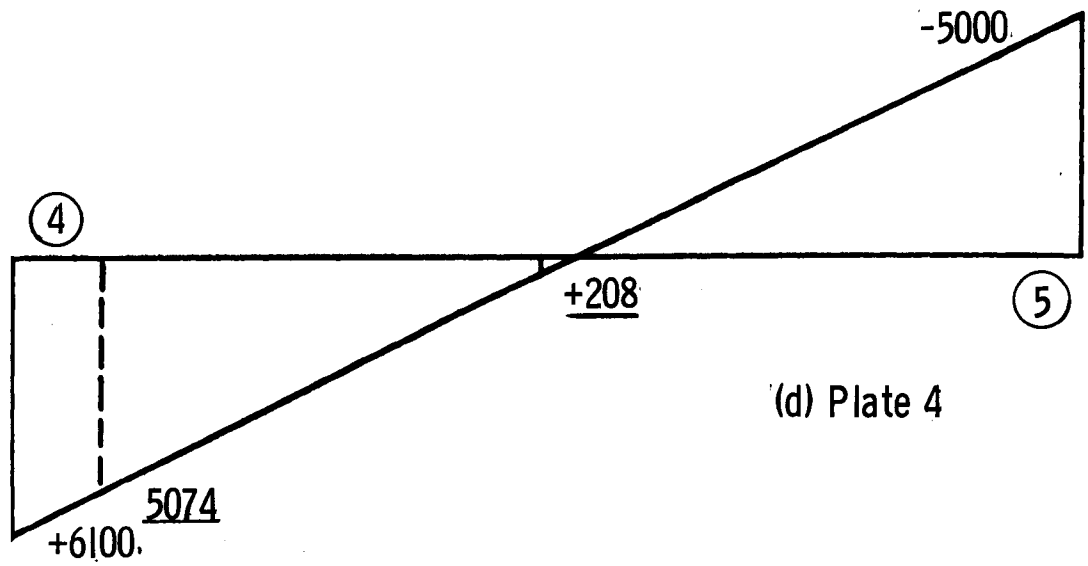

(d) Plate 4

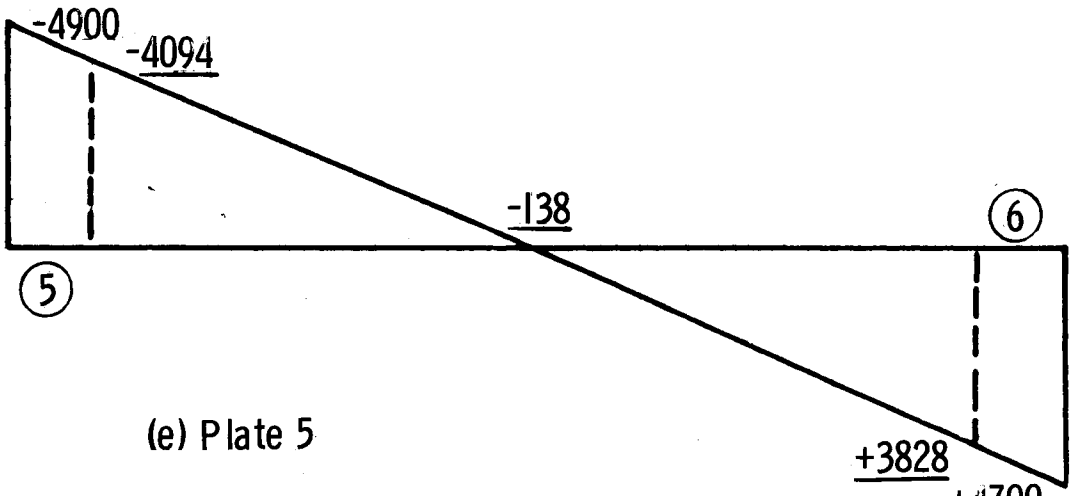

(e) Plate 5

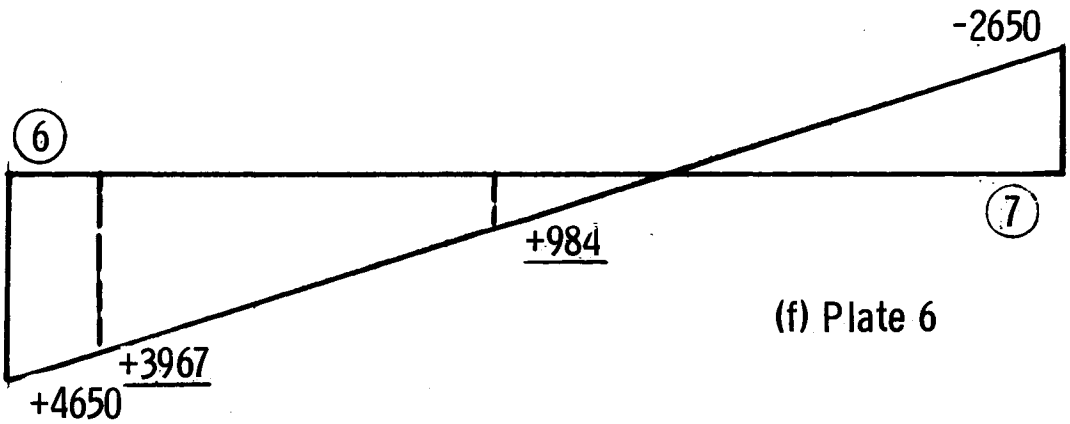

(f) Plate 6

FIG. 75 (continued)

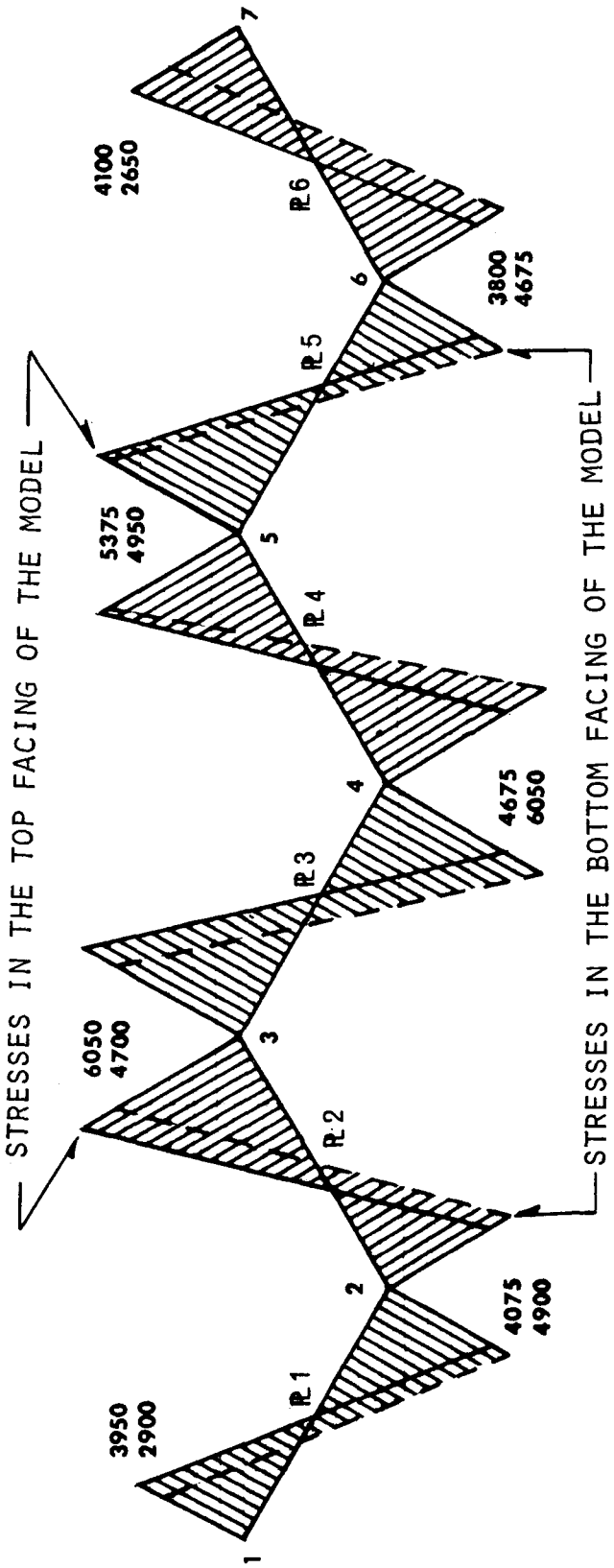

FIG. 76. EXPERIMENTAL LONGITUDINAL STRESSES IN PSI IN THE TOP AND BOTTOM FACINGS TAKEN AT THE MIDSPAN SECTION OF THE 9.5-FOOT FOLDED PLATE MODEL WHEN LOADED AS SHOWN IN FIG. 63

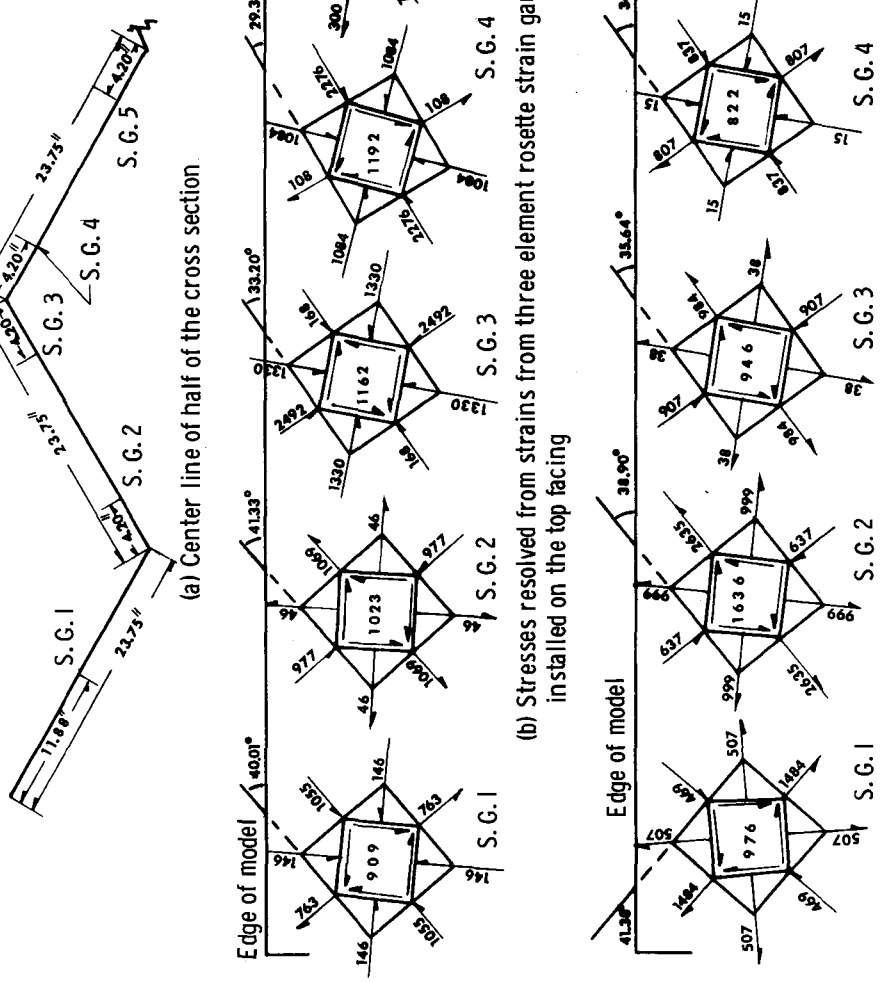

(a) Center line of half of the cross section

(b) Stresses resolved from strains from three element rosette strain gauges installed on the top facing

(c) Stresses resolved from strains from three element rosette strain gauges installed on the bottom facing.

FIG. 77. EXPERIMENTAL STRESSES IN PSI IN TOP AND BOTTOM FACINGS AT A SECTION 12" FROM FACE OF SUPPORT FOR THE TEN-FOOT FOLDED PLATE MODEL WHEN LOADED AS SHOWN IN FIG. 63

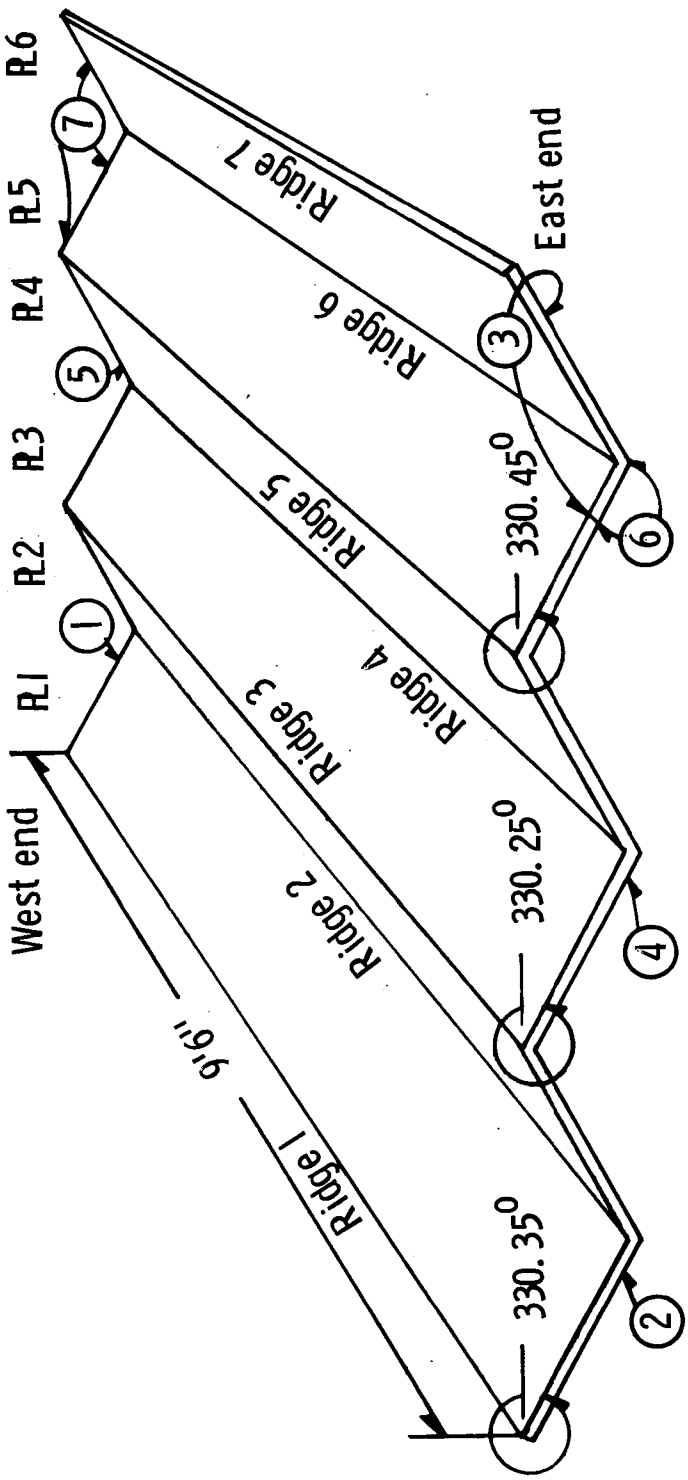

FIG. 78. SEQUENCE OF FAILURES IN THE 9.5-FOOT FOLDED PLATE MODEL (ULTIMATE LOAD = 17,750 POUNDS)

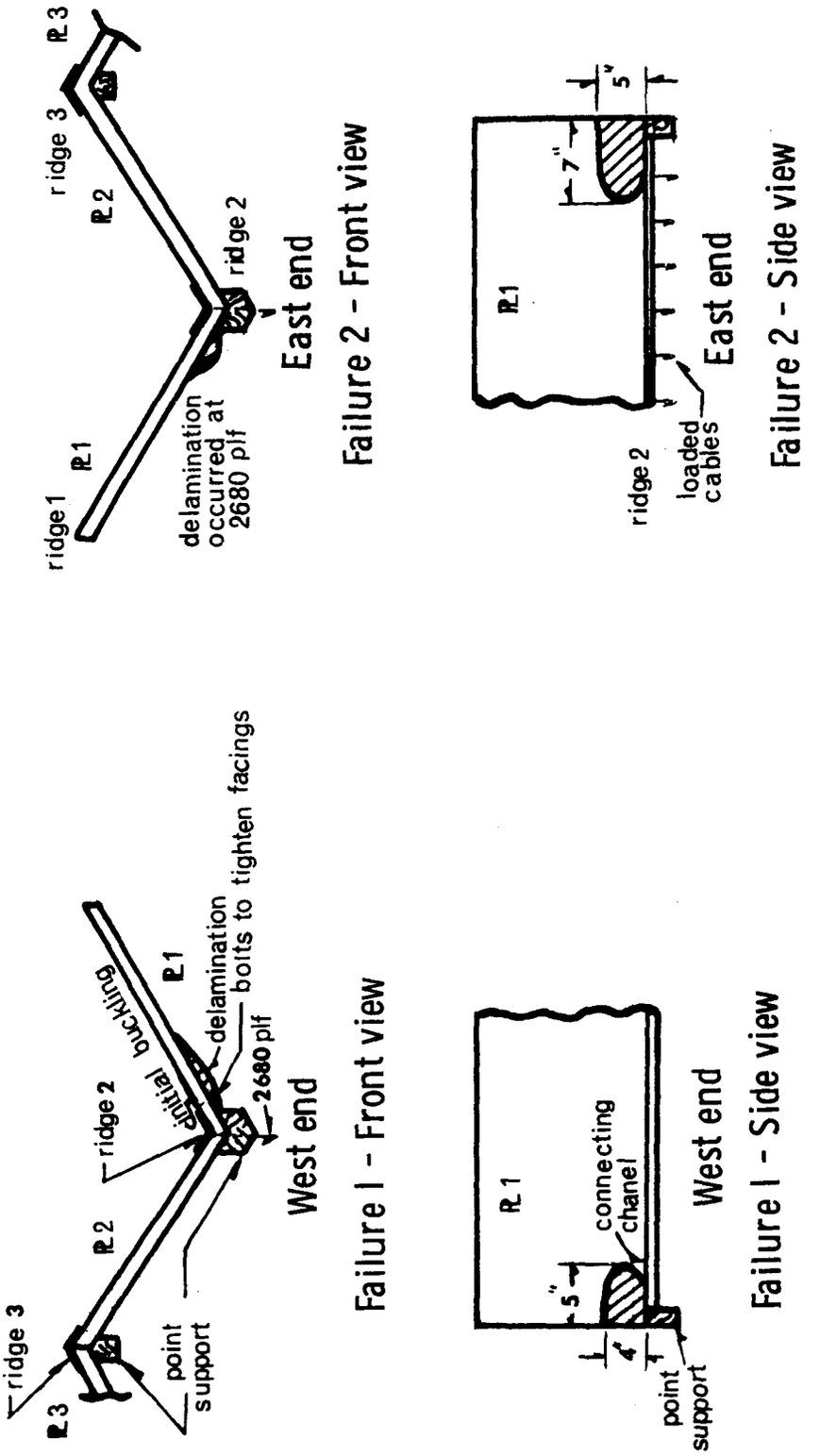

FIG. 79. INITIAL DELAMINATIONS ABOVE POINT-SUPPORTS - RIDGE 2 ONLY BEING LOADED

FIG. 80. FAILURE 1 (FIG. 78) IN PLATE 1 (FIG. 44)
AT THE WEST END.

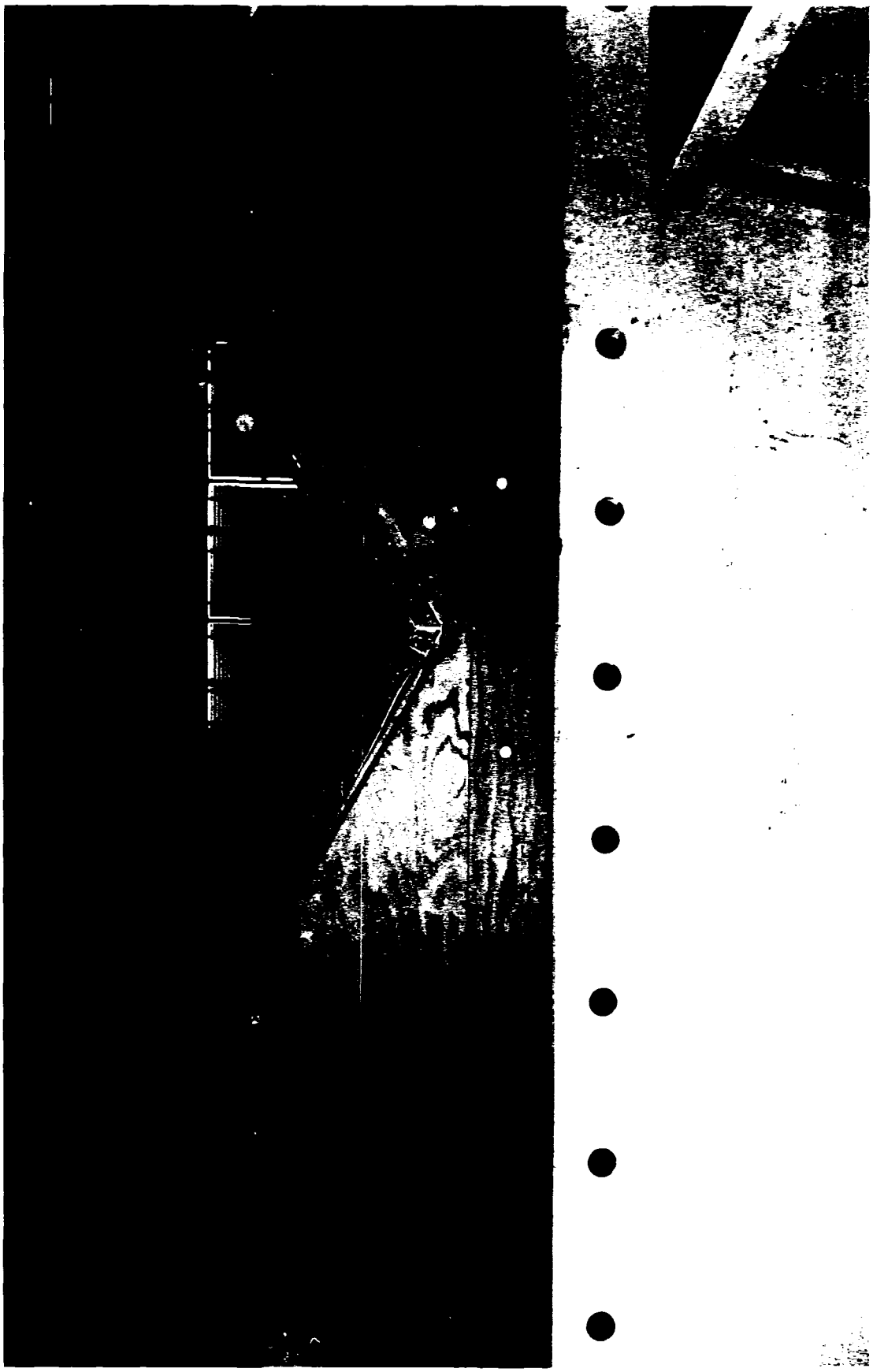

FIG. 81. FAILURE 4 (SEE FIG. 78) AT THE EAST END OF PLATE 3
CAUSED BY A UNIFORM LOAD OF 13,000 LBS
DISTRIBUTED ALONG THE FIVE INTERIOR RIDGES.

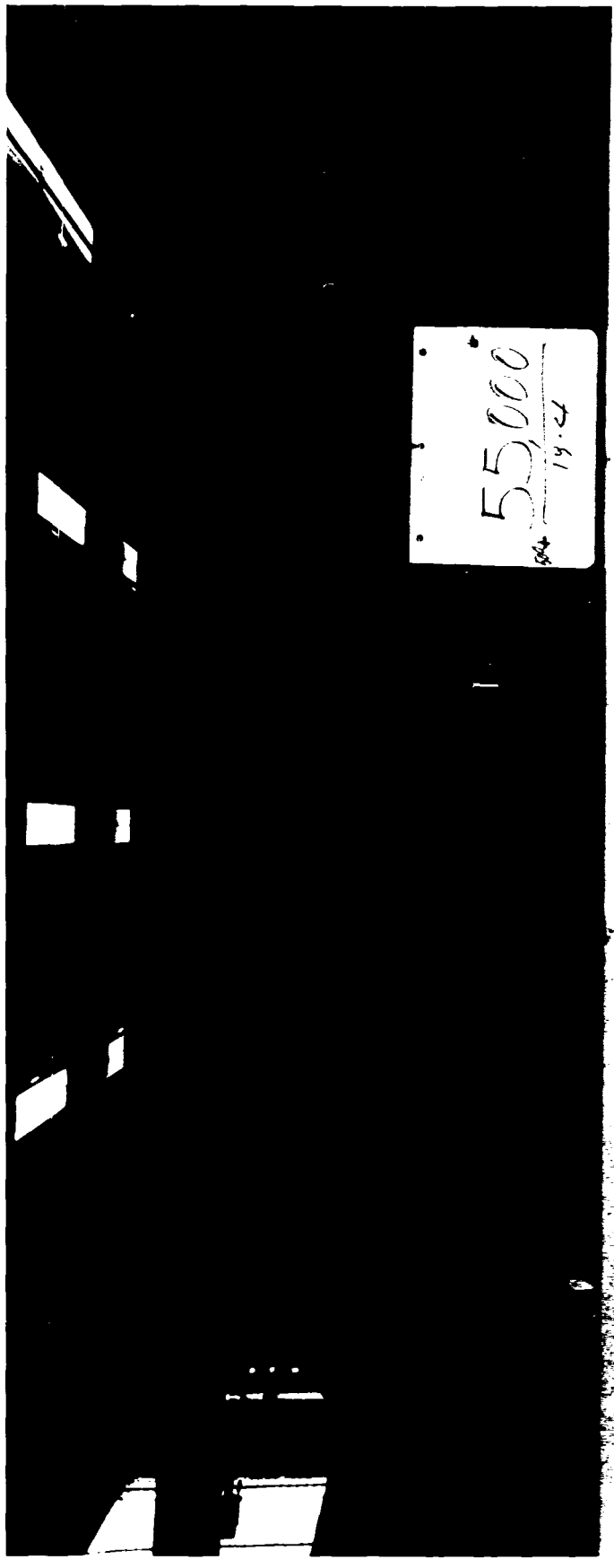

FIG. 82. FAILURE 5 AT THE WEST END OF PLATE 4 AT A TOTAL LOAD OF 14,700 LBS UNIFORMLY DISTRIBUTED ALONG THE INTERIOR FIVE RIDGES

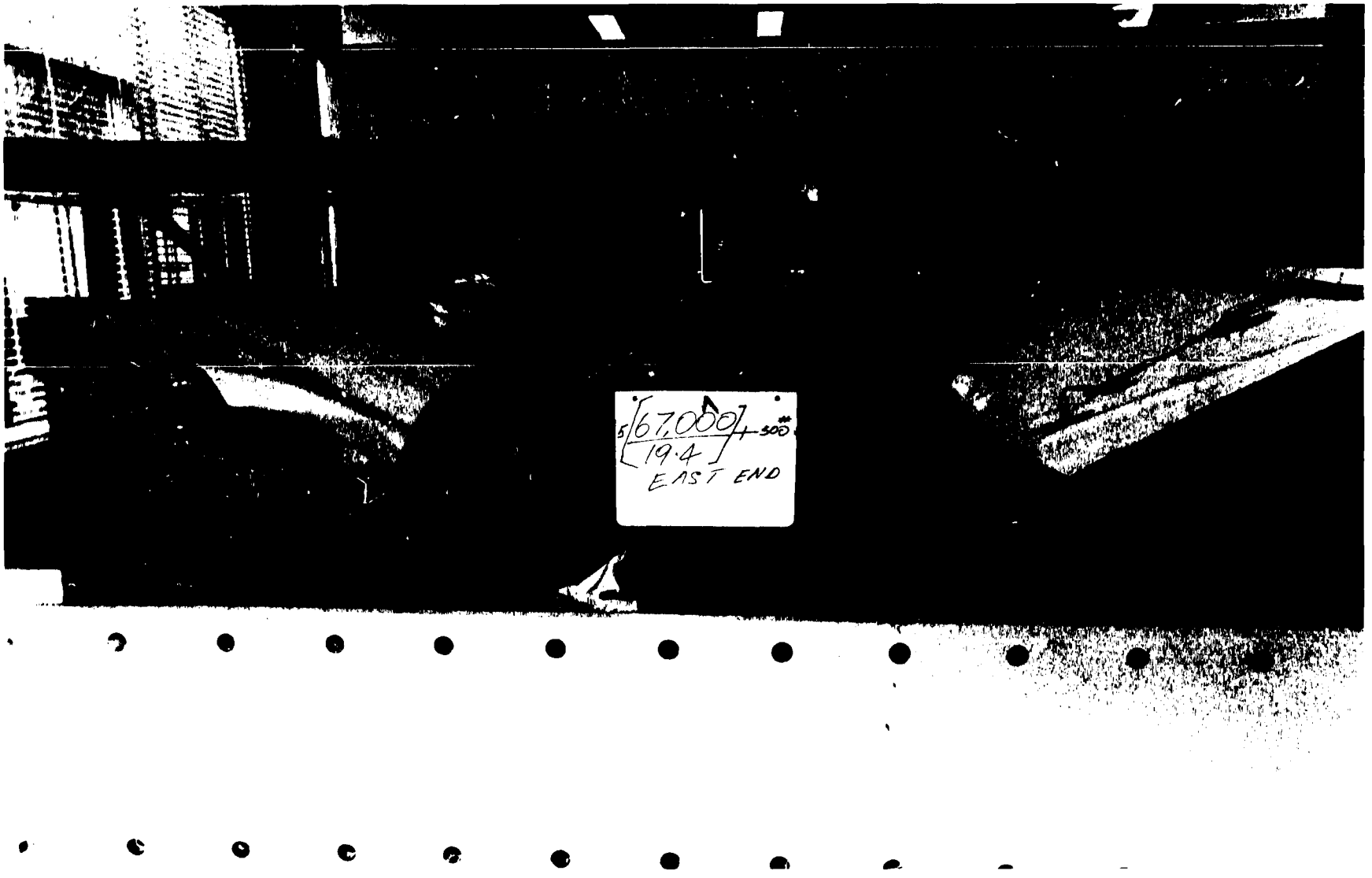

FIG. 84. SHEAR FAILURES OCCUR AT THE WEST ENDS OF PLATES 6, 5, 4 AND 3, AT LOADS RANGING FROM 17,200 TO 17,750 POUNDS.

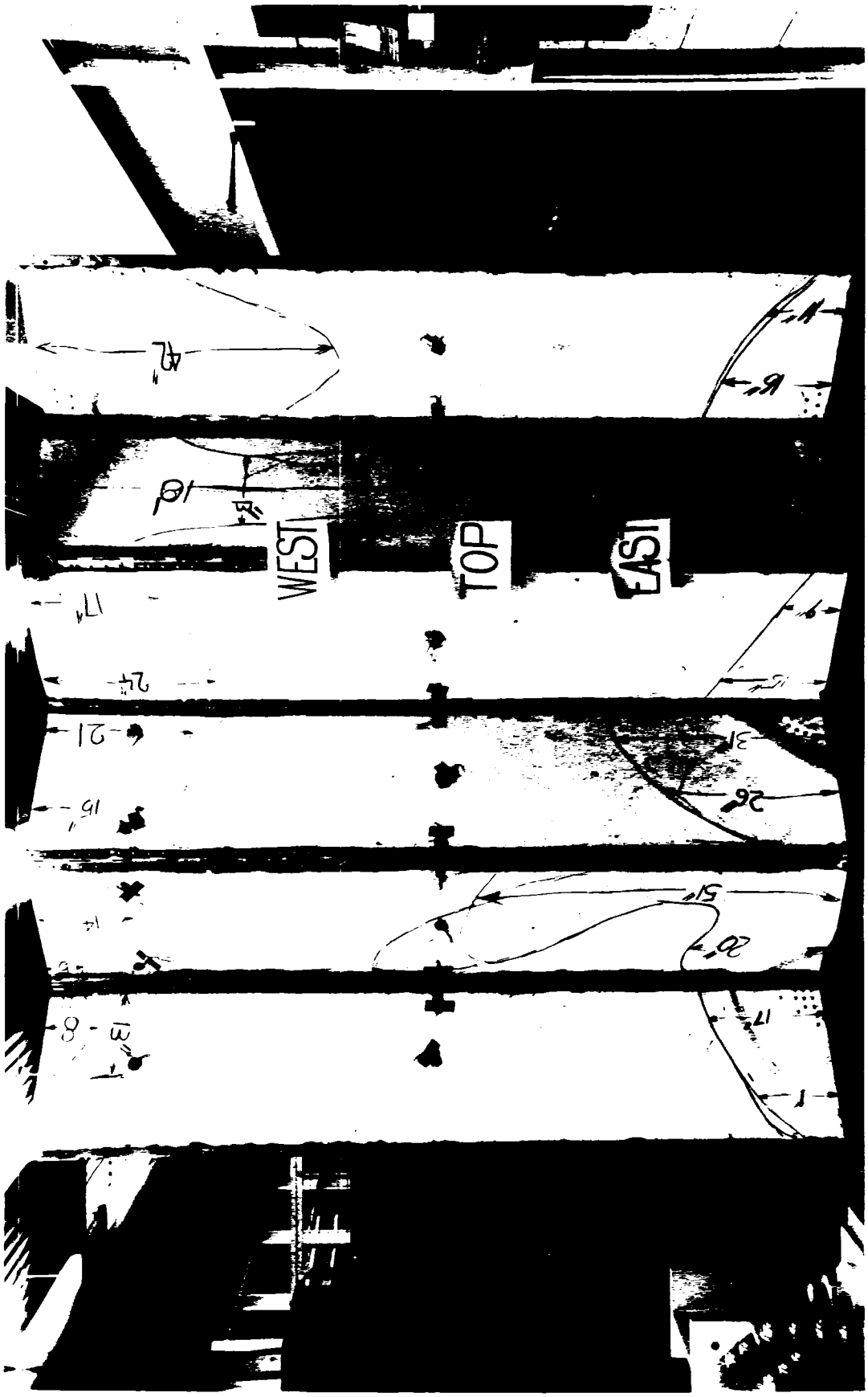

FIG. 85. TOP VIEW OF THE 9.5-FOOT MODEL AFTER FAILURE.
THE CONTOUR LINES INDICATE DELAMINATION BOUNDARIES.

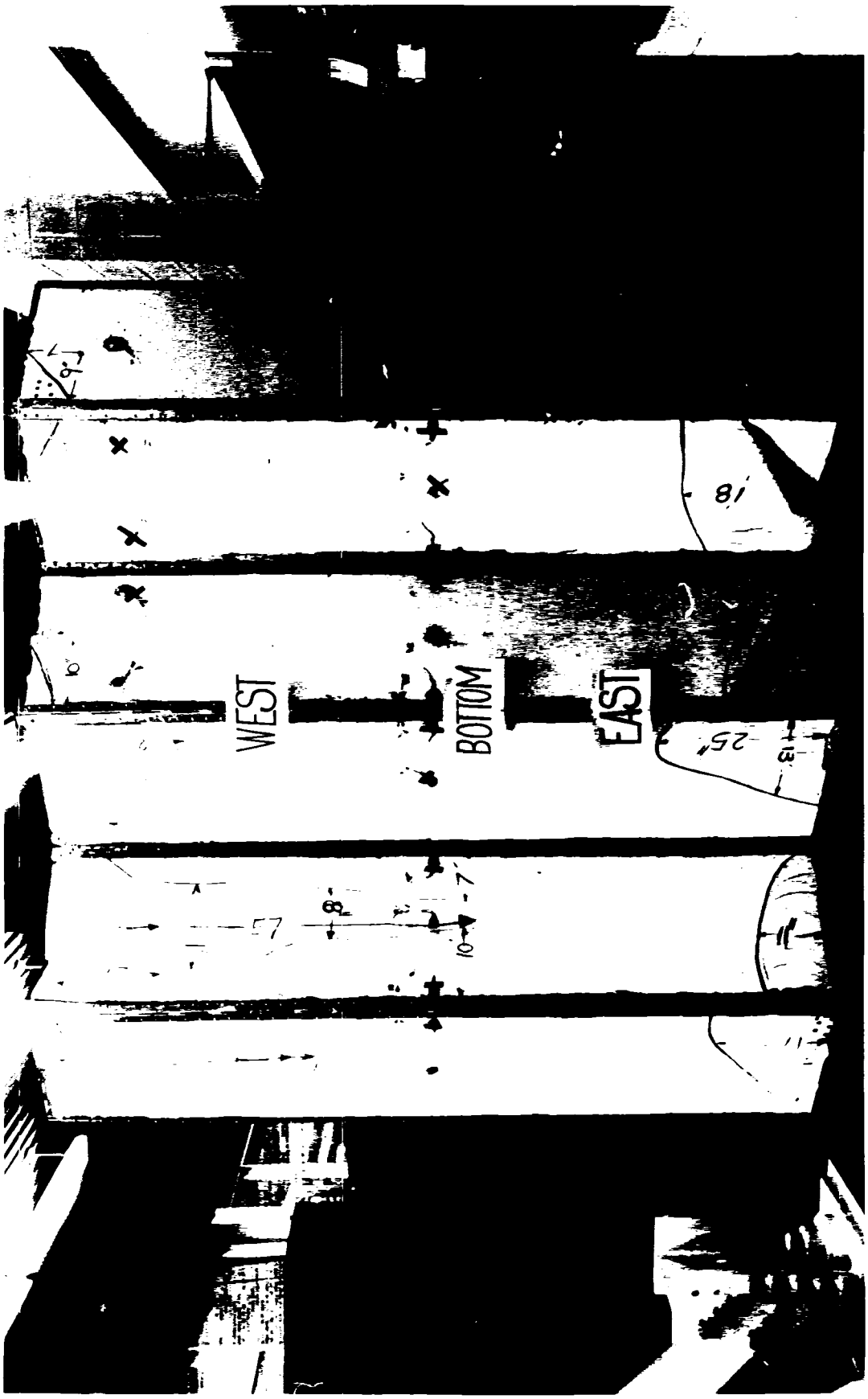

FIG. 86. BOTTOM VIEW OF THE 9.5-FOOT MODEL AFTER FAILURE.
THE CONTOUR LINES INDICATE DELAMINATION BOUNDARIES.

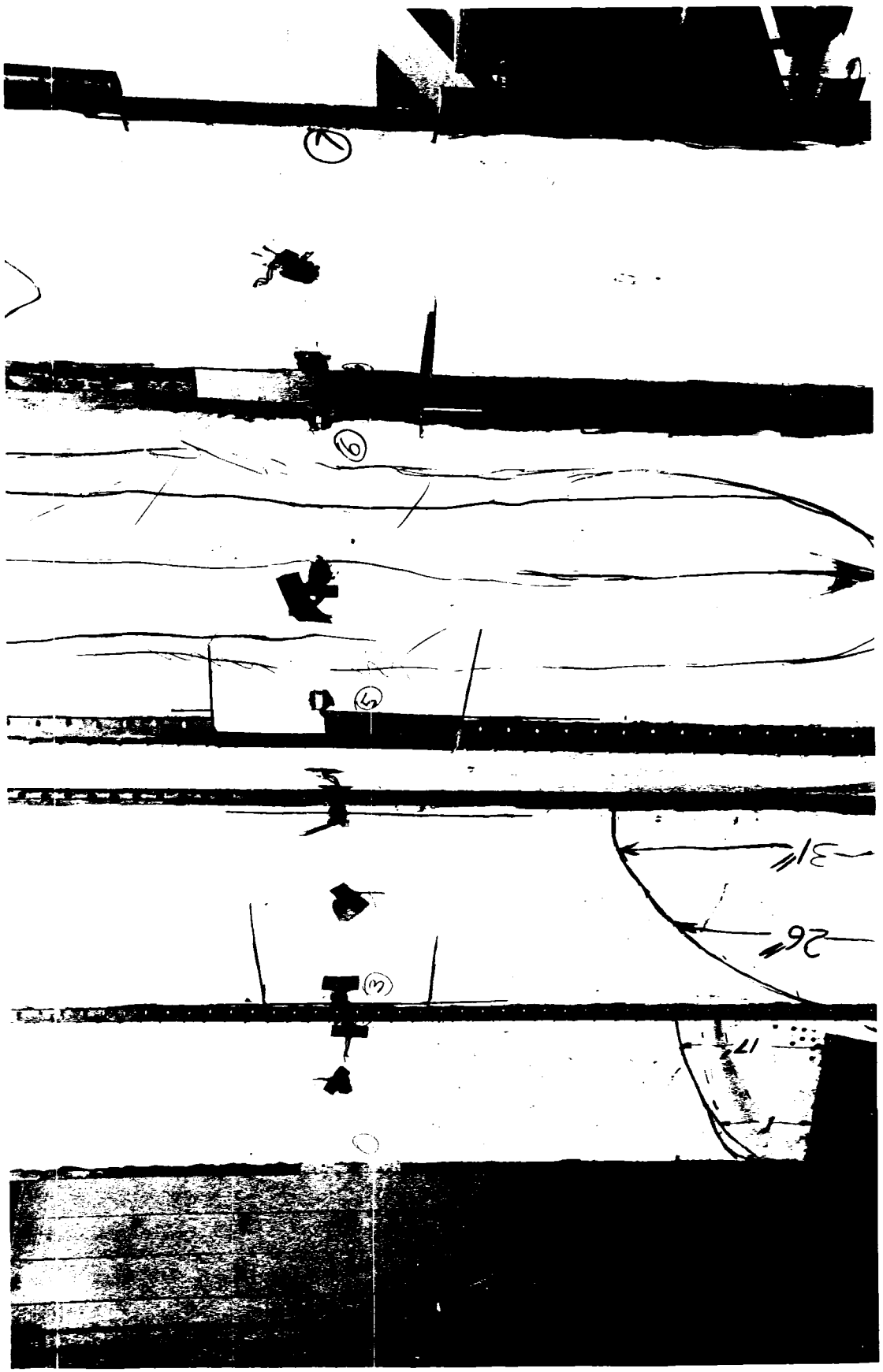

FIG. 87. TWELVE-INCH SAMPLES OF CONNECTING CHANNELS WERE CUT OUT AT MIDSPAN OF EACH RIDGE.

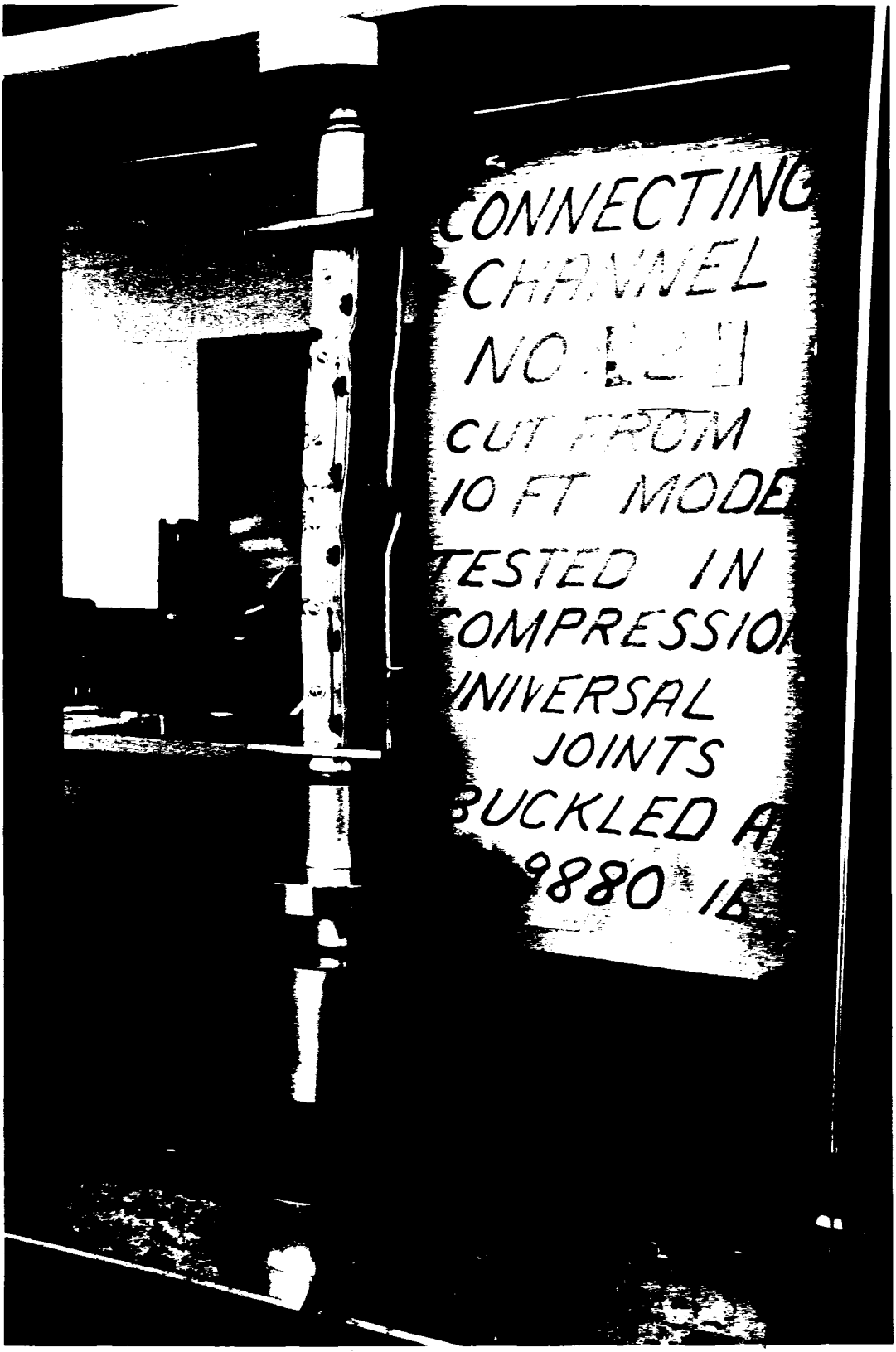

FIG. 88. A SAMPLE OF CONNECTING CHANNEL TESTED IN COMPRESSION.

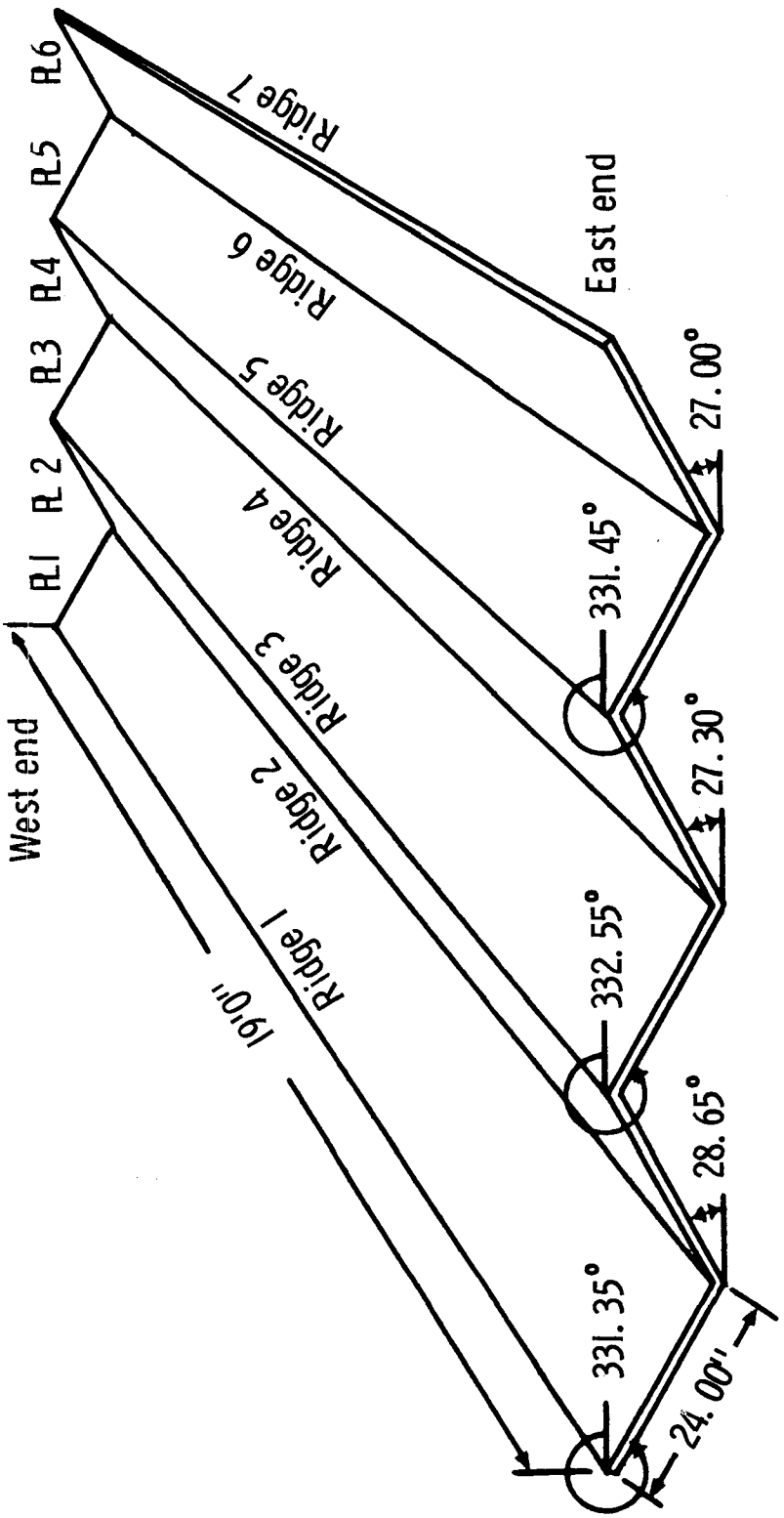

FIG. 89. FOLDED PLATE MODEL MADE UP OF SANDWICH PANELS HAVING ALUMINUM FACINGS (.025" THICK) AND STYROLITE CORE (1" THICK)

FIG. 90. BOTTOM OF THE MODEL. SIDE OF PRESSURE BOX. DATA ACQUISITION SYSTEM.
TOP OF PRESSURE BAG ON THE FLOOR.

FIG. 91. TWO SHEETS OF PLASTIC LAID ON THE MODEL AND SEALED AROUND THE RIM OF THE PRESSURE BOX CONSTITUTE THE BOTTOM OF THE PRESSURE BAG

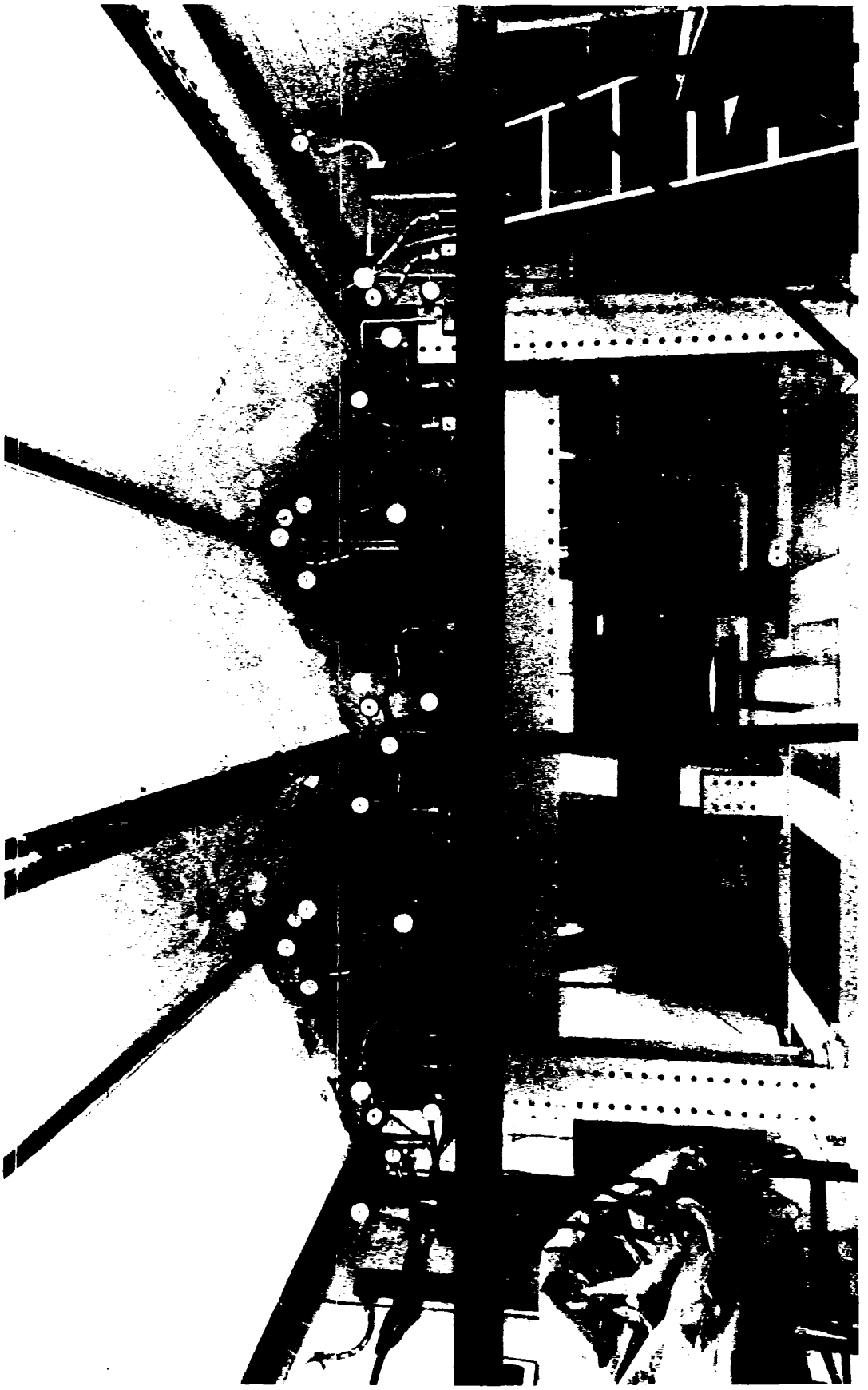

FIG. 92. TWENTY-SEVEN DIAL INDICATORS SET ACROSS THE MIDSPAN SECTION OF THE 19-FOOT FOLDED SANDWICH PLATE MODEL

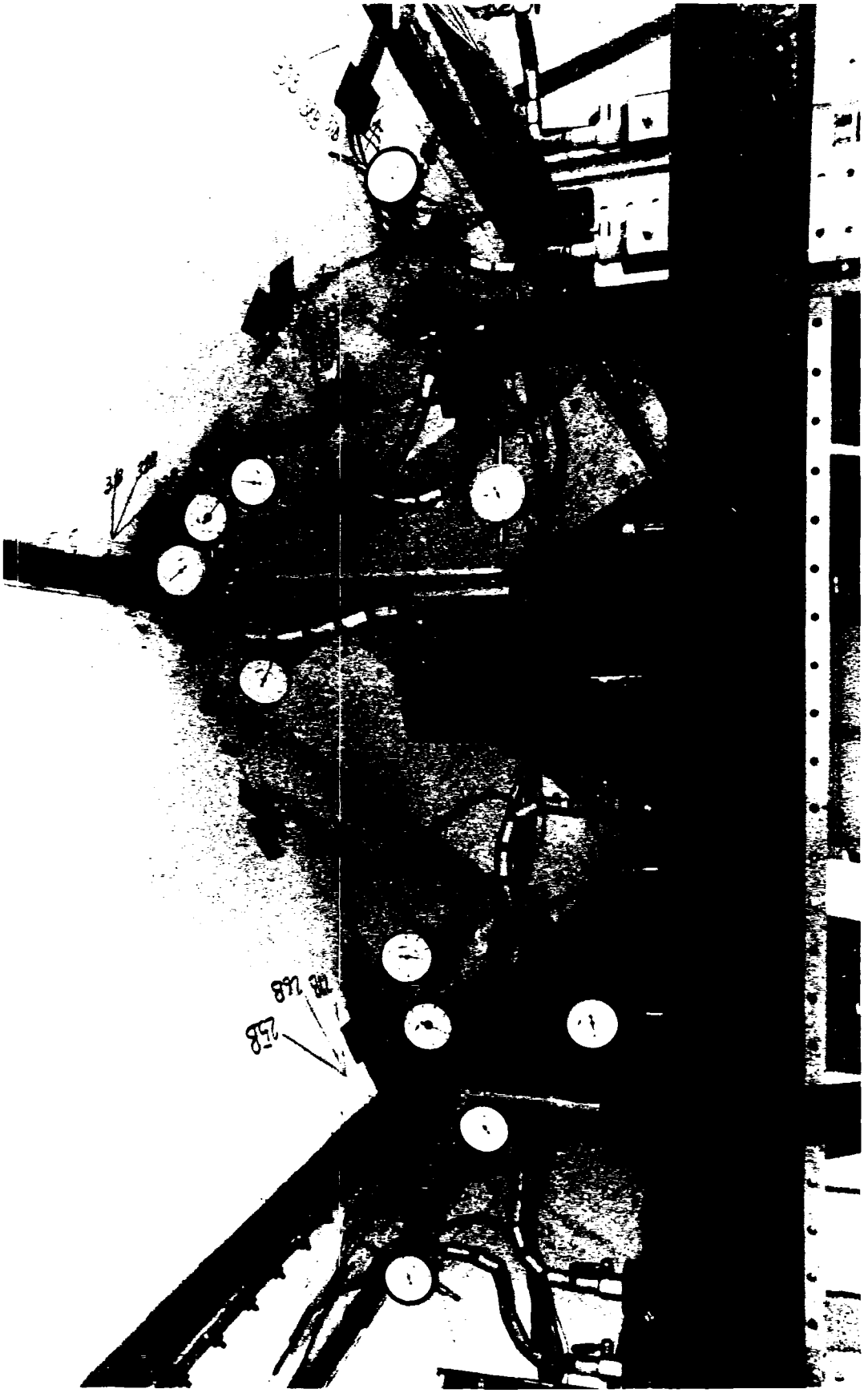

FIG. 93. CLOSE-UP OF DIAL INDICATORS SET AT MIDSPAN OF RIDGES 4 AND 5

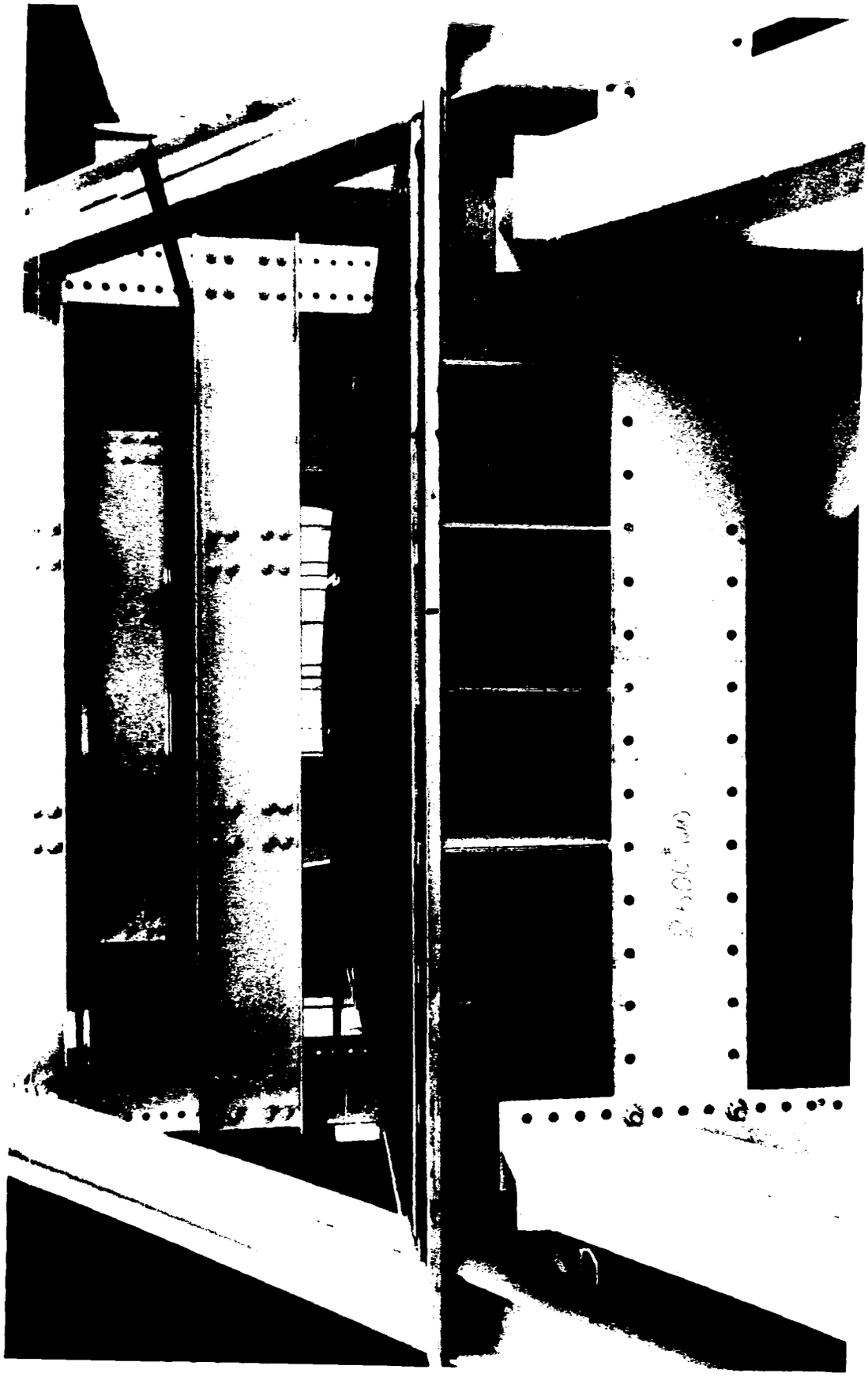

FIG. 94. PRESSURE BAG TESTED FOR LEAKS - VIEW FROM THE EAST END

FIG. 95. GENERAL VIEW OF COMPLETED EXPERIMENTAL SET-UP FOR THE 19-FOOT MODEL

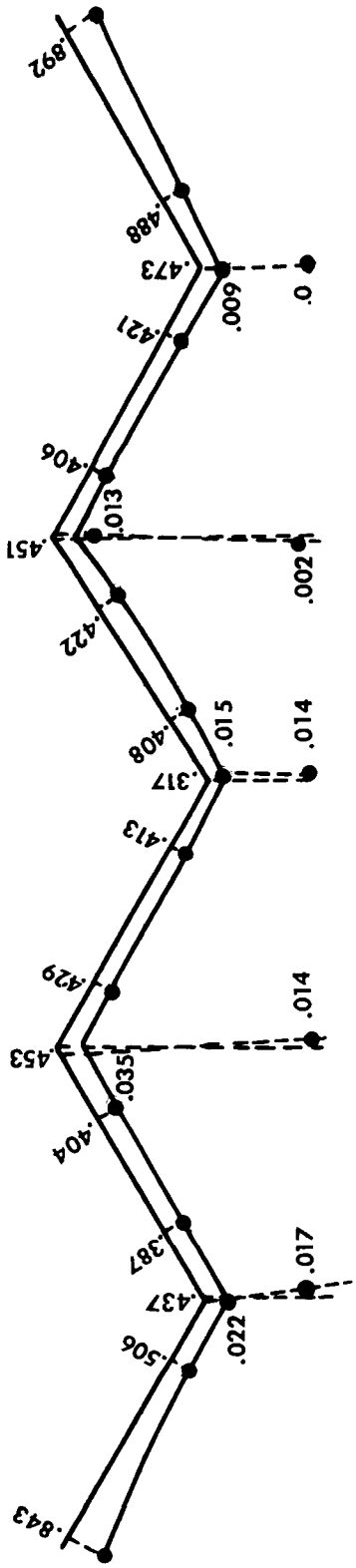

FIG. 96. EXPERIMENTAL DEFLECTIONS IN INCHES AT MIDSPAN OF THE NINETEEN-FOOT FOLDED PLATE MODEL LOADED WITH A UNIFORM PRESSURE OF 23.4 POUNDS PER SQUARE FOOT

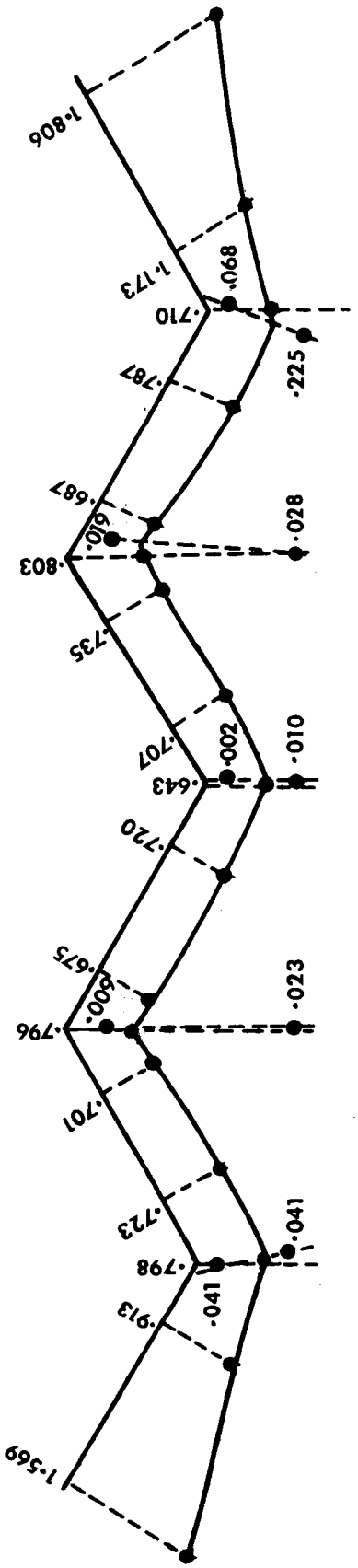

FIG. 97. EXPERIMENTAL DEFLECTIONS IN INCHES AT MIDSPAN OF THE NINETEEN-FOOT FOLDED PLATE MODEL LOADED WITH A UNIFORM PRESSURE OF 40 POUNDS PER SQUARE FOOT

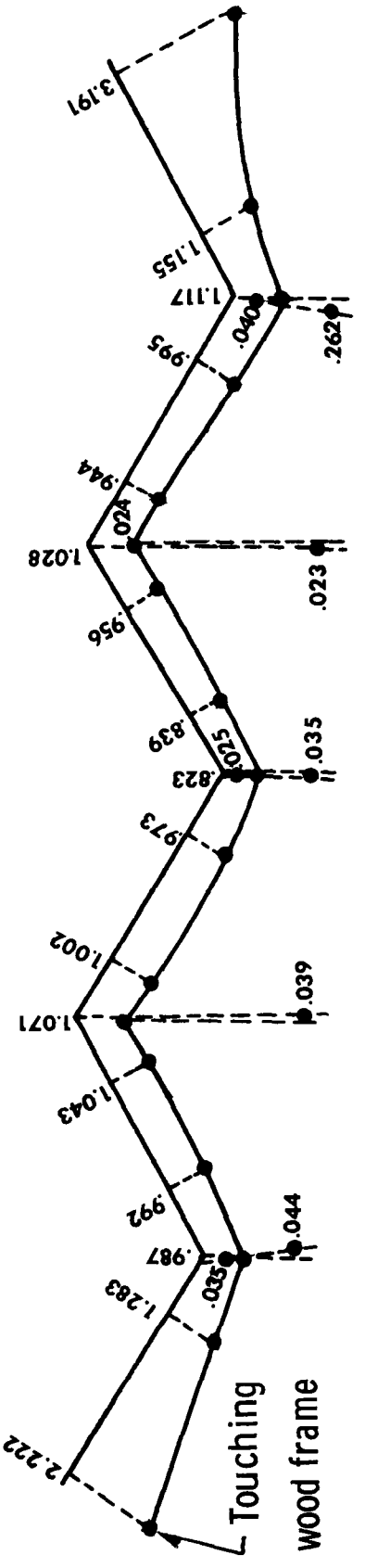

FIG. 98. EXPERIMENTAL DEFLECTIONS IN INCHES AT MIDSPAN OF THE NINETEEN-FOOT FOLDED PLATE MODEL LOADED WITH A UNIFORM PRESSURE OF 49.4 POUNDS PER SQUARE FOOT

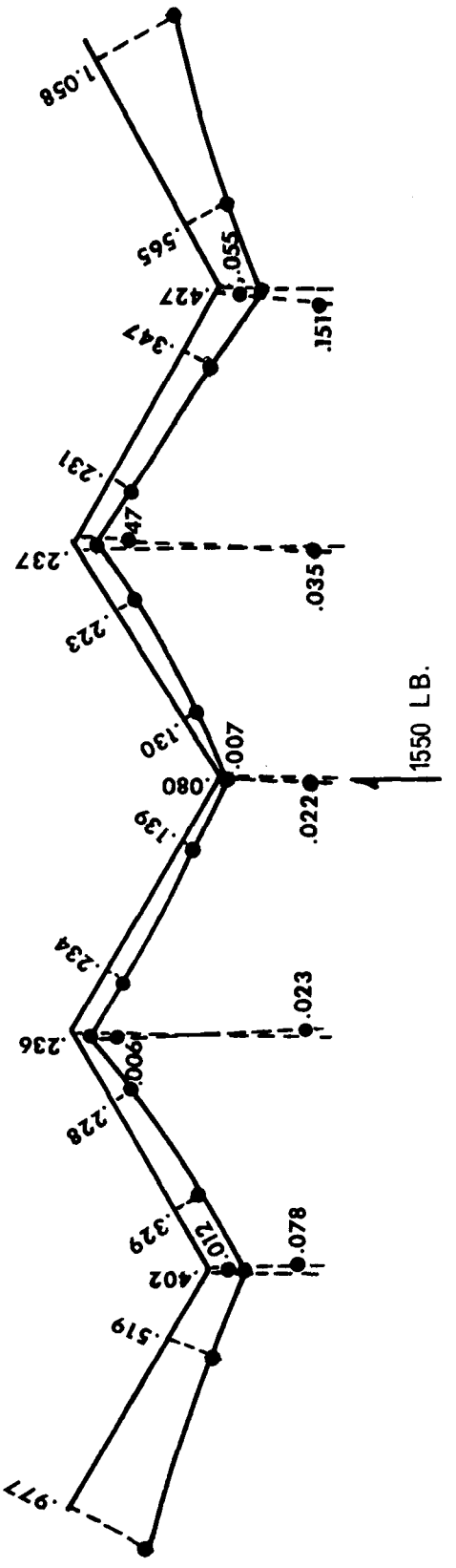

FIG. 99. EXPERIMENTAL DEFLECTIONS IN INCHES AT MIDSPAN OF THE NINETEEN-FOOT FOLDED PLATE MODEL LOADED WITH A UNIFORM PRESSURE OF 26 POUNDS PER SQUARE FOOT - INTERMEDIATE SUPPORT AT RIDGE 5

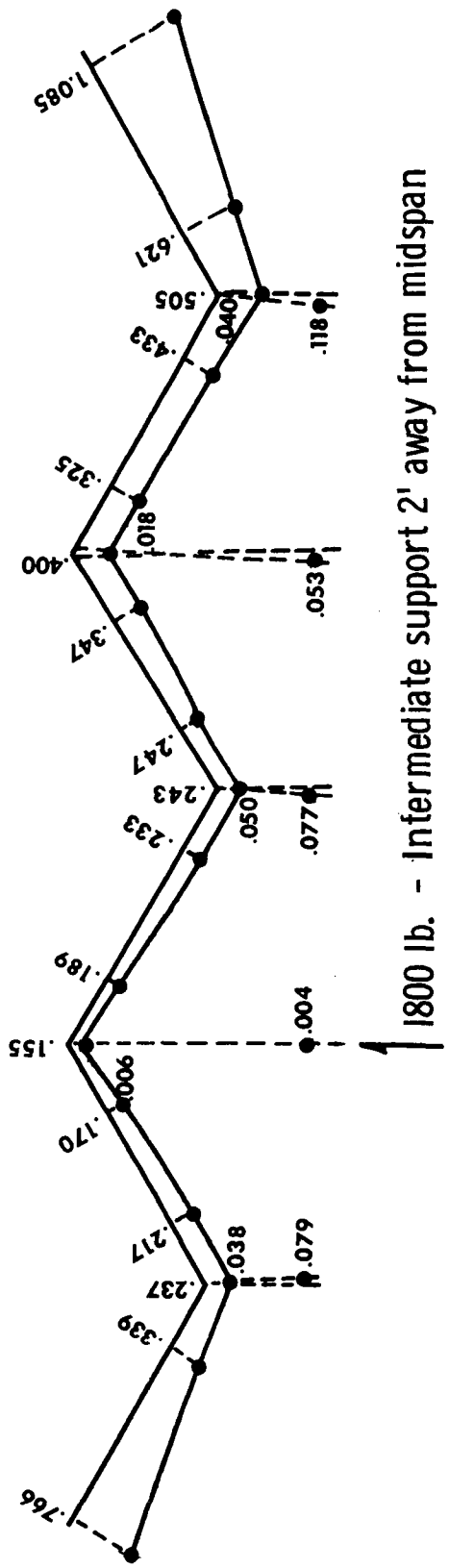

FIG. 100. EXPERIMENTAL DEFLECTIONS IN INCHES AT MIDSPAN OF THE NINETEEN-FOOT FOLDED PLATE MODEL LOADED WITH A UNIFORM PRESSURE OF 26 POUNDS PER SQUARE FOOT - INTERMEDIATE SUPPORT AT RIDGE 3

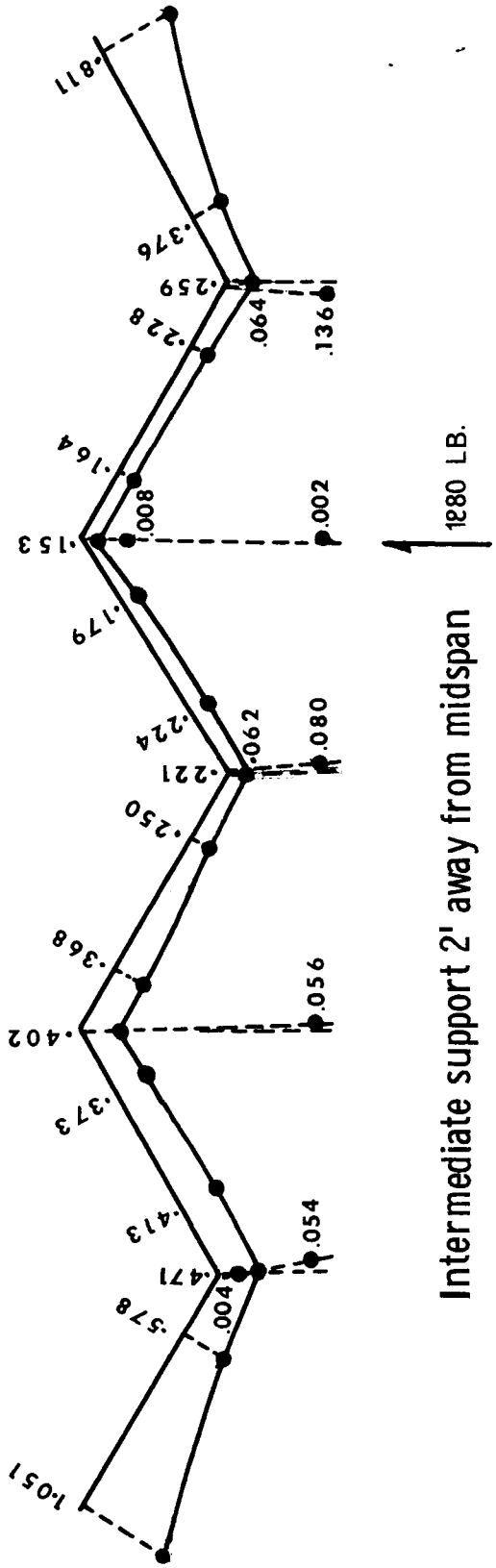

FIG. 101. EXPERIMENTAL DEFLECTIONS IN INCHES AT MIDSPAN OF THE NINETEEN-FOOT FOLDED PLATE MODEL LOADED WITH A UNIFORM PRESSURE OF 26 POUNDS PER SQUARE FOOT - INTERMEDIATE SUPPORT AT RIDGE 5

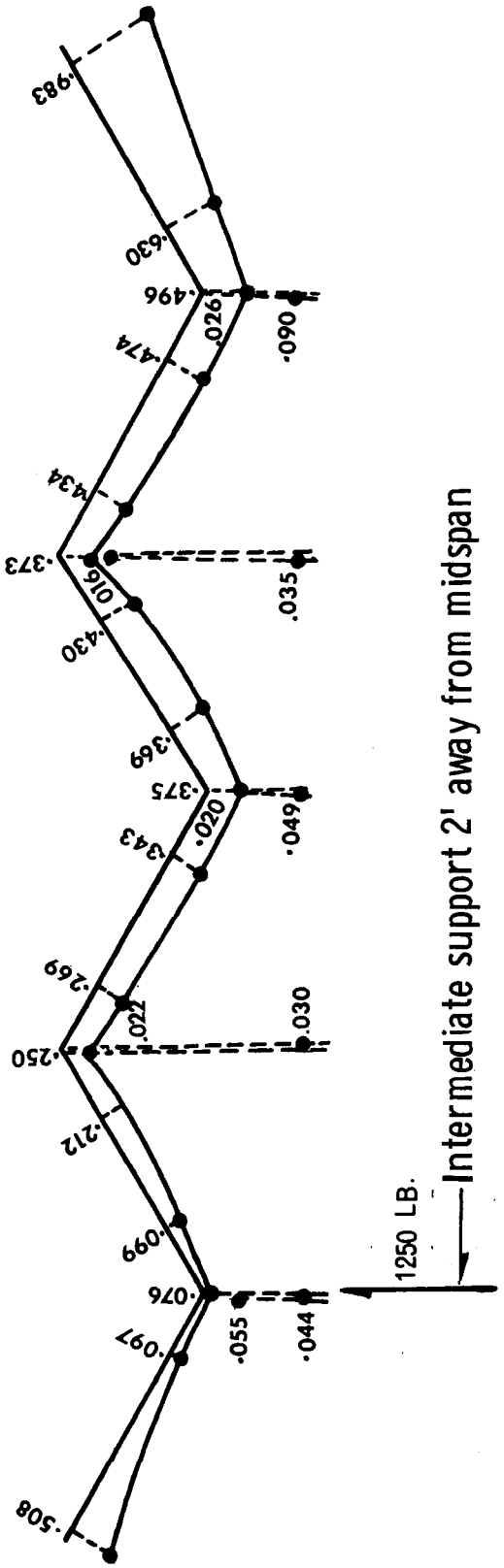

FIG. 102. EXPERIMENTAL DEFLECTIONS IN INCHES AT MIDSPAN OF THE NINETEEN-FOOT FOLDED PLATE MODEL LOADED WITH A UNIFORM PRESSURE OF 26 POUNDS PER SQUARE FOOT - INTERMEDIATE SUPPORT AT RIDGE 2

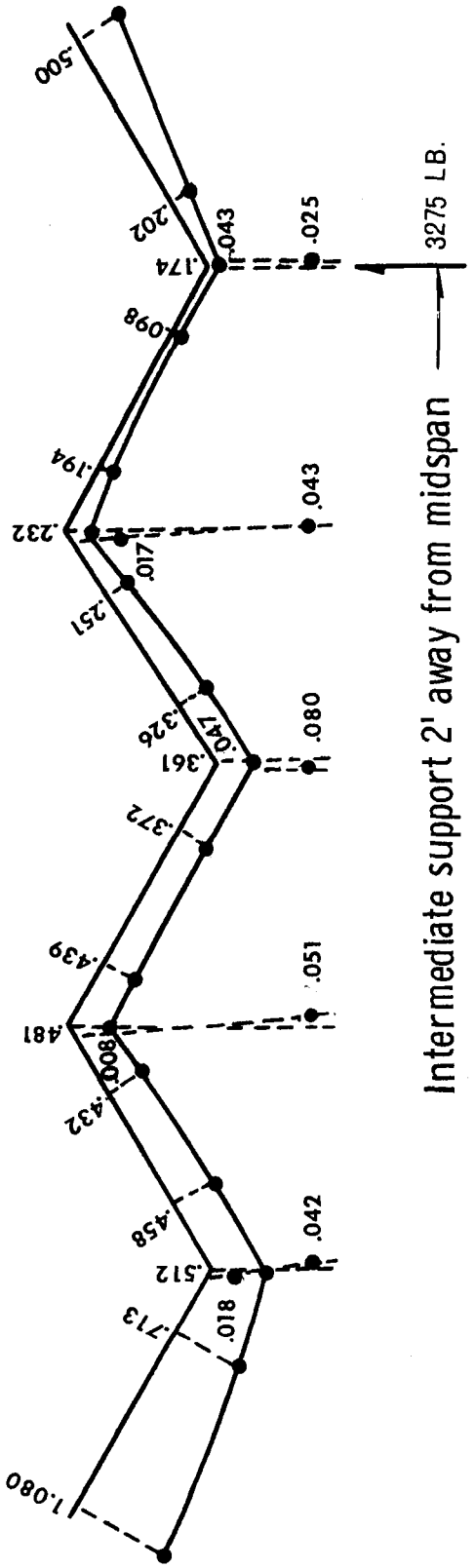

FIG. 103. EXPERIMENTAL DEFLECTIONS IN INCHES AT MIDSPAN OF THE NINETEEN-FOOT FOLDED PLATE MODEL LOADED WITH A UNIFORM PRESSURE OF 26 POUNDS PER SQUARE FOOT - INTERMEDIATE SUPPORT AT RIDGE 6

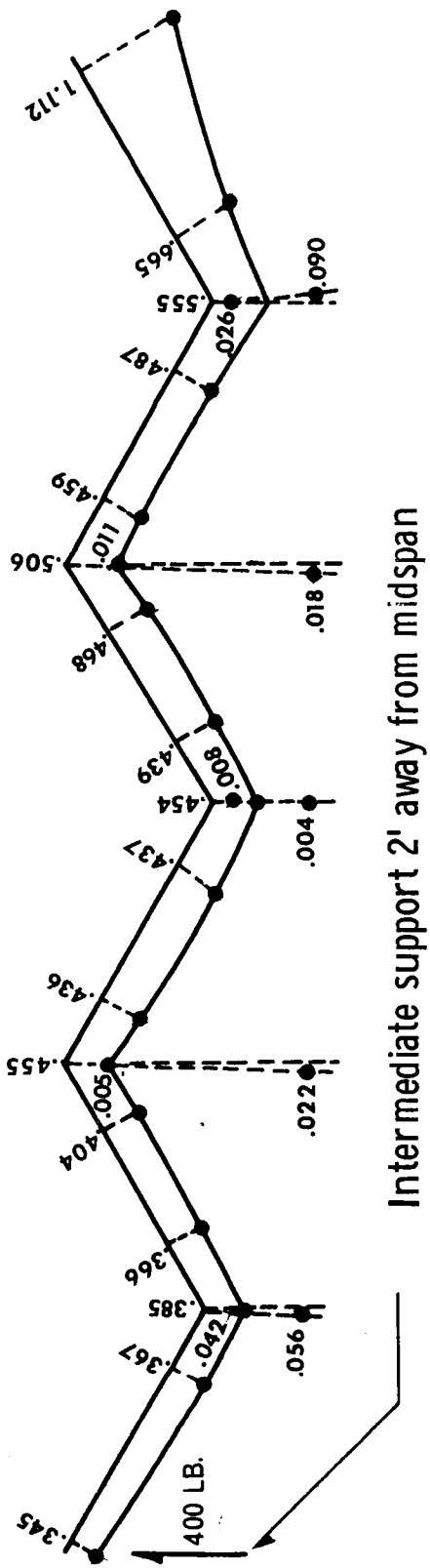

FIG. 104. EXPERIMENTAL DEFLECTIONS IN INCHES AT MIDSPAN OF THE NINETEEN-FOOT FOLDED PLATE MODEL LOADED WITH A UNIFORM PRESSURE OF 26 POUNDS PER SQUARE FOOT - INTERMEDIATE SUPPORT AT RIDGE I

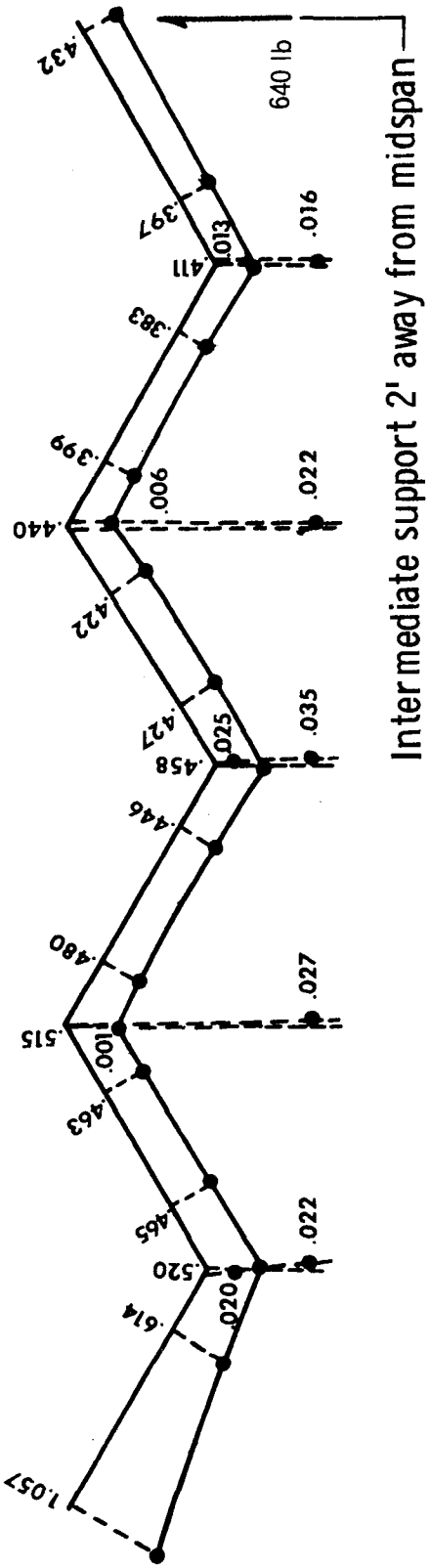

FIG. 105. EXPERIMENTAL DEFLECTIONS IN INCHES AT MIDSPAN OF THE NINETEEN-FOOT FOLDED PLATE MODEL LOADED WITH A UNIFORM PRESSURE OF 26 POUNDS PER SQUARE FOOT - INTERMEDIATE SUPPORT AT RIDGE I

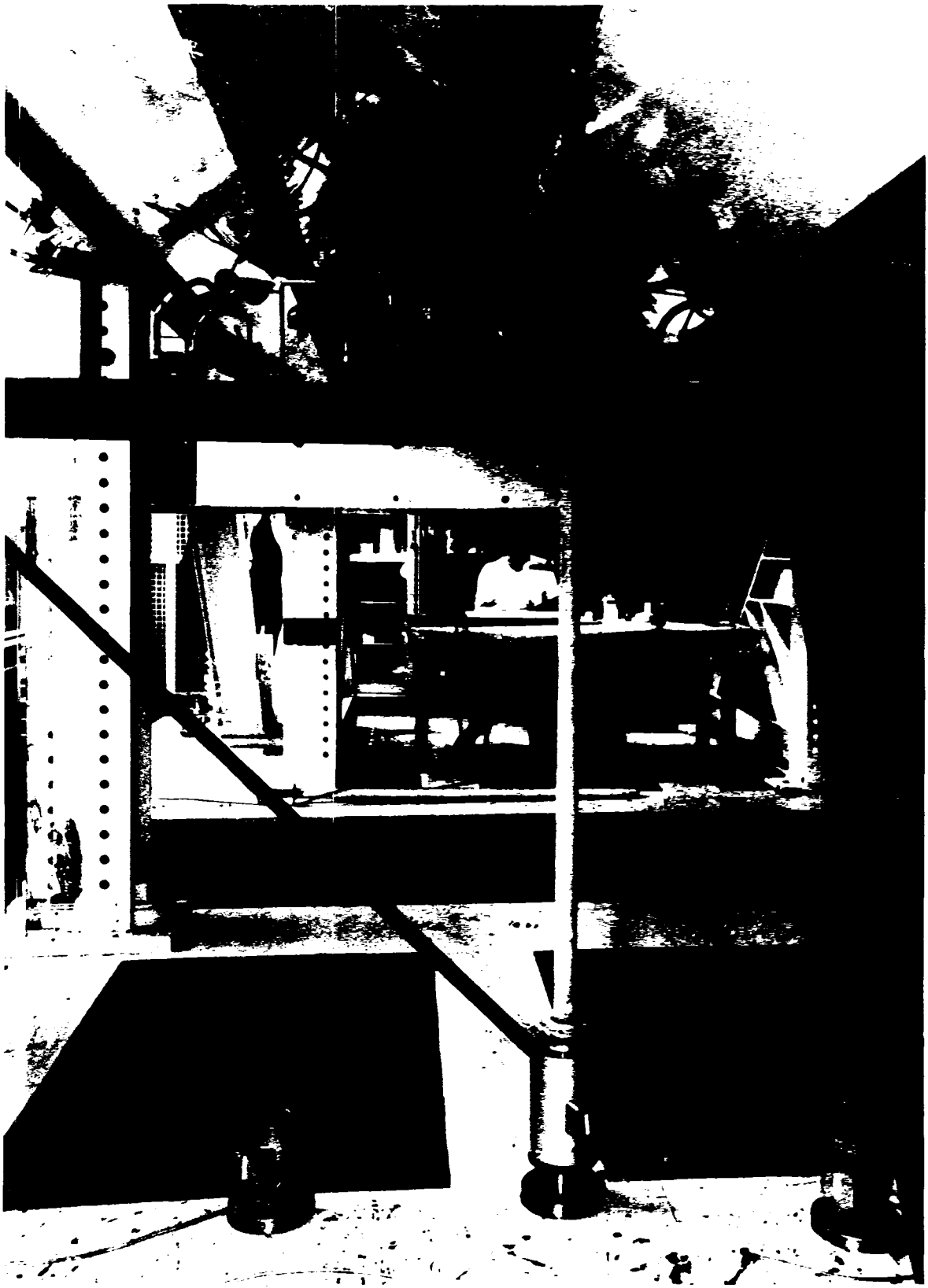

FIG. 106. INTERMEDIATE POINT SUPPORT AT RIDGE 5
SET AT TWO FEET WEST OF MIDSPAN

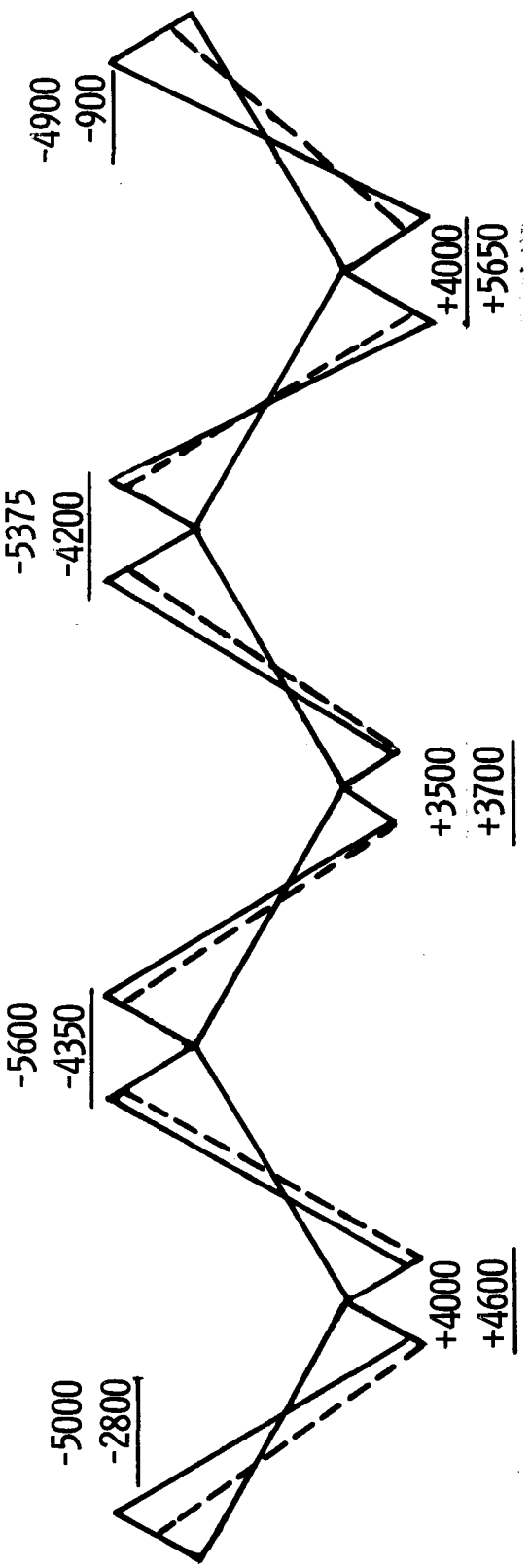

FIG. 107. EXPERIMENTAL LONGITUDINAL STRESSES IN PSI IN THE TOP AND BOTTOM FACINGS AT THE MIDSPAN SECTION OF THE NINETEEN-FOOT FOLDED PLATE MODEL WHEN LOADED WITH A UNIFORM PRESSURE OF 26 POUNDS PER SQUARE FOOT

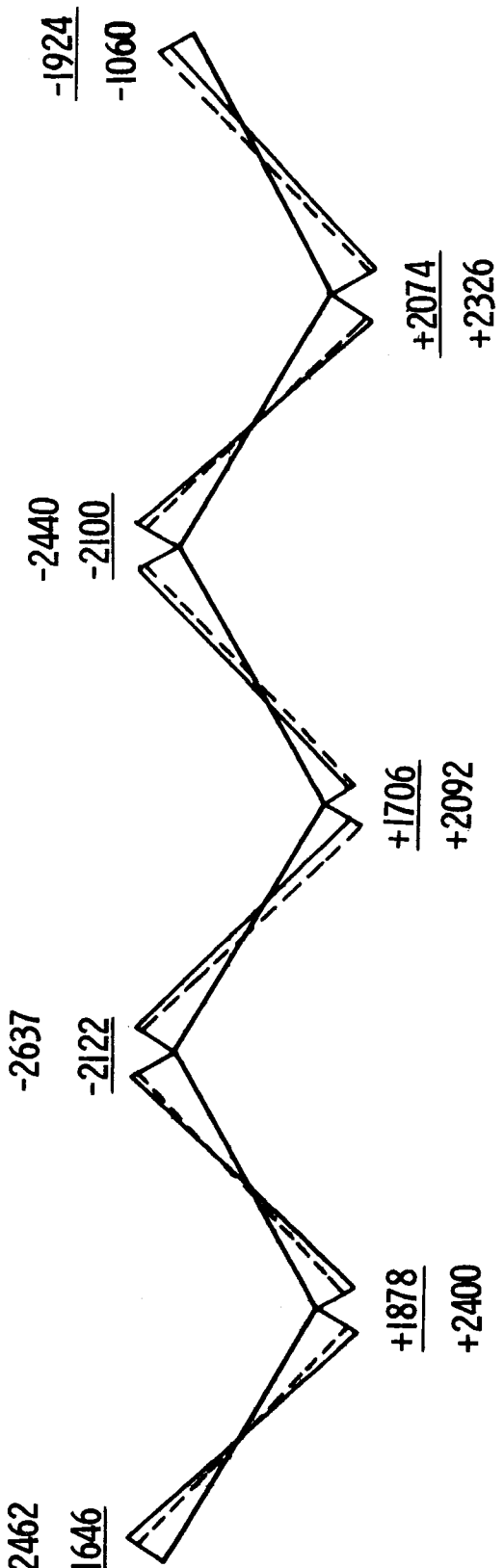

FIG. 108. EXPERIMENTAL LONGITUDINAL STRESSES IN PSI IN THE TOP AND BOTTOM FACINGS AT THE MIDSPAN SECTION OF THE NINETEEN-FOOT FOLDED PLATE MODEL WHEN LOADED WITH A UNIFORM PRESSURE OF 13 POUNDS PER SQUARE FOOT

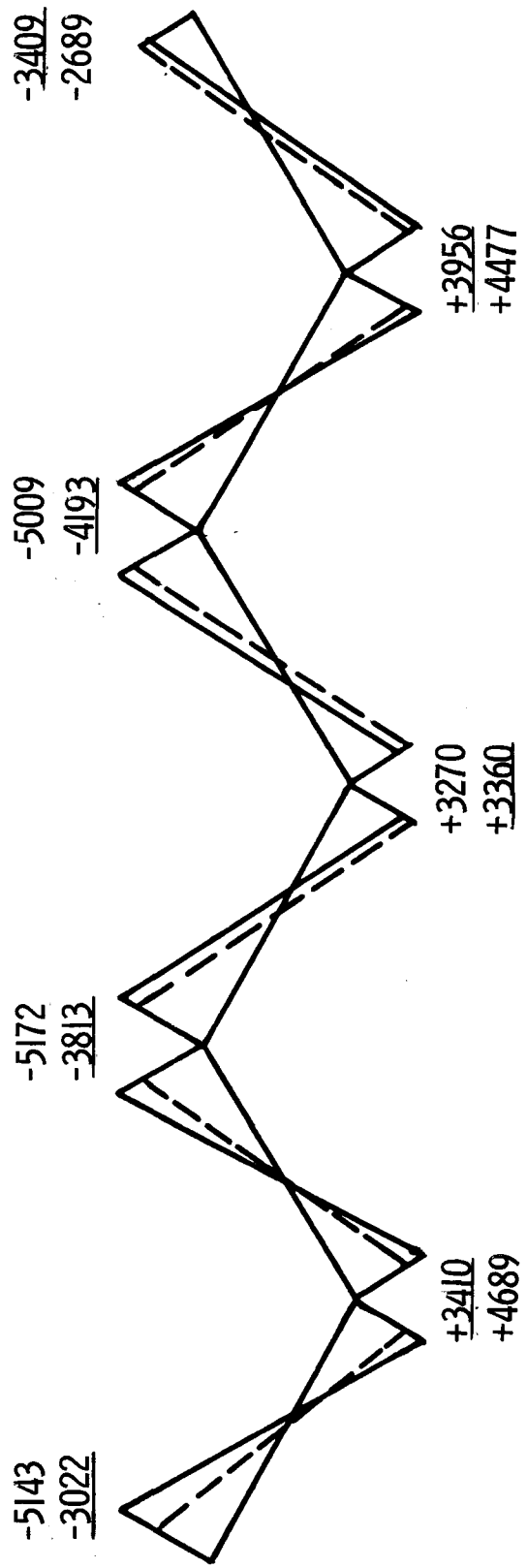

FIG. 109. EXPERIMENTAL LONGITUDINAL STRESSES IN PSI IN THE TOP AND BOTTOM FACINGS AT THE MIDSPAN SECTION OF THE NINETEEN-FOOT FOLDED PLATE MODEL LOADED WITH 23.4 POUNDS PER SQUARE FOOT

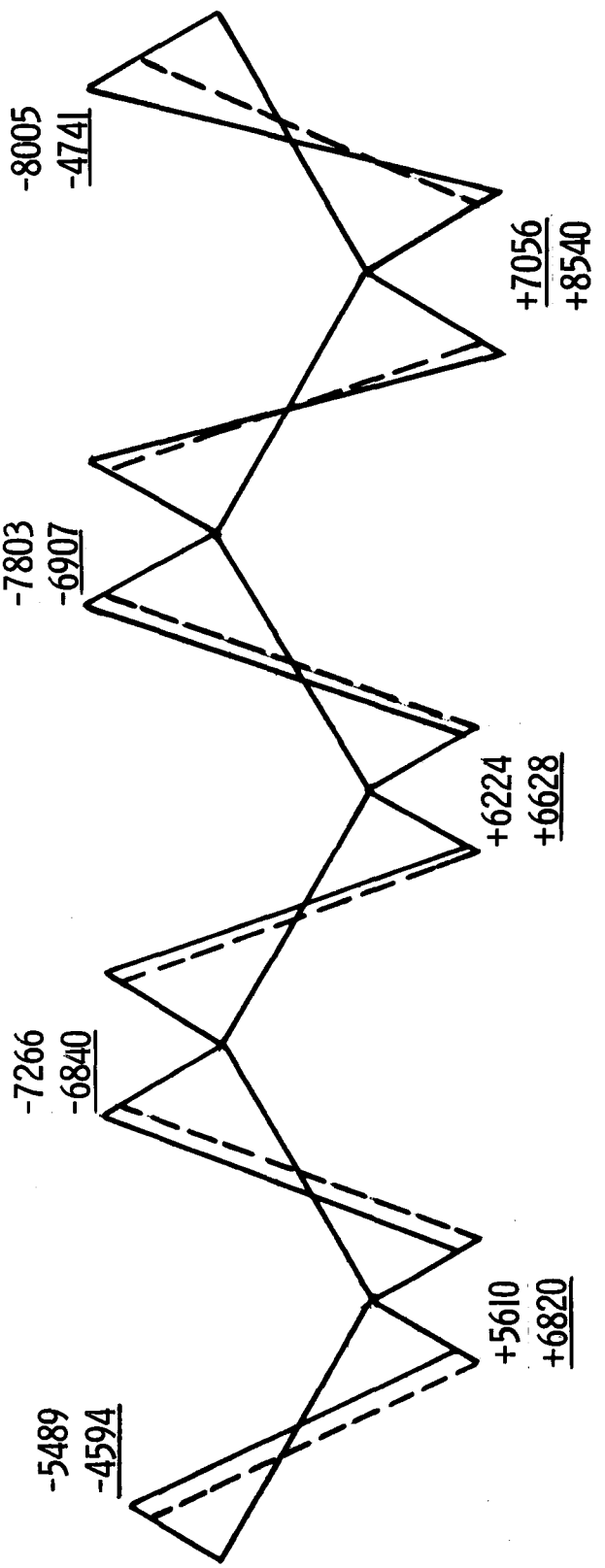

FIG. 110. EXPERIMENTAL LONGITUDINAL STRESSES IN PSI IN THE TOP AND BOTTOM FACINGS AT THE MIDSPAN SECTION OF THE NINETEEN-FOOT FOLDED PLATE MODEL WHEN LOADED WITH A UNIFORM PRESSURE OF 39 POUNDS PER SQUARE FOOT

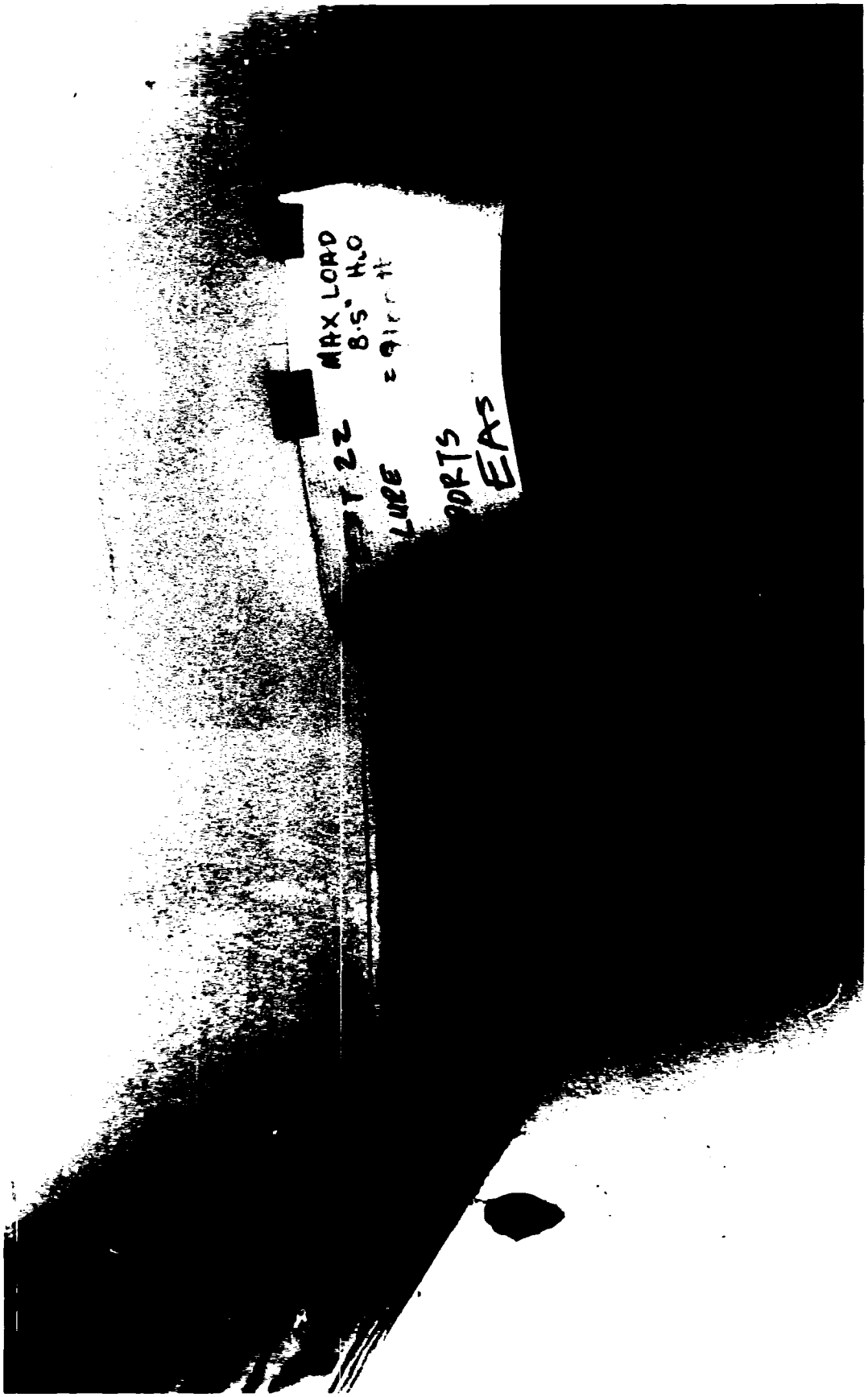

FIG. 111. DELAMINATION BETWEEN FACINGS AND CONNECTING CHANNEL AT THE EAST END OF RIDGE 6

FIG. 112. AT A LOAD OF 46.8 PSF RIDGE 1 IS SHOWN BENT BELOW THE BOTTOM OF THE PRESSURE BOX

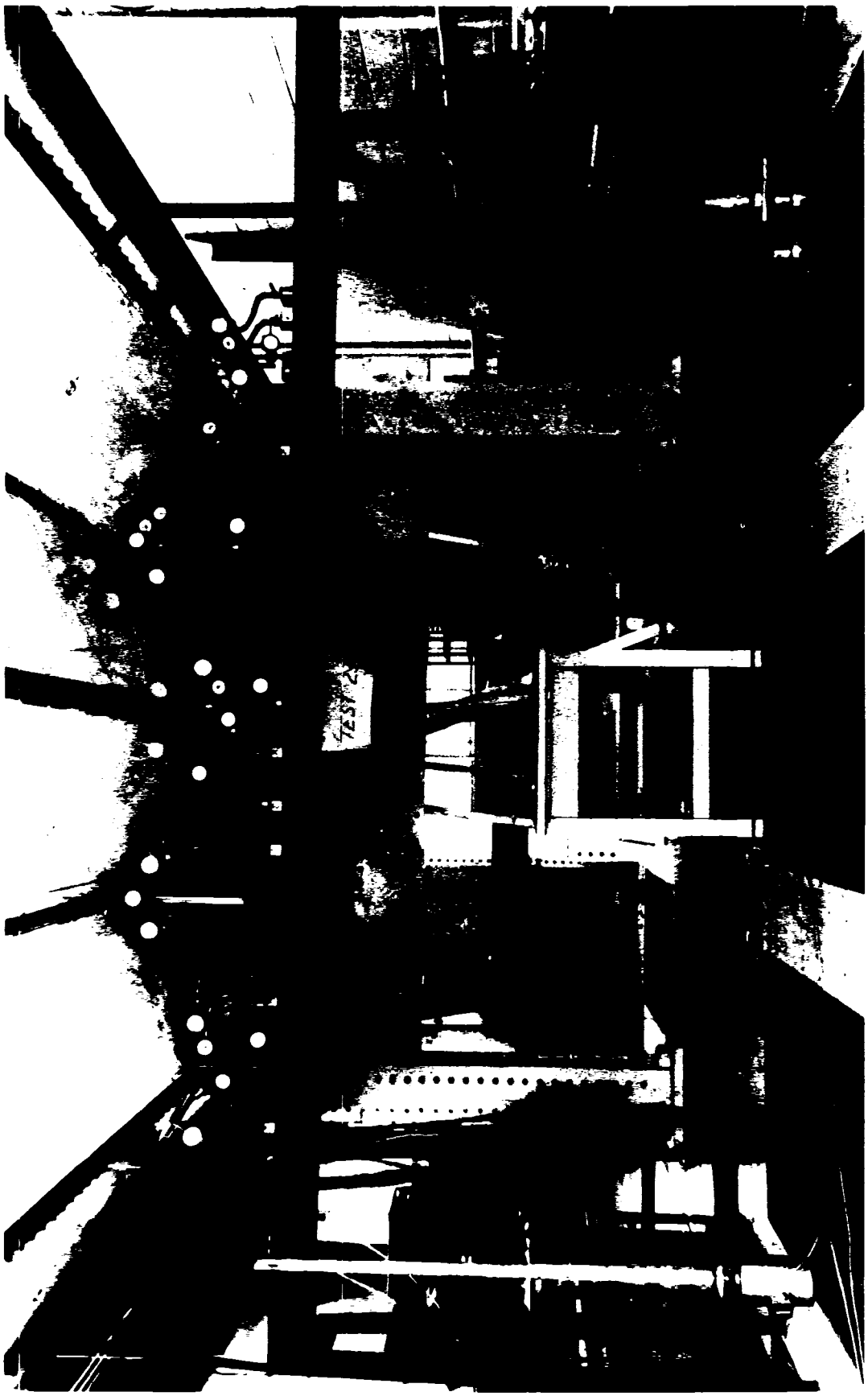

FIG. 113. ATTEMPT TO FAIL THE 19-FOOT MODEL HAVING INTRODUCED POINT SUPPORTS AT MIDSPAN OF RIDGES 1 AND 7

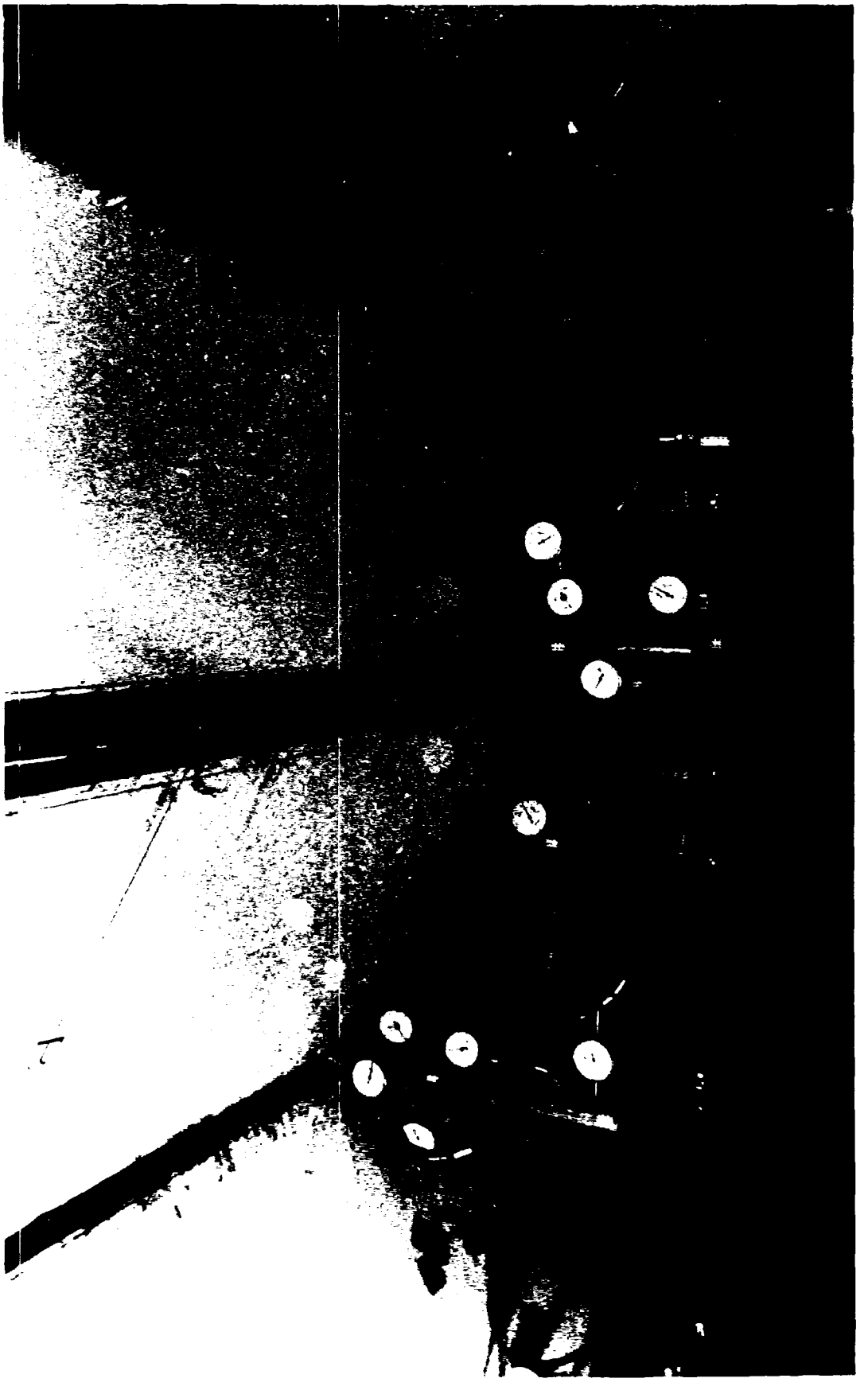

FIG. 114. FAILURE AT RIDGE 7 DUE TO STRESS CONCENTRATIONS CAUSED BY THE POINT SUPPORT

FIG. 115. RIDGES 1 AND 7 WERE UNIFORMLY SUPPORTED WITH CLAMPS TO AVOID LOCAL FAILURE AT THE EXTERIOR PANELS

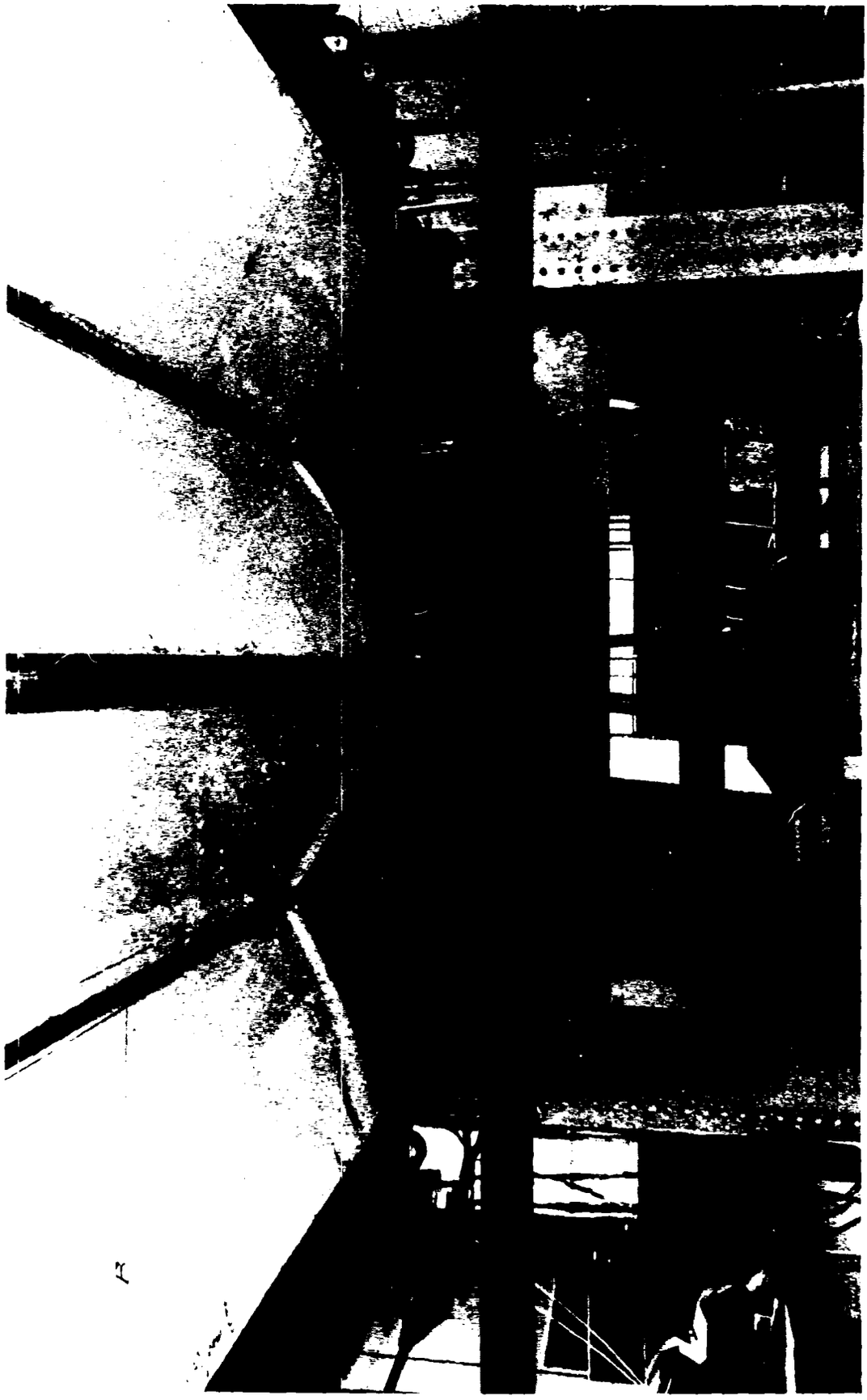

FIG. 116. FAILURE OF THE 19-FOOT FOLDED SANDWICH PLATE MODEL
BOTTOM VIEW

FIG. 117. TOP VIEW OF THE FAILED MODEL AFTER HAVING REMOVED THE PRESSURE BAG

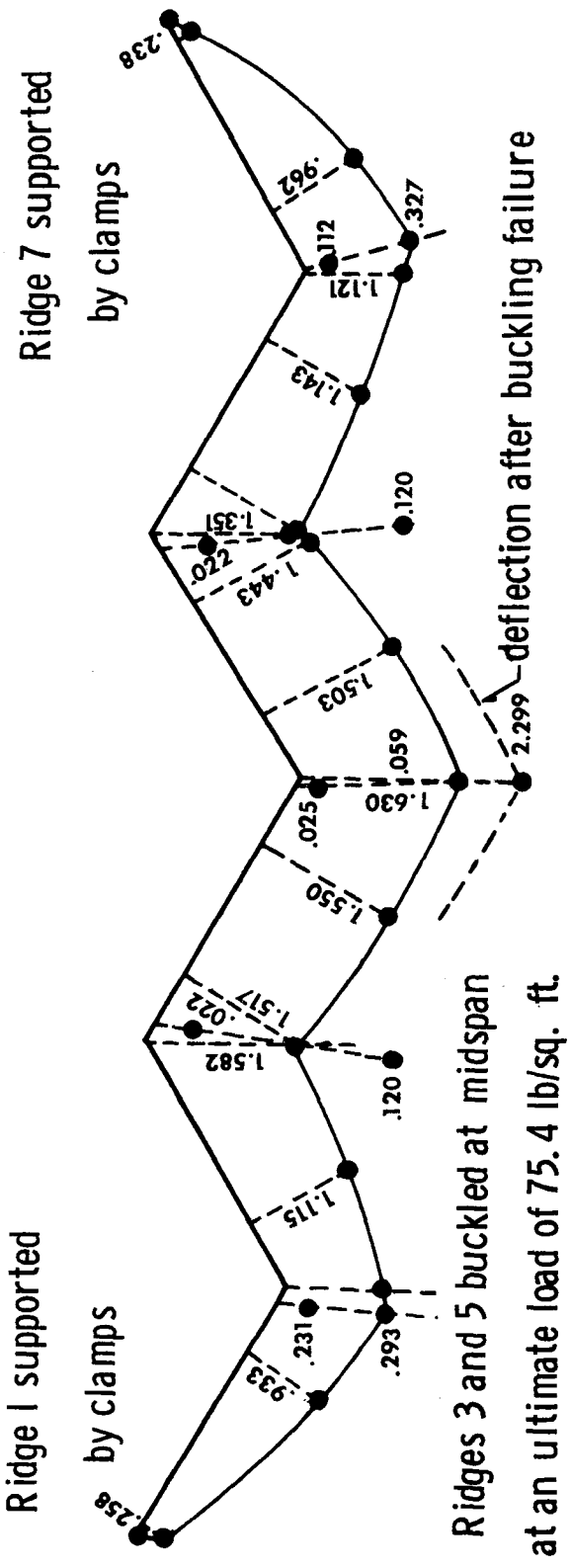

FIG. 118. EXPERIMENTAL DEFECTIONS IN INCHES AT MIDSPAN OF THE NINETEEN-FOOT FOLDED PLATE MODEL BEFORE AND AFTER RIDGES 3 AND 5 BUCKLED AT AN ULTIMATE LOAD OF 75.4 POUNDS PER SQUARE FOOT

FIG. 119. THE FAILED 19-FOOT MODEL IS LIFTED OFF THE PIPE SUPPORT BY ONE MAN

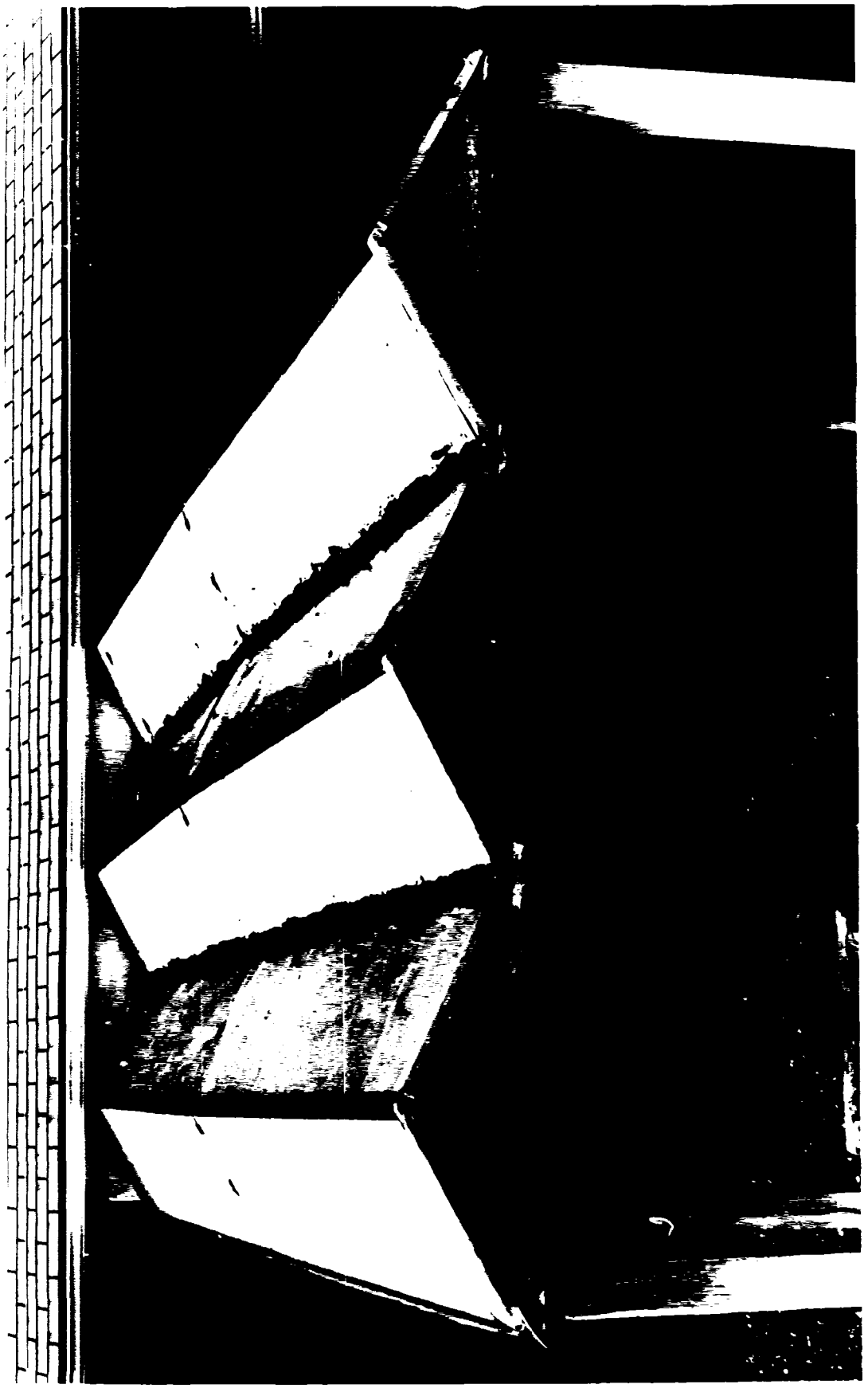

FIG. 120. THE FAILED 19-FOOT FOLDED SANDWICH MODEL EXPOSED TO WEATHER

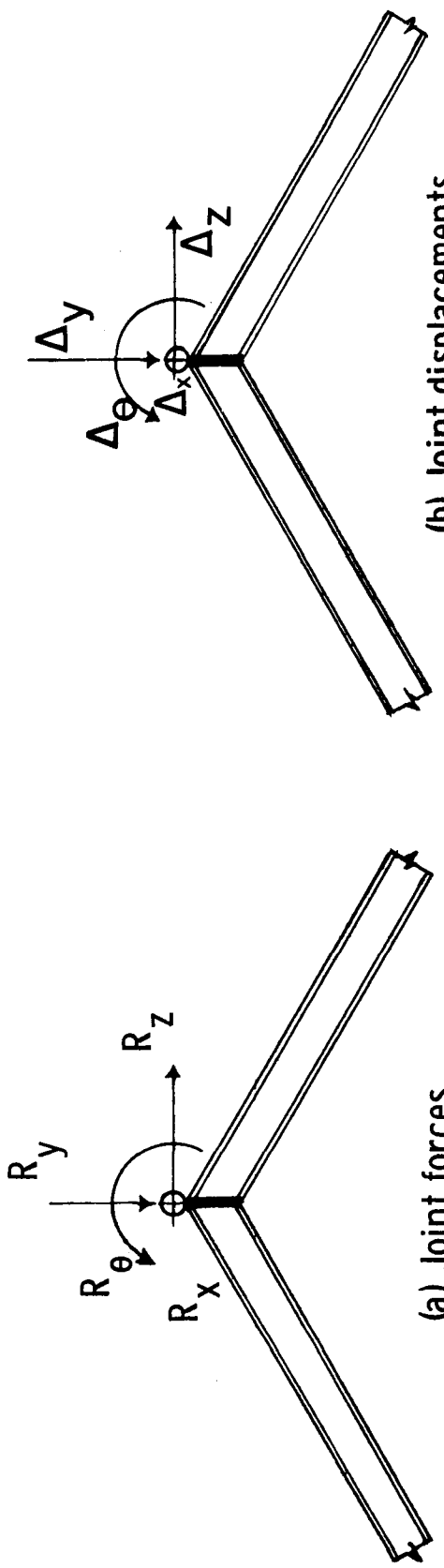

FIG. 121. POSITIVE JOINT FORCES AND DISPLACEMENTS IN THE FIXED COORDINATE SYSTEM

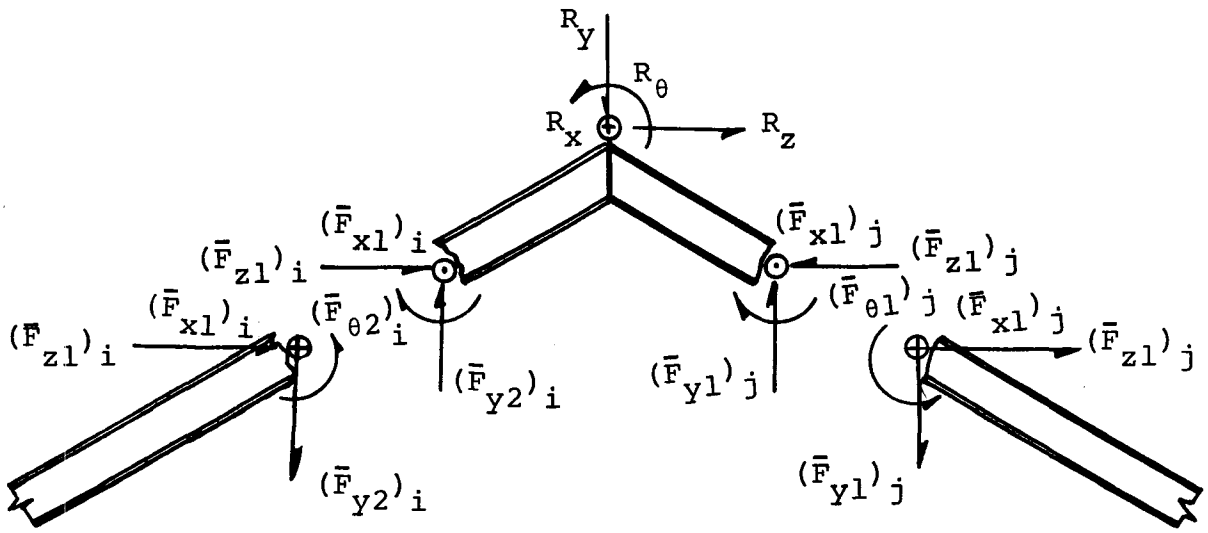

(a) Forces

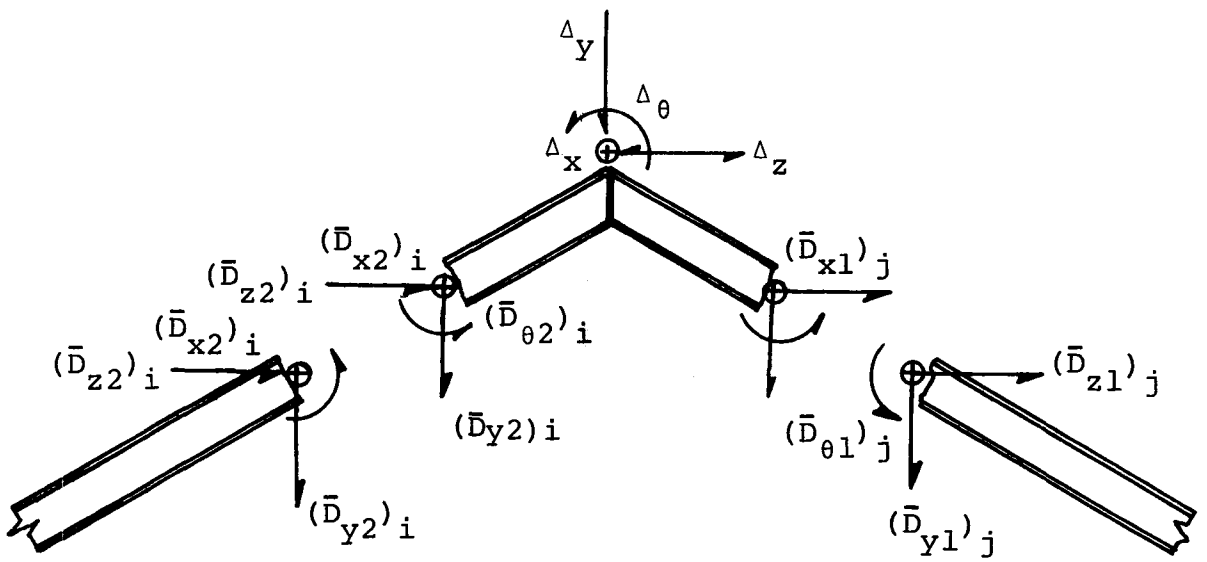

(b) Displacements

FIG. 122. RELATIONSHIPS AT A JOINT OF FORCES AND DISPLACEMENTS IN THE FIXED COORDINATE SYSTEM

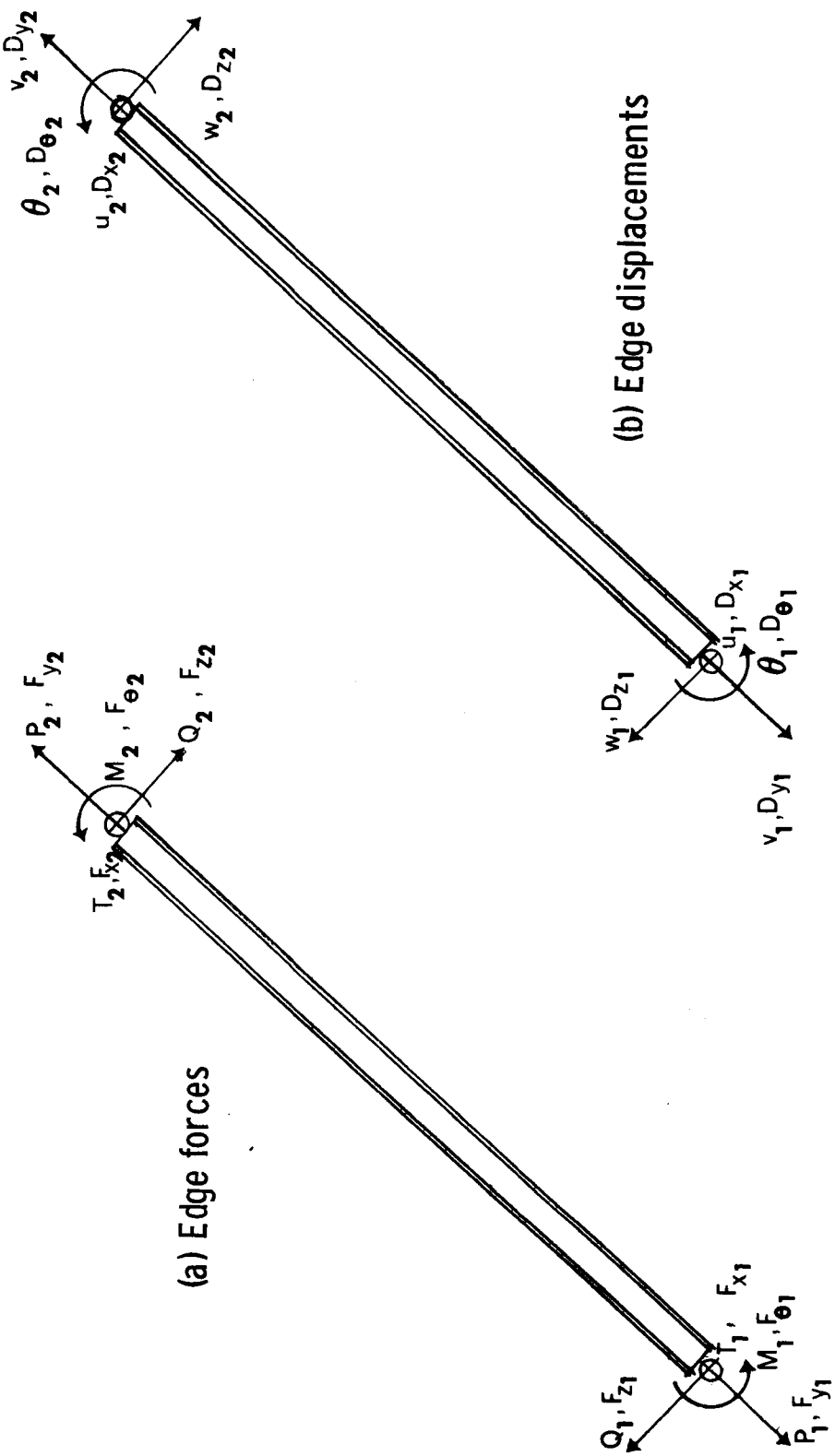

FIG. 123. POSITIVE EDGE FORCES AND DISPLACEMENTS IN THE RELATIVE COORDINATE SYSTEM

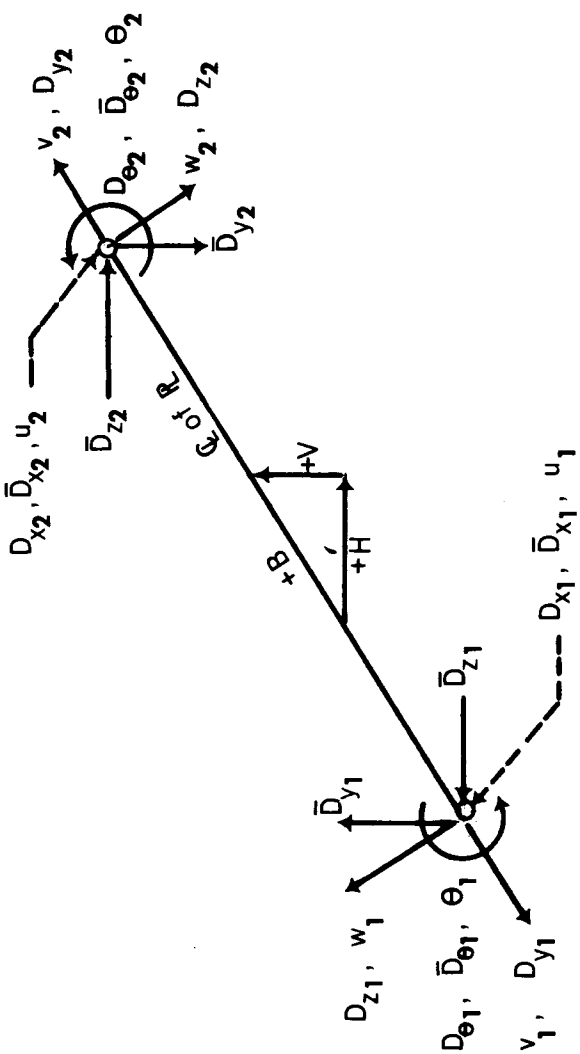

FIG. 124. RELATIONSHIP BETWEEN DISPLACEMENTS IN THE RELATIVE SYSTEM AND THOSE IN THE FIXED SYSTEM

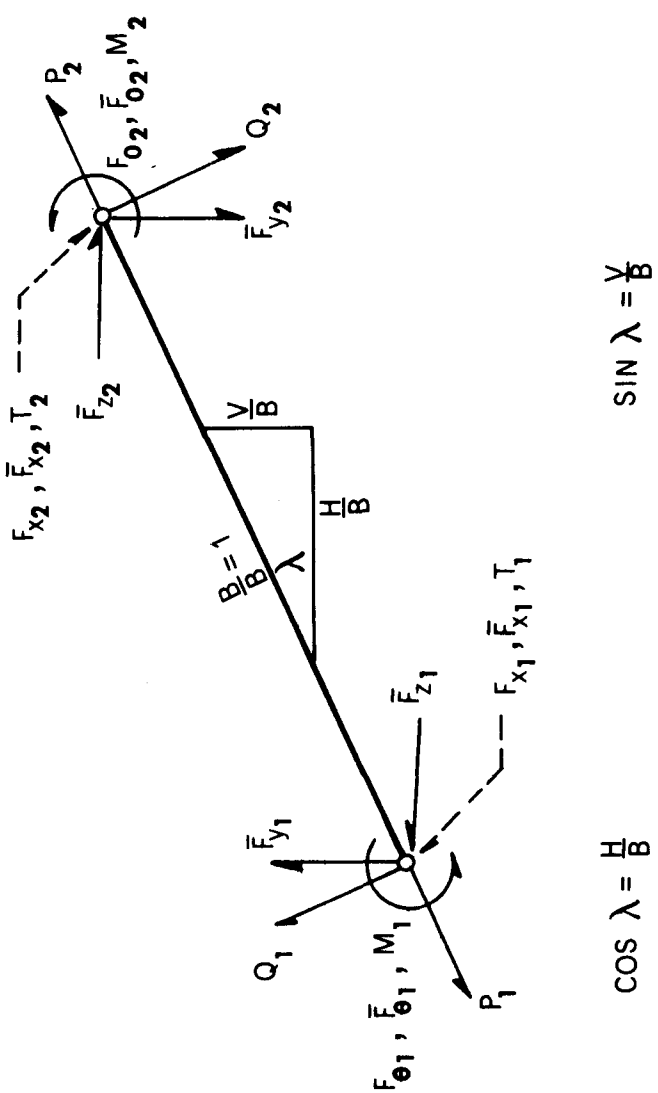

FIG. 125. RELATIONSHIP BETWEEN FORCES IN THE RELATIVE SYSTEM AND THOSE IN THE FIXED SYSTEM

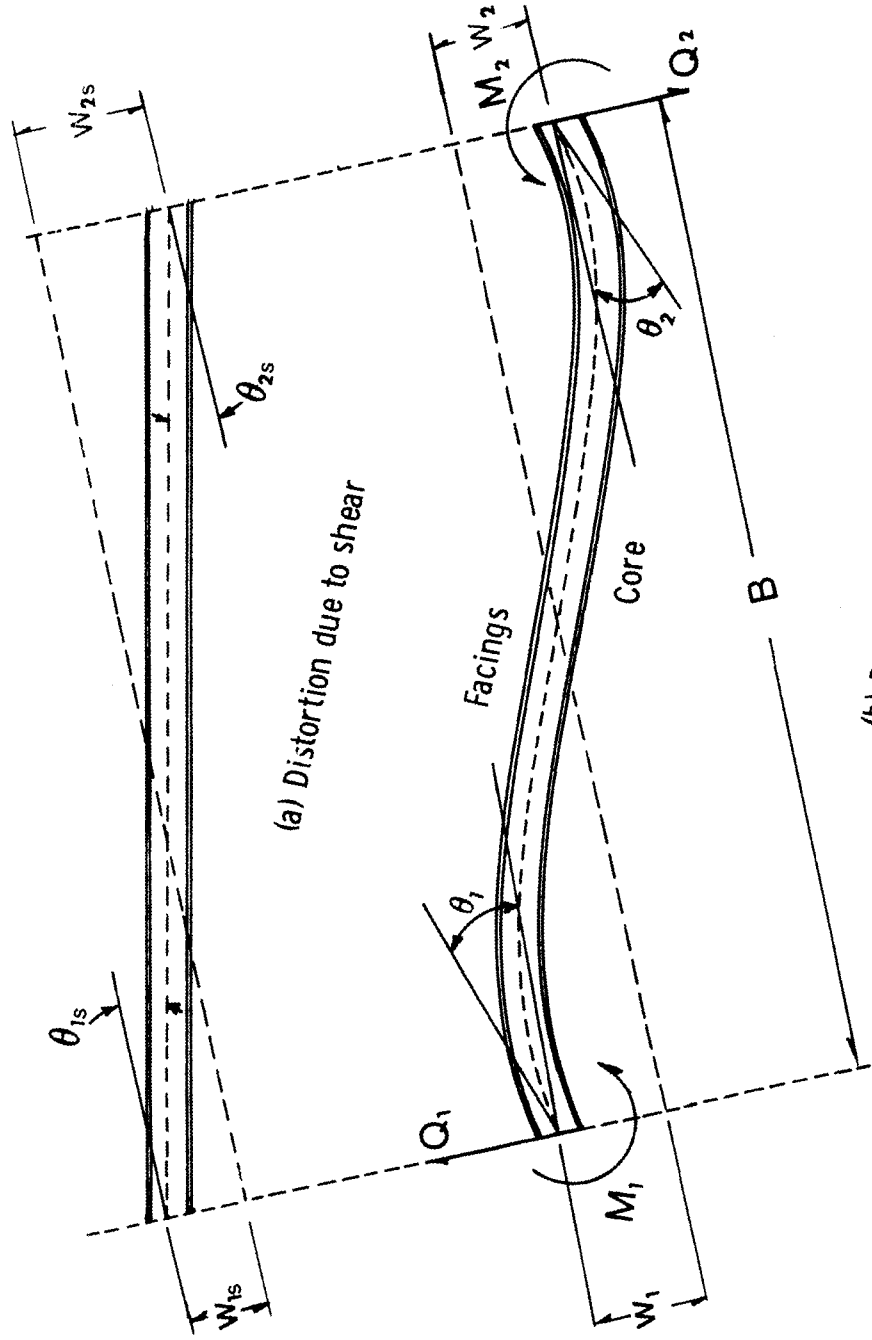

FIG. 126. SLOPE DEFLECTION OF A SANDWICH STRIP

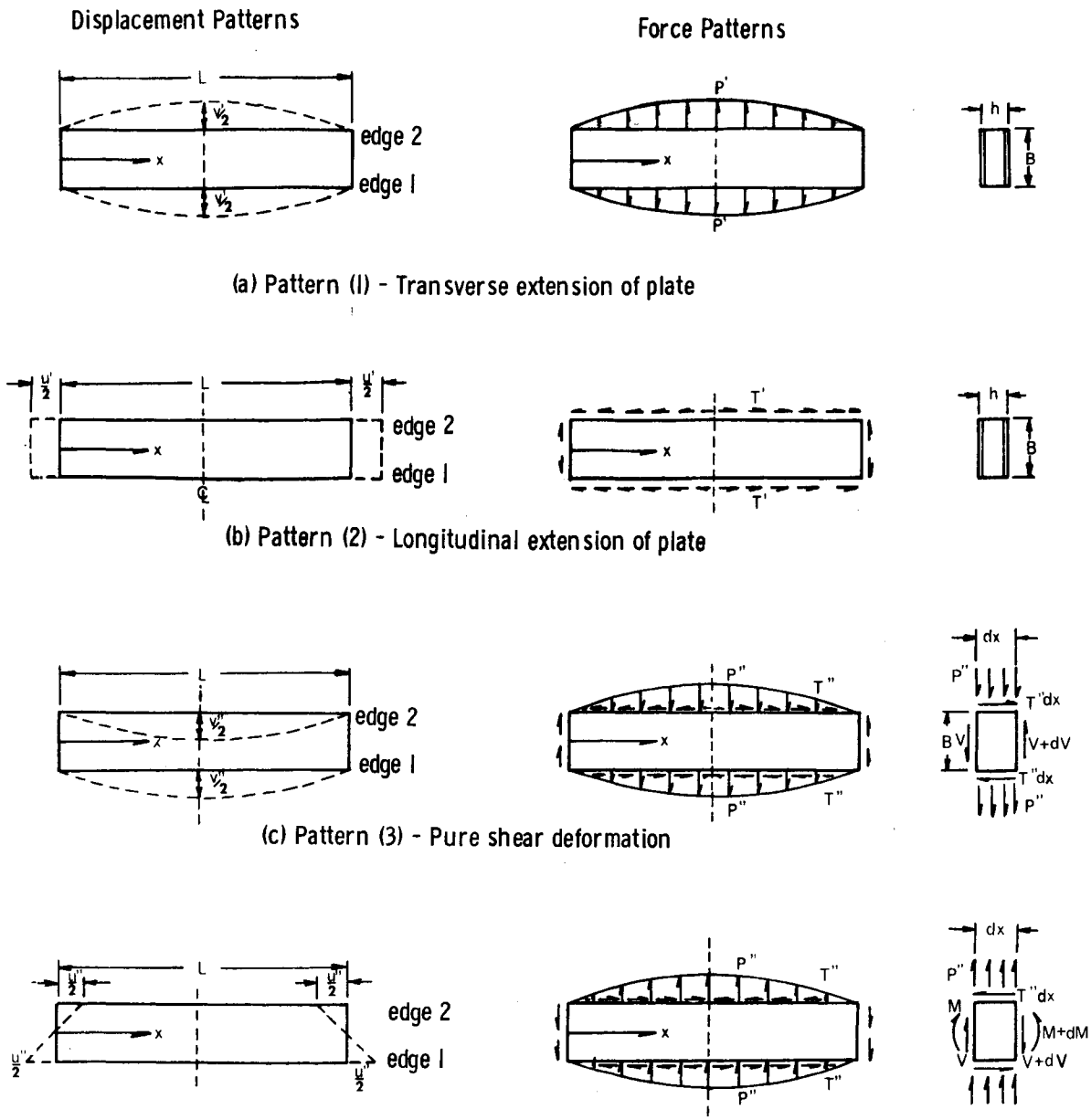

(a) Pattern (1) - Transverse extension of plate

(b) Pattern (2) - Longitudinal extension of plate

(c) Pattern (3) - Pure shear deformation

(d) Pattern (4) - Combination of flexural and shear deformation

FIG. 127. DISPLACEMENT AND FORCE PATTERNS FOR DETERMINING PLATE STIFFNESS MATRIX

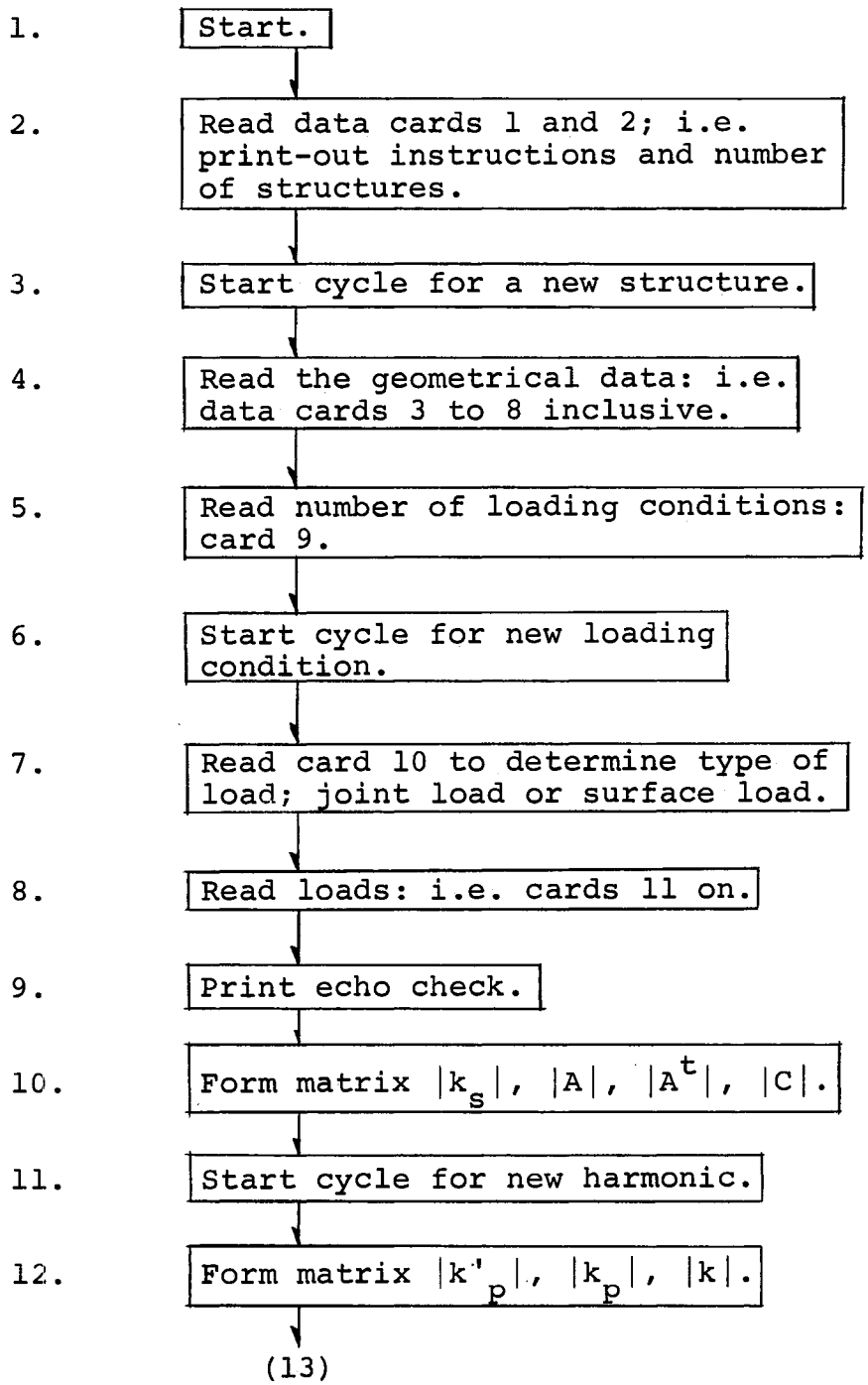

FIG. 128. FLOW CHART

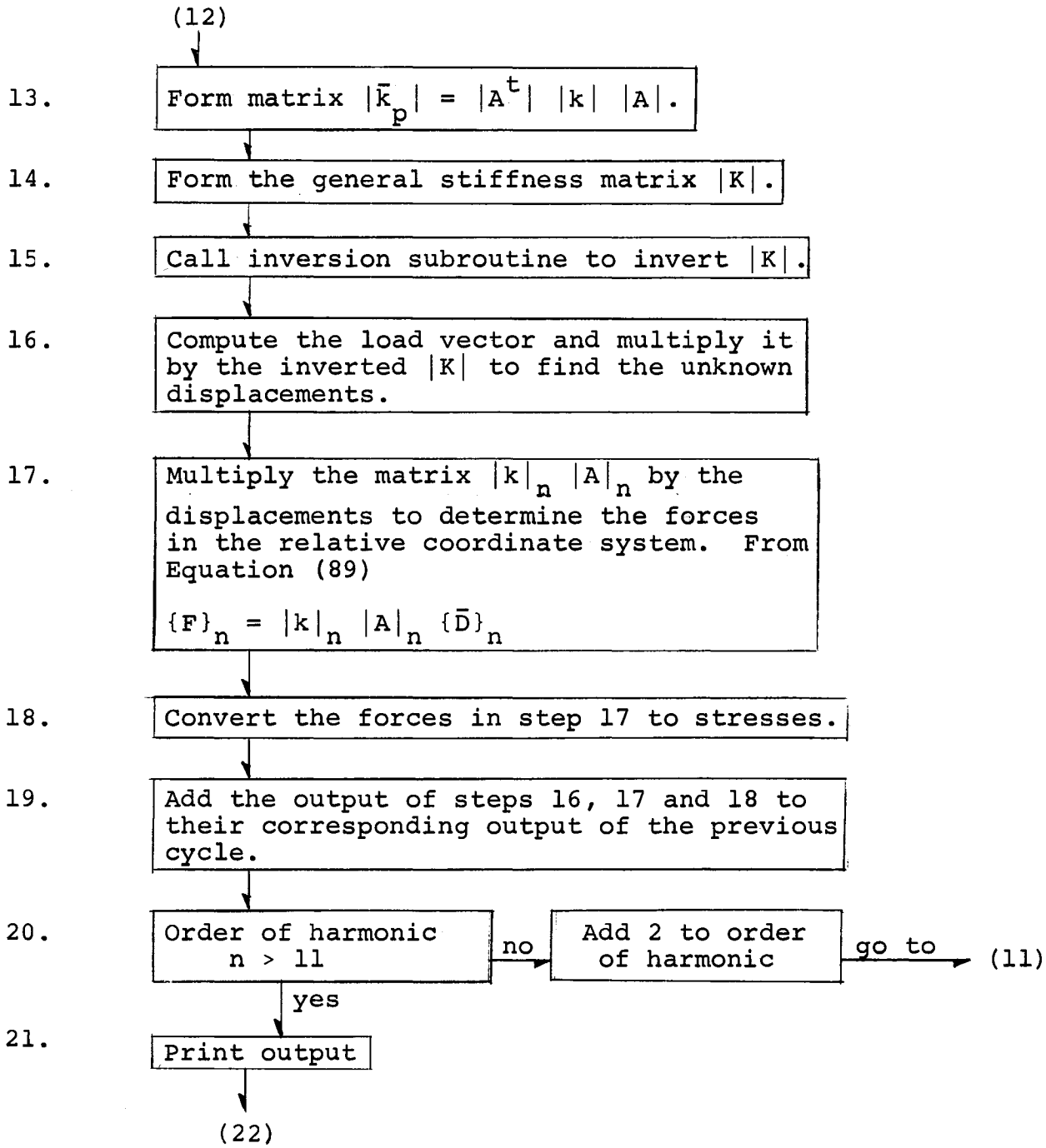

FIG. 128. CONTINUED.

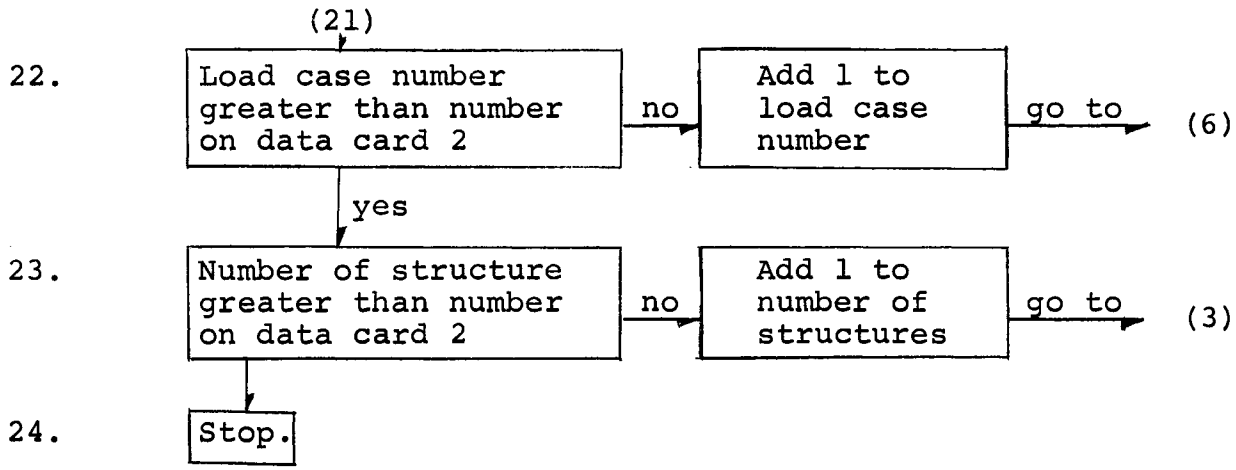

FIG. 128. CONTINUED

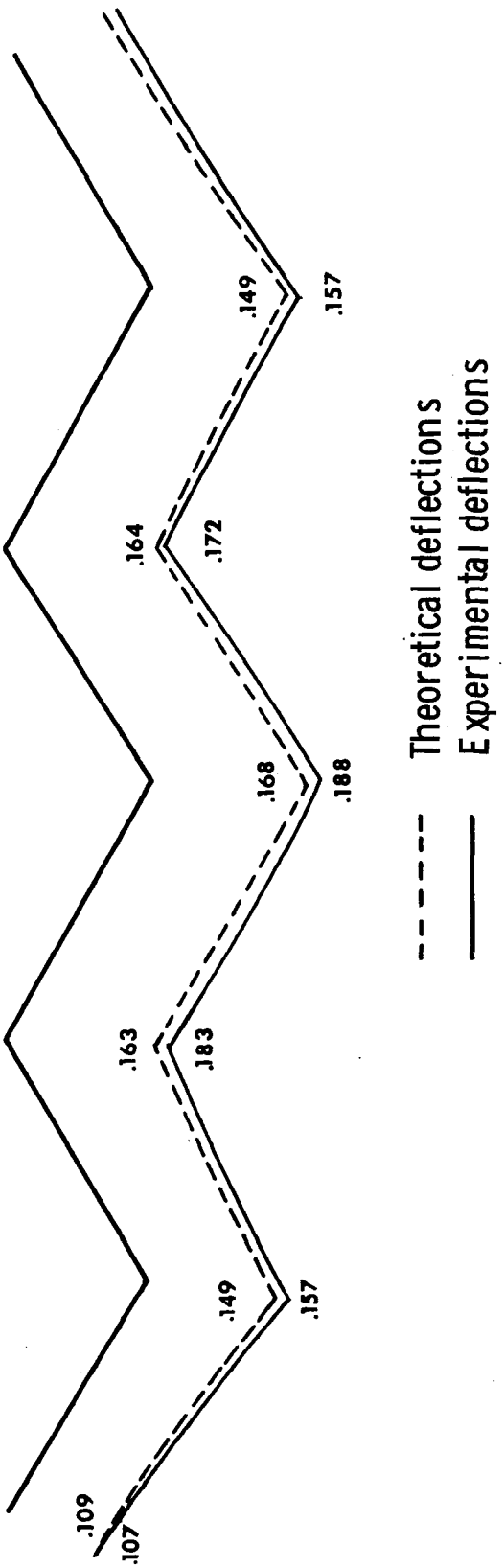

FIG. 129. THEORETICAL AND EXPERIMENTAL DEFLECTIONS IN INCHES AT MIDSPAN OF THE 9.5-FOOT FOLDED PLATE MODEL WHEN RIDGES 2 TO 6 ARE EACH UNIFORMLY LOADED WITH 2260 POUNDS

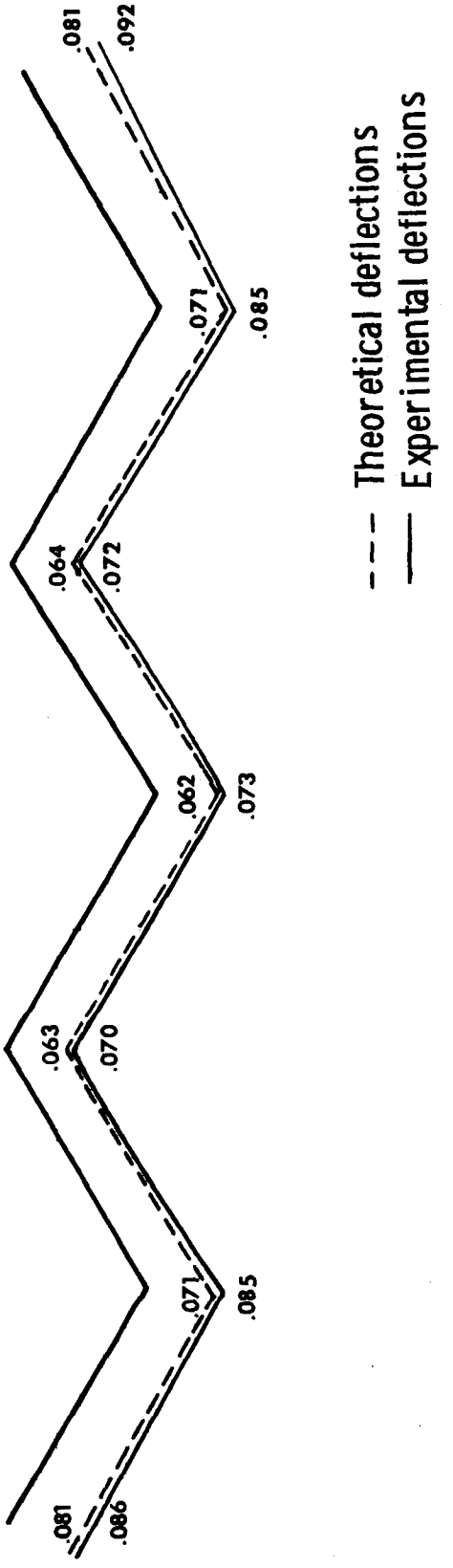

FIG. 130. THEORETICAL AND EXPERIMENTAL DEFLECTIONS IN INCHES AT MIDSPAN OF THE 9.5-FOOT FOLDED PLATE MODEL WHEN RIDGES 2, 4, AND 6 ARE EACH UNIFORMLY LOADED WITH 1600 POUNDS

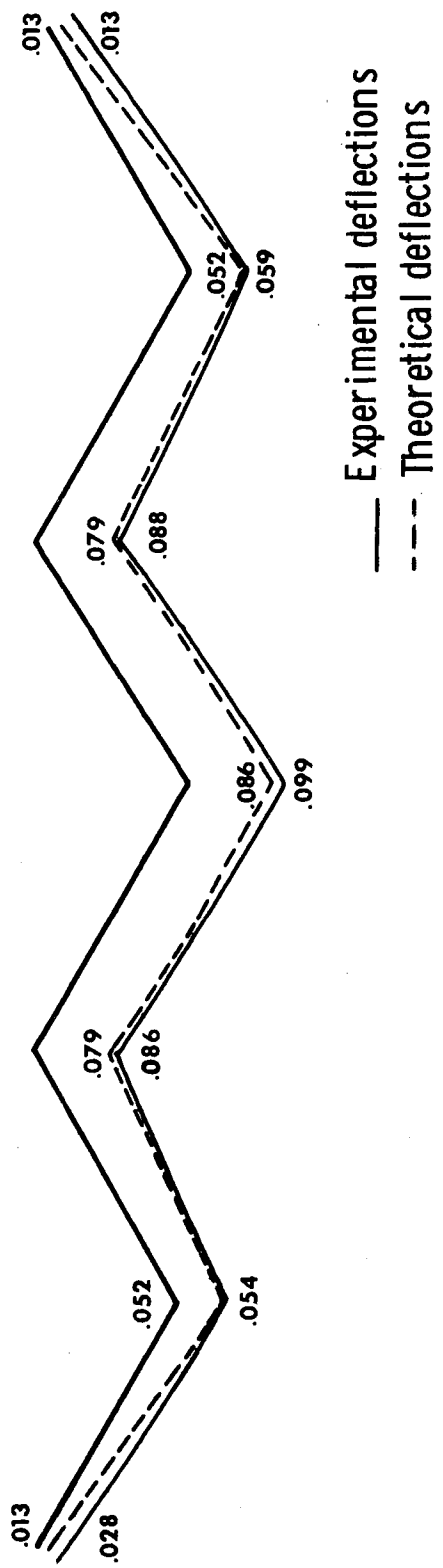

FIG. 131. THEORETICAL AND EXPERIMENTAL DEFLECTIONS IN INCHES AT MIDSPAN OF THE 9.5-FOOT FOLDED PLATE MODEL WHEN RIDGES 3 AND 5 ARE UNIFORMLY LOADED WITH 2400 POUNDS

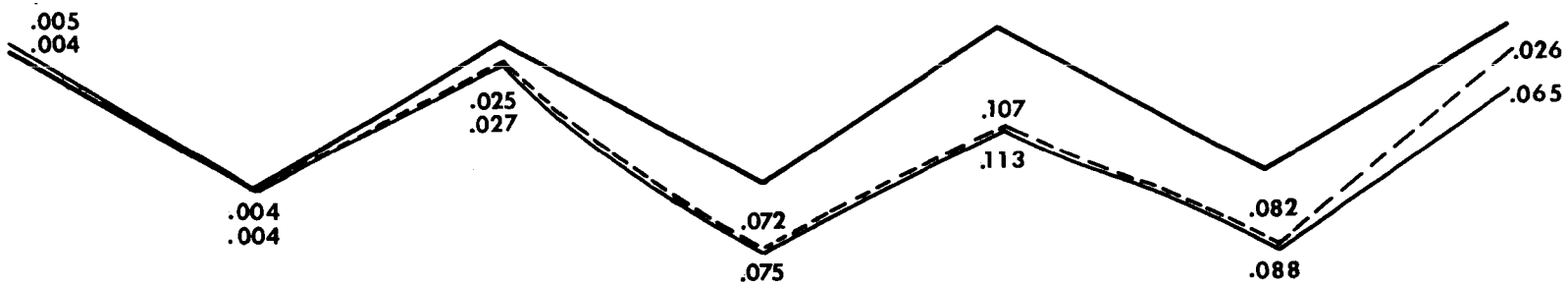

FIG. 132. THEORETICAL AND EXPERIMENTAL DEFLECTIONS IN INCHES AT MIDSPAN OF THE 9.5-FOOT FOLDED PLATE MODEL WHEN RIDGE 5 IS UNIFORMLY LOADED WITH 3980 POUNDS

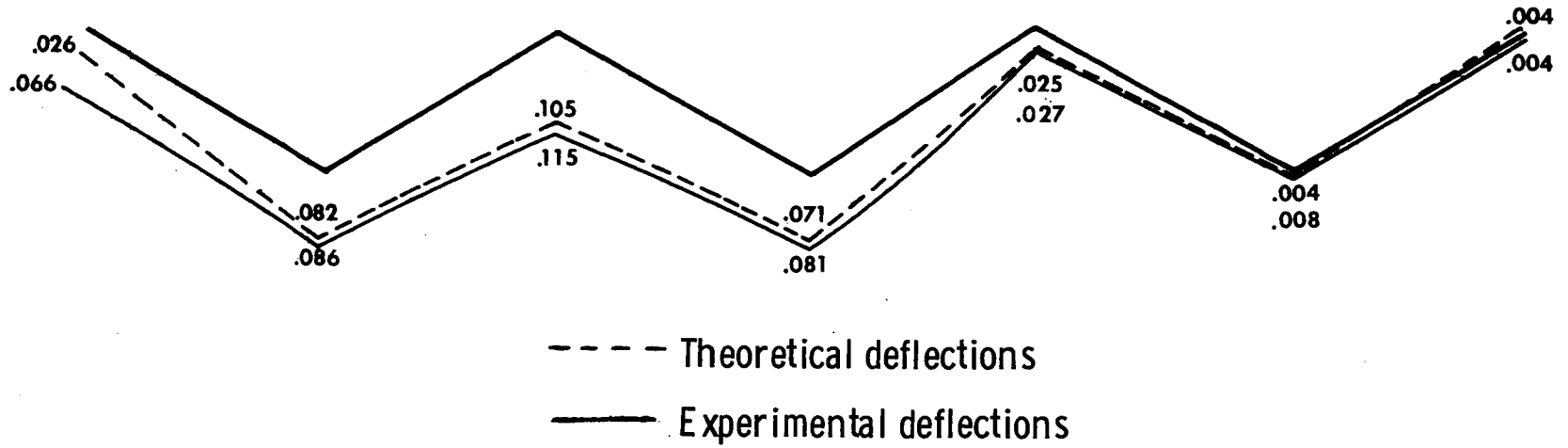

FIG. 133. THEORETICAL AND EXPERIMENTAL DEFLECTIONS IN INCHES AT MIDSPAN OF THE 9.5-FOOT FOLDED PLATE MODEL WHEN 3 IS UNIFORMLY LOADED WITH 3980 POUNDS

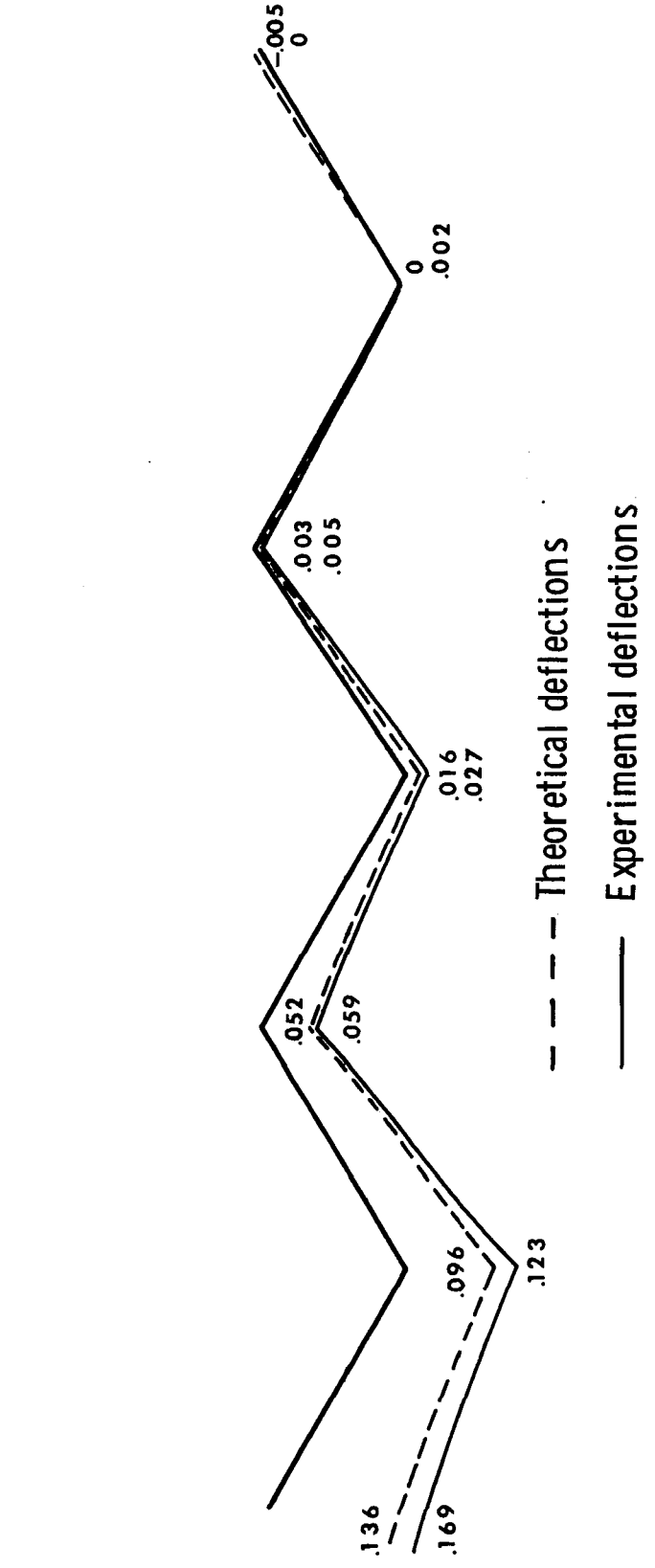

FIG. 134. THEORETICAL AND EXPERIMENTAL DEFLECTIONS IN INCHES AT MIDSPAN OF THE 9.5-FOOT FOLDED PLATE MODEL WHEN RIDGE 2 IS UNIFORMLY LOADED WITH 2550 POUNDS

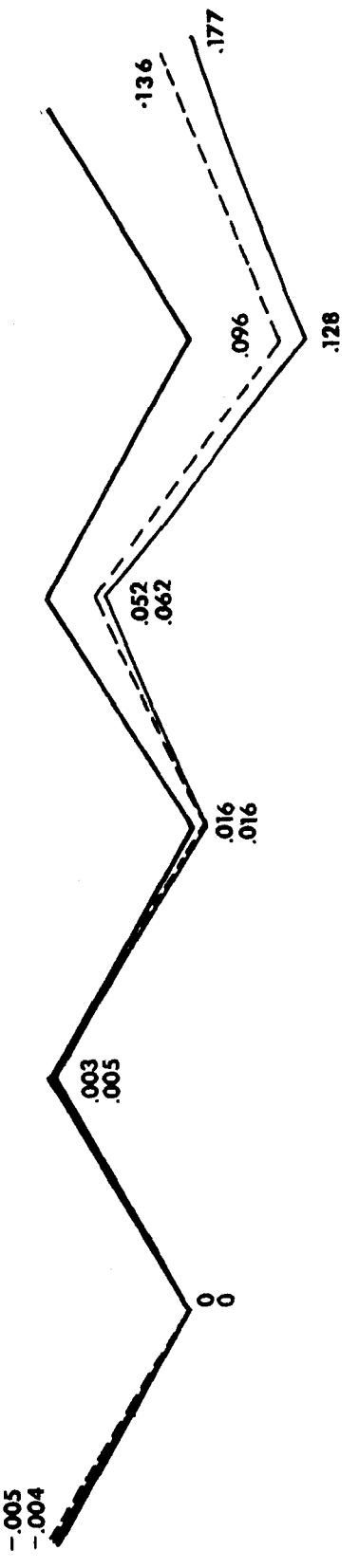

Theoretical deflections - - - - -

Experimental deflection ———

FIG. 135. THEORETICAL AND EXPERIMENTAL DEFLECTIONS IN INCHES AT MIDSPAN OF THE 9.5-FOOT FOLDED PLATE MODEL WHEN RIDGE 6 IS UNIFORMLY LOADED WITH 2550 POUNDS

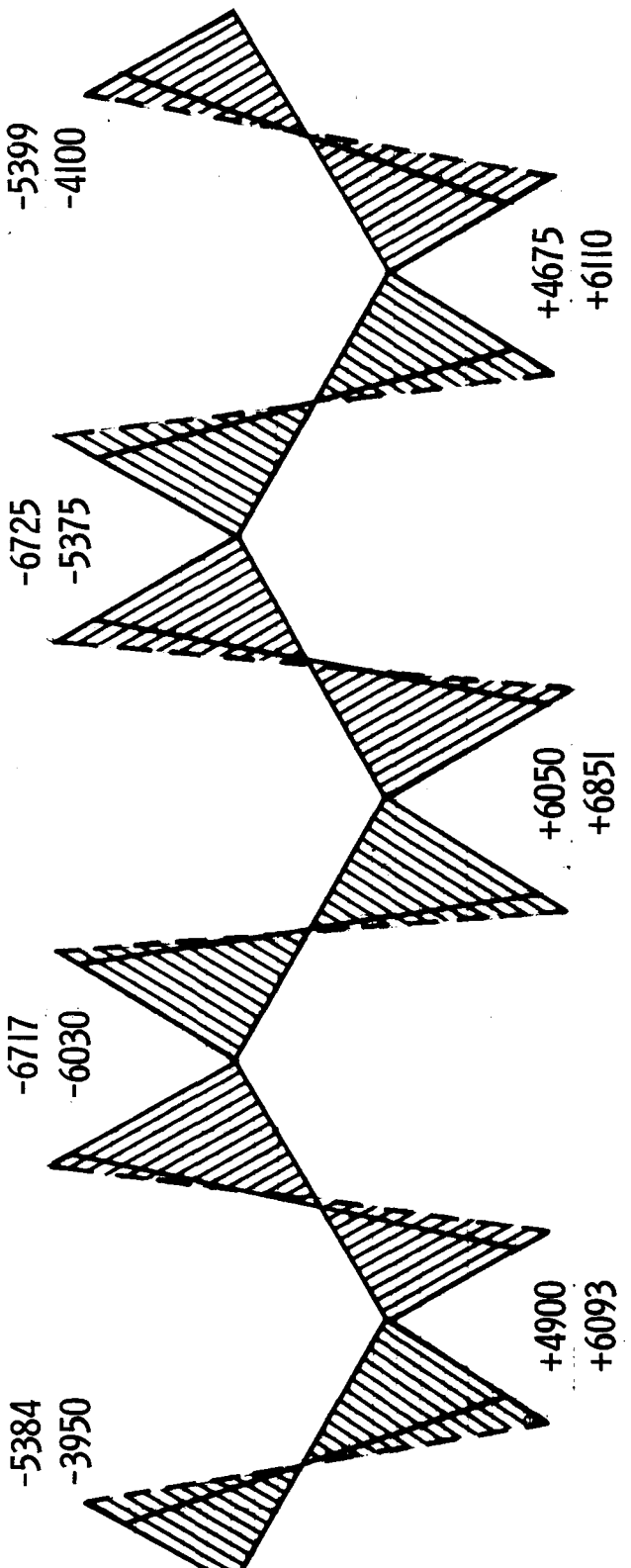

FIG. 136. EXPERIMENTAL AND THEORETICAL LONGITUDINAL STRESSES IN PSI AT MIDSPAN OF THE 9.5-FOOT FOLDED PLATE MODEL WHEN RIDGES 2 TO 6 ARE EACH UNIFORMLY LOADED WITH 2260 POUNDS

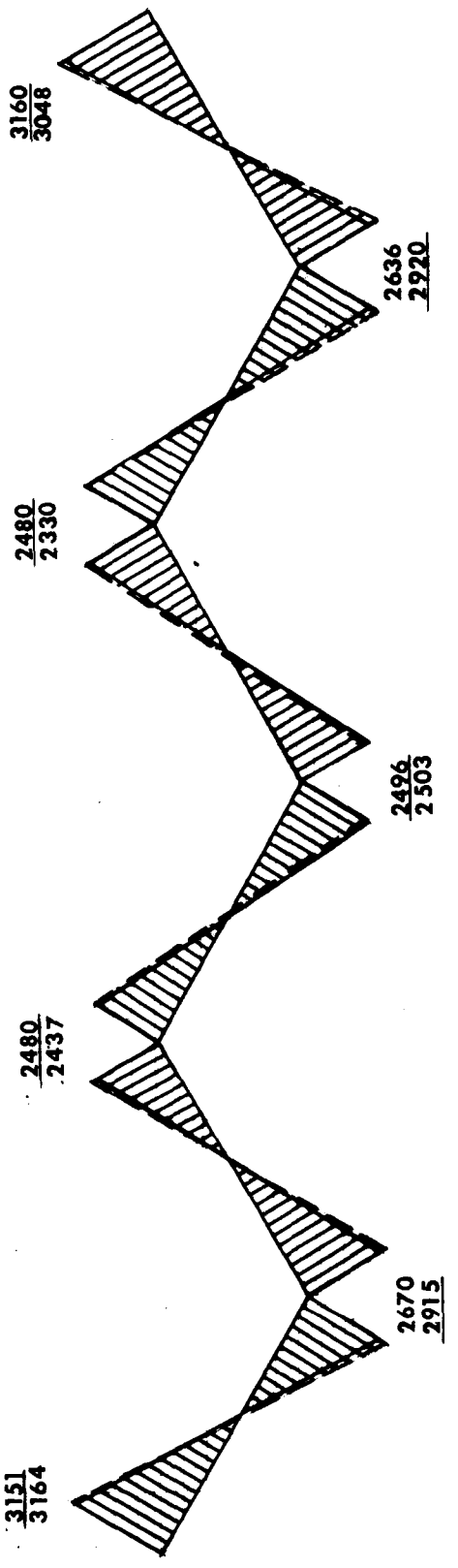

FIG. 137. EXPERIMENTAL AND THEORETICAL LONGITUDINAL STRESSES IN PSI AT THE MIDSPAN SECTION OF THE 9.5-FOOT FOLDED PLATE MODEL WHEN RIDGES 2, 4 AND 6 ARE EACH UNIFORMLY LOADED WITH 1600 POUNDS

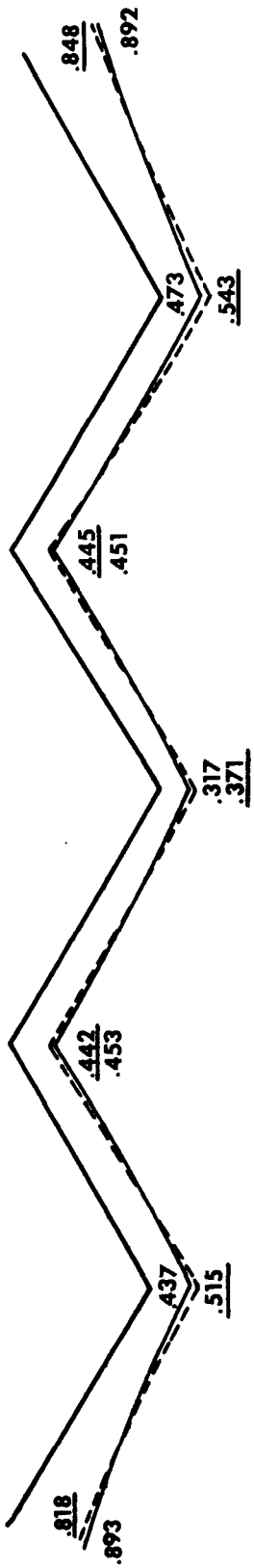

FIG. 138. THEORETICAL AND EXPERIMENTAL DEFLECTIONS IN INCHES AT MIDSPAN OF THE NINETEEN-FOOT FOLDED PLATE MODEL LOADED WITH A UNIFORM PRESSURE OF 23.4 POUNDS PER SQUARE FOOT

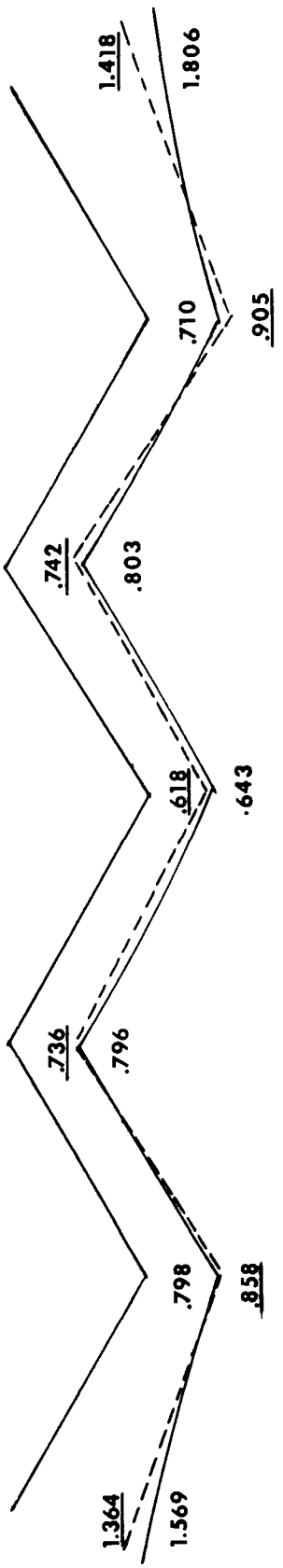

FIG. 139. THEORETICAL AND EXPERIMENTAL DEFLECTIONS IN INCHES AT MIDSPAN OF THE NINETEEN-FOOT FOLDED PLATE MODEL LOADED WITH A UNIFORM PRESSURE OF 40 POUNDS PER SQUARE FOOT

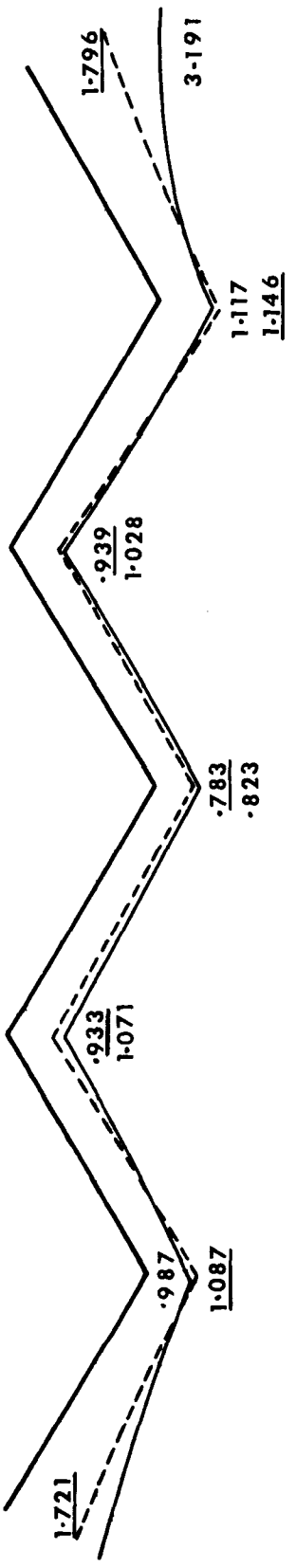

---- Theoretical deflections (underlined)

—— Experimental deflections

FIG. 140. THEORETICAL AND EXPERIMENTAL DEFLECTIONS IN INCHES AT MIDSPAN OF THE NINETEEN-FOOT FOLDED PLATE MODEL LOADED WITH A UNIFORM PRESSURE OF 49.4 POUNDS PER SQUARE FOOT

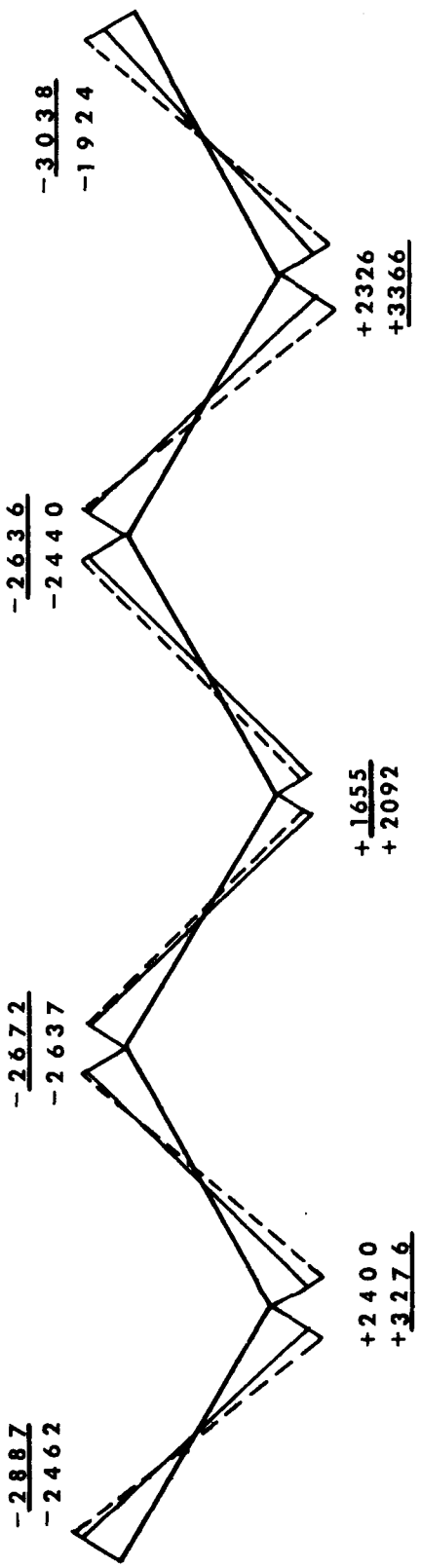

FIG. 141. THEORETICAL AND EXPERIMENTAL LONGITUDINAL STRESSES IN PSI AT MIDSPAN OF THE NINETEEN-FOOT FOLDED PLATE MODEL WHEN LOADED WITH A UNIFORM PRESSURE OF 13 POUNDS PER SQUARE FOOT

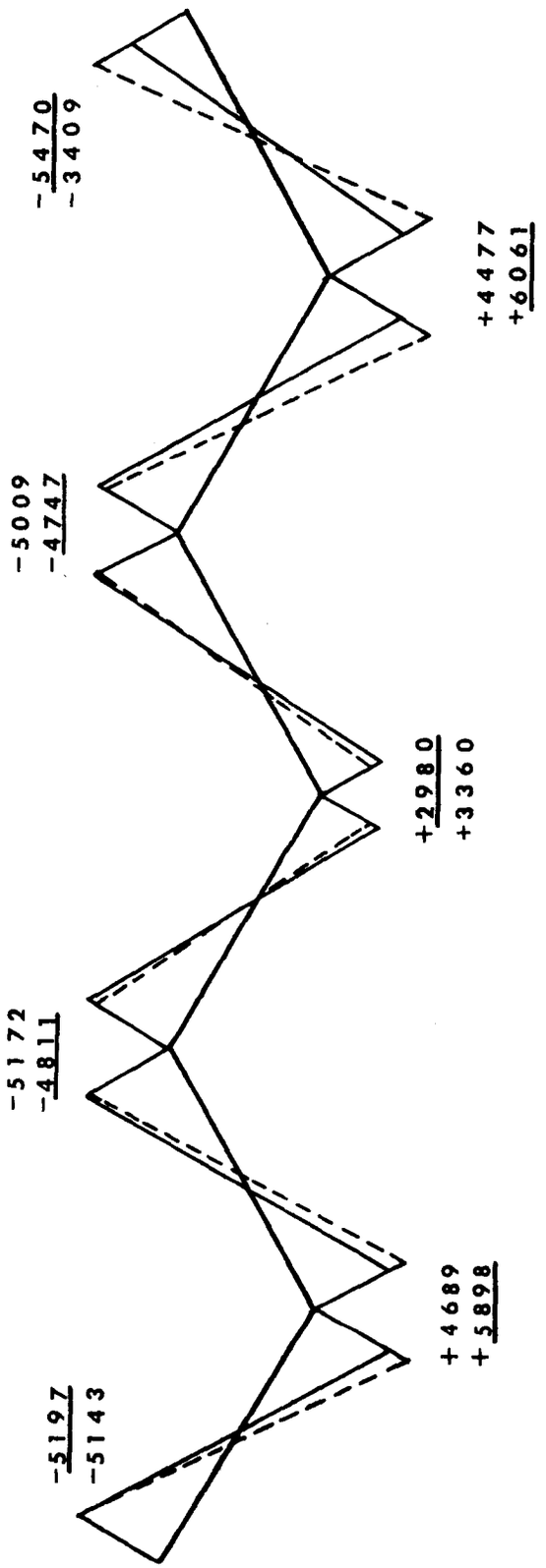

FIG. 142. THEORETICAL AND EXPERIMENTAL LONGITUDINAL STRESSES IN PSI AT MIDSPAN OF THE NINETEEN-FOOT FOLDED PLATE MODEL WHEN LOADED WITH A UNIFORM PRESSURE OF 23.4 POUNDS PER SQUARE FOOT

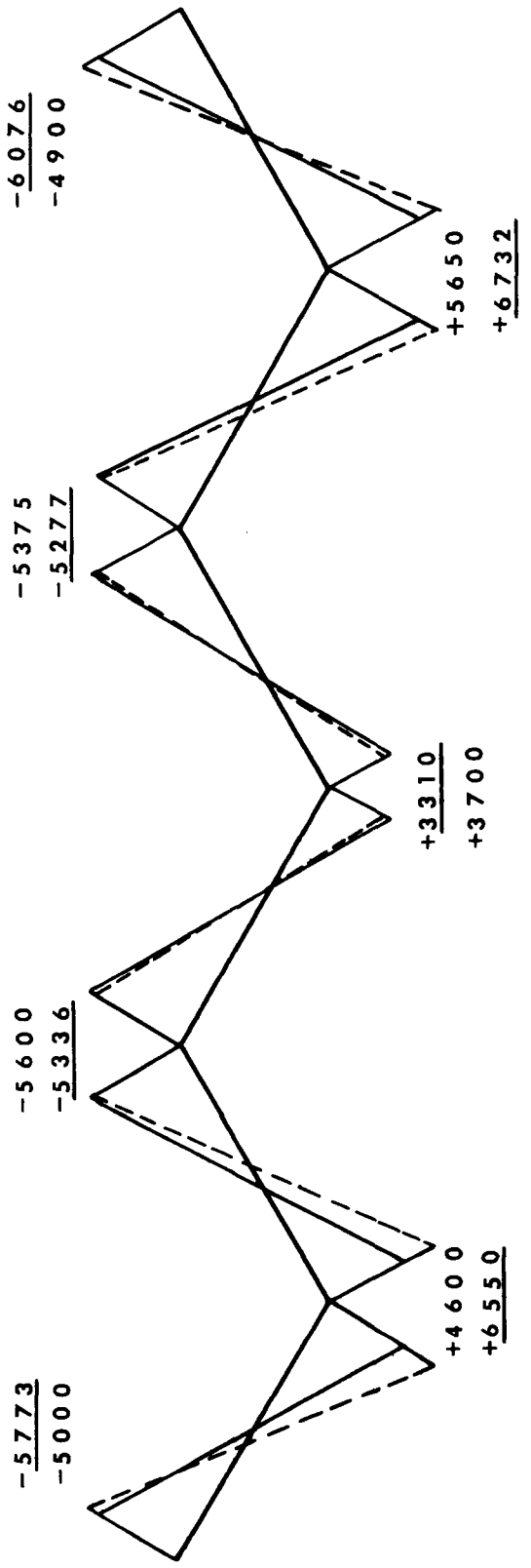

FIG. 143. THEORETICAL AND EXPERIMENTAL LONGITUDINAL STRESSES IN PSI AT MIDSPAN OF THE NINETEEN-FOOT FOLDED PLATE MODEL WHEN LOADED WITH A UNIFORM PRESSURE OF 26 POUNDS PER SQUARE FOOT

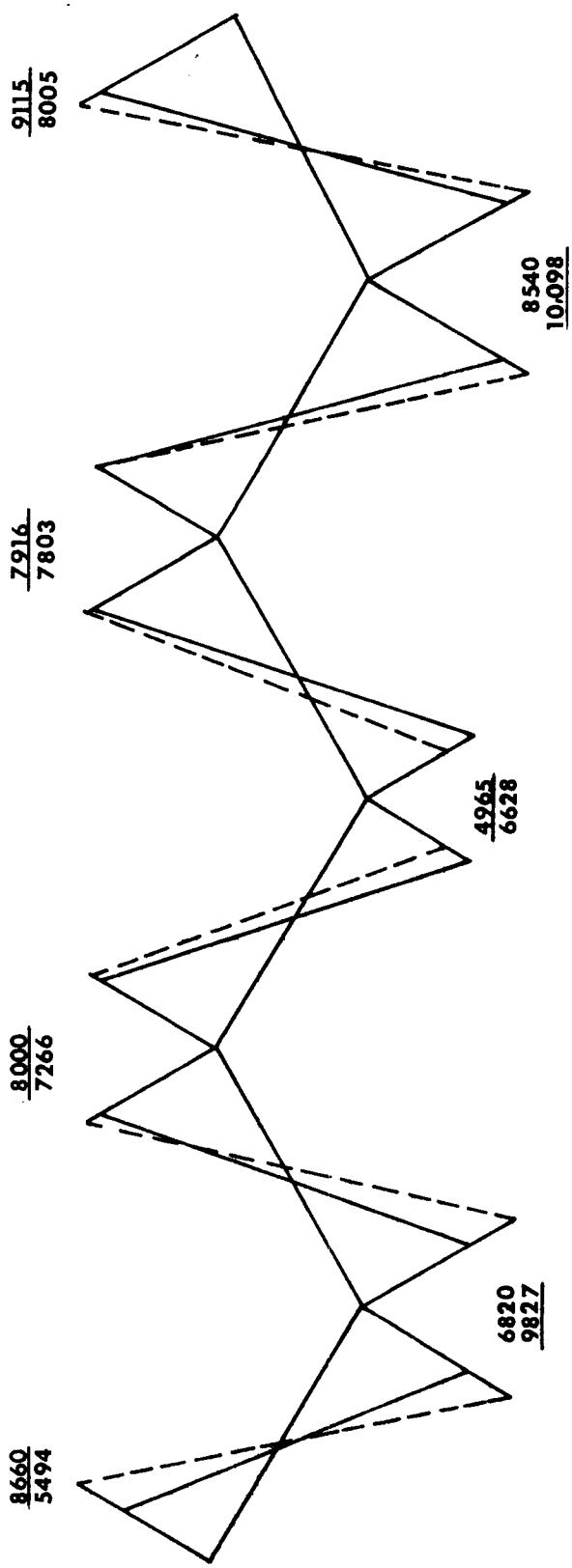

---- Theoretical stresses (underlined)

—— Experimental stresses

FIG. 144. THEORETICAL AND EXPERIMENTAL LONGITUDINAL STRESSES IN PSI AT MIDSPAN OF THE NINETEEN-FOOT FOLDED PLATE MODEL WHEN LOADED WITH A UNIFORM PRESSURE OF 39 POUNDS PER SQUARE FOOT

FIG. 145. THE 9.5-FOOT FOLDED SANDWICH PLATE MODEL IS EASILY LIFTED AT ONE END BY ONE MAN

VITA AUCTORIS

The writer, P. Fazio, was born in Italy, in 1939; immigrated to Canada in 1953; became a Canadian citizen in 1957.

In 1963 he received his B.A.Sc. in Civil Engineering at the University of Windsor; He was granted the M.A.Sc. degree by the same Department in 1964. From 1964 to 1967, he taught, part-time, at the above University; in addition, he pursued the required studies and research leading to the Ph.D. Degree.

In 1967 he accepted a position of Assistant Professor in the Engineering Faculty of Sir George Williams University in Montreal.